NEW MEXICO DEPARTMENT OF TRANSPORTATION

RESEARCH BUREAU

Innovation in Transportation

Solution to Interfacial Delamination of NMDOT's Asphalt Pavements

Final Report

Prepared by:
University of New Mexico
Department of Civil Engineering
Albuquerque, NM 87131

Prepared for:
New Mexico Department of Transportation
Research Bureau
7500B Pan American Freeway NE
Albuquerque, NM 87109

In Cooperation with:
The US Department of Transportation
Federal Highway Administration

MAY 25, 2026

USDOT FHWA SUMMARY PAGE

1. Report No.	2. Government Accession No.	3. Recipient's Catalog No.
4. Title and Subtitle Solution to Interfacial Delamination of NMDOT's Asphalt Pavements		5. Report Date May, 2026 6. Performing Organization Code 456-A
7. Author(s): Muhammad Tasnim Alam and Rafi Tarefder		8. Performing Organization Report No. 456-374
9. Performing Organization Name and Address University of New Mexico Department of Civil Engineering MSC01 1070 1 University of New Mexico Albuquerque, NM 87131		10. Work Unit No. (TRAIS) 11. Contract/Grant No. C06372
12. Sponsoring Agency Name and Address NMDOT Research Bureau 7500B Pan American Freeway PO Box 94690 Albuquerque, NM 87199-4690		13. Type of Report and Period Covered Final Report, 7/1/2022– 6/25/2026 14. Sponsoring Agency Code
15. Supplementary Notes		

16. Abstract

This study investigated interfacial delamination in NMDOT's asphalt pavements and developed improved methods for evaluating and improving bonding between asphalt layers. Laboratory testing evaluated four tack coat types: trackless tack, SS-1H, SS-1HP, and CSS-1H. Direct shear tests were used to measure interface shear strength under different tack coat types, residual application rates, curing times, surface textures, surface aging conditions, normal stresses, loading rates, temperatures, and moisture conditions. Based on rheological properties, such as high-temperature performance grade, elastic recovery, and non-recoverable creep compliance, trackless tack showed superior performance, followed by SS-1HP, SS-1H, and CSS-1H. In direct shear testing, the highest interface shear strength for SS-1H was 252 psi at a residual application rate of 0.04 gal/yd². For SS-1HP, the highest interface shear strength was 275.29 psi at 0.06 gal/yd². For CSS-1H, the highest interface shear strength was 234 psi at 0.04 gal/yd². For trackless tack, the highest interface shear strength was 298.02 psi at 0.10 gal/yd². Overall, trackless tack produced the highest interface shear strength, followed by SS-1HP, SS-1H, and CSS-1H. The minimum curing times were about 120 minutes for SS-1H, 100 minutes for CSS-1H, 50 minutes for SS-1HP, and 25 minutes for trackless tack. Additional results showed that moisture conditioning and high temperature reduced interface shear strength, while rougher and controlled-textured surfaces improved bonding performance. Mechanistic-empirical pavement analysis showed that reduced bonding between asphalt layers can increase predicted pavement distresses, including rutting, fatigue cracking, and International Roughness Index. Finite element modeling using a cohesive zone approach was used to simulate interface shear stress and was validated with laboratory direct shear test results. Other detailed results are presented in the report. Overall, this study provides NMDOT with practical guidelines for tack coat selection, residual application rate, curing time, surface preparation, and quality control to help reduce the risk of interfacial delamination in asphalt pavements.

17. Key Words NMDOT asphalt pavements, Interfacial delamination, Tack coat, Interface shear strength, Direct shear test, Application rate, Milled surface texture, Curing time, Finite element modeling		18. Distribution Statement Available from NMDOT Research Bureau	
19. Security Classification of the Report None	20. Security Classification of this page None	21. Number of Pages 191	22. Price N/A

SOLUTION TO INTERFACIAL DELAMINATION OF NMDOT'S ASPHALT PAVEMENTS

Final Report

Report Submitted to

Research Bureau
New Mexico Department of Transportation
7500B Pan American Freeway NE, PO Box 94690
Albuquerque, NM 87199-4690
(505)-841-9145

Prepared by

Muhammad T. Alam and Rafiqul A. Tarefder

University of New Mexico
Department of Civil Engineering
Albuquerque, N.M. 87131

The University of New Mexico

PREFACE

This report evaluates interfacial delamination in NMDOT's asphalt pavements. It examines how tack coat type, residual application rate, curing time, surface texture, temperature, and moisture affect bonding between asphalt layers. The report presents laboratory direct shear testing, mechanistic analysis, and finite element modeling to evaluate interface bonding behavior.

NOTICE

DISCLAIMER

ACKNOWLEDGEMENTS

This project was funded by the New Mexico Department of Transportation's (NMDOT) Research Bureau. The University of New Mexico (UNM) research team would like to express their sincere gratitude and appreciation to Kelly Montoya, State Materials Director, NMDOT, for serving as the advocate of this project and for her continued support, sponsorship, long-term vision, and valuable suggestions.

The research team also extends its sincere appreciation to Dr. Can Chen, P.E., State Asphalt Engineer, NMDOT, and Dr. Hashem Faidi, Pavement Management and Design Manager, NMDOT, for their valuable guidance and technical suggestions throughout the research. Dr. Chen's extended help in coordinating and collecting the materials and other supports were crucial to the successful completion of this project and are greatly appreciated.

UNM research team sincerely appreciates the valuable time and assistance provided by Angelo Armijo, Staff Manager, and Abigail Moya, Project Manager.

The UNM research team would also like to thank the other Project Technical Panel members for their valuable suggestions during the quarterly meetings. The authors further acknowledge the support provided by all personnel from NMDOT and the University of New Mexico.

TABLE OF CONTENTS

LIST OF FIGURES

LIST OF TABLES

CHAPTER 1
INTRODUCTION

1.1 Research Need and Significance

Asphalt Concrete (AC) pavement is a layered structure; each layer has a different thickness and material. These layers are typically arranged in descending order of load-bearing capacity of the materials to transfer the wheel load efficiently and economically from the top layer to the subgrade layer. The top AC layer is the main structural element of the pavement and is responsible for spreading the wheel load over a relatively large area underneath the base and subgrade. However, it is a common practice to pave several AC layers with smaller thicknesses (known as lifts, thickness less than 3 in) instead of one thicker layer to achieve better compaction (or due to the compactor’s limitation). Two layers are usually laminated or bonded using tack coat materials or other interface materials. As such, the lamination or bonding between two thin AC layers is responsible for transferring loads between layers. If the interface bonds or laminations are intact, then the AC layers function as a monolithic layer, allowing loads to transfer efficiently on the underlying base and subgrade. If an interfacial delamination occurs, the pavement's load transfer mechanism gets impeded, resulting in pavement distress and premature failure. During routine field exploration, the presence of delamination is found as shown in FIGURE 1.1.

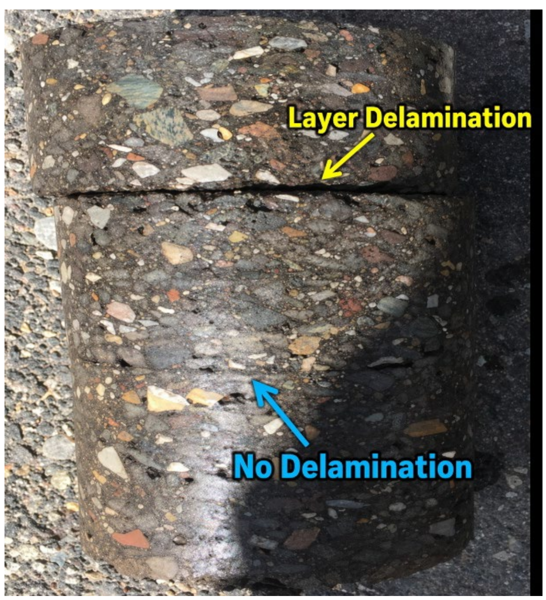

FIGURE 1.1: Field core (I-40)

Interfacial delamination represents one of the critical mechanisms affecting the performance and durability of asphalt pavements. The loss of bonding between AC layers alters the stress distribution within the pavement structure and reduces the efficiency of load transfer across the interface. As a result, localized stresses and strains may increase within AC layers. These changes in structural response can accelerate pavement deterioration and significantly reduce service life.

Numerous pavement distresses have been associated with inadequate interlayer bonding. One of the most commonly observed distresses is slippage cracking (FIGURE 1.2a), which frequently occurs at locations where vehicles apply significant braking forces. Examples include intersections, signalized approaches, ramps, and areas subjected to heavy traffic congestion. At these locations, horizontal shear stresses develop near the pavement surface. If the interface bond is insufficient to resist these stresses, the top AC layer may slide relative to the underlying layer.

Other forms of pavement distress may also develop when the interface bond is weak. Surface debonding (FIGURE 1.2b) has also been reported in pavement sections where interlayer bonding has deteriorated.

(a)

(b)

FIGURE 1.2: Pavement distress due to delamination

(a) Slippage Cracking (b) Surface debonding

Importantly, these distresses may occur even when the asphalt mixtures used in the pavement layers remain structurally sound. In such cases, the deterioration is not associated with deficiencies in the mixture design or material quality, but rather with the loss of bonding between layers. Consequently, the interface between asphalt layers represents a critical zone within the pavement structure where structural performance can be significantly influenced.

Because of the importance of interlayer bonding, transportation agencies have long recognized the need to improve adhesion between asphalt pavement layers. The most common method used to promote bonding between layers is the application of a tack coat. Tack coat typically consists of a thin layer of asphalt binder or asphalt emulsion applied to the surface of an existing pavement layer prior to placement of a new asphalt course. The purpose of the tack coat is to create an adhesive bond between layers so that the pavement structure can behave as a monolithic system under traffic loading.

When properly applied, tack coat enhances the shear resistance at the interface between pavement layers. The resulting bond allows horizontal stresses generated by traffic loading to be transferred across the interface without causing slippage or separation. By maintaining continuity between AC layers, tack coat helps ensure that the pavement structure behaves as an integrated composite system. This interaction contributes to improved load distribution, reduced structural deterioration, and increased pavement service life.

Despite the widespread use of tack coat in asphalt pavement construction, achieving consistent bonding performance in the field remains a challenge. The effectiveness of tack coat bonding depends on several factors related to materials, construction practices, and environmental conditions. The type of tack coat material used may influence the adhesive properties of the interface. Conventional asphalt emulsions, polymer-modified binders, and other materials may exhibit different bonding characteristics.

The amount of tack coat applied is also a critical parameter. Application rate is typically expressed as the residual binder content remaining after the water component of the emulsion has evaporated. If the application rate is too low, insufficient binder may be available to establish adequate bonding between layers. Conversely, excessive tack coat application may create a lubricating layer that reduces friction and shear resistance at the interface. Achieving the appropriate residual application rate is therefore essential for optimal bonding performance.

Surface condition is another important factor influencing interlayer bonding. The presence of dust, debris, or moisture on the existing pavement surface can interfere with adhesion between layers. Proper surface preparation prior to tack coat application is therefore necessary to ensure adequate bonding. Surface texture also plays an important role in bonding performance. Rough or milled surfaces may enhance mechanical interlocking between asphalt layers, while smooth surfaces may provide limited mechanical interaction.

Variations in construction practices can introduce additional variability in tack coat performance. Uneven spray patterns, improper equipment, and insufficient curing time may lead to inconsistent tack coat application. Environmental conditions during construction, such as temperature and humidity, may also influence the behavior of tack coat materials. Because of these factors, the field performance of tack coat bonding may vary significantly across different pavement projects.

Previous research has demonstrated that interface shear strength between asphalt layers is influenced by several interacting parameters. Important factors include tack coat type, residual application rate, surface texture, temperature, moisture condition, and loading rate. Laboratory studies have been conducted to evaluate the influence of these parameters on interlayer bonding performance. Various experimental devices have been developed to measure the shear strength of asphalt interfaces.

Interlayer shear testing has become one of the most widely used laboratory approaches for evaluating bonding performance between asphalt layers. In these tests, a layered asphalt specimen is subjected to controlled horizontal displacement or shear loading until failure occurs at the interface. The measured shear strength indicates the bonding capacity between the pavement layers. These experimental methods allow researchers to compare the performance of different tack coat materials and application rates under standardized laboratory conditions. Studies have shown that variations in tack coat materials and construction variables can significantly influence the measured interface shear strength.

Although considerable research has been conducted on interlayer bonding, several important challenges remain. Different research institutions and transportation agencies have used a variety of testing devices, specimen configurations, and loading conditions. As a result, measured interface strengths can vary significantly between studies.

Furthermore, the relationship between laboratory measurements and field performance is not always clearly established. Pavement interfaces in the field are subjected to complex loading and environmental conditions that may not be fully replicated in laboratory experiments.

Another challenge is the complex nature of bonding mechanisms at the asphalt interface. Interlayer bonding occurs through a combination of adhesive, frictional, and mechanical interactions. Adhesion is governed by the bonding characteristics of the asphalt binder, while frictional and mechanical interlocking result from aggregate texture and surface roughness. The relative contribution of these mechanisms may vary depending on surface preparation, tack coat properties, and environmental conditions.

Traffic loading introduces additional complexity into the behavior of asphalt pavement interfaces. Wheel loads generate shear stresses within the pavement structure that vary depending on load magnitude, vehicle speed, pavement thickness, and temperature conditions. Temperature gradients within the pavement structure can alter the stiffness of asphalt materials and influence stress distribution across the interface. Moisture infiltration and long-term aging of the asphalt binder may further affect the bonding characteristics between layers.

Recent advances in pavement analysis have introduced new tools for evaluating the mechanics of interlayer bonding. Mechanistic–empirical pavement design methods provide a framework for analyzing pavement responses under realistic loading and environmental conditions. These methods allow researchers to assess the structural implications of different bonding conditions between pavement layers.

Numerical modeling techniques have been used to study the mechanics of interfacial damage and delamination. Finite element models allow researchers to simulate pavement behavior under complex loading conditions and evaluate interface shear response, damage initiation, and progressive degradation of bonding between layers. When validated using laboratory testing data, these models provide valuable insight into the parameters that control interfacial failure.

For transportation agencies responsible for maintaining pavement infrastructure, improving the understanding of interlayer bonding is essential. Premature pavement failures caused by delamination can result in increased maintenance costs, reduced pavement service life, and disruptions to traffic operations. Reliable evaluation methods are therefore needed to assess interface bonding performance and guide construction practices.

The research presented in this report focuses on improving the understanding of bonding performance between asphalt pavement layers and the mechanisms that contribute to interfacial delamination. The study evaluates the influence of tack coat parameters on interface behavior and examines the mechanical response of pavement layers under different loading and environmental conditions.

A combination of laboratory testing, mechanistic analysis, and numerical modeling is used to investigate interlayer behavior. Direct shear testing is conducted to quantify interface shear strength and to evaluate the effects of tack coat type, application rate, curing condition, surface characteristics, and loading conditions. The experimental results are interpreted using mechanistic concepts to understand the roles of adhesion, friction, and mechanical interlocking in controlling interface resistance.

The study also considers the influence of environmental factors, particularly temperature and moisture, on bonding performance. In addition, finite element modeling is employed to simulate interfacial behavior and to investigate damage initiation and progression using a cohesive zone modeling approach. The numerical model is calibrated and validated using laboratory test results to ensure consistency between measured and simulated responses.

The results of this research are expected to contribute to the development of improved testing protocols and design guidelines for preventing delamination in asphalt pavements. By identifying the parameters that influence interface performance, this study aims to provide practical tools to improve pavement construction practices and enhance the long-term durability of asphalt pavement systems.

1.2 Objectives

The main objective of this research is to evaluate the bonding behavior between asphalt concrete layers and to identify the key parameters influencing interfacial delamination under mechanical and environmental conditions.

The specific objectives of this study are:

a) To review current practices related to tack coat materials, application methods, and interface bonding evaluation techniques.

b) To evaluate the influence of tack coat type, application rate, and curing condition on interface bonding performance through laboratory testing.

c) To investigate the shear behavior of asphalt interfaces under different loading conditions, including the effects of normal stress and loading rate.

d) To evaluate the effects of full and partial bonding conditions on pavement performance using Pavement Mechanistic-Empirical Design (PMED) analysis.

e) To interpret interface behavior using mechanistic principles by quantifying the contributions of adhesion, friction, and mechanical interlocking.

f) To evaluate the influence of environmental conditions, particularly temperature and moisture, on interface shear strength.

g) To identify the key parameters controlling interfacial failure and provide recommendations to improve bonding performance and reduce the risk of delamination in asphalt pavements.

h) To develop and validate a finite element model capable of simulating pavement interface behavior under complex field conditions, including geometry, traffic loading, and material characteristics.

1.3 Scope of The Study

This study focuses on interfacial delamination between asphalt pavement layers. The work includes a review of current tack coat practices, application rates, testing methods, and factors affecting interface bonding. Laboratory tests are conducted to evaluate the effects of tack coat type, application rate, curing time, surface texture, temperature, moisture, normal stress, and loading rate on interface shear strength.

The study also uses mechanistic-empirical pavement analysis to examine the effects of full and partial bonding conditions on pavement distresses such as rutting, fatigue cracking, and roughness. In addition, finite element modeling using a cohesive zone approach is used to simulate interface shear stress between asphalt layers. Overall, this study aims to identify important bonding parameters and provide guidance to reduce delamination in asphalt pavements.

1.4 Organization of the Report

This report is organized into six chapters:

Chapter 1, Introduction, presents the research need, objectives, and scope of the study. It establishes interfacial delamination as a critical pavement distress mechanism and articulates the need to evaluate bonding behavior between asphalt concrete layers.

Chapter 2, Review of Current Practices, synthesizes existing knowledge and practice related to interlayer bonding and delamination. The chapter examines factors that influence interface performance, laboratory and field methods used to assess bond strength, and tack coat practices adopted by various state Departments of Transportation. It concludes by identifying gaps in current evaluation approaches.

Chapter 3, Evaluation of Tack Coat Parameters, presents the laboratory evaluation of tack coat materials, covering residual binder content, rheological properties, curing behavior, and direct shear test results. The effects of tack coat type, residual application rate, and curing condition on interface shear strength are examined and discussed.

Chapter 4, Determination of Mechanics of Delamination, investigates how interface bonding conditions affect pavement structural response and predicted performance. Using mechanistic–empirical pavement analysis, the chapter evaluates the influence of bond condition, binder grade, truck traffic level, and climate on asphalt concrete rutting, top-down fatigue cracking, bottom-up fatigue cracking, and international roughness index. It demonstrates how the loss of composite action between asphalt layers alters stress transfer, amplifies critical strains, and accelerates pavement distress.

Chapter 5, Selection of Delamination Design Parameters and Limiting Values, identifies the key parameters governing interfacial delamination. The chapter evaluates the effects of normal stress, shear rate, moisture conditioning, temperature, surface roughness, texture, aging, and texture orientation on interface shear strength. A finite element modeling framework is also presented to simulate interface shear stress and fracture energy.

Chapter 6, Conclusions, summarizes the major findings of the study and offers recommendations for improving interlayer bonding and reducing the risk of delamination in asphalt pavements

CHAPTER 2
REVIEW OF CURRENT PRACTICES

Delamination failure is induced by interlayer stress that develops due to effects such as heavy wheel loads, layers and interface materials, structural discontinuities, moisture movements, freeze-thaw and temperature differences between layers, localized disturbances and slippage formations, lateral confinements, and aging. Delamination is a gradual, cyclic process that can occur in conjunction with fatigue failure (Hakimzadeh et al., 2012). The increase in interface shear from braking and turning operations is a major contributor to interfacial delamination (Yoo et al., 2006). When interfacial shear stress due to applied wheel load exceeds the strength of the interface bond, delamination occurs (Mohammad et al., 2009). If the temperature distribution along the depth is not uniform, shear stress can be generated along the AC interfaces due to differential expansions and/or contractions of the layers. The AC interfaces can be damaged by the moisture effects because moisture damage reduces the strength of the interface bond. Also, during tack coat applications, the existing surface needs to be clean and dry before application of the tack coat. If tack coat is applied without drying the existing surface or if tack coat is contaminated with dust or dirt, the interface bond will be hampered. In addition, improper choice of tack coat (type) and lack of tack coat or low application rate are potential reasons for delamination at the interfaces.

Past field investigations reported that delamination between layers can cause slippage, cracking, and premature deformations (Shaat, 1992; Charmot et al., 2005; Tayebali et al., 2004; Romanoschi and Metcalf, 2002). Shaat (1992) stated that a poor interlayer bond is responsible for the slippage cracking in the pavement. Charmot et al. (2005) reported that poor interlayer bond caused interface slippage on 44% of an overlay project in Nevada, soon after completion of the works. Besides the regular highway pavements, many researchers investigated the effects of interface quality on airport pavement performance. This is because the traffic-induced loads are comparatively higher in airport pavements than in highway pavements. In Japan, the interface delamination problem is one of the main problems that causes airport runway pavement failures (Hachiya & Sato, 1997; Tsubokawa et al., 2007).

Several researchers used various numerical analyses to demonstrate the importance of interface quality on pavement performance. These analyses included the calculation of stresses and strains based on various interface conditions and the prediction of pavement performance. Uzan et al. (1978) used the finite element method (FEM) to show that the pavement responses (stress and strain) under wheel loads are significantly affected by the degree of interface bonding. Brown & Brunton (1984) reported a 30% reduction in pavement life due to the degradation in interface bonding quality. Several researchers used FEM tools to create a model to perform the surface layer stress analysis of aircraft during landing and braking (Kruntcheva et al., 2006; Su et al., 2008; Buonsanti & Leonardi, 2012; Ali Shafabakhsh & Akbari, 2013; Shafabakhsh & Akbari, 2013). Some studies have shown that tire tread patterns, contact load shapes, and interface conditions can significantly influence the stress distribution and peak stress imparted on the pavement’s surface (De Beer et al., 2002; Yoo et al., 2006; Al-Qadi & Wang, 2011). Wang et al. (2012) investigated the interaction between tire and pavement by considering actual tire contact geometry. They found that the tire pressure is not uniform; the pressure is significantly higher at the center than on the outer side. They concluded that longitudinal contact stresses increase as a tire's motion changes from free rolling to braking. They also reported that both vertical and transverse contact stresses can become greater than those at the free rolling condition. Su et al. (2008) used a three-dimensional tire-pavement interaction model to demonstrate that the modelled slip between the surface and the underlying layer had a significant impact on pavement stresses due to poor load transfer to the underlying layer. The layer elastic theory was used by Maina et al. (2008) to assess surface layer delamination and model the risk of shear slippage inside the pavement. Kruntcheva et al. (2006) studied the effect of bond condition on pavement stresses by modeling the interface as a 10-mm thick layer of variable stiffness. They used linear elastic and two-dimensional FEM analysis to demonstrate that delamination between the pavement layers reduces pavement life. From the above studies, it can be concluded that the effects of interface delamination on pavement performance are significant.

2.1 Factors that Influence Interfacial Delamination

2.1.1 Tack coat type

Tack coat is used in the field to promote adhesion between the layers (West et al., 2005). Tack coat can be conventional asphalt binder, cutback asphalt, or asphalt emulsion. However, due to improved workability and lower cost, asphalt emulsion is the most commonly used tack coat in the pavement industry (TRB, 2012). The emulsified tack coats are usually made from either conventional or polymer-modified asphalt binders. Several studies have examined the interface strengths made from different tack coat materials. They reported that the polymer-modified emulsions produce greater interface strengths. Mohammad et al. (2002) utilized a direct shear test to investigate six tack coats (four emulsions and two traditional asphalt binders) at different application rates and different temperatures. They concluded that the tack coat with the highest viscosity has the highest interface shear strength. Tayebali et al. (2004) compared conventional binder and rapid-setting emulsion tack coats. They found that the conventional binder delivered 20–50 percent stronger strength across a range of temperatures and load application rates when the test was done in tension mode. This is because actual binder content varies depending on the tack coat substance, and it affects the strength. For example, the binder content of a neat binder is 100%. On the other hand, asphalt emulsion has a binder content from 30 to 70 percent. However, at an identical application rate, conventional binder and asphalt emulsion tack coatings would have dramatically different residual application rates after curing because the emulsion's 30–40 percent water content evaporated during this time. Moreover, the conventional binder has a substantially higher viscosity than the emulsion binder. Tayebali et al. (2004) also found that the difference is negligible when the test was performed in shear mode. Because aggregate interlock and friction were dominant components in the direct shear strength test, this was most likely the reason for this behavior.

Mohammad et al. (2011) compared neat emulsion and polymer-modified emulsion tack coats at 20 °C. The interface shear strength and modulus values of the polymer-modified tack coat are roughly double those of the neat emulsion tack coat. Canestrari & Santagata (2005) found a similar trend when they evaluated interfaces with no tack coat, neat emulsion, and polymer-modified emulsion at 20 °C. At 40 °C, however, the interface shear strength values of the modified and unmodified emulsion tack coats performed fairly similarly. Bae et al. (2010) tested neat emulsion and polymer-modified emulsion tack coats at varied temperatures (-10 to 60 °C) and application rates (0.14–0.70 l/m2). The results revealed that the two tack coats have similar interface shear strength at low temperatures. The difference in strength becomes significant when the temperature rises above 10 °C. They also reported that the polymer-modified emulsion can have a significantly higher strength (about 10 times) than a neat emulsion. Chen & Huang (2010) discovered the same results. The polymer-modified emulsion performs better than conventional emulsions at medium temperatures, typically 25–55 °C.

2.1.2 Application rate

Several studies evaluated the effect of application rate on the interface bond performance. It should be mentioned that the residual rate (after breaking and curing) must be controlled rather than the total or gross application rate when comparing tack coat types and application rates. These studies aim to determine the optimum tack coat application rate. However, mixed results have been reported by the researchers. Some have proposed that too much tack coat can result in a slip plane at the interface (Mohammad et al., 2010), whereas too little tack coat can result in free dust at the interface, preventing adhesion (Bae et al., 2010; Tran et al., 2011). The shear strength increases approximately linearly with increasing tack coat application rate in the range of 0.1–0.7 l/m2, according to Mohammad et al. (2009) and Mohammad et al. (2011). However, in another study, Mohammad et al. (2010) reported that higher tack coat application rates resulted in lower shear strength results. Romanoschi & Metcalf (2002) investigated the interface shear strength with and without a tack coat using cores from field trials. The field trial with tack coat was created by applying tack coat at a low rate of 0.11 l/m2 to the interface. They found that the average difference of shear strengths between with and without tack coat field cores is 210 kPa. The interface shear modulus is reduced by an average of 40 MPa/mm if no tack coat is applied. A similar observation is also reported by Canestrari & Santagata (2005).

In contrast, Lysenko (2006) reported that the interface shear strength is high when no tack coat is applied in the case of laboratory-prepared specimens. Tashman et al. (2008) used both the direct shear test and pull-off test to evaluate milled and un-milled surfaces, as well as the influence of different tack coat application rates (0.08–0.32 l/m2). They found that the tensile strength (as measured by the pull-off test) of both milled and non-milled sections decreases as the tack coat rate increases. They also reported that the application rate of tack coat does not affect direct shear strength for milled interface sections as it does for non-milled sections. Mrawira & Damude (1999) found that the presence of any tack coat caused a slip plane and reduced the measured interface shear strength for field cores with non-milled interfaces.

2.1.3 Interface texture

The effect of the texture of the interface on the shear resistance of the interface has been evaluated by many researchers (D'Andrea et al., 2013). Tozzo et al. (2014) reported that there is a relationship between the textures of the layers and shear stress at the interface. Tashman et al. (2008) used direct shear, torsional shear, and tensile tests to compare the textured and non-textured interface shear strengths. They found that the direct shear strength for the textured interface is almost three times higher than the value for the non-textured interface. The torsional shear strength of the textured interface is slightly higher than that of the non-textured interface. The tensile test shows that the textured interface has a tensile strength that is around double for non-textured interface. According to Mohammad et al. (2010), a textured surface has greater interface shear strength than a non-textured surface. A similar observation was made by Santagata et al. (2008). Sholar et al. (2002) showed that the milled (textured) interface has 10–25 percent more shear strength than the non-milled (non-textured) interface. It is also reported in the literature (TRB,

2012) that bottom-layer surface roughness and interface shear strength are directly related, and milled surfaces consistently have higher strength than non-milled surfaces.

2.1.4 Interface condition

Before applying a new AC layer, it is critical to ensure that the surface of the existing layer is dry and clean. However, the field practice is not always ideal, and there are many cases when paving is done in the presence of rainwater or dust on the existing surface. Therefore, many efforts have been undertaken to evaluate the effect of existing surface conditions on the performance of the interface, and the results are interesting. Interface performance is expected to be reduced due to wet or dusty interfaces. Sangiorgi et al. (2002) found that the presence of dust on the existing surface has a detrimental effect on interface bond performance. On the other hand, Lysenko (2006) found that the presence of dust near the interface enhanced the strength of laboratory-prepared samples. The dust acts like filler and creates an asphalt mastic at the interface. Because mastic is stiffer than the binder, this increase in tack coat stiffness would have boosted interface adherence by increasing the tack coat material's adhesive potential (TRB, 2012). In full-scale trials on two highways in the United States, Sholar et al. (2002) investigated the effect of the presence of rainwater on the interface performance. They found that there is a significant (approximately 50–60%) reduction in shear strength for the moist interface compared to the dry interface. In contrast, some studies found that there is no significant difference in shear strengths between dry and wet conditions (TRB, 2012).

2.1.5 Test temperature

Both AC and tact coat are temperature-sensitive materials. Therefore, many researchers have found that interface shear strength decreases as temperature increases. However, the magnitude of the decline varies from study to study. With increasing temperature, Bae et al. (2010) found a significant drop in interface shear strength. According to Diakhate et al. (2006), shear strength dropped due to temperature in a non-linear manner. At higher temperatures, where tack coat viscosity is low, texture, according to Chen and Huang (2010), becomes more significant in obtaining optimal shear resistance. Canestrari & Santagata (2005) measured a 200 kPa reduction in interfacial shear strength due to a change of temperature from medium to high. The interface shear modulus also drops at the higher test temperature, but to a significantly lesser degree. For various asphalt mixtures and interface conditions, Sholar et al. (2002) showed a 92% drop in shear strength from 25 °C to 60 °C. West et al. (2005) discovered that temperature change significantly affects bond strength. Tayebali et al. (2004) reported an approximate 80% reduction in shear strength at the higher temperature. A similar trend was observed by Hachiya & Sato (1997). It is also revealed by Romanoschi & Metcalf (2002) that the decline in shear strength is true for the interfaces where no tack coat is applied. Like shear strength, the tensile strength of the tack coat is also a function of temperature (TRB, 2012). TRB (2012) also confirmed that the polymer-modified emulsions are less sensitive to temperature changes than neat emulsions.

2.1.6 Curing time

It is recommended to wait until the tack coat breaks (cured) after it is applied before paving the top layer. The tack coat is considered to be broken (cured) when water separates from the emulsion due to evaporation, and the color of the tack coat begins to change from brown to black. A thin coating of asphalt binder on the existing layer forms when the water has entirely separated from the emulsion. The emulsions are considered to have set at this point. However, sometimes paving is done before the curing of the tack coat. Therefore, some studies investigate the effect of curing of tack coat on the interface bond performance, and the findings are not uniform. For example, a few studies, such as West et al. (2005, Tashman et al., 2008 concluded that paving over an unbroken tack coat does not affect bond strength, while other studies, such as Hachiya & Sato (1997), Buchanan & Woods (2004), reported that interface bond strength improves if the tack coat is cured properly. According to past literature, an overlay can be applied immediately after the tack has been applied, whether it is broken or not. It is also reported that the bond will be established between the layers regardless of the curing condition of the applied tack coat.

2.1.7 Normal stress

Like other materials, the magnitude of normal stress directly affects the direct shear strength of an AC interface. Uzan et al. (1978 stated that the interface bond strength is linearly correlated with the applied normal stress. Mohammad et al. (2009) reported that the significance of normal is more critical for a dusty interface than a clean interface. According to West et al. (2005), normal stress is not significant at 10 °C test temperature, but is linearly related to shear strength at 60 °C. The reason is that the frictional component is more dominant than the adhesion at higher temperatures. Romanoschi & Metcalf (2002) used normal stresses ranging from 138 to 522 kPa to examine surfaces with and without tack coat in a direct shear test and found that bond interface shear strength and modulus increase with increment of normal stress at a rate that is equivalent to a friction angle of approximately 45°. Similar trends have been reported by other researchers, such as Chen & Huang (2010) and D’Andrea et al. (2013).

2.1.8 Loading rate

Because both AC and tack coat are viscoelastic materials, their mechanical responses are time-dependent. Like any other viscoelastic material, interface shear strength decreases as the rate of loading increases (Uzan et al., 1978). Sutanto et al. (2007) applied different deformation rates (10, 50, and 100 mm/min) and found that shear strength varied by approximately 33%, in proportion to the rate of loading. By comparing two different loading rates (19 and 50 mm/min), Sholar et al. (2002) found that the faster rate causes 55% increment in shear strength than the slower rate. However, Tayebali et al. (2004) reported that the loading rate is more critical in tension mode than in shear mode. They reported that the tensile strength measured at a 2.5 mm/min load rate is about two to four times the tensile strength measured at a 1.0 mm/min load rate. The difference in strength between the 1.0- and 2.5-mm load rates was minimal when a direct shear test was used.

2.2 Review of Testing

Past studies show that interfacial delamination hinders the pavement's load transfer mechanism and results in other pavement distress and premature failure. Giving importance to this fact, several researchers have attempted to develop their own test methods and apparatuses for evaluating interfacial delamination. It is worth mentioning that no standard test method or protocol has yet been established despite these attempts. The tests mentioned in the literature can be categorized into three major groups based on the applied loading modes: shear, torque, and tension tests, as shown in FIGURE 2.1.

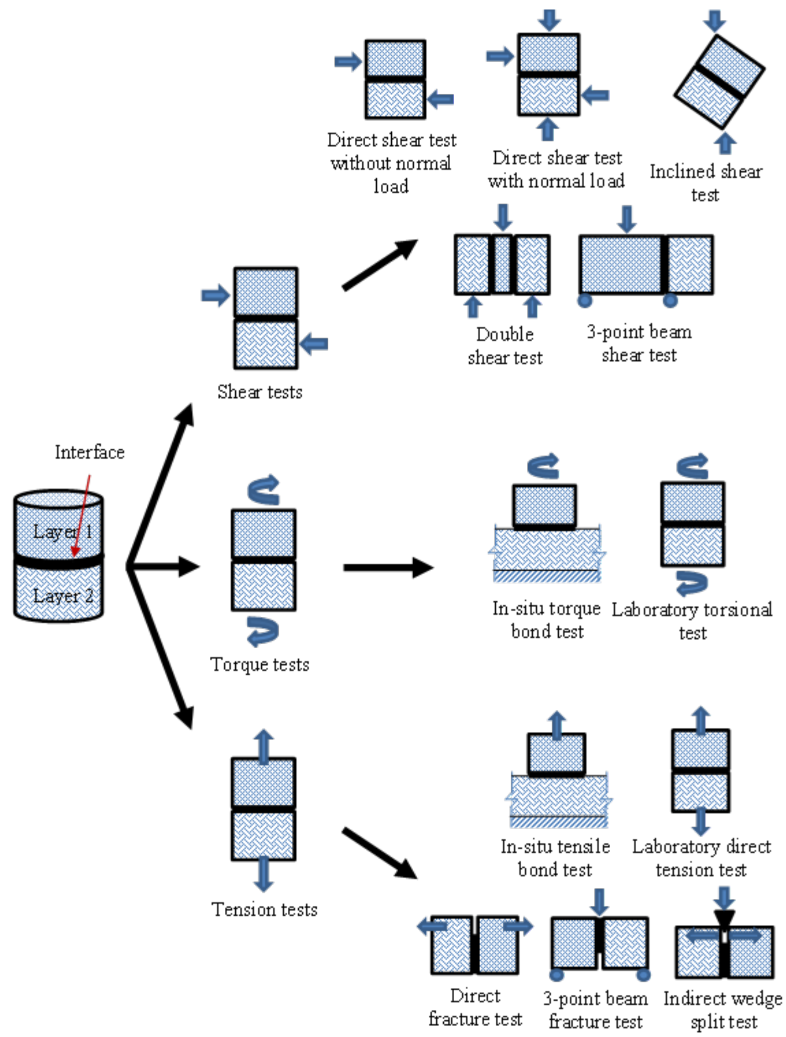

FIGURE 2.1: Types of test methods for evaluation of interfacial delamination

2.2.1 Direct Shear Tests

The direct shear tests are the most commonly used tests to evaluate interfacial delamination because of their ease of use and suitability. The shear test is performed by applying shear load on a two-layered (or three-layered) specimen with or without the presence of normal load. The test is also conducted in two different modes: monotonic and cyclic loadings. Descriptions of a few direct shear tests are summarized in this section.

The simplest direct shear test is the Leutner test, as shown in FIGURE 2.2, developed in Germany in 1979 (Sangiorgi et al., 2002). The test is done by applying a constant rate of shear displacement to a 150 mm diameter layered cylindrical specimen until interface failure occurs without the presence of any normal load. The loading rate is 50 mm/min to make the test compatible with any ordinary Marshal or California bearing ratio (CBR) devices, which are widely available. It uses the maximum shear strength as the delamination performance parameter. The limitation of this test is that the mounting molds put extra pressure on the specimen (Sholar et al., 2002), which can affect the results.

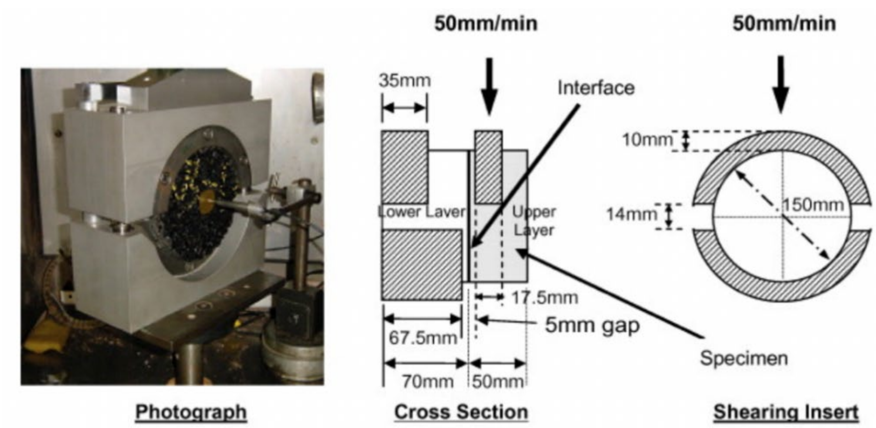

FIGURE 2.2: Leutner simple direct shear test (Sangiorgi et al., 2002)

Many researchers later adopted and modified the Leutner test to make it more suited for their objectives due to its relatively basic configuration and easy operation. For example, Raab et al. (2010) developed the layered parallel direct shear (LPDS) test in Switzerland to examine delamination of the asphalt pavement's interface. The LPDS test uses 150 mm diameter layered specimens with a standard displacement rate of 50 mm/min, just like the Leutner test. The LPDS device is seen schematically in FIGURE 2.3. Like the Leutner test, the mounting molds also put extra pressure on the specimen.

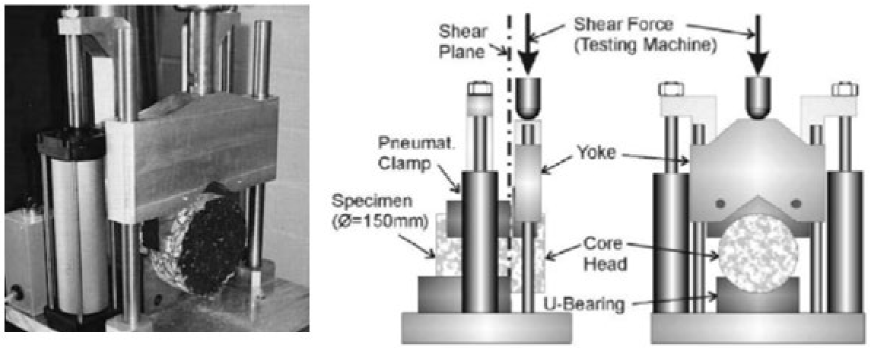

FIGURE 2.3: Layered parallel direct shear (LPDS) test (Raab & Partl, 2004)

Sholar et al. (2002) reported that the loading arms of the original Leutner test put additional load on the specimen, and this load can affect the test results. They designed a simple shear test device for the Florida Department of Transportation (FDOT) that holds a layered specimen with two ring-shaped arms (as shown in FIGURE 2.4), where one arm is fixed, and another can move to apply load. The device is designed in such a way that the gap between the two arms can be adjusted. In addition, other test configurations, such as temperature, loading mode (stress or strain), loading rate, etc., are also configurable. However, in this test, the normal load cannot be applied to the specimen, and there is a great chance of flexural stress on the interface if the interface is not completely vertical (Diakhate, 2007).

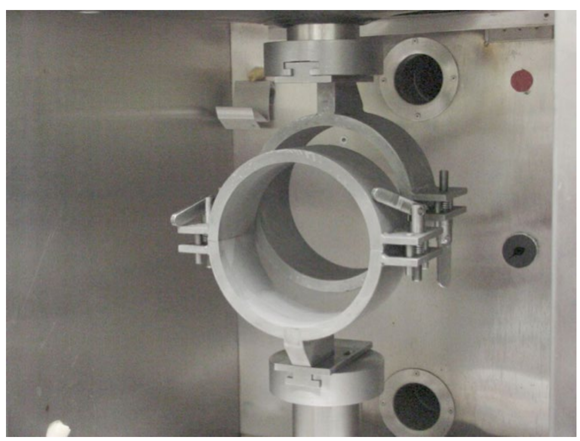

FIGURE 2.4: Florida Department of Transportation (FDOT) shear test (Sholar et al., 2002)

To accommodate the facility for applying normal load to the specimen, the Louisiana Interlayer Shear Strength Tester (LISST) was developed to characterize pavement's interfacial delamination (Mohammad et al., 2012). It uses a custom-made mold with two shearing platens (one of which is a stable response frame and the other a mobile shearing frame) separated by a 12.7 mm gap. The device also facilitated applying a normal load to the specimen. The test is done at a constant displacement rate of 2.54 mm/min. FIGURE 2.5 shows the LISST device developed by Mohammad et al. (2012). Like other direct shear tests, there is a chance of flexural stress on the interface if the interface is not completely vertical.

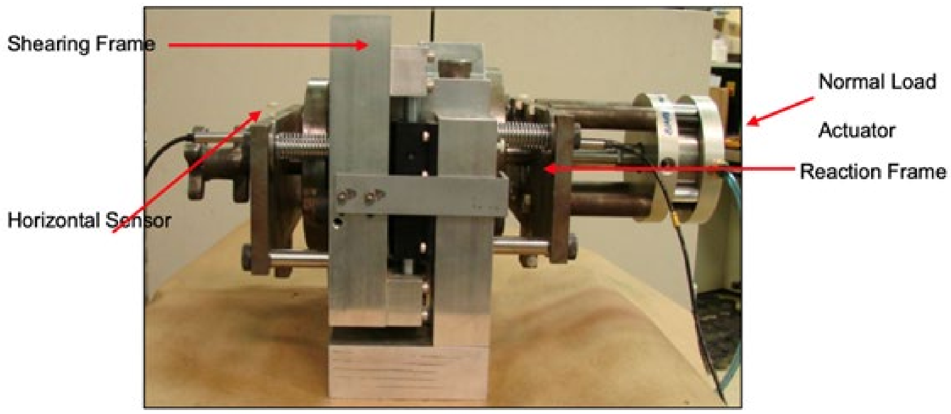

FIGURE 2.5: Louisiana interlayer shear strength tester (LISST) (Mohammad et al., 2012)

The National Centre for Asphalt Technology (NCAT) also used a similar shear test device to evaluate the interfacial delamination in the presence of normal stress (West et al., 2005). The device (as shown in FIGURE 2.6) is similar to the FDOT shear tester, and likewise, this device can be attached to a universal testing or Marshall loading frame for the loading of specimens. The test applies a shear load at 50.8 mm/min on a 150 mm diameter specimen. A gap width of 6.35 mm ± 0.8 mm is recommended between two shearing platens. The test can be performed in the presence of a normal load. However, the applied load may produce a bending moment on the interface due to the eccentricity effect.

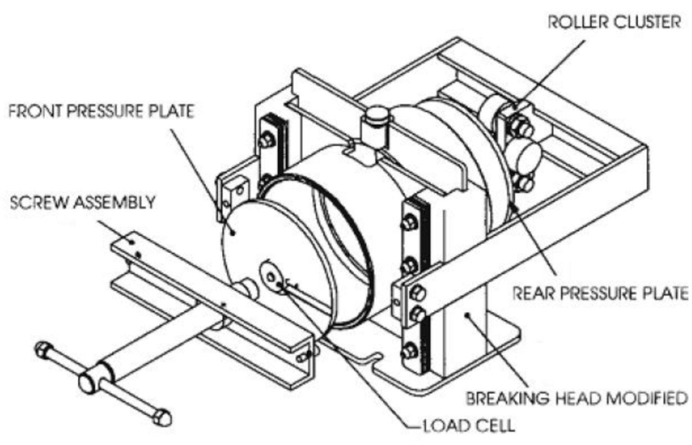

FIGURE 2.6: National Centre for Asphalt Technology (NCAT) shear test (West et al., 2005)

To remove the gravitational force from the mounting mold, some tests were developed where the interface is kept parallel to the horizontal plane. An example of such a test is the Ancona Shear Testing Research and Analysis (ASTRA) test developed by Santagata et al. (1994). One unique feature of the test apparatus is that it can measure the displacements in both normal and shear directions, which allows to determine the dilation (or volumetric expansion) at the interface. The apparatus can also test both prismatic and cylindrical specimens. The test is carried out at a constant displacement rate of 2.5 mm/min with a constant normal load perpendicular to the plane of the tested interface. The ASTRA equipment is depicted schematically in FIGURE 2.7.

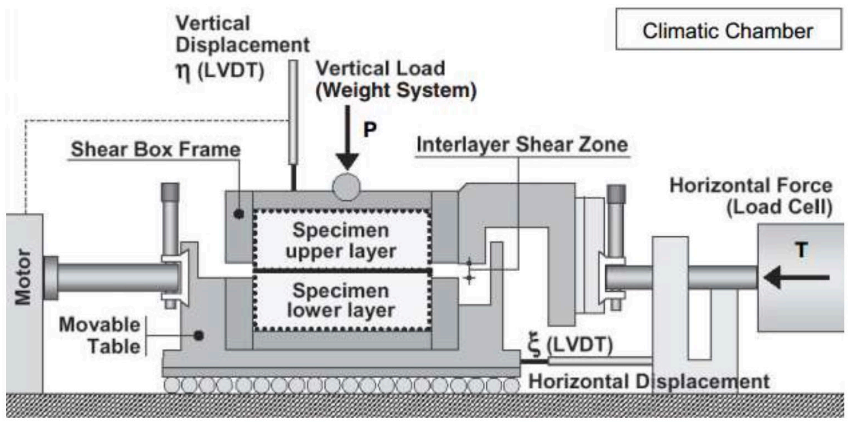

FIGURE 2.7: Ancona Shear Testing Research and Analysis (ASTRA) test

In real conditions, the pavements are subjected to repeated traffic loading; therefore, many researchers urged that the cyclic or dynamic test would be a better choice than the monotonic testing. As a consequence, there are some tests that have been proposed by the researcher to investigate the interface delamination in cyclic loading. Donovan et al. (2000) developed another direct shear test fixture, as shown in FIGURE 2.8, to apply cyclic shear load at the interface of a layered specimen in the vertical direction with the presence of a normal load, which is applied in the horizontal direction. The test aims to track the degradation of interface delamination due to cyclic loading. Al-Qadi et al. (2012) later used a modified version of the apparatus. However, they performed the test in monotonic mode instead of cyclic mode to reduce the effect of the bending moment caused by the eccentricity of the shear force.

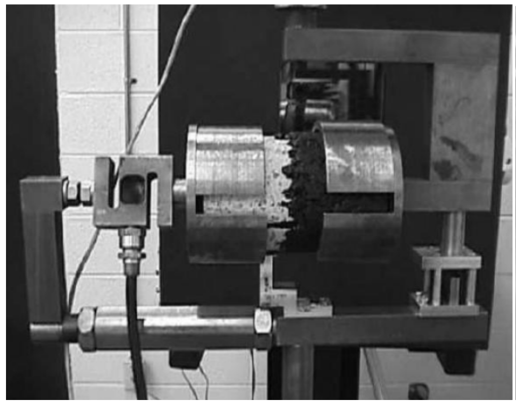

FIGURE 2.8: Donovan et al. dynamic shear test (Donovan et al., 2000)

Another dynamic shear test was used in Germany in 2007 to investigate the interface delamination between AC layers (Wellner et al., 2015). This dynamic shear testing equipment is designed to assess the degradation of the dynamic shear reaction modulus at interfaces of 100 mm diameter layered specimens due to repeated shear displacement in the presence of normal load. The dynamic shear testing apparatus is depicted in FIGURE 2.9.

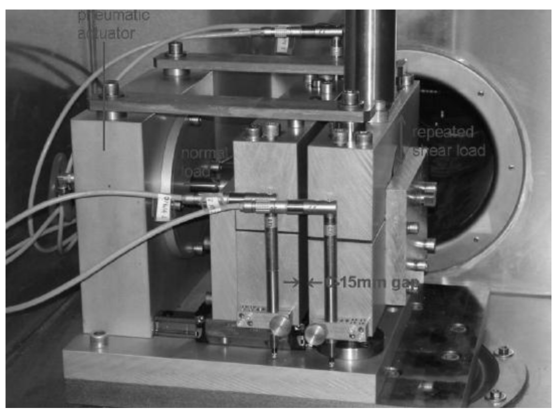

FIGURE 2.9: Ascher et al. dynamic shear test (Wellner et al., 2015)

Isailovic et al. (2018) also used a dynamic shear test to track the delamination at the interface due to cyclic loading. They performed the test on the 150 mm cylindrical specimen at three different normal stress levels (0 to 0.5 MPa) and five temperature levels (-10 to 50 °C). However, they recommend using the test without applying the normal load for practical purposes. FIGURE 2.10 shows the cyclic test used by Isailovic et al.

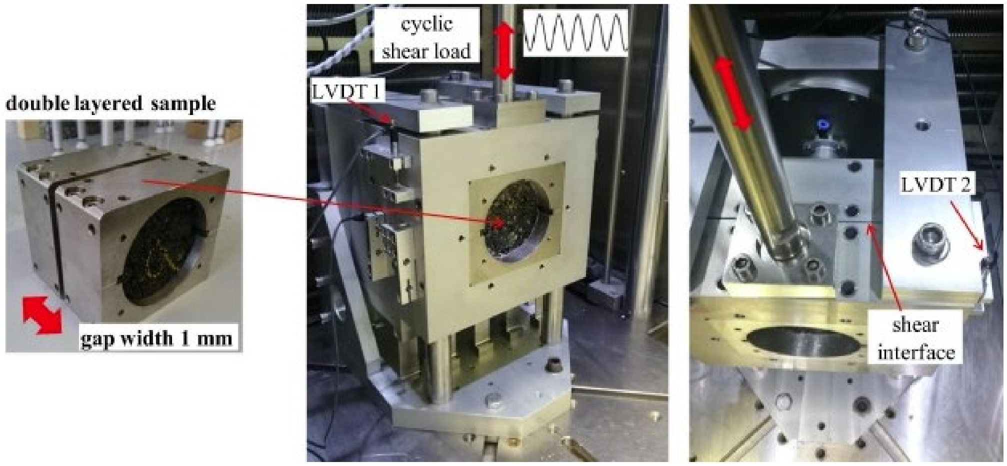

FIGURE 2.10: Isailovic et al. dynamic shear test; (Isailovic et al., 2018)

In a simple direct shear test on a two-layered specimen, the applied load may produce a bending moment on the interface due to the eccentricity effect. This situation can alter the measured shear stress value, and the reliability of the test result becomes questionable. To avoid the bending effect, Diakhate (2007) developed a double shear test to determine the interfacial delamination performance in pure shear mode. FIGURE 2.11 shows the double shear test apparatus used by Diakhate (2007). In this test, the outside layers are fixed while the central part is subjected to displacement, resulting in (near) pure shearing forces at the two interfaces. The original test can be done in both monotonic and dynamic loadings without the presence of normal load (Canestrari et al., 2013).

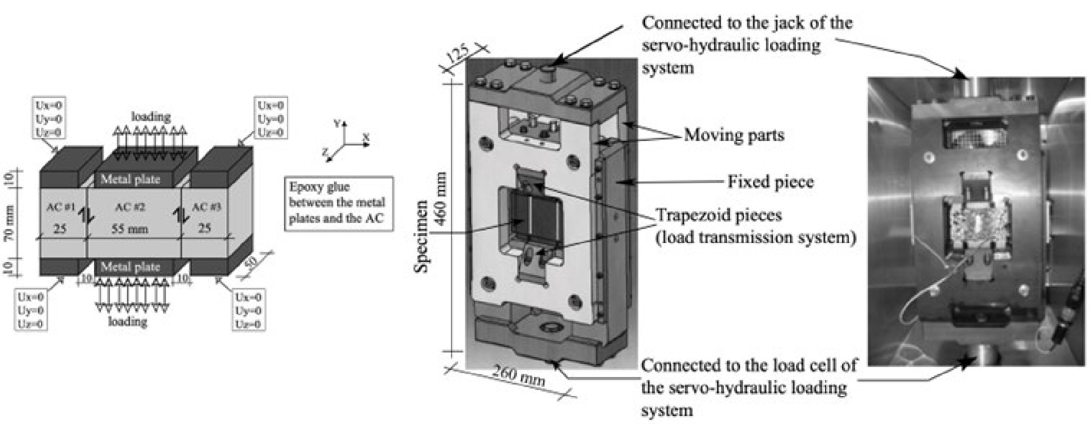

FIGURE 2.11: Double shear test (Diakhate et al., 2011)

Rotating the interface plane and applying a vertical load on the inclined interface is another approach to evaluate delamination at the interface in the presence of normal stress. In this method, the applied vertical load transforms into two resultant forces: one acts normal to the interface and the other acts parallel to the interface. Based on this principle, Romanoschi & Mercalf (2002) developed a shear fatigue test in which the shear plane is set at a 25.50 angle to the horizontal plane, allowing both normal and shear force to be applied to the interface at the same time. However, the researchers concluded that further analysis is required to capture the ratio between shear stress and normal stress for more accurate predictions. FIGURE 2.12 depicts a schematic illustration of the test.

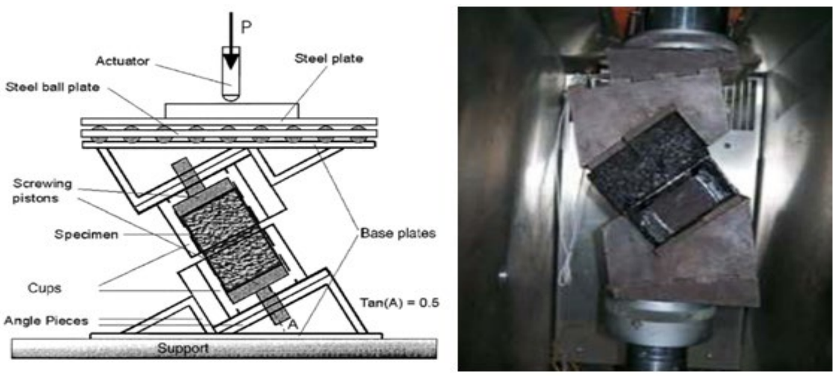

FIGURE 2.12: Inclined shear test (Romanoschi & Metcalf, 2002)

Another inclined shear test device is the Spienza inclined shear test machine (SISTM), as shown in FIGURE 2.13. The uniqueness of this device is that it can run the test in both monotonic and cyclic loading modes (Tozzo et al., 2014). In this test, the inclination angle is 60° in the longitudinal direction of the specimen. The angle was chosen such that the normal and shear stress response measured would relate to 30.0 mm from the edge of a tire wheel load.

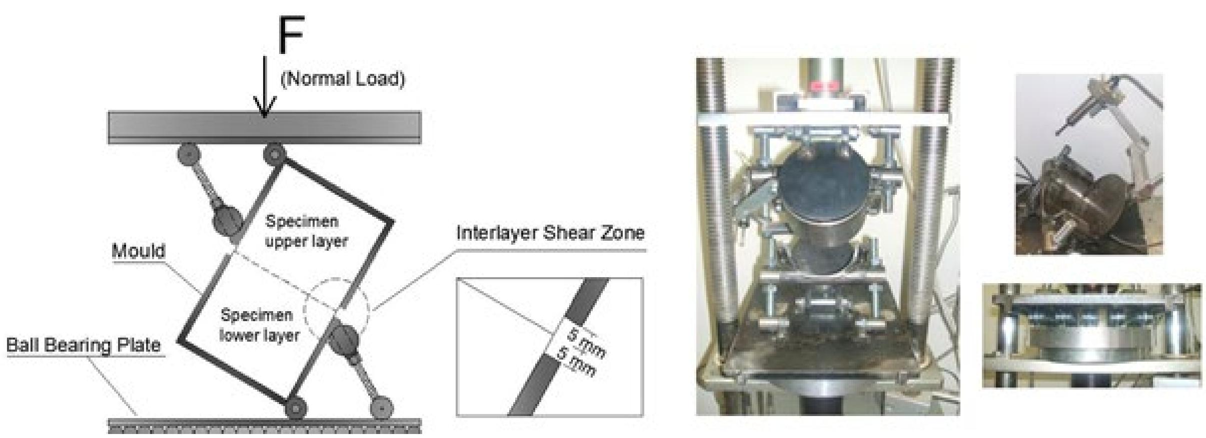

FIGURE 2.13: Spienza inclined shear test machine (SISTM) (Tozzo et al., 2014)

The three-point bending beam configuration is also being used to evaluate delamination of asphalt layers. A three-point bending shear test was proposed by Laboratorio de Caminos de Barcelona (LCB) in Spain (Canestrari et al., 2013), as shown in FIGURE 2.14, where the interface of two-layered specimens is located just outside of one support, and a vertical load is applied at the middle of the beam. Due to this configuration, it is hypothesized that the bending moment at the interface is nearly zero, and it is under pure shear stress. The vertical load increases until the specimen fails. Shear strength, shear modulus, and breaking energy are all measured in this test. However, this test needs a longer specimen, which is not practically feasible.

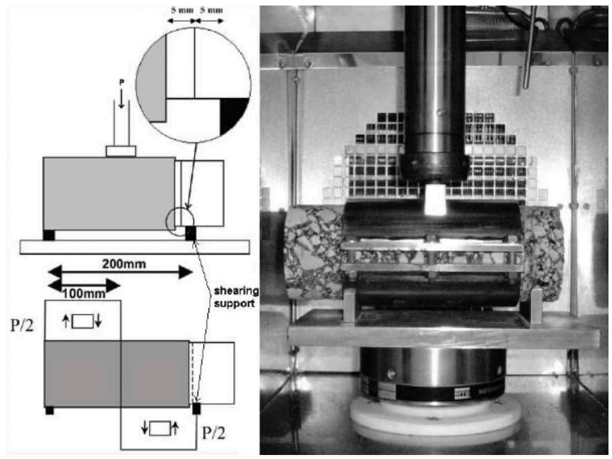

FIGURE 2.14: Three-point bending shear test (Canestrari et al., 2013)

2.2.2 Torque Tests

The torque (or torsional shear) test is done by applying a twisting moment on a two-layered specimen. While most of the torque tests are in-situ tests that are performed in the field, a few torque tests are available, which are done in the laboratory in a controlled environment. Descriptions of a few torque tests are summarized in this section:

An in-situ torque bond test, as shown in FIGURE 2.15, was developed in Sweden for investigating in-situ interfacial delamination of asphalt pavement layers (Tashman et al., 2008). This test requires a core up to 20mm below the interface. Then, the top surface of the core is attached to the device's metal plate and connected to a torque wrench. After that, a torque is supplied manually to the specimen at a consistent rate until the adhesion between the specimen surface and the metal plates has grown to the point where no failure is expected at this interface. When the maximum torque is reached, or the recorded torque exceeds 300 N · m, the torque stress is turned off. The test can be done on specimens either 100mm or 150mm in diameter. In a practical scenario, it is difficult to maintain the torque rate steady using manual operation. It is known that the strength is directly related to the loading rate. Thus, it is very likely to get erroneous test results from the in-situ tests.

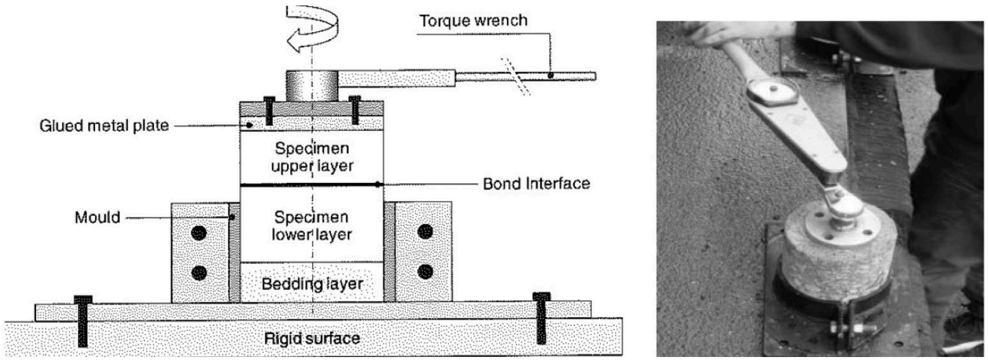

FIGURE 2.15: Swedish in-situ torque bond test (Tashman et al., 2008)

Another in-situ torque test for the evaluation of delamination of asphalt layers is the ATacker test (West, 2005). The uniqueness of this apparatus is that it can perform both a torque and a tensile test (FIGURE 2.16). It was developed by the Mississippi Transportation Research Centre. A smooth, round aluminum contact plate, a torque and force gauge, and a force-driven lever are the main components of this apparatus. The diameters of the contact plates can be varied from 12.7 mm to 127.0 mm, depending on the tack coat materials employed. To maximize the contact surface area of the contact plate, a typical normal force of 178N is applied for 60 seconds after the tack coat material is put in the correct amount on the plate, which breaks and sets. Torsion or tensile force is applied until the tack coat materials fail, depending on the type of test required.

FIGURE 2.16: ATacker in-situ torque bond test (West, 2005)

In the aforementioned in-situ tests, the load is applied manually to rotate the shaft. In a practical scenario, it is difficult to maintain the torque rate steady using manual operation. It is known that the strength is directly related to the loading rate. Thus, it is very likely to get erroneous test results from the in-situ tests. Therefore, an automatic laboratory torque test was developed that can apply a constant torque to delaminate the specimen, as shown in FIGURE 2.17. Therefore, it is possible to get the load-displacement results from the test. The test is done by gluing the two-layered specimen to two metal plates. In this configuration, one plate is fixed, and torque is applied to the other plate until the specimen fails. The peak load is considered the torque bond strength of the interface. The test can be done in both monotonic and cyclic loading modes. Sutanto (2011) found higher bond strength values compared to the manual torque bond test when operated at a contact rate of 600 Nm/min. The main disadvantage of this test is that it is difficult to execute the test.

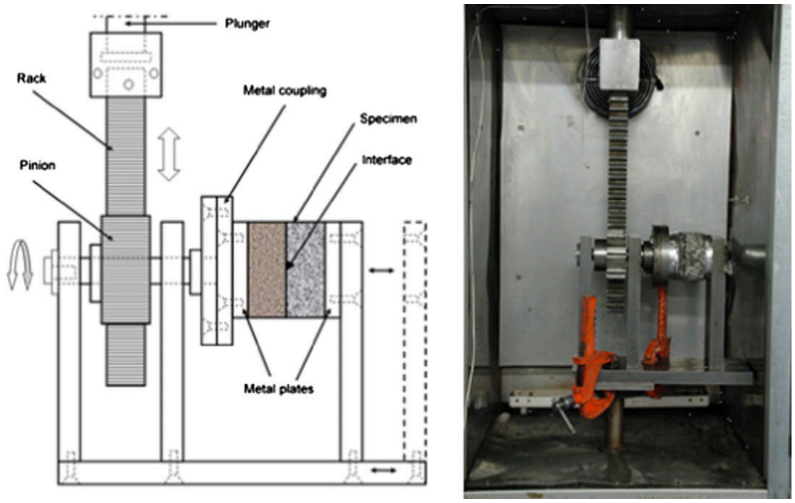

FIGURE 2.17: Automatic torsional shear test (Sutanto, 2011)

2.2.3 Tension Tests

The tension test is conducted by applying tension load on two-layered specimens until the specimens fail. Like the torque tests, most of the tension tests are also performed mainly in the field. There are some fracture-based tensile tests that are done in the presence of notches, and the objective of these tests is to determine the delamination propagation properties. Descriptions of some tension tests are summarized in this section:

An in-situ pull-off test equipment (FIGURE 2.18) was developed by the Swiss Federal Laboratories in 1999 to investigate delamination between asphalt layers (Canestrari et al., 2013). This test is done by attaching the top layer of the pavement to the device, and then, a tensile force is applied manually to delaminate the top layer (Mohammad et al., 2012). Though this test is easy to execute, human subjectivity is an issue for this test.

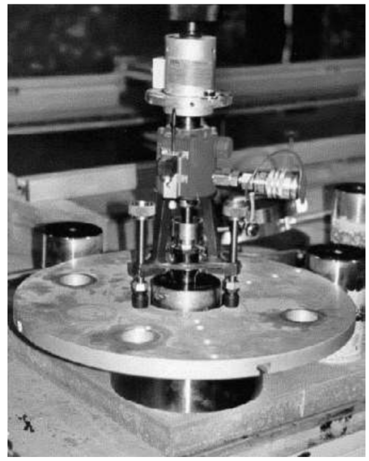

FIGURE 2.18: Swiss in-situ pull-off test (Canestrari et al., 2013)

Another in-situ pull-off test for investigating delamination was developed by the University of Texas at El Paso (UTEP) (White, 2015). In this test, the test device, as shown in FIGURE 2.19, is leveled on the pavement surface where the tack coat has just been applied. Then, the contact plate is lowered until it touches the tack coat. A 40-pound load is placed on top of the contact plate, and the plate is then allowed to set for 10 minutes. After that, the torque wrench of the device is turned counterclockwise to pull out the contact plate until it separates from the tack coat material. The force required to separate the contact plate from the tack substance is tracked. The torque wrench reading is then translated to the tack material's strength using a calibration factor.

FIGURE 2.19: University of Texas at El Paso (UTEP) in-situ pull-off test (Hakimzadeh, 2015)

Besides the in-situ tests, laboratory tests are also available to evaluate the interfacial delamination of asphalt layers in the laboratory environment. For example, a direct tension (pull-off) test, as shown in FIGURE 2.20, was developed at Kansas State University to determine optimum application rates of tack coat materials at the pavement interface (Chang et al., 2014). In this test, a constant pulling rate is applied on a two-layer specimen until the specimen fails, and the peak load in load displace curve is referred to as the tensile strength. The specified pulling rate is 25mm/min, and the diameter of the coring specimen is 50 mm. The main disadvantage of this test is that if the specimen is not aligned vertically, the results will be erroneous.

FIGURE 2.20: KDOT direct tension test (Chang et al., 2014)

Hakimzadeh et al. (2012) urged that peak tensile strength data are not sufficient for FEM modeling. They proposed a new fracture-based test, called the interface bond test (IBT), for evaluating interfacial delamination of asphalt pavement layers. In this test, a notch is created at the interface, and a tensile load is applied to open the crack at a rate of 0.5 mm/min (FIGURE 2.21). Hence, the fracture parameters can be calculated from the load-displacement curve. They reported that fracture energy can be a promising indicator for characterizing delamination performance. The test can be successfully applied to the thin-layer systems.

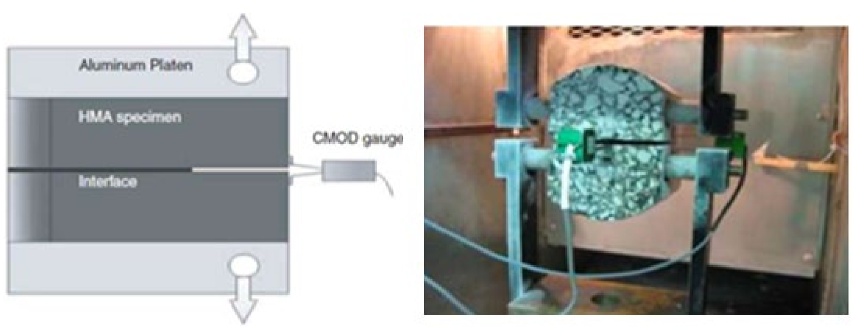

FIGURE 2.21: Interface bond test (IBT) (Hakimzadeh et al., 2012)

In the IBT, the thin layers need to be glued with aluminum platens to apply the tensile load. This step is difficult, and an improper bond between the layer and platen can give erroneous results. To avoid these circumstances, Hakimzadeh (2015) proposed another new test that determines fracture properties at the pavement interface in a bending beam configuration, as shown in FIGURE 2.22. In this case, a two-layered beam is prepared in such a way that the interface is at the middle of the beam. Then, a notch is introduced at the interface, and load is applied to break the specimen. The test can be done in both tensile loading mode and mixed loading mode. However, preparing specimens with thicker layers is difficult and practically not feasible.

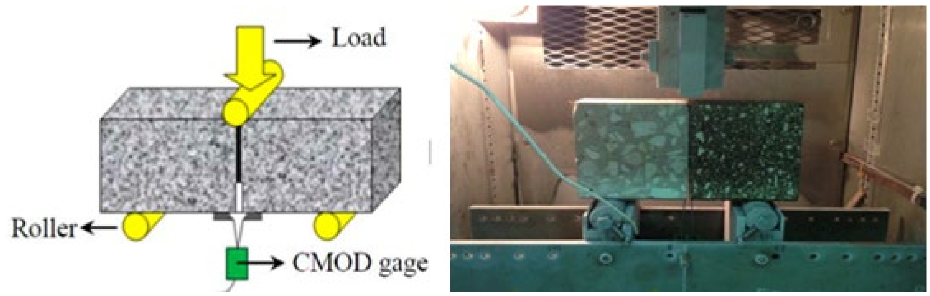

FIGURE 2.22: Three-point bending fracture test (Hakimzadeh, 2015)

Another fracture-based test for investigating delamination between asphalt layers is the wedge splitting fracture test. This test was developed by Tschegg et al. (1995) in Austria to investigate the fracture parameters of the AC interface. In this test, a vertical compressive force is applied to a metal wedge, and the wedge converts it to horizontal forces to break a layer at the interface. The maximum load and fracture energy are derived from the load-displacement curve. FIGURE 2.23 is a schematic illustration of the wedge splitting test. Though the test is easier to execute, it does not provide the actual load versus crack opening curve (Hakimzadeh, 2015).

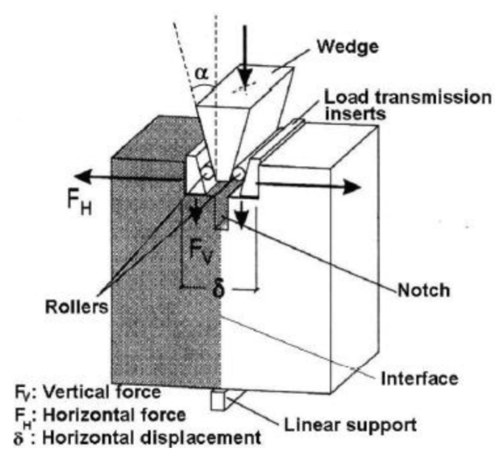

FIGURE 2.23 Indirect wedge splitting fracture test (Tschegg et al., 1995)

2.2.4 Summary

TABLE 2.1 summarizes the advantages and limitations of each test that is used to investigate interfacial delamination between asphalt concrete layers. For example, some tests, specifically the direct shear tests in vertical loading conditions, are affected by load eccentricity if the interfaces are not perpendicular to the applied loads and/or the gap widths between the mounting molds are wider. In these circumstances, failure can be affected by a flexural stress in addition to the applied shear stress. The direct tension test's results can be erroneous if the alignment of the specimen is not properly vertical. Results of these tests can also be affected by the glue materials, which are required to attach specimens to the devices. Similarly, results from manually operated (in-situ torque or tension) tests are subjected to human bias. The dynamic tests are difficult to execute, and complicated loading frames are required that may not be available elsewhere. Some tests offer very little information about bonding properties that can be further used for modeling purposes. Past literature also reported that the variability of results from these tests is quite high.

TABLE 2.1: Advantages and disadvantages of different tests for evaluation of delamination

Test method	Advantages	Disadvantages
Direct shear tests (monotonic with and without normal load)	• Quick and simple (Sutanto, 2011). • Repeatable (Sutanto, 2011). • Can be conducted using common laboratory equipment	• Mounting mold can put additional pressure (Sholar et al., 2004) • Possible load eccentricity causes a bending moment. (Diakhate, 2007) • Complexity associated with the application of normal stress (Sutanto, 2011). • Cannot separate friction from the bond. • Loading condition is not field representable (Donoval et al., 2000)
Direct shear tests (dynamic)	• The loading condition is field representable. (Donoval et al., 2000)	• Very difficult to execute (Al-Qadi, 2012) • Time consuming
Double shear tests	• No possibility of load eccentricity that causes a bending moment. (Diakhate, 2007)	• Preparing specimens is difficult.
Inclined shear tests	• Allows the application of both normal and shear forces to the interface at the same time. (Romanoschi & Metcalf, 2002)	• Further analysis is required to capture the ratio between shear stress and normal stress for more accurate prediction (Tozzo et al., 2014)
Three-point shear test	• Reduced bending moment at the interface ('pure shear' configuration). (Canestrari et al., 2013)	• Difficult to prepare the specimen
Torque test (in-situ)	• Portable can be performed in situ or in the laboratory (Chang et al., 2014). • Quick.	• Poor repeatability (Sutanto, 2011). • Temperature cannot be controlled. • The adhesive property between the metal plate and the upper surface can affect the results.

Torque test (laboratory)	• Controlled environment • Repeatable	• Difficult to execute

TABLE 2.1: (continued): Advantages and disadvantages of different tests for evaluation of delamination

Test method	Advantages	Disadvantages
Direct tension (in-situ)	• Portable, can be performed in situ or in the laboratory (Chang et al., 2014). • Quick.	• Poor repeatability (Chang et al., 2014). • Temperature cannot be controlled (Tschegg et al., 1995) • The adhesive property between the metal plate and the upper surface can affect the results • Can give only the tensile strength (Hakimzadeh et al., 2012)
Direct tension (lab)	• Temperature controllable	• Can give only the tensile strength (Hakimzadeh et al., 2012) • The adhesive property between the metal plate and the upper surface can affect the results • Difficult to align the specimen
Fracture-based tension tests	• Can give fracture properties (Hakimzadeh, 2015)	• Difficult to prepare the specimen
Indirect tensile test	• Can give fracture properties (Tschegg et al., 1995) • Easier to execute	• Computational difficulty. • A proper load versus crack opening curve cannot be achieved (Hakimzadeh, 2015).

2.3 Tack Coat Practices in DOTs

In the United States, a survey by Paul and Scherocman collected responses from 42 state DOTs and the District of Columbia. The findings indicated that most agencies use slow-setting emulsions. The commonly used types are SS-1, SS-1h, CSS-1, and CSS-1h. Only one state reported regular use of hot asphalt binders for tack coat (Paul & Scherocman, 2012). Another survey of midwestern and western states reported similar trends. Slow-setting emulsions were the primary materials in most states. California was an exception, where AR-4000 was widely used. In some cases, SS-1 or CSS-1 was also used. Limited use of cutback asphalt was reported in Kansas. New Mexico and Texas indicated occasional use of performance-grade asphalt binders (Cross & Shrestha, 2012). Guidelines from the Unified Facilities Guide Specification (UFGS) state that slow-setting emulsions can be diluted. Dilution increases the application volume and improves spray control at low application rates. It also helps achieve more uniform coverage during placement (UFGS, 2012). However, diluted emulsions require more time to break and set. This process may take several hours or longer. During this period, the interface may be weak. Early traffic can cause slippage if the other layer is placed too soon (UFGS, 2012).

This subsection presents detailed information on specifications and guidelines regarding the tack coat of some DOTs. The states considered in this comparison are New Mexico, Arizona, California, Colorado, Oklahoma, and Texas. These agencies were selected because their specifications are commonly referenced in projects within the southwestern and southern United States and are relevant to pavement construction conditions in New Mexico.

2.3.1 New Mexico

The NMDOT outlines the requirements for applying a thin layer of asphalt material, known as tack coat, to an existing hot mix asphalt (HMA), warm mix asphalt (WMA), or portland cement concrete pavement surface before placing new pavement. The Contractor must select one of the following approved emulsified asphalts for the tack coat: CSS-1, CSS-1H, SS-1, or SS-1H. Alternatively, performance-graded asphalt binder or other products from the Department's Approved Products List may be used. The surface must be dry, clean, patched, free of dirt, moisture, vegetation, and irregularities. Tack coat should be applied uniformly using a pressure distributor at a rate determined by the Project Manager, typically targeting a residual asphalt content of 0.04 to 0.06 gallons per square yard. Application is prohibited on wet surfaces or when air temperatures fall below the manufacturer's recommended level. Traffic must generally be kept off the tack coat, though it may be placed up to 24 hours ahead if the roadway is closed; limited traffic is allowed only if approved by the Project Manager.

2.3.2 Arizona

The ADOT standard specifications outline requirements for applying tack coat before placing a bituminous mixture on an existing bituminous surface or an existing Portland cement concrete pavement. A light coat of bituminous material is also applied to edges or vertical surfaces against which a bituminous mixture is placed. The Contractor selects the bituminous material, subject to approval by the Engineer, who specifies the application rate for the specific use. Approximate tack coat application rates are provided:

- Emulsified Asphalt (Special Type): 0.08 to 0.12 gallons/square yard for all tack coats;
- Asphalt Cement – 0.06 to 0.08 gallons/square yard.

The Engineer may adjust the application rate. If emulsified asphalt is used, it must break before the bituminous mixture is placed. Tack coat is applied only as far in advance as necessary to achieve proper bonding; no more material is applied in one day than can be covered by the bituminous mixture that same day. Traffic is not permitted on the tack coat until covered.

2.3.3 California

The California Department of Transportation (Caltrans) provide detailed recommendations for applying tack coat, a light layer of asphaltic emulsion or asphalt binder, to ensure bonding between existing pavement surfaces (including planed ones) and new hot mix asphalt (HMA) overlays, between HMA layers, or against vertical surfaces like curbs and gutters; it is not required for chip seals (though flush coats may be needed) or typically for slurry seals/micro-surfacing unless the surface is dry/raveled or concrete. Approved materials include slow-setting emulsions (SS-1, SS-1h, CSS-1, CSS-1h), rapid-setting (RS-1, RS-2, CRS-1, CRS-2, PMRS-2, PMRS-2h, PMCRS-2, PMCRS-2h), quick-setting (QS-1, QS-1h, CQS-1, CQS-1h), or any grade of asphalt binder with selection based on local experience, weather (e.g., rapid/quick-setting for cool/night work), and compatibility (cationic/anionic not mixed). Estimating quantity considers paving layers (e.g., 1-4 based on HMA thickness), application rates, and area, using minimum rates like 0.05-0.11 gal/sq yd for HMA Type A/RHMA-G overlays and 0.07-0.12 gal/sq yd for OGFC for estimation. Slow/quick-setting emulsions may be diluted by the supplier up to a 1:1 water: emulsion ratio to aid uniform coverage, but not rapid-setting; diluted rates are higher to achieve residual asphalt (e.g., 0.08-0.22 gal/sq yd for 1:1 diluted on HMA). Application must use a calibrated distributor for uniform coverage at specified minimum residual rates on clean/dry surfaces free of dust/dirt (swept/washed if needed), with spray bar at proper height/angle for double/triple overlap, avoiding puddling/streaking; apply only what can be covered same day, keep traffic off until broken/set (brown to black color change), blot excess with sand/roller if needed, and repair tracking/damage at contractor's expense.

2.3.4 Colorado

The CDOT specifications outline the requirements for preparing and treating an existing pavement surface with asphalt material to ensure proper adhesion before placing new layers. The surface preparation includes all necessary work such as patching, brooming, shaping to the required grade and section, compaction, and removal of unstable corrugated areas to provide a smooth, dry, uniform base; edges of adjacent pavements must be cleaned for adhesion. Asphalt material for tack coat is specified by type and grade in the contract. Application is prohibited when the surface is wet or when weather conditions would prevent proper construction. The Contractor must provide equipment for heating and uniformly applying the asphalt material, including a distributor capable of variable widths up to 15 feet at rates from 0.05 to 2.0 gallons per square yard with specified tolerances, equipped with a tachometer, pressure gauges, volume measuring devices, thermometer, and adjustable full circulation spray bars. Asphalt material is applied uniformly via pressure distributor in continuous spreads, limited to half the section width when maintaining traffic, with care to avoid excess at spread junctions (which must be removed or redistributed); skipped or deficient areas are corrected, and material is not placed where traffic will travel on the fresh application—rates, temperatures, and areas require pre-approval by the Engineer.

2.3.5 Oklahoma

The ODOT specifications detail the preparation and treatment of existing bituminous or concrete surfaces with bituminous material, defined as an original emulsion (mixture of asphalt, water, and emulsifying agent for a uniform blend) or diluted emulsion (further watered to reduce viscosity for easier spraying), with residual asphalt content being the amount remaining on the pavement after all water evaporation. Construction methods require cleaning the existing roadbed surface before placing tack coat, painting a thin, uniform tack coat on all contact surfaces, such as curbs, gutters, manholes, and other structures that will come in contact with hot mix asphalt to minimize damage and inconvenience to traffic while allowing one-way traffic without pickup or tracking of the bituminous material. Application is prohibited during wet or cold weather, in windy conditions that would cause the tack coat emulsion to drift, or on damp surfaces with free-standing water; the Department will allow tack coat application to damp surfaces. The Resident Engineer must approve the quantity, rate of application, temperature, and areas to be treated before application. Tack coat or NT (non-tracking) tack material is applied with rates altered by the Resident Engineer based on weather and surface type or layer, such as 0.060 gal/yd² original emulsion (0.035 gal/yd² residual); ensure the tack breaks before application of the next surfacing layer. Reapply tack at a rate that ensures proper bonding if the tack loses its adhesive properties or is damaged by traffic before being covered by the next surfacing layer, as directed by the Resident Engineer. The Resident Engineer will measure the volume of emulsion for Tack Coat and NT Tack Material as delivered, before dilution. Bituminous material will be measured by the gallon [liter] or ton [metric ton].

2.3.6 Texas

Tack Coat Specifications from the TxDOT require using CSS-1H, SS-1H, EBL, or a PG binder with a minimum high-temperature grade of PG 58 for tack coat binder; specialized tack coat materials listed on the Department's MPL for Tracking Resistant Asphalt Interlayer (TRAIL) will be allowed or required when shown on the plans. The contractor should not dilute emulsified asphalts at the terminal, in the field, or at any other location before use, unless in conformance with the manufacturer's recommendation for approved TRAIL product use or when shown on the plans. Tack coat and mixture may be placed only when the roadway surface temperature is 45°F or higher, unless otherwise approved, measured using a handheld infrared thermometer, and only when the Engineer determines that general weather conditions of the road surface are suitable. The Engineer may waive the requirement to place tack coat. For application, clean the surface before placing the tack coat; the Engineer will set the rate between 0.04 and 0.10 gal. of residual asphalt per square yard of surface area, applying a uniform tack coat at the specified rate unless otherwise directed in a uniform manner to avoid streaks and other irregular patterns. Apply the tack coat to all surfaces that will come in contact with the subsequent material placement, allowing adequate time for the emulsion to break completely before placing any material, and prevent splattering when placed adjacent to curb, gutter, and structures. The Engineer will notify the Contractor when the sampling will occur and will witness the collection of the sample from the asphalt distributor immediately before use, labeling the can with the producer name, producer facility location, grade, district, date sampled, all applicable bills of lading (if available), and project information, including highway and control number. For emulsions, the Engineer may test as often as necessary to ensure the residual of the emulsion is greater than or equal to the specification requirement.

2.3.7 Summary

State departments of transportation establish specifications for the application of tack coat to ensure proper bonding between asphalt pavement layers. Although the purpose of tack coat is consistent among agencies, the detailed requirements differ from state to state. These differences occur in material types, application rates, construction procedures, and measurement methods.

Such variations are often related to regional construction practices, environmental conditions, and agency standards.

CHAPTER 3
EVALUATION OF TACK COAT PARAMETERS

Previous chapters discussed the role of interlayer bonding in asphalt pavements. They also reviewed previous research on interfacial delamination and tack coat performance. The literature shows that bonding between asphalt layers is affected by several factors. These factors include tack coat type, application rate, surface texture, curing condition, temperature, moisture, loading rate, and normal stress. The individual and combined interaction among these variables has not been studied in detail. Their relative contribution to interface shear strength has also not been clearly quantified.

This chapter evaluates tack coat parameters that influence bonding between asphalt pavement layers. The investigation focuses on parameters that can be controlled during pavement construction. These include tack coat type, application rate, curing condition, and surface characteristics. These parameters affect both adhesion and mechanical interaction at the interface between asphalt layers.

This chapter concentrates on variables associated with tack coat materials and construction practices. This separation allows the present chapter to focus on parameters directly related to tack coat application, while later chapters address mechanical and environmental influences on interface performance.

The results presented in this chapter provide experimental information on the influence of tack coat materials and application conditions on bonding between asphalt layers. The findings also support the development of laboratory procedures capable of producing consistent measurements of interface shear strength. Such information can assist transportation agencies in improving construction practices and reducing the risk of interfacial delamination in asphalt pavements.

3.1 Tack Coat Materials

According to ASTM International (ASTM D8), a tack coat (or bond coat) is a thin application of bituminous material placed on an existing, relatively non-absorptive surface. Its purpose is to ensure proper bonding between the existing layer and a new asphalt layer. Several materials have been used for tack coats, including hot asphalt cement, cutback asphalt, and emulsified asphalt. Cutback asphalt, which contains solvents such as kerosene or diesel, is no longer commonly used. This is mainly due to environmental and safety concerns. Emulsified asphalt is now the most widely used tack coat material. It is a nonflammable liquid made by blending asphalt with water and an emulsifying agent, such as soap or fine clay particles.

Common emulsions for tack coat applications include slow-setting types (SS-1, SS-1h, CSS-1, CSS-1h) and rapid-setting types (RS-1, RS-2, CRS-1, CRS-2). Modified versions, such as CRS-2P (polymer-modified) and CRS-2L (latex-modified), are also used in practice.

Several key terms related to tack coat application are given below:

- ***Diluted Emulsion****:* An emulsion to which water has been added in an amount permitted by the specification.

- ***Emulsion****:* A mixture of asphalt binder, water, and emulsifying agent.

- ***Residual Asphalt Content****:* The amount of asphalt binder remaining on the pavement surface after the water has evaporated from the emulsion.

- ***Application Rate****:* The quantity of tack coat material applied to a unit area of pavement surface.

- ***Residual Application Rate****:* The quantity of residual asphalt binder remaining on a unit area of pavement surface after breaking and curing.

- ***Tack Coat Break****:* The stage at which water begins to separate from the emulsion and the color changes from brown to black.

- ***Tack Coat Cure****:* The stage at which all water has evaporated, and the tack coat is ready to receive the next asphalt layer.

Several tack coat materials commonly used in pavement construction were evaluated in this study. The materials included both conventional emulsified tack coats and modified products.

Two primary types of tack coat emulsions used in pavement construction are anionic (e.g., SS-1H) and cationic (e.g., CSS-1H) emulsions. If the emulsifying agent is cationic, the droplets bear a positive charge, and vice versa (Al-Qadi, Hasiba et al., 2012). Cationic emulsions carry the "C" suffix. Slow-setting versions have SS. The "H" ending—for instance, in CSS-1H—indicates a harder asphalt base. Polymers have expanded emulsion options. The P suffix marks polymer-modified types. These emulsions differ in their chemical composition and breaking mechanisms, which can affect their performance under various environmental conditions. These emulsions differ in their chemical composition and breaking mechanisms, which can affect their performance under various environmental conditions.

To investigate the performance of conventional tacks modified by nanopolymers, a silane-based nanopolymer additive was added to SS-1H and CSS-1H tack coats. For convenience, these polymer-modified tack coats will be mentioned as SS-1HP and CSS-1HP in this article. This additive works as a “molecular bridge” and can enhance the interface strength by forming a covalent bond. This additive is typically mixed in the emulsion at a volume of 1.5% to 3%. This study uses a 2% additive.

Trackless/non-tracking tack has recently been introduced to the paving industry. They set rapidly after application. This process eliminates tackiness. Wilson et al. (2016) explained that tracking potential can be defined by a few strength ratios as shown below:

$$Tracking\ condition: \frac{\sigma_{A_{Tire-Tack}}}{\sigma_{C_{Tack}}} \text{ and/or } \frac{\sigma_{A_{Tire-Tack}}}{\sigma_{A_{Tack-AC\ layer}}} > 1 \qquad \text{Eq.1}$$

$$Trackless\ condition: \frac{\sigma_{A_{Tire-Tack}}}{\sigma_{C_{Tack}}} \text{ and } \frac{\sigma_{A_{Tire-Tack}}}{\sigma_{A_{Tack-AC\ layer}}} < 1 \qquad \text{Eq.2}$$

Where,

$\sigma_{A_{Tire-Tack}}$ = Adhesive strength between tire and tack ;

$\sigma_{C_{Tack}}$ = Cohesive strength of tack coat;

$\sigma_{A_{Tack-AC\ layer}}$ = Adhesive strength between tack and ac layer.

These equations (Eq. 1 and Eq. 2) define when a tack coat tends to track or remain stable. Tracking happens if the bond between the tire and tack is stronger than the tack's own strength or its bond to the asphalt layer. A trackless condition occurs when the tire-tack bond is weaker than both. These strength ratios provide a simple way to judge the likelihood of tack tracking during paving.

The following tack coat materials were used in the study:

- SS-1H emulsified asphalt
- CSS-1H emulsified asphalt
- SS-1HP polymer-modified emulsified asphalt
- Trackless tack coat

FIGURE 3.1 shows different parts of these tack coats:

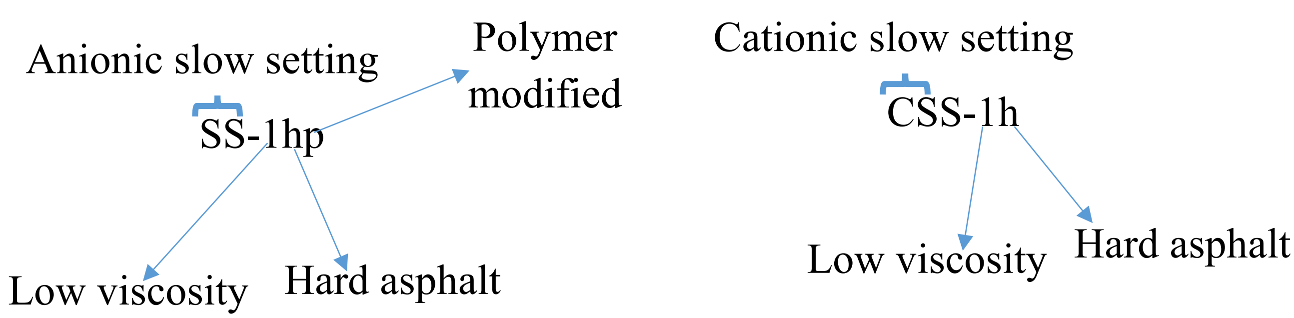

FIGURE 3.1: Types of Tack Coat Emulsions and Their Properties

3.1.1 Residual Binder Content Measurement

This study will use the residual application rate for the comparison instead of the gross application rate. The residual rate was needed to determine the amount of the collected tack coat emulsion.

TABLE 3.1 shows the residual binder content determination of SS-1H. The residue asphalt content of the tack coat emulsion was measured using the evaporation method. In this procedure, the weight of a breaker with a stirring rod was measured. Next, the tack coat emulsion was poured into the beaker, and the total weight was measured, as shown in FIGURE 3.1. After that, the breaker with stirrer rod and tack coat was placed in an oven at 163ºC for 2 hours, as shown in FIGURE 3.2. During the two-hour-long heating period, the tack coat was manually stirred thoroughly using a stirrer rod. After 2 hrs, the beaker was removed from the oven and allowed to cool down. When the beaker was cooled at room temperature, the final weight was measured (FIGURE 3.3). From the initial and final weights, the residual asphalt content was determined. In this study, three replicate tests were done, and the results are presented in TABLE 3.1. It shows that the average residual asphalt content is 62.13% and the standard deviation is 0.02%. TABLE 3.1 shows the residual binder content determination of SS-1H. A similar way was followed to measure the residual binder content of other tack coats.

FIGURE 3.2: Weight of beaker, stirrer rod, and emulsion before heating phase

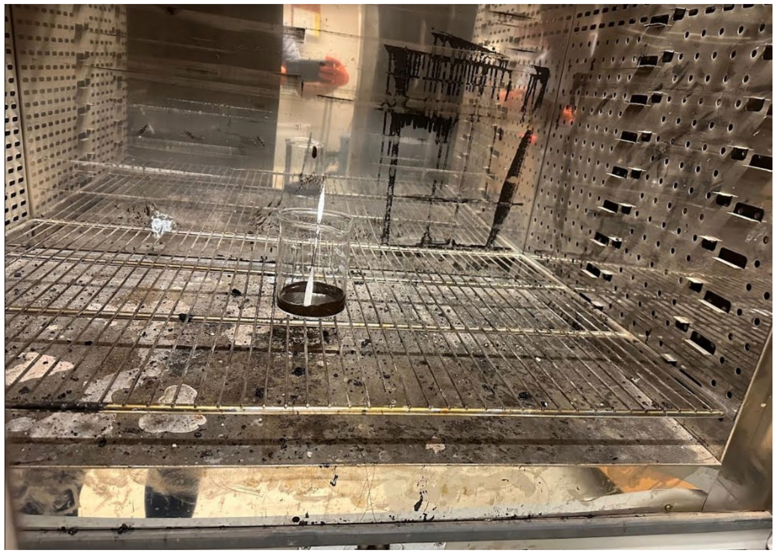

FIGURE 3.3: Emulsion placed in an oven

FIGURE 3.4: Weight of breaker, stirrer rod, and emulsion after heating phase

TABLE 3.1: Determination of residual asphalt content

Descriptions	Weights (gm)
Replicate 1	
Beaker + stirrer rod	282.9
Beaker + stirrer rod + emulsion (before evaporation)	337.2
Emulsion (before evaporation)	54.3
Beaker + stirrer rod + emulsion (after evaporation)	316.8
Emulsion (after evaporation)	33.9
% residual content	62.43%
Replicate 2	
Beaker + stirrer rod	283.4
Beaker + stirrer rod + emulsion (before evaporation)	340.1
Emulsion (before evaporation)	56.7
Beaker + stirrer rod + emulsion (after evaporation)	317.2
Emulsion (after evaporation)	33.8
% residual content	59.61%
Replicate 3	
Beaker + stirrer rod	284.0
Beaker + stirrer rod + emulsion (before evaporation)	335.9
Emulsion (before evaporation)	51.9
Beaker + stirrer rod + emulsion (after evaporation)	317.4
Emulsion (after evaporation)	33.4
% residual content	64.35%
Average % residual content	62.13%
Standard deviation	0.02%

3.1.2 Tack Coat Rheological Properties

The rheological properties of the tack coat materials were evaluated. Binder rheology influences the deformation and recovery response of asphalt materials under loading. Standard binder tests were used to measure the rheological properties of the tack coats. The measured parameters included high-temperature performance grade, elastic recovery, and non-recoverable creep compliance.

The high-temperature performance grade indicates the temperature range over which the binder can resist permanent deformation. Elastic recovery represents the ability of the binder to recover after deformation. Non-recoverable creep compliance describes the amount of permanent deformation that remains after repeated loading. These properties provide information about the stiffness and elastic behavior of the tack coat binders. Differences in rheological properties influence the adhesive characteristics of the tack coat and the shear resistance developed at the AC interface.

3.1.3 Residual Asphalt and Rheological Tests with SS-1H

To get the rheological properties of the residual asphalt of the tack coat emulsion, it is required to separate the water from the emulsion. In this study, water from tack coat emulsion was separated using a filtration method.

In the filtration method, the tack coat emulsion was first properly stirred in the collected pail to make the mixture homogenous. Then, tack coat emulsion was collected in a small beaker. In the next step, the weights of a break, a filter paper, and a funnel were measured. After that, the filter paper was folded and placed inside the funnel. A small amount of water was applied to wet the filter paper to ensure that it stuck to the funnel. The funnel with the filter paper was placed on a beaker. Then, tack coat emulsion was poured into the funnel and left for a sufficient amount of time (at least 24 hours) to drain the water. After 24 hrs., it was found that the water had drained out through the filter, and residual asphalt remained on the filter paper. Finally, the residual asphalt was removed from the filter, as shown in FIGURE 3.5. The final weights of residual asphalt, filter paper with asphalt, and the beaker with water were measured.

TABLE 3.2 shows the measured weights for different conditions for a tack coat. A similar way was followed for other tack coats. It can be found that the residual asphalt content is 67.49%. The percentage of drained water is 27.27%. Some portions of water may be evaporated, and the remaining may be trapped inside the asphalt.

FIGURE 3.5: Residual Asphalt Removed from Filter

TABLE 3.2: Filtration Results

Descriptions	Weights (gm)
Beaker	200.83
Filter	2.56
Funnel	32.2
Beaker + Filter + Funnel	234.76
Beaker + Filter + Funnel + Tack coat emulsion	301.85
Tack coat emulsion	67.10
Residual asphalt removed	42.12
Left over + filter	5.72
Leftover residual asphalt	3.16
Total residual asphalt	45.28
% residual asphalt	67.49%
Beaker + water	219.125
Drained water	18.299
% water	27.27%

3.1.4 Dynamic Shear Rheometer (DSR) Test

The dynamic shear rheometer (DSR) test was used to determine the high-temperature grade of the asphalt residue of the collected tack coat. FIGURE 3.6 shows a DSR device.

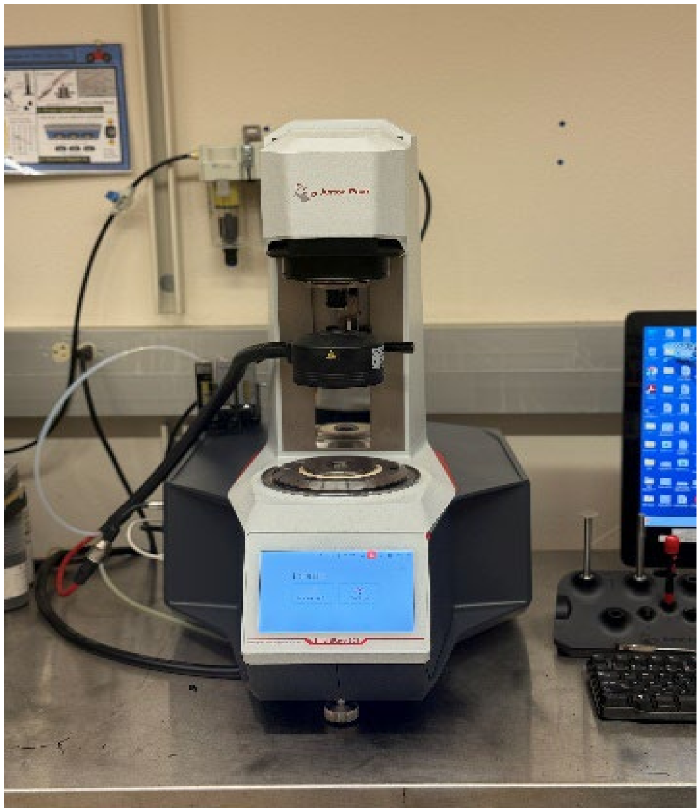

FIGURE 3.6: Dynamic Shear Rheometer (DSR)

It measures the complex modulus, G*, and phase angle, δ, at different temperatures. Hence, the high temperature grade is determined based on the rutting parameter, G*/sinδ requirement (minimum 1.0 kPa). The test is performed on a cylindrical binder sample with a 25 mm diameter and 1 mm height by applying a constant oscillating strain at 10 rad/s. To prepare the cylindrical samples, a sufficient amount of diluted tack coat was drawn down on the 25-mm silicone mat (FIGURE 3.7) in such a way that a minimum of 1 mm-thick asphalt residue film was left on the mat after evaporation of water. When the sample was completely dry, it was peeled and loaded onto the 25-mm DSR plate to perform the DSR test.

FIGURE 3.7: Prepared Sample for DSR Test

This study performed the DSR test on 4 replicate specimens. FIGURE 3.8 shows the DSR results for the tested tack coat residue. It shows that the G*/sinδ value decreases as the temperature increases for all replicates. It can also be seen that the G*/sinδ values of all replicate specimens are close to each other at each temperature. FIGURE 1 presents the high-temperature performance grades (PG) of the tack coats determined from the DSR test results. The SS-1H and CSS-1H tack coats exhibit a high-temperature grade of 64°C, while the SS-1HP tack coat shows an improved grade of 70°C, indicating enhanced resistance to permanent deformation at elevated temperatures. In contrast, the trackless tack coat demonstrates the highest performance grade of 82°C. Based on the DSR test results, this higher grade indicates superior stiffness and improved resistance to permanent deformation under high-temperature loading conditions. Overall, the results suggest that the trackless tack coat provides the best high-temperature performance among the evaluated materials.

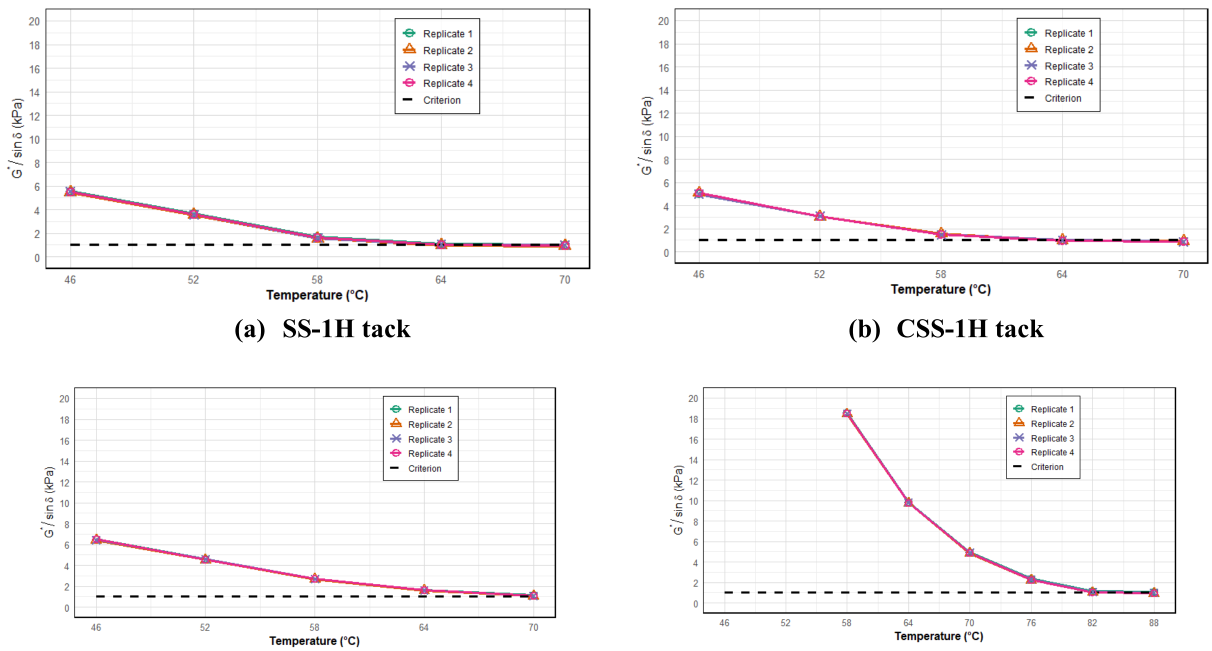

(a) SS-1H tack (b) CSS-1H tack

(c) SS-1HP (d) Trackless Tack

FIGURE 3.8: DSR Test Results

TABLE 3.3 shows the high-temperature PG of tack coats used in this study.

TABLE 3.3: High Temperature PG of Tack Coats Used in This Study

Tack Coats	High Temperature PG
SS-1H Tack	64 °C
SS-1HP Tack	70 °C
CSS-1H Tack	64 °C
Trackless Tack	82 °C

3.1.5 Multiple Stress Creep Recovery (MSCR) Test

The multiple stress creep recovery (MSCR) test is used to determine the creep-recovery performance of the asphalt binder. In this test, a one-second creep load is applied to the binder sample using the DSR device. After one second, the load is removed to allow the sample to recover for 9 seconds. After the recovery period, the total, recoverable, and non-recoverable strains are measured, as shown in FIGURE 3.9.

Next, two different test parameters are determined: percentage of recovery and non-recoverable creep compliance using Eq. 3 and 4, respectively. To evaluate stress dependency, the test is performed at two different stress levels: 0.1 kPa and 3.2 kPa. For better repeatability, several cycles of load recovery are used at each stress level.

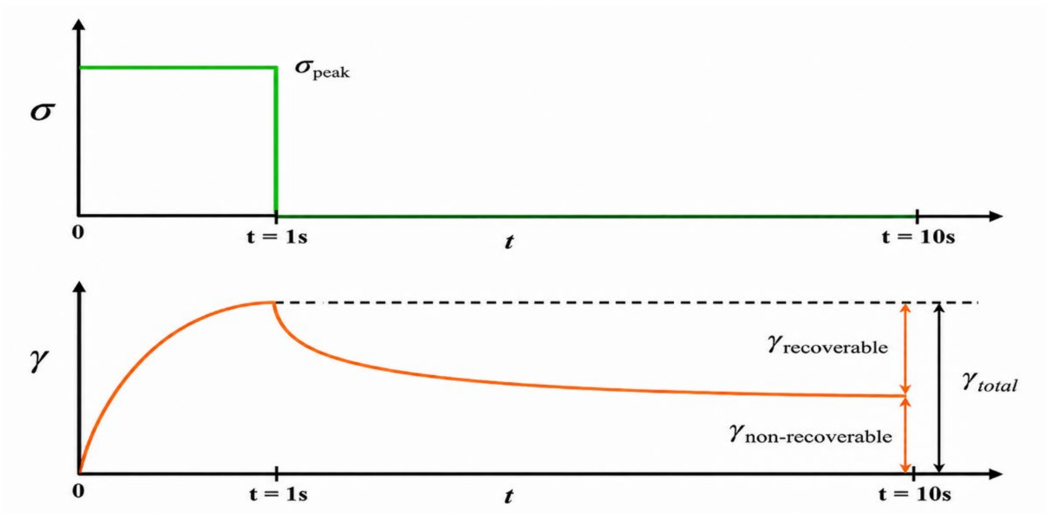

FIGURE 3.9: Strain Behavior During MSCR Testing

$$\%R = \frac{\varepsilon_{recoverable}}{\varepsilon_{total}} \cdot 100 \ \ (\%) \qquad \text{Eqn.3}$$

$$J_{nr} = \frac{\varepsilon_{non-recoverable}}{\sigma_0} \qquad (1/\text{kPa}) \qquad \text{Eqn. 4}$$

In this study, the MSCR test was performed on the tack coat residue at 50°C. 4 replicate samples were tested in this study, and the results are shown in FIGURE 3.10. FIGURE 3.10 presents the MSCR test results of all tack coats in terms of percent recovery (%R) and non-recoverable creep compliance (J_{nr}) at 0.1 and 3.2 kPa stress levels. For the SS-1H tack coat (FIGURES 3.10a and 3.10b), the replicate results are closely grouped, indicating good repeatability. The average % recovery decreases from 38.11% at 0.1 kPa to 25.23% at 3.2 kPa, while the corresponding J_{nr}

values increase from 0.34 to 0.45 kPa⁻¹, reflecting reduced elastic response and increased susceptibility to permanent deformation at higher stress levels. A similar trend is observed for the SS-1HP tack coat (FIGURES 3.10c and 3.10d), where higher % recovery values of 56.05% and 36.48% are obtained at 0.1 and 3.2 kPa, respectively, along with lower Jnr values of 0.25 and 0.39 kPa⁻¹, indicating improved elastic behavior compared to SS-1H.

In contrast, the CSS-1H tack coat (FIGURES 3.10e and 3.10f) exhibits significantly lower % recovery values of 21.81% and 8.11% and higher J_{nr} values of 0.56 and 0.62 kPa⁻¹ at 0.1 and 3.2 kPa, respectively, indicating a predominantly viscous response and poor resistance to permanent deformation. The trackless tack coat (FIGURES 9g and 9h) demonstrates the best overall performance, with the highest % recovery values of 87.76% and 65.42% and the lowest J_{nr} values of 0.13 and 0.27 kPa⁻¹ at the respective stress levels. Overall, all materials show consistent replicate behavior, and the results (Tables 3.4 and 3.5) clearly indicate that the trackless tack coat provides superior elastic recovery and lower non-recoverable creep compliance, followed by SS-1HP, SS-1H, and CSS-1H.

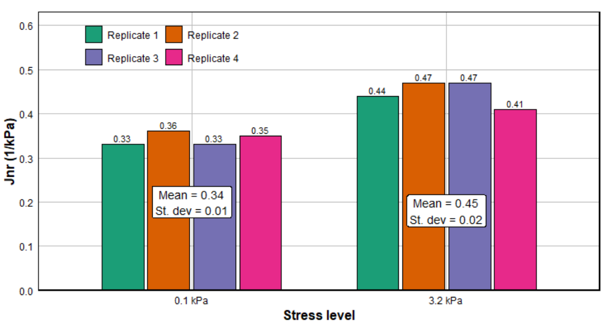

(a) SS-1H J_{nr}

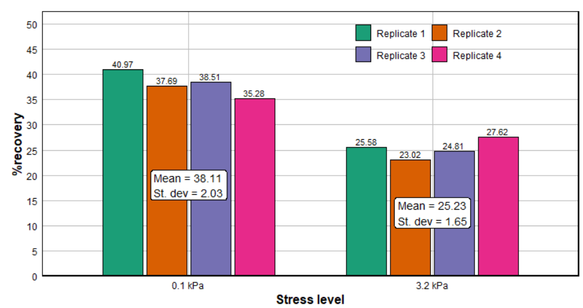

(b) SS-1H %R

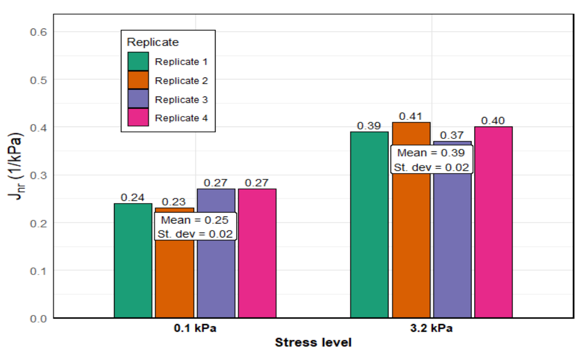

(c) SS-1HP J_{nr}

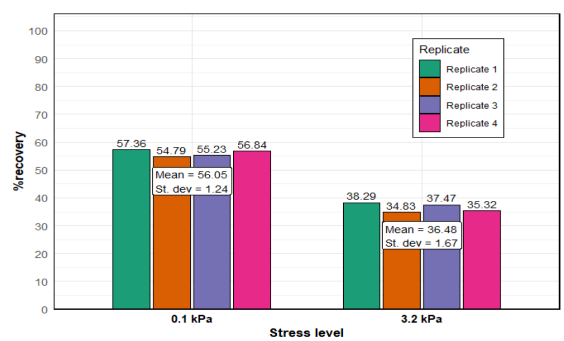

(d) SS-1HP %R

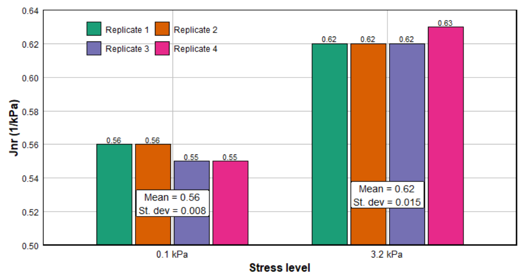

(e) CSS-1H J_{nr}

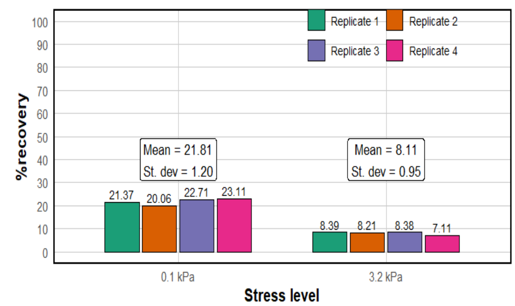

(f) CSS-1H %R

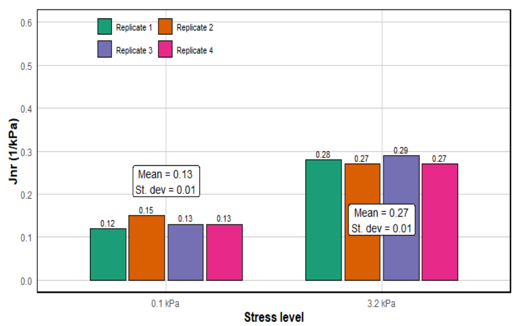

(g) Trackless tack J_{nr}

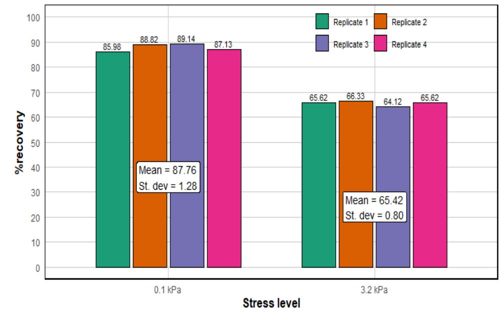

(h) Trackless tack *%R*

FIGURE 3.10: MSCR Test Results

TABLE 3.4: MSCR Summary

MSCR	SS-1H Tack	SS-1HP Tack	CSS-1H Tack	Trackless Tack
% *R* at 0.1, 3.2 kPa	38, 25	56, 36	21, 8	87, 65`
J_{nr} at 0.1, 3.2 kPa	0.34, 0.45	0.25, 0.39	0.56, 0.62	0.13, 0.27

TABLE 3.5: Significance among different tack coats

Tack Coat	%*R* at 0.1 kPa	%*R* at 3.2 kPa	J_{nr} at 0.1 kPa	J_{nr} at 3.2 kPa
SS-1H	38.11	25.23	0.34	0.45
SS-1HP	56.05	36.48	0.25	0.39
CSS-1H	21.81	8.11	0.56	0.62
Trackless	87.86	65.42	0.13	0.27
$P < 0.05$	**Yes**	**Yes**	**Yes**	**Yes**

3.2 Double Layer AC Sample Preparation

Double-layer AC specimens were prepared for the interface shear tests. The samples were prepared using a Superpave gyratory compactor (as shown in FIGURE 3.11).

FIGURE 3.11 Superpave Gyratory Compactor

The interface between the two layers was located at the mid-height of the specimen. This configuration allowed the shear load to act directly along the interface during testing. In this study, a laboratory-produced AC mixture was used to create AC specimens with two layers. As shown in FIGURE 3.12, an SP-IV aggregate gradation was used to prepare the AC mixture. The binder's grade is PG 64-22. The asphalt content and the desired air void are, respectively, 6.5% and 7 ± 0.3 %.

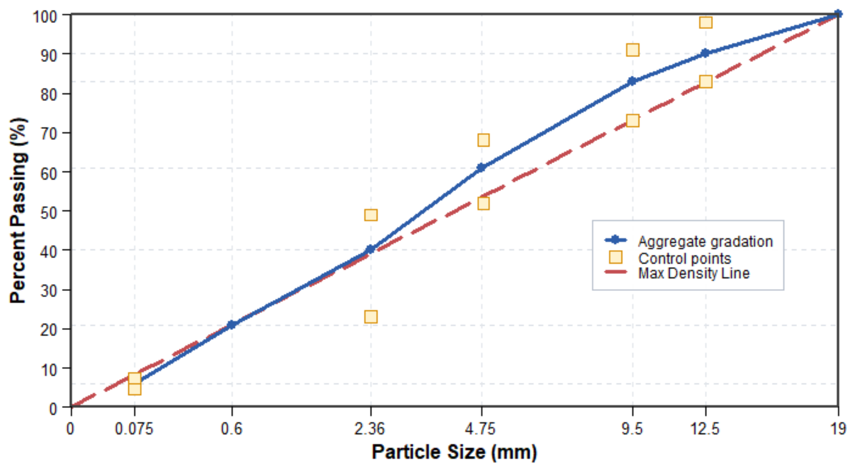

FIGURE 3.12: Aggregate gradation

This study has prepared double-layered asphalt concrete (AC) specimens using a Superpave gyratory compactor. The procedure consists of three main steps: compaction of the bottom layer, application and curing of the tack coat, and compaction of the top layer (see FIGURE 3.13).

A preliminary step is also carried out for each layer to determine the mass of loose mix required to achieve the target height and design air void level.

First, the loose mix is compacted in the Superpave gyratory compactor to form a cylindrical specimen with a height of 75 mm and a diameter of 150 mm at the design air void level. After compaction, the specimen is removed from the mold and allowed to cool for at least 24 hours. Because the diameter of the compacted specimen becomes slightly larger than the mold diameter, the sides of the specimen are sanded so that it can be reinserted into the mold. A belt sander is used for this step, and a paintbrush removes sanding dust from the specimen surface.

Next, the required quantity of tack coat is measured and applied evenly on the top surface of the bottom layer using a paintbrush. The amount is calculated from the specimen surface area, the residual asphalt content of the tack coat, and the planned application rate. The tack coat is applied only when the ambient temperature is above 15.5°C, which is the minimum recommended application temperature. After application, the specimen is cured until the coating changes from brown to black, indicating that the emulsion has broken and set.

Meanwhile, the loose mix for the top layer is conditioned in the oven at compaction temperature for two hours. The bottom specimen is then reinserted into the mold with the tack-coated surface facing upward. The conditioned loose mix is placed on top in a quantity sufficient to produce a 75 mm thick layer at the design air void level. Finally, the compaction mold is placed in the gyratory compactor to produce the combined double-layer specimen at the desired total height.

The compacted double-layer specimen is removed from the mold and left to cool at room temperature for at least 24 hours. The prepared specimens are then available for further conditioning or direct shear testing.

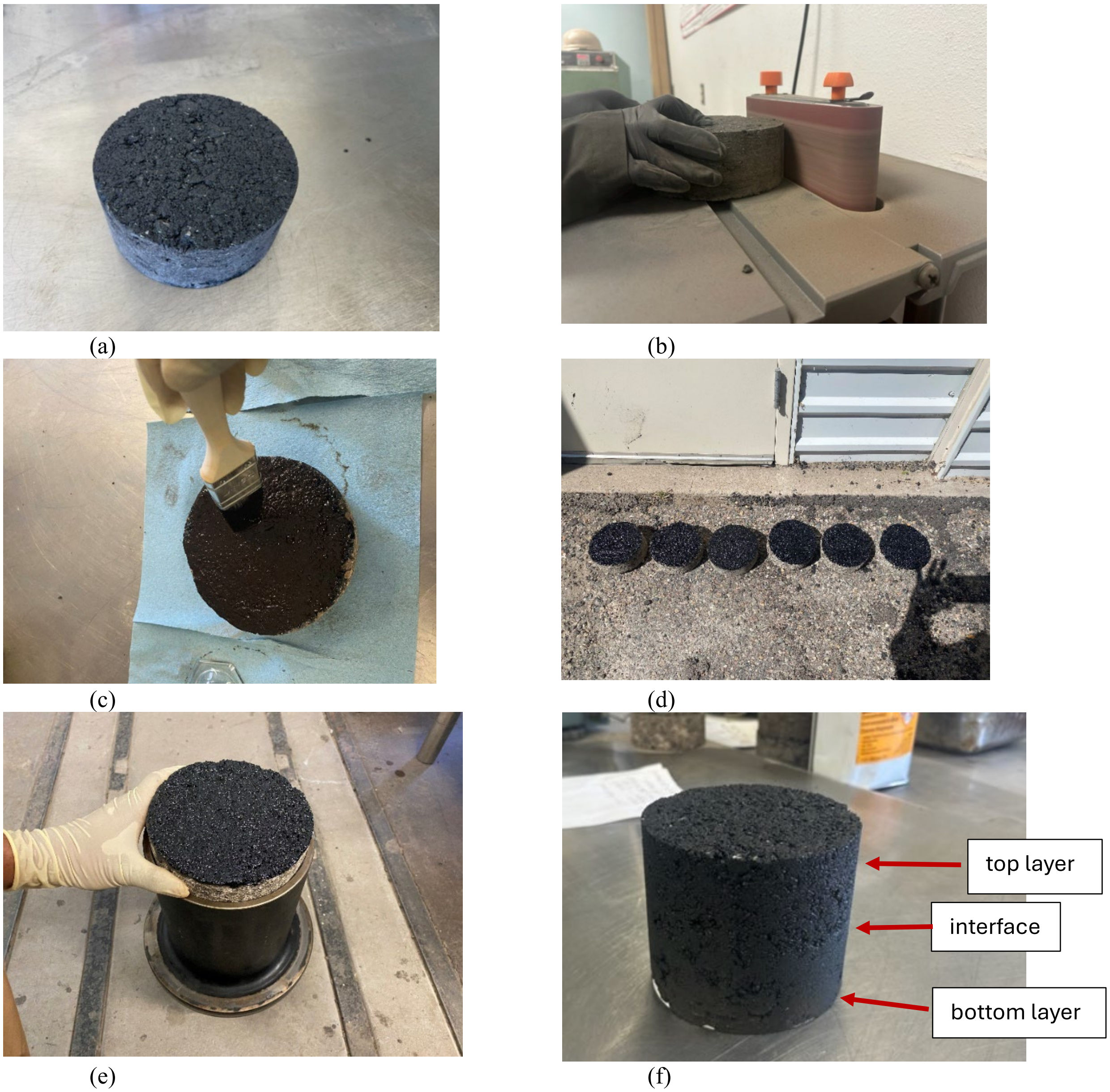

FIGURE 3.13: Preparation of Double-Layered AC Specimen Using Gyratory Compactor: (a) Bottom Layer; (b) Sanding the Bottom Layer's Peripheral Side; (c) Tack Coat Apply with a Paintbrush; (d) Tack Coat Curing; (e) Placing the Bottom Layer into the Mold; and (f) The Double-Layered Specimen

3.3 Experimental Program

The experimental program examines variables that can be controlled during pavement construction. These variables include tack coat type, application rate, surface condition, and curing time. Laboratory testing was conducted using layered asphalt specimens prepared under controlled conditions. Direct shear testing was used to measure the resistance of the interface to horizontal shear loading. The results provide information on how construction-related parameters influence the development of interlayer bonding. Variables related to environmental effects, such as moisture, temperature, including surface texture, loading rate, and applied normal stress, are examined in a later chapter.

Four tack coat materials were evaluated in this study. Different application rates were also examined. Application rate determines the amount of residual asphalt present between asphalt layers. A low application rate may not provide sufficient binder to develop adequate bonding. A high application rate may create a slip plane between layers. After application, the emulsified tack coat requires time to break and develop adhesive properties. The curing period may influence the bond formed between the asphalt layers.

3.4 Direct Shear Test

Laboratory investigations provide a practical method for examining the influence of tack coat parameters on bonding performance. Laboratory testing allows variables to be controlled during specimen preparation and testing. This approach makes it possible to evaluate the influence of individual parameters under defined conditions. It also helps identify the conditions that produce adequate bonding between asphalt layers.

The literature shows that there is no widely accepted laboratory procedure for evaluating interlayer bonding in asphalt pavements. Several experimental methods have been proposed to investigate interfacial delamination. These methods include direct shear tests, torsional tests, and tensile pull-off tests. Each method provides useful information about bond performance. However, the test configurations often differ. Differences in specimen geometry, loading conditions, and testing procedures make direct comparison of results difficult. A consistent experimental approach is therefore needed to better understand the factors that control interlayer bond behavior. Direct shear testing has gained preference because it is straightforward, easy to interpret, and sensitive to changes in tack coat type, application rate, and test conditions. Research across multiple states has shown that shear testing clearly distinguishes the effects of materials, application rates, and conditioning factors.

Direct shear tests rarely produce equal results under similar settings. Even if experimentalists are trying to standardize methods, random errors still happen. Some variables can't be fully controlled; thus, analysts have to take into consideration the accepted differences in how data is interpreted. Inter-laboratory comparisons are useful for checking the general uniformity and accuracy of tests. When one technician does repeated tests in the same facility, repeatability is required to check for uniformity. This statistic shows how accurate a laboratory is within itself, which is usually measured by combining the variance or the root mean square. Reproducibility looks at discrepancies between facilities that use different experimentalists and the same specimens. Strong repeatability means that repeated measurements will be quite similar to each other. Inter-laboratory results, on the other hand, can have wider ranges. Standard deviation is the main measure for both; however, the coefficient of variation (COV) can be used in some cases. According to NCHRP Report 712, a COV of less than 10% means that the measurement is accurate enough.

Outliers are values that are very different from the rest of the group. They can be thrown out if an experimentalist can show that there are problems with the process. If tests go wrong, they need to be retested. However, unfavorable data must persist unless proven invalid. Statistical consistency tests and other tools can help to find unusual results in an objective way.

The tests were conducted using a Geotechnical Consulting and Testing System (GCTS) servo-hydraulic testing machine SDS-150 (FIGURE 3.14). The system features automated electro-hydraulic closed-loop digital servo control of the shear and normal loads. The normal and shear displacements are measured by a linear variable differential transducer (LVDT). Experimental data, including normal and shear stresses, shear displacement, and normal displacement, are acquired automatically by the data collection software.

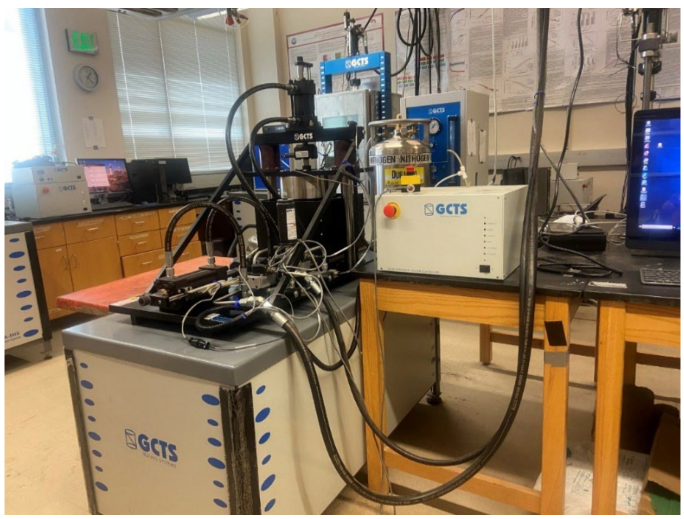

FIGURE 3.14: GCTS SDS-150 closed-loop servo-controlled direct shear machine

The direct shear test was done as shown in FIGURE 3.15 to determine the interface shear strength of the tested specimens. FIGURE 3.15a shows the shear actuator, the normal actuator, and the sample chamber. FIGURE 3.15b shows a tested specimen after failure. The sample failed at the interface, and the shear load direction is also shown in FIGURE 3.15b.

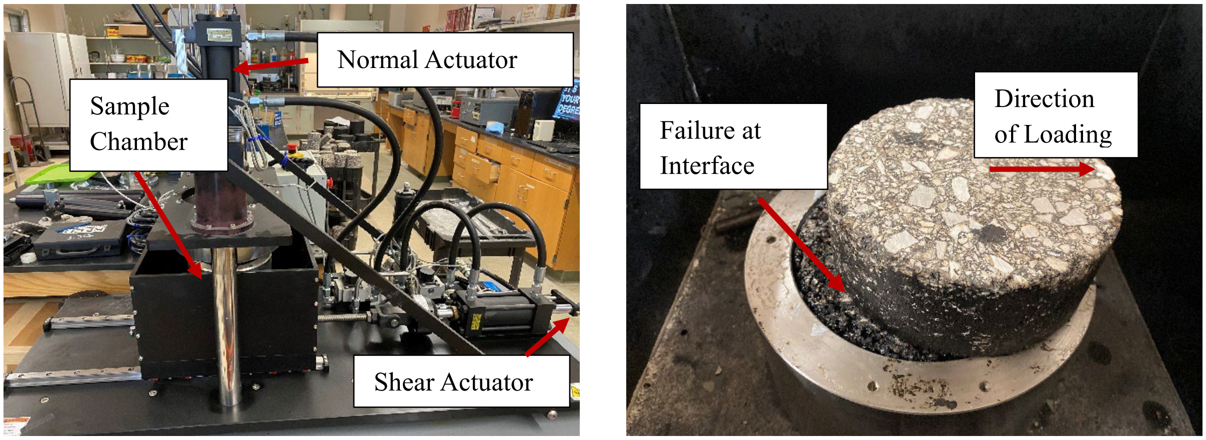

(a) (b)

FIGURE 3.15: Direct shear test setup

3.5 Determination of Curing Time

The curing time of emulsified asphalt is crucial for achieving the desired performance and durability of the pavement. In the field, the curing time of emulsified asphalt is influenced by various factors, such as the action of rolling equipment, traffic, temperature, humidity, and wind (Estakhri, Saylak et al. 1991). Wind speed can accelerate the curing process, resulting in shorter curing times compared to laboratory conditions (Estakhri, Saylak et al. 1991). The curing process of emulsified asphalt involves the evaporation of water from the emulsion. Evaporation is the transformation of liquid water into a gaseous state and its diffusion into the atmosphere (Li 2016).

The saturation vapor pressure, which represents the maximum amount of water vapor that a given volume of air can carry, can be calculated using Boyle's law (Banerjee, Prozzi et al. 2010):

$$e_s = 0.6108 * e^{\frac{T+17.27}{T+237.3}}$$ Eqn.
5

e_S = saturation vapor pressure in psi, and

T = ambient temperature in ºF.

To accurately quantify and predict evaporative behavior, it is essential to understand the concept of the vapor pressure deficit (VPD).

VPD is influenced by various environmental factors, including temperature, relative humidity, and atmospheric pressure. As temperature increases, the saturation vapor pressure rises, potentially increasing the VPD if the ambient vapor pressure remains constant. Conversely, an increase in relative humidity leads to a higher ambient vapor pressure, reducing the VPD and consequently the evaporative potential. The VPD represents the difference between the saturation vapor pressure and the ambient vapor pressure. The saturation vapor pressure is the maximum amount of water vapor that the air can hold at a given temperature, while the ambient vapor pressure is the actual amount of water vapor present in the air (Banerjee, Prozzi et al. 2010).

$$VPD = e_s * (1 - \frac{RH}{100}) \quad \text{Eqn.6}$$

Where,

VPD = vapor pressure deficit, and

RH = relative humidity (%)

Meyer's empirical formula has shown a positive correlation between wind speed and evaporation (Banerjee 2012). Therefore, to understand the combined effect of wind speed and VPD, this study conducted a variable transformation, which is a common advanced statistical approach. This study has multiplied wind speed and VPD.

Before investigating the effect of curing time on shear strength, the curing time or time for complete evaporation of water from the tack coat emulsion (without any additional heating) was determined. To do that, this study monitored the change in water content with time from a thin layer of tack coat filed in a metal pan placed under the natural sun. First, the weight of a flat metal pan was measured. Next, about 20 g of asphalt emulsion was poured into the pan and spread over the pan (FIGURE 3.16a). The color of the emulsion at this time was brown. The total weight was measured. After that, the pan with the emulsion was kept in the sun to evaporate the water, as illustrated in FIGURE 3.16b. During this time, their weight was measured at designated intervals, and this continued until the weight did not change with time. FIGURE 3.16c shows the final status of the emulsion after complete evaporation of water. It can be seen that the color of the emulsion became black, and there are several break lines across the specimen.

(a) Initial status (b) Under the sun (c) Final status

FIGURE 3.16: Steps associated with determining curing time

3.5.1 Curing Time of CSS-1H

FIGURE 16 presents the evaporation status at different times. It can be seen that the evaporation initially increases rapidly with time, followed by a phase where the evaporation slowly increases with time. It can also be observed that after 100 minutes, the evaporation becomes stable. This indicates that after 100 minutes, naturally possible evaporation was completed. Thus, it can be said that the curing time of CSS-1H tack emulsion is 100 minutes.

The behavior as shown in FIGURE 3.17 can also be represented as an exponential function, as presented in Eq. 7.

$$E = 98.85 * (1 - e^{-0.07785*t}) \qquad \text{Eq. 7}$$

Where: *E* is the percentage of material (water) evaporated from the emulsion, and *t* represents the time in minutes.

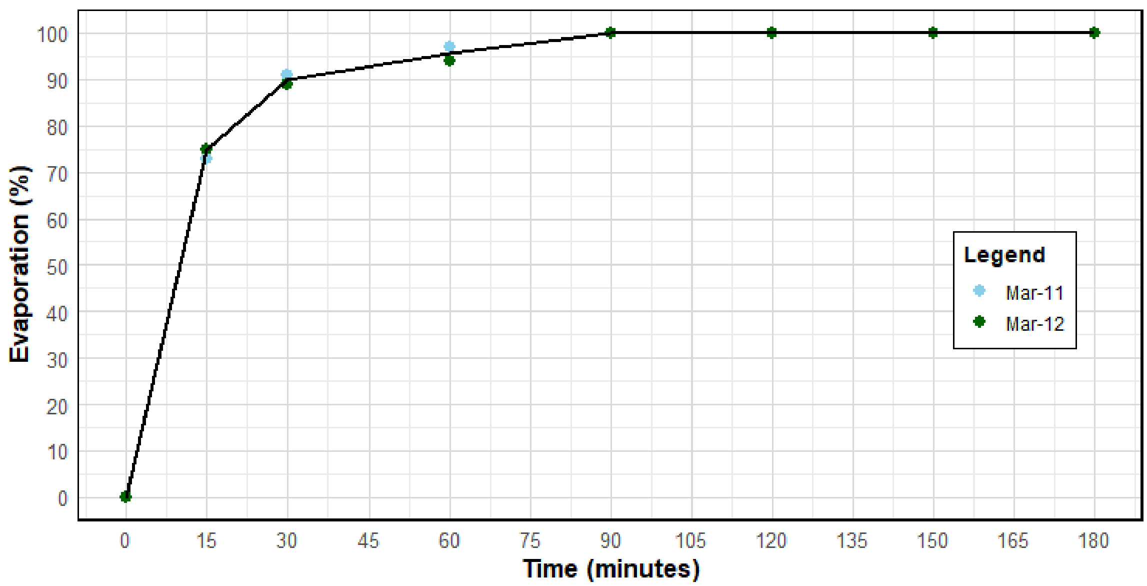

FIGURE 3.17: Determination of curing time of CSS-1H

TABLE 3.6 presents meteorological data from the National Weather Service database of Albuquerque International Airport (the nearest station to the place of test samples) and derived parameters that influence evaporation rates for three different dates. More data from different days of different months are needed to reach a concrete conclusion. The key parameters included are temperature, wind speed, relative humidity, saturation vapor pressure (SVP), vapor pressure deficit (VPD), and a combined factor of wind speed and VPD. Additionally, the TABLE includes a column for evaporation percentage, which likely represents the relationship between VPD and evaporation rate.

TABLE 3.6: Evaporation rates and influencing meteorological factors

Date	Temperature (°F)	Wind Speed (mph)	Relative humidity (%)	SVP (psi)	VPD (psi)	Wind speed* VPD	Evaporation (%) at 100 minutes
Mar-11	50	5	24	0.258	0.120	0.59	100
Mar-12	52	5	29	0.181	0.130	0.65	100

3.5.2 Curing Time of SS-1H

For SS-1H, the same days of CSS-1H were chosen. TABLE 3.7 presents meteorological data for SS-1H.

TABLE 3.7: Evaporation rates and influencing meteorological factors

Date	Temperature (°F)	Wind Speed (mph)	Relative humidity (%)	SVP (psi)	VPD (psi)	Wind speed* VPD	Evaporation (%) at 120 minutes
Mar-11	50	5	24	0.258	0.120	0.59	100
Mar-12	52	5	29	0.181	0.130	0.65	100

The behavior as shown in FIGURE 3.18 can also be represented as an exponential function, as presented in Eq. 8.

$$E\ (\%) \approx 38.76 * \left[1 - \exp\left(-\frac{t}{14.96}\right)\right] \qquad \text{Eqn.8}$$

Where: *E* is the percentage of material (water) evaporated from the emulsion, and *t* represents the time in minutes.

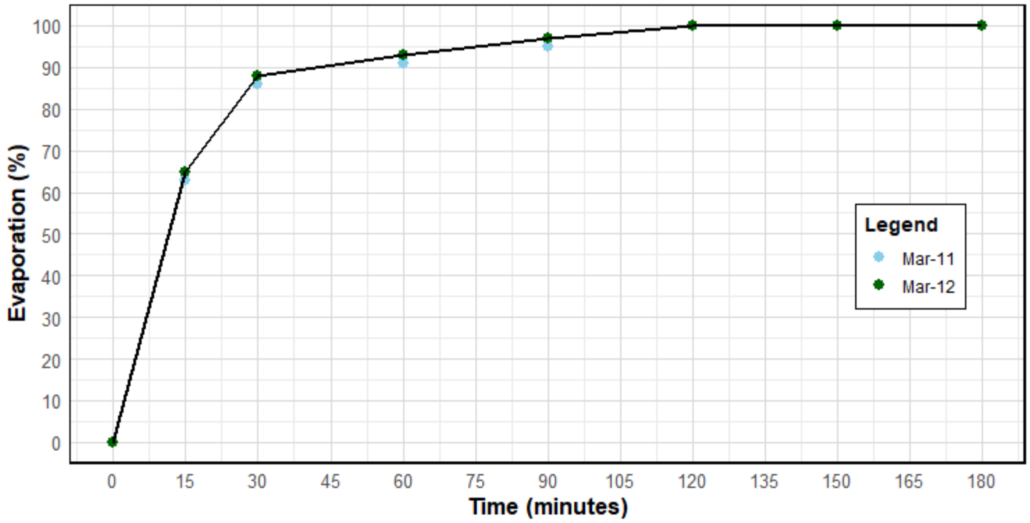

FIGURE 3.18: Determination of curing time of SS-1H

3.5.3 *Curing Time Determination of SS-1HP*

TABLE 3.8 presents meteorological data for SS-1HP.

TABLE 3.8: Evaporation Rates and Influencing Meteorological Factors

Date	**Temperature (°F)**	**Wind Speed (mph)**	**Relative humidity (%)**	**SVP (psi)**	**VPD (psi)**	**Wind speed* VPD**	**Evaporation (%) at 40 min**
Aug-17	82	6	28	0.099	0.072	0.43	100
Aug-18	79	8	44	0.098	0.055	0.44	100
Aug-22	80	3	29	0.099	0.070	0.21	100
Aug-30	77	3	43	0.098	0.056	0.17	100

A nonlinear logistic model was fitted to the data, and the estimated parameters along with their statistical metrics are presented in TABLE 3.9.

TABLE 3.9: Nonlinear Logistic Model Parameter

Parameter	Estimate	Std. Error	t value	Pr(>|t|)
a	100.25	3.13	32.07	5.64e-06
b	0.153	0.021	7.22	0.001951
c	16.23	1.31	12.35	0.000247

**Number of iterations to convergence: 8*

The fitted model is shown in Eq. 9:

$$E\ (\%)\ \approx\ \frac{100.25}{1 + \exp\left(-0.153 \cdot (T - 16.23)\right)} \qquad \text{Eq. 9}$$

Where: E is the percentage of material (water) evaporated from the emulsion, and T represents the time in minutes.

FIGURE 3.19 shows evaporation vs. time for the four dates when the curing time determination test was conducted.

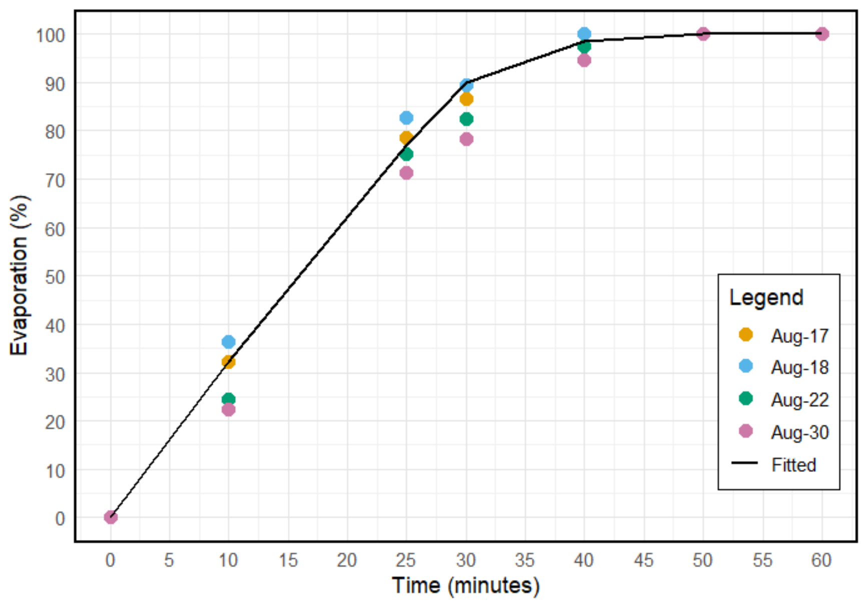

FIGURE 3.19: Determination of Curing Time of SS-1HP

3.5.4 Curing Time Determination of Trackless Tack

TABLE 3.10 presents meteorological data for trackless tack.

TABLE 3.10: Evaporation Rates and Influencing Meteorological Factors

Date	**Temperature (°F)**	**Wind Speed (mph)**	**Relative humidity (%)**	**SVP (psi)**	**VPD (psi)**	**Wind speed* VPD**	**Evaporation (%) at 0.5 hr**
May-25	78	9	8	0.0978	0.089	0.81	100
May-28	80	13	18	0.0982	0.078	1.05	100
June-01	77	8	30	0.0975	0.068	0.55	100
June-03	78	7	29	0.0978	0.070	0.49	100

A nonlinear logistic model was fitted to the data, and the estimated parameters along with their statistical metrics are presented in TABLE 3.11.

TABLE 3.11: Nonlinear Logistic Model Parameter

Parameter	**Estimate**	**Std. Error**	**t value**	**Pr(>|t|)**
a	96.97362	5.86065	16.547	7.81E-05
b	0.26988	0.07726	3.493	0.02505
c	7.09752	1.18087	6.01	0.00386

**Number of iterations to convergence: 13*

The fitted model is shown in Eq. 10:

$$E\ (\%) \approx \frac{96.97362}{1 + \exp\big(-0.26988 \cdot (T - 7.09752)\big)} \qquad \text{Eq.10}$$

Where: E is the percentage of material (water) evaporated from the emulsion, and T represents the time in minutes.

FIGURE 3.20 shows evaporation vs time for the four dates when the curing time determination test was conducted.

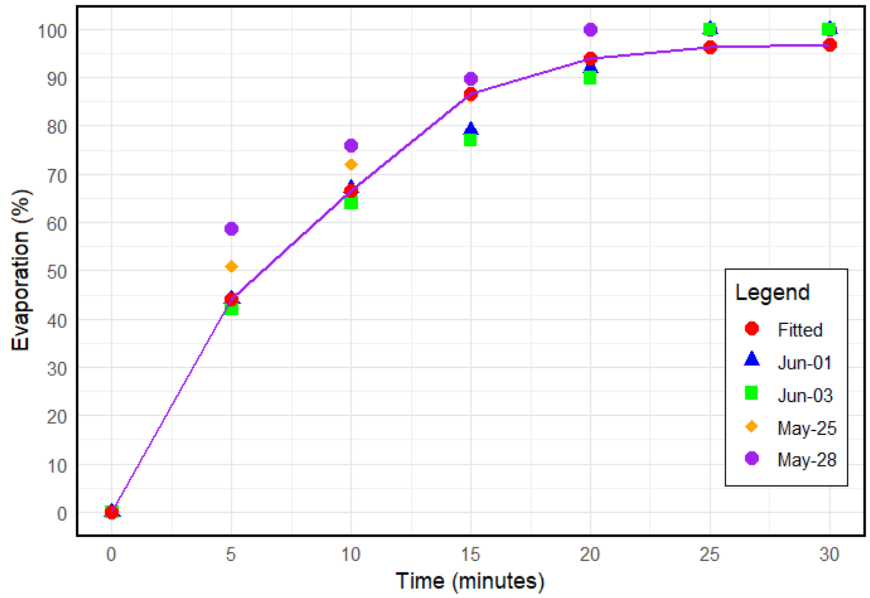

FIGURE 3.20: Determination of Curing Time of Trackless Tack

3.6 Effect of Curing Time

To investigate the effect of curing time, laboratory-produced double-layered specimens were used. The application rate was selected as 0.08 gal/yd^2. The specimens were produced at different curing times. The effect of curing time on the interface shear strength has been discussed below.

3.6.1 Curing Effect on Trackless Tack

The specimens were produced at four different curing times: 0 (no curing), 15 min, 25 min, and 30 min. FIGURE 3.21 shows the status of the interface at different curing times. It can be observed that the interface looks completely wet at 0 minutes, and it still looks slightly wet at 15 minutes. However, at 25 minutes and 30 minutes, it becomes dry.

FIGURE 3.21(a) - 3.21(d) shows that the average shear strength for the specimens prepared with no curing time is 201.21 psi. On the other hand, the average shear strengths of specimens prepared with 15 min, 25 min, and 30 min are 289.74, 303.64, and 301.58 psi, respectively.

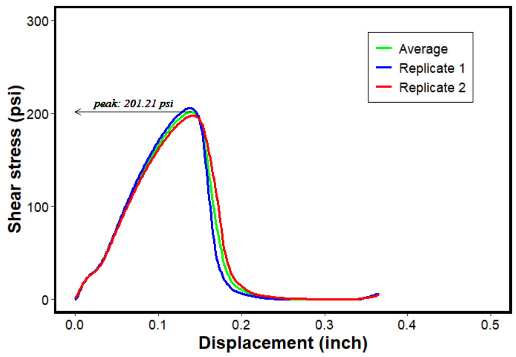

(a) No curing (0 min)

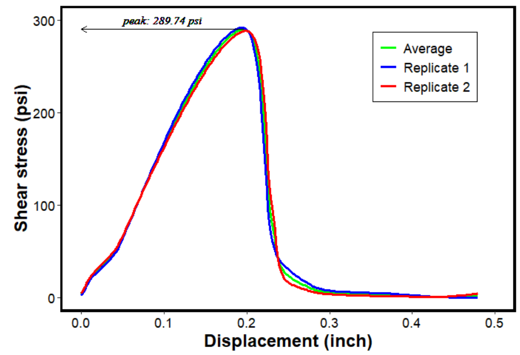

(b) 15 min

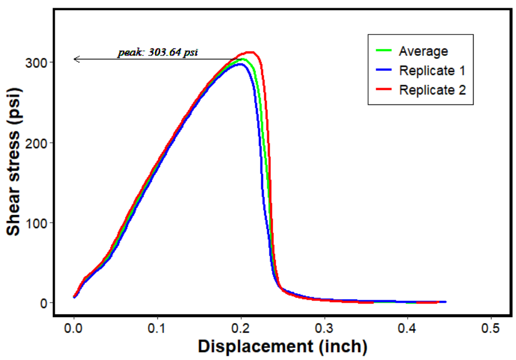

(c) 25 min

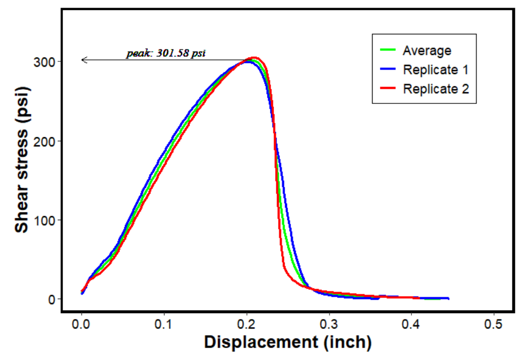

(d) 30 min

FIGURE 3.21: Direct Shear Test Results for Different Curing Times of Trackless Tack

FIGURE 3.22 shows the relationship between shear strength (psi) and percentage of evaporation.

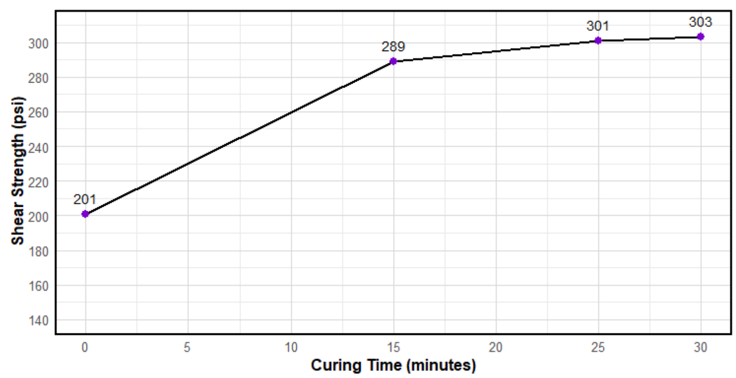

FIGURE 3.22: Relationship between Shear Strength and Curing Time of Trackless Tack

3.6.2 *Curing Effect on SS-1HP*

FIGURE 3.23 (a) - 3.23 (d) shows that the average shear strength for the specimens prepared with no curing time is 204.48 psi. The loading rate was 1.97 inches/min. On the other hand, the average shear strengths of specimens prepared with 10 min, 50 min, and 60 min are 231.29, 270.08, and 269.45 psi, respectively.

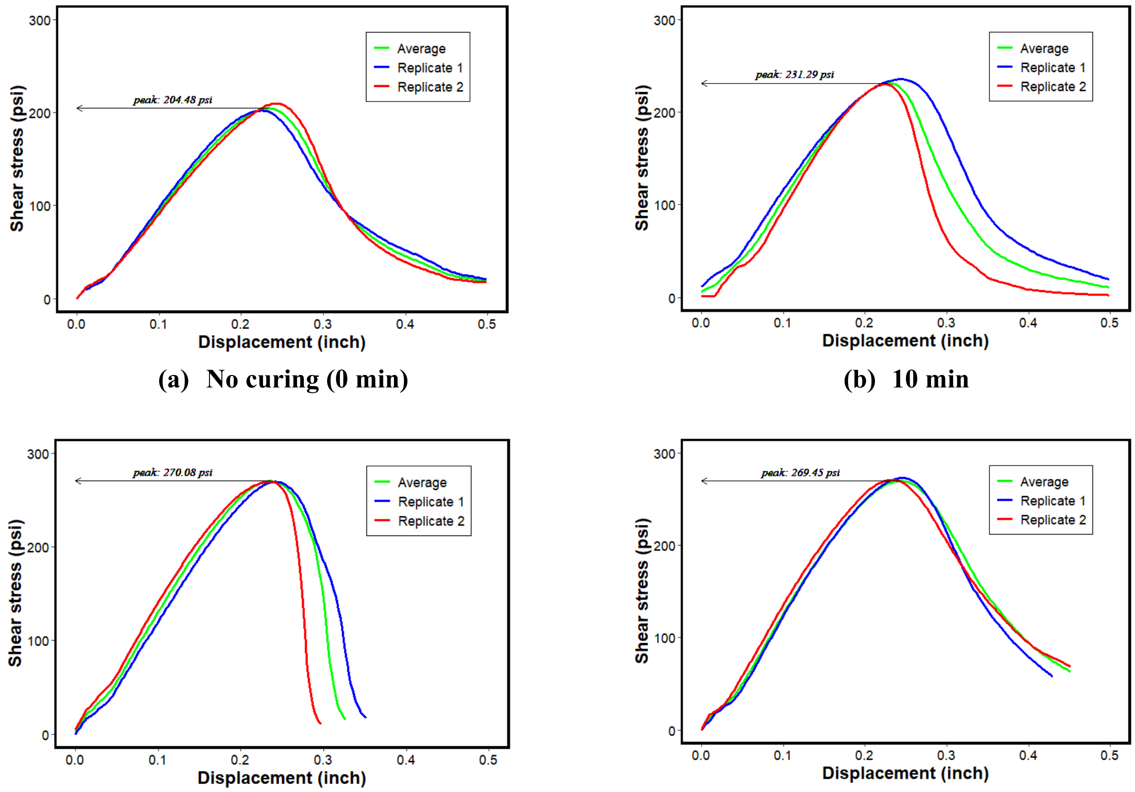

(a) No curing (0 min)

(b) 10 min

(c) 50 min

(d) 60 min

FIGURE 3.23: Direct Shear Test Results for Different Curing Times of SS-1HP

FIGURE 3.24 shows the relationship between shear strength (psi) and percentage of evaporation.

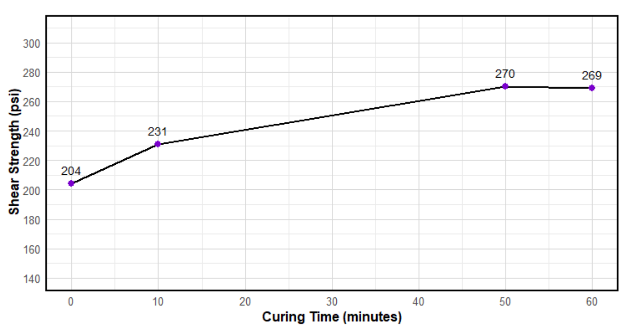

FIGURE 3.24: Relationship between Shear Strength and Curing Time of SS-1HP

3.6.3 Curing Effect on SS-1H

FIGURE 3.25 shows the results found from the direct shear test results for specimens prepared at different curing times. FIGURE 3.25 (a) shows the direct shear test results of two specimens prepared with no curing time. In both cases, the specimens failed at a lower stress level than the specimens prepared with some curing times, as shown in FIGURES 3.25 (b)- 3.25 (e). It can also be noticeable that the strength initially increases rapidly with an increment of curing time, but becomes asymptotic or reaches a plateau after 2 hrs. The average shear strength for the specimens prepared with no curing time is 173.19 psi. On the other hand, the average shear strengths of specimens prepared with 15 min, 30 min, 60 min, and 120 min are 196, 200.01, 215, and 218 psi, respectively. FIGURE 3.26 presents the relationship between shear strength and curing time.

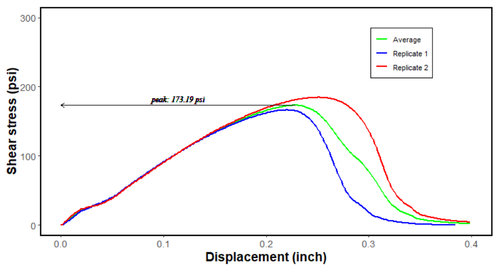

(a) No curing

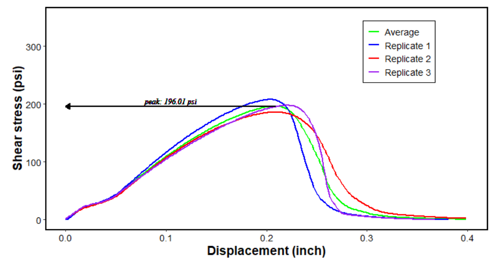

(b) 15 minutes

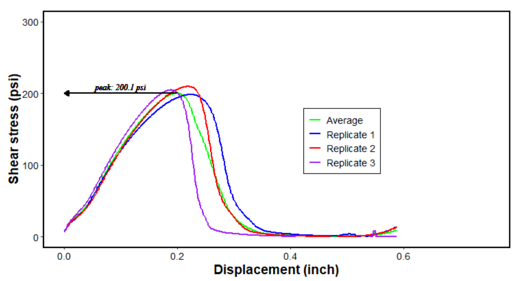

(c) 30 minutes

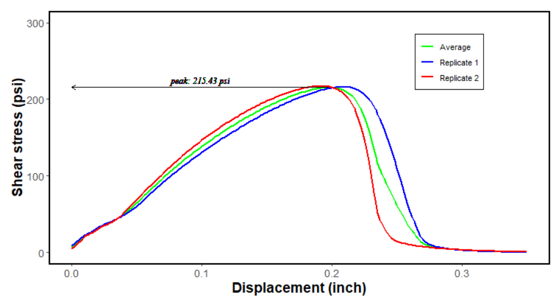

(d) 60 minutes

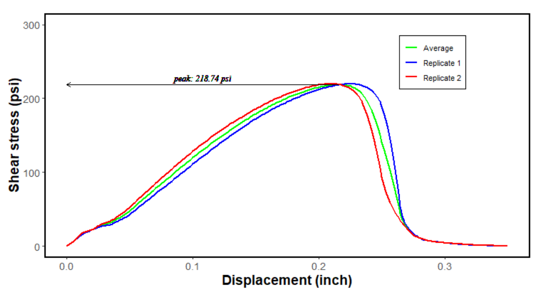

(e) 120 minutes

FIGURE 3.25: Direct shear test results for different curing times of SS-1H

FIGURE 3.26 presents the relationship between shear strength and percentage of material (water) evaporated from the emulsion. It can be observed that shear strength linearly increases as the evaporation increases. This relationship indicates that the highest shear strength can only be achieved if the tack coat is fully cured, or in other words, all water needs to be evaporated from the emulsion to get the maximum bonding.

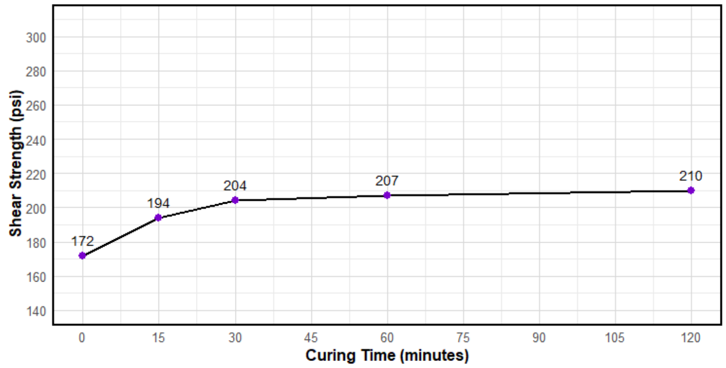

FIGURE 3.26: Relationship between Shear Strength and Curing Time of SS-1H

3.6.4 Curing Effect on CSS-1H

FIGURE 3.27 shows the results found from the direct shear test results for specimens prepared at different curing times. FIGURE 3.27(a) shows the direct shear test results of two specimens prepared with no curing time. In both cases, the specimens failed at a lower stress level than the specimens prepared with some curing times, as shown in FIGURES 3.27 (b)- 3.27 (e). It can also be noticeable that the strength initially increases rapidly with an increment of curing time, but becomes asymptotic or reaches a plateau after 2 hrs. The average shear strength for the specimens prepared with no curing time is 145 psi. On the other hand, the average shear strengths of specimens prepared with 15 min, 30 min, 60 min, and 120 min are 160, 180, 183, and 194 psi, respectively. FIGURE 3.28 presents the relationship between shear strength and curing time.

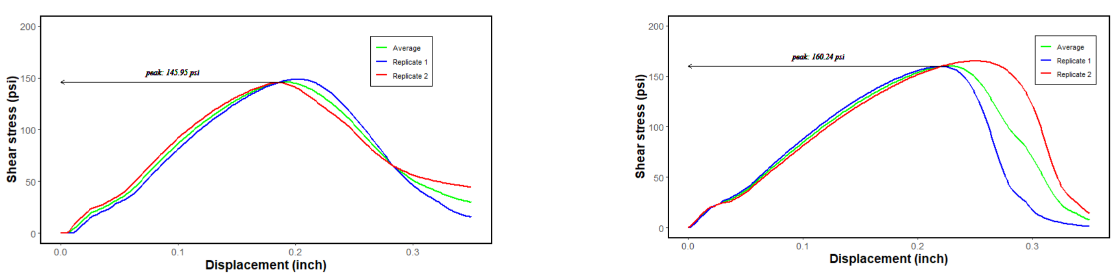

(a) No curing **(b) 15 minutes**

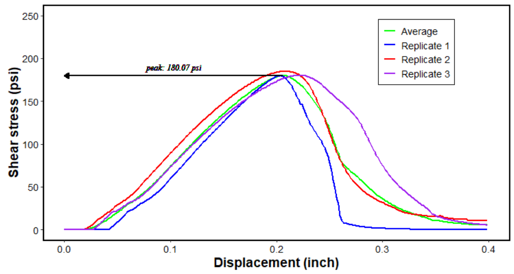

(c) 30 minutes

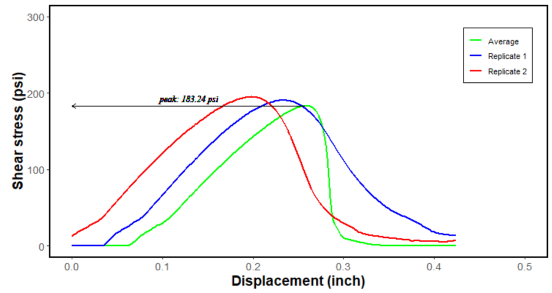

(d) 60 minutes

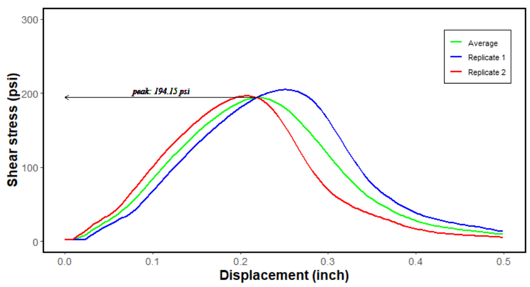

(e) 120 minutes

FIGURE 3.27: Direct shear test results for different curing times of CSS-1H

FIGURE 3.28 presents the relationship between shear strength and percentage of material (water) evaporated from the emulsion. It can be observed that shear strength linearly increases as the evaporation increases. This relationship indicates that the highest shear strength can only be achieved if the tack coat is fully cured, or in other words, all water needs to be evaporated from the emulsion to get the maximum bonding.

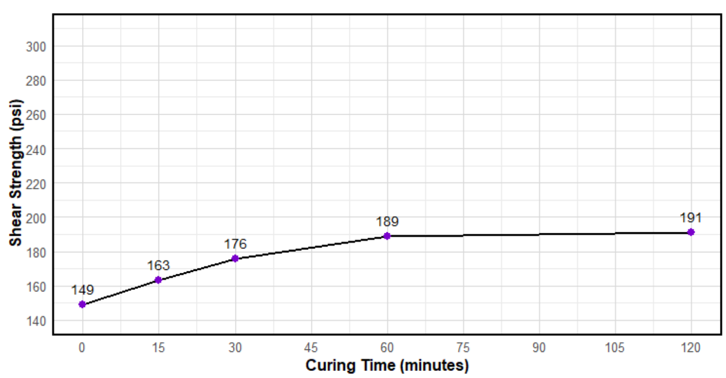

FIGURE 3.28: Relationship between Shear Strength and Curing Time of CSS-1H

3.7 Effect of Tack Coat Type and Application Rate

Differences in interface strength were observed among the evaluated materials. Conventional emulsified tack coats produced measurable bonding between asphalt layers. However, the magnitude of the interface shear strength varied among the materials. Polymer-modified tack coats generally produced higher interface strength than conventional emulsions. The modified binders showed greater resistance to shear displacement at the interface. The trackless tack coat also showed strong bonding performance. In several cases, the measured interface strength was comparable to or greater than that obtained with conventional emulsions. These results indicate that the rheological properties of the tack coat influence bonding behavior at the pavement interface.

The effect of tack coat application rate was examined as part of the experimental program. Application rate controls the amount of residual asphalt available at the interface. Several application rates were evaluated during testing. The objective was to determine how the amount of tack coat influences interface shear strength.

Low application rates produced relatively low interface strength. In these cases, the amount of binder present at the interface was limited. Increasing the application rate generally increased interface shear strength. An additional binder improved adhesion between the asphalt layers. However, excessive application rates did not always produce additional improvement. When the binder layer became too thick, the interface tended to behave as a slip plane under shear loading.

These observations suggest that an optimum application rate exists. Within this range, the tack coat provides sufficient adhesion without creating excessive lubrication between layers. The interface shear strength of different tack coat types at different application rates is discussed below.

3.7.1 Trackless Tack Application Rate Effect

This study prepared double-layered AC specimens at four different residual asphalt contents: 0 (no tack coat), 0.04, 0.06, 0.08, and 0.10 gal/yd^2 to evaluate the effect of tack coat application rate on the interfacial bond performance. After applying the tack coat, all specimens were cured under the natural sun for 0.5 hr.

FIGURE 28 shows the results found from the direct shear test results for tested specimens prepared with different amounts of tack coat emulsion. FIGURE 3.29(a) shows the direct shear test results of two specimens prepared with no tack coating. For both cases, there are two different phases in the load-displacement curves. In the first phase, the load initially increases as the displacement increases until it reaches a maximum value. This load increment is attributed to bonding between two layers due to adhesion from tack coating and interlocking from aggregate embedment. The maximum value of load is related to the bonding strength of the interface material. After reaching the peak point, the bonding between the interface materials starts to fail (second phase), when the load decreases rapidly as the displacement increases. Finally, the load becomes zero or negligible, which indicates the complete deterioration in interface bonding. It should be mentioned that the load-displacement curves of two replicate specimens are close to each other, which confirms the repeatability of the direct shear test. The average shear strength for the specimens prepared with no tack coat is 215.67 psi. Similarly, direct shear test results for specimens prepared with 0.04, 0.06, 0.08, and 0.10 gal/yd^2 tack coat are presented in FIGURES 3.29 (b)- 3.29 (e). The average shear strengths of specimens prepared with 0.04, 0.06, 0.08, and 0.10 gal/yd^2 tack coat are 241.54, 271.85, 290.92, and 298.02 psi, respectively. Therefore, it can be said that the interface shear strength increases for trackless tack coat with increasing application rates.

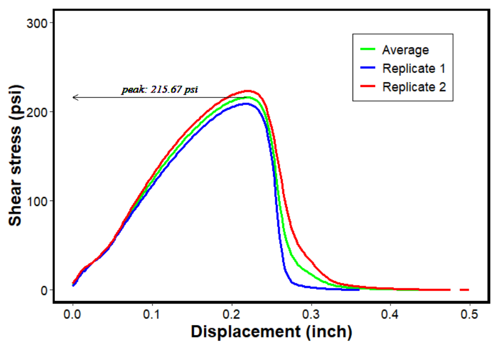

(a) No tack coat (0 gal/yd^2)

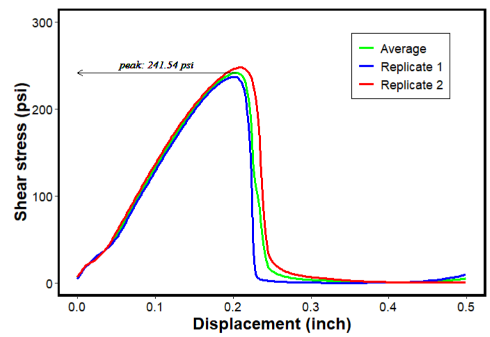

(b) 0.04 gal/yd^2

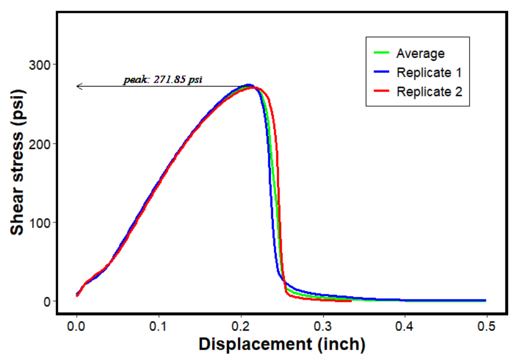

(c) 0.06 gal/yd^2

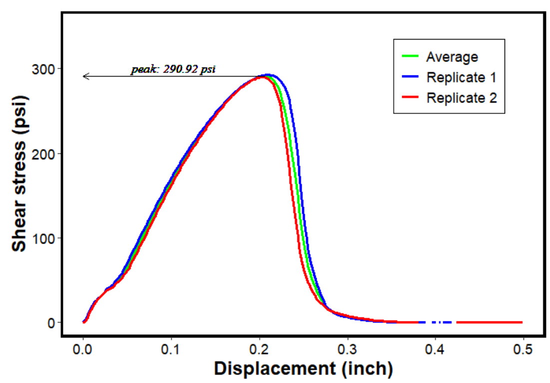

(d) 0.08 gal/yd^2

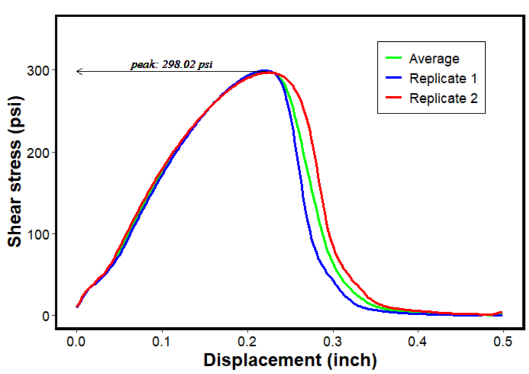

(e) 0.10 gal/yd^2

FIGURE 3.29: Direct Shear Test Results for Different Application Rates of Trackless Tack

FIGURE 3.30 shows the relationship between residual application rate and shear strength. It can be seen that the shear strength increases with increasing application rates.

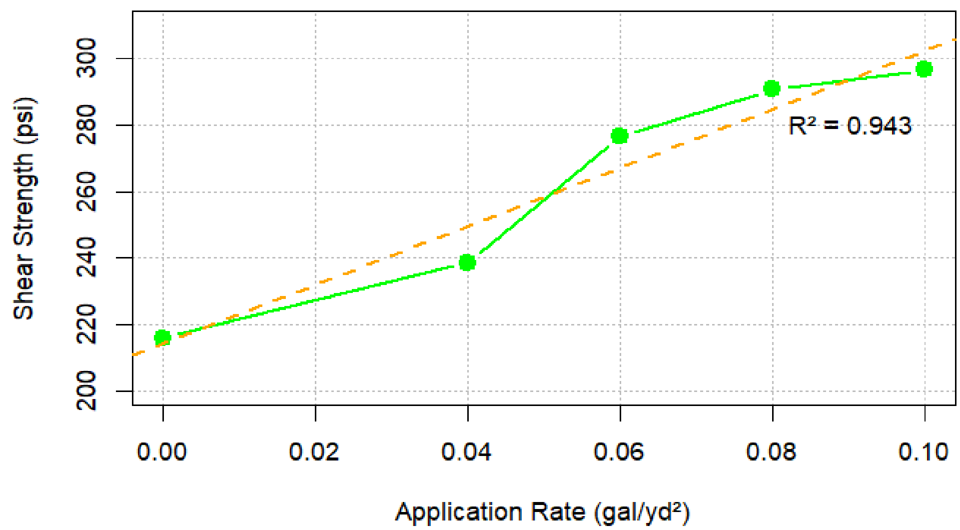

FIGURE 3.30: Shear Strength Versus Residual Application Rate Plot of Trackless Tack

3.7.2 SS-1HP Application Rate Effect

FIGURE 3.31 shows the results found from the direct shear test results for tested specimens prepared with different amounts of tack coat emulsion. FIGURE 3.31 (a) shows the direct shear test results of two specimens prepared with no tack coating. The average shear strength for the specimens prepared with no tack coat is 202.85 psi. Similarly, direct shear test results for specimens prepared with 0.04, 0.06, and 0.08 gal/yd^2 tack coat are presented in FIGURES 3.31 (b)- 3.31 (e). The average shear strengths of specimens prepared with 0.04, 0.06, and 0.08 gal/yd^2 tack coat are 264.22, 275.29, and 253.61 psi, respectively. Therefore, it can be said that the optimum application rate of SS-1HP is 0.06 gal/yd^2.

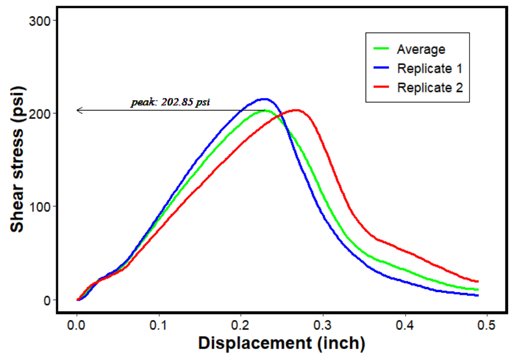

(a) No tack coat (0 gal/yd^2)

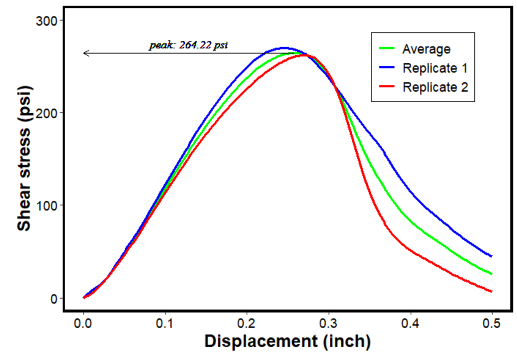

(b) 0.04 gal/yd^2

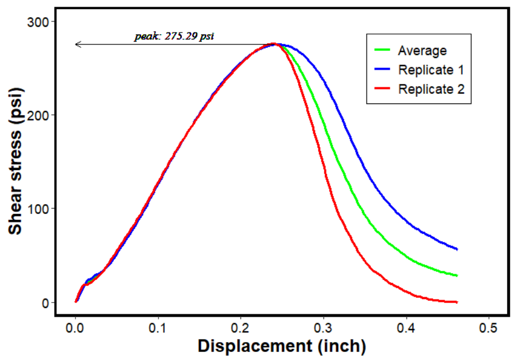

(c) 0.06 gal/yd^2

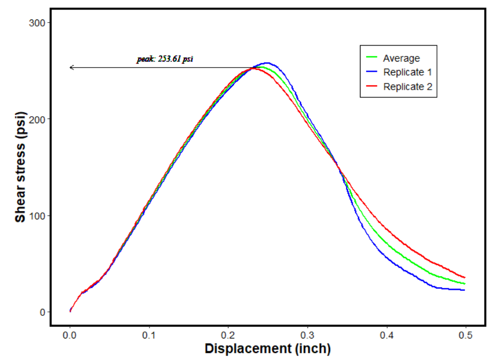

(d) 0.08 gal/yd^2

FIGURE 3.31 Direct Shear Test Results for Different Application Rates of SS-1HP

FIGURE 3.32 shows the relationship between residual application rate and shear strength. It can be seen that the shear strength increases with increasing application rates.

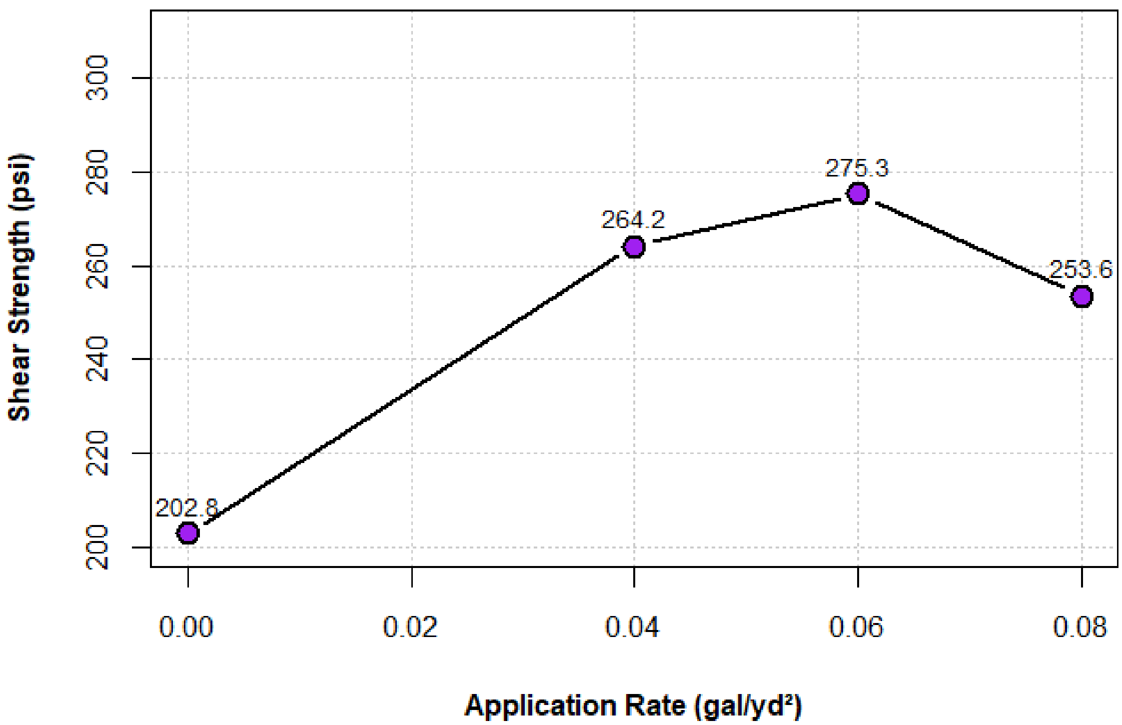

FIGURE 3.32 Shear Strength Versus Residual Application Rate Plot of SS-1HP

3.7.3 SS-1H Application Rate Effect

FIGURE 3.33 shows the results found from the direct shear test results for tested specimens prepared with different amounts of tack coat emulsion. FIGURE 3.33 (a) shows the direct shear test results of two specimens prepared with no tack coating. The average shear strength for the specimens prepared with no tack coat is 231 psi. Similarly, direct shear test results for specimens prepared with 0.04, 0.06, and 0.08 gal/yd^2 tack coat are presented in FIGURES 3.33 (b)- 3.33 (d). The average shear strengths of specimens prepared with 0.04, 0.06, and 0.08 gal/yd^2 tack coat are 252, 250, and 223 psi, respectively. Therefore, it can be said that the application of a lower amount of tack coat can increase the shear strength compared to not applying tack coat. But applying too much tack coat can decrease the shear strength.

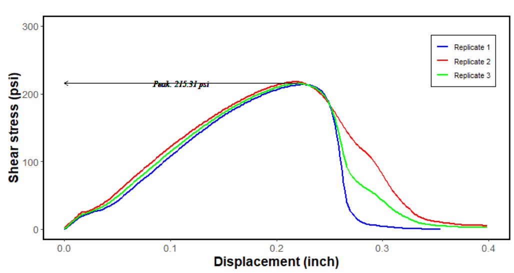

(a) No tack coat (0 gal/yd^2)

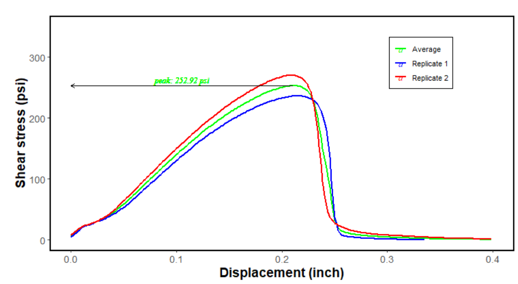

(b) 0.04 gal/yd^2

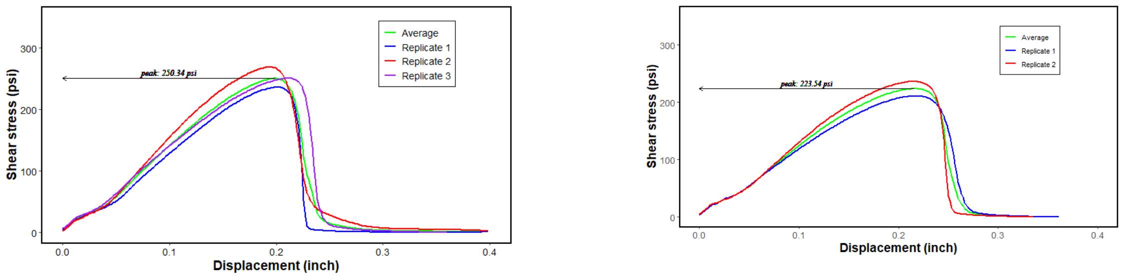

(c) 0.06 gal/yd² **(d) 0.08 gal/yd²**

FIGURE 3.33: Direct Shear Test Results for Different Application Rates of SS-1H

FIGURE 3.34 shows the relationship between residual application rate and shear strength. It can be seen that the shear strength initially increases until a peak point, then it decreases as the residual application rate increases.

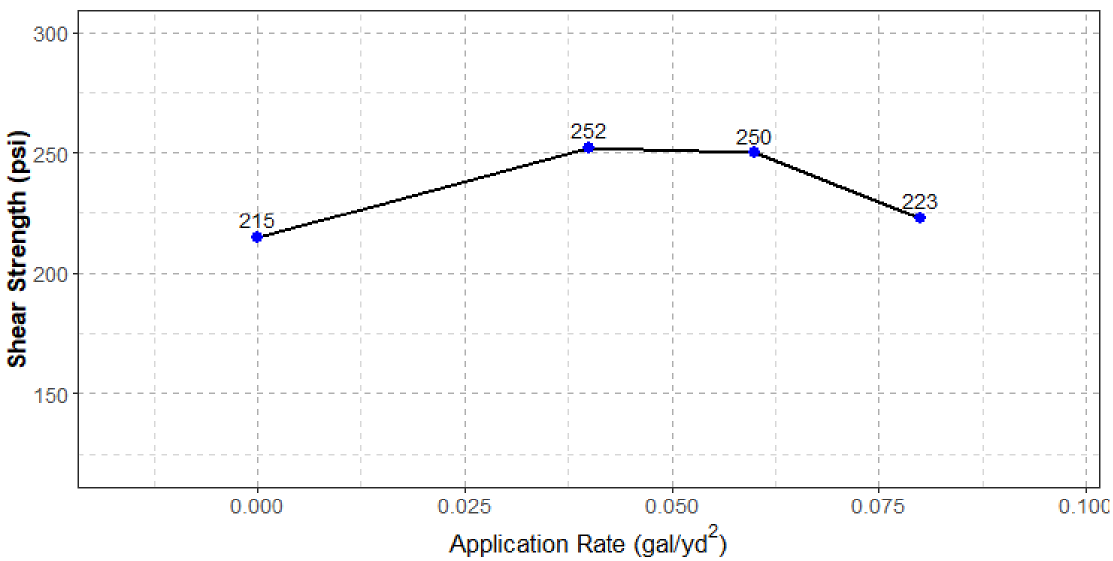

FIGURE 3.34: Shear Strength Versus Residual Application Rate Plot of SS-1H

3.7.4 CSS-1H Application Rate Effect

FIGURE 34 shows the results found from the direct shear test results for tested specimens prepared with different amounts of tack coat emulsion. FIGURE 3.35(a) shows the direct shear test results of two specimens prepared with no tack coating. The average shear strength for the specimens prepared with no tack coat is 145 psi. Similarly, direct shear test results for specimens prepared with 0.04, 0.06, and 0.08 gal/yd^2 tack coats are presented in FIGURES 3.35 (b)- 3.35 (d). The average shear strengths of specimens prepared with 0.04, 0.06, and 0.08 gal/yd^2 tack coats are 234 psi, 223 psi, and 186 psi, respectively. Therefore, it can be said that the application of a lower amount of tack coat can increase the shear strength compared to not applying tack coat. However, applying too much tack coat can decrease the shear strength.

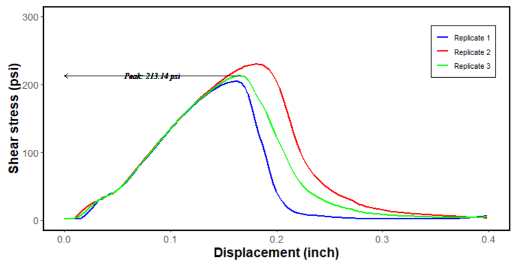

(a) No tack coat (0 gal/yd^2)

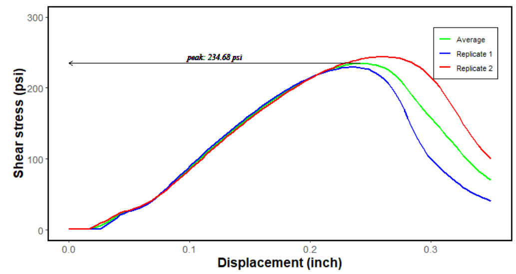

(b) 0.04 gal/yd^2

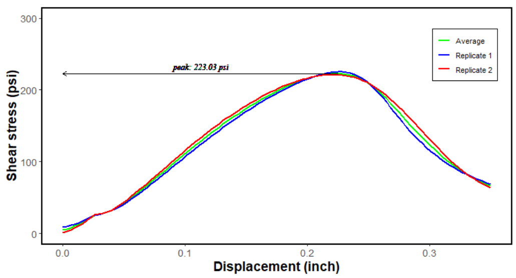

(c) 0.06 gal/yd^2

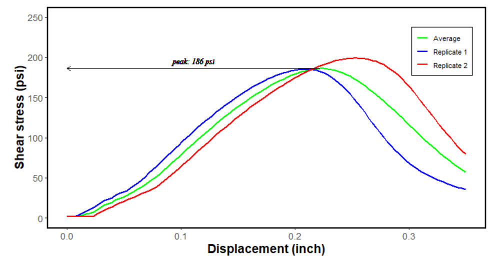

(d) 0.08 gal/yd^2

FIGURE 3.35: Direct shear test results for different tack coat application rates of CSS-1H

FIGURE 3.36 shows the relationship between residual application rate and shear strength. It can be seen that the shear strength initially increases until a peak point, then it decreases as the residual application rate increases.

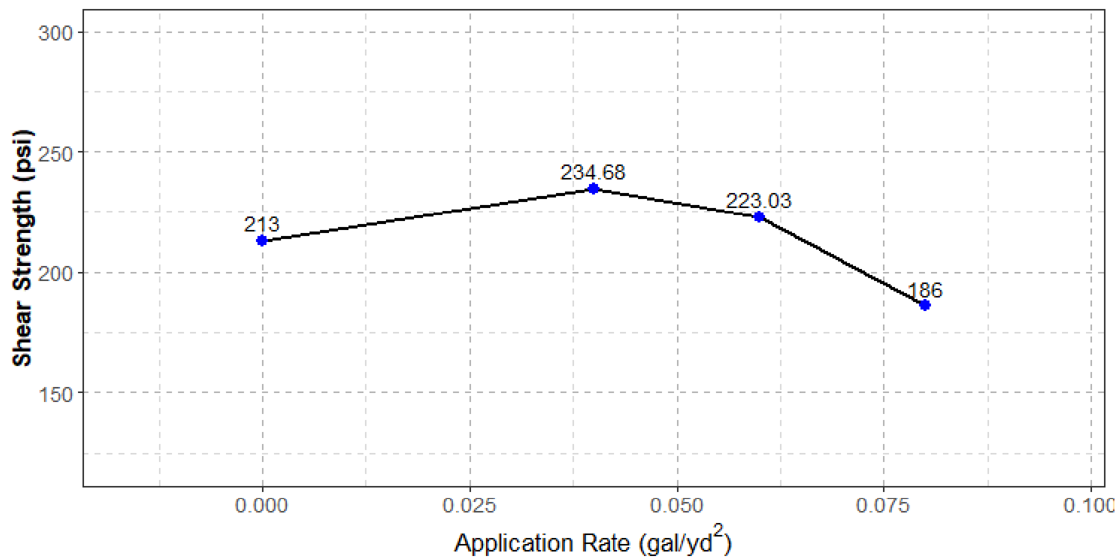

FIGURE 3.36: Shear Strength Versus Residual Application Rate Plot of CSS-1H

3.8 Summary

This chapter evaluates the effects of selected construction parameters on interlayer bonding in asphalt pavements. Laboratory testing was performed on double-layer asphalt concrete specimens prepared under controlled conditions. Interface behavior was quantified using direct shear testing. The study focused on controllable variables, including tack coat type, application rate, surface condition, and curing time.

The results show that tack coat material significantly influences interface shear strength. Differences in binder composition and rheological properties affect adhesion and resistance to shear displacement at the interface. Modified emulsions generally exhibited improved performance compared to conventional materials.

Application rate was identified as a key factor governing bond development. Increasing the rate improved interface strength up to a threshold. Beyond this level, additional binder reduced performance, likely due to the formation of a lubricating layer at the interface.

The curing condition also played a critical role. Insufficient curing resulted in low interface strength due to incomplete emulsion break. Strength increased with curing time and approached a plateau after adequate curing.

The principal findings are summarized as follows:

Finding 1: The optimum residual application rate for emulsified tack coats (SS-1HP, SS-1H, and CSS-1H) was 0.04–0.06 gal/yd², while the trackless tack coat showed better performance at 0.08–0.10 gal/yd².

Finding 2: The optimum curing time varied by material. It was approximately 25 min for trackless tack, 50 min for SS-1HP, and 120 min for SS-1H and CSS-1H.

Finding 3: Tack coat type influences bond strength. Polymer-modified and trackless emulsions produced higher interface shear strength than conventional emulsions.

Finding 4: Excessive application reduces bonding efficiency. It can cause a slip plane under shear loading.

Overall, the results demonstrate that interlayer bonding is governed by material selection, application rate, and curing conditions. Proper control of these parameters is required to achieve reliable interface bond performance.

CHAPTER 4
DETERMINATION OF MECHANICS OF DELAMINATION

Flexible pavement analysis treats asphalt concrete (AC) layers as a composite system. Under this assumption, all layers act together as a single structural unit. This simplification is necessary for mechanistic design calculations. It also reduces the complexity of modeling stress and strain distributions within the pavement.

Field conditions are less ideal. The bond at every AC layer interface can vary. Construction practice, surface preparation quality, tack coat type, curing condition, traffic loading history, and long-term climate exposure all influence the actual level of bonding achieved. None of these factors operates independently. Their interaction determines how well adjacent asphalt lifts transfer load across the interface.

When the interface bond is intact, load transfer across the interface is efficient. The pavement layers deflect together. Shear and tensile strains remain within acceptable limits at every depth. When the bond degrades, the layers begin to move relative to each other. Shear stress concentrates at the interface. Critical strain locations shift. The pavement accumulates damage faster than predicted by fully bonded design models.

This analysis evaluates three interface bond factors: 1.0 for full bonding, 0.8 for a partially bonded condition, and 0.5 for a weaker interface. These values span the realistic range of interlayer contact that may develop in a constructed pavement. The chapter uses these three levels to examine how changes in bond continuity affect predicted pavement distress across multiple combinations of binder grade, traffic level, and climate input.

4.1 Mechanics of Interface Debonding

Asphalt pavement functions as a multi-layer elastic structure. Each layer has its own stiffness, thickness, and material properties. The layers interact through their interfaces. The quality of that interaction governs how the load is distributed through the structure.

Under full bonding, the strain at the bottom of one AC lift equals the strain at the top of the layer immediately below it. Displacement continuity is maintained across the interface. No relative movement occurs between layers. The structure responds as a monolithic composite under traffic loading.

When bonding is partial or absent, this displacement continuity breaks down. The layers can slip relative to each other. The strain is no longer continuous across the interface. Each layer behaves more like a separate beam. Tensile and shear stresses concentrate at the interface rather than distributing through the full depth of the asphalt structure.

The consequences are significant. Tensile strains near the bottom of the upper lift increase. Rutting resistance drops because the layers no longer act together to resist shear deformation. Top-down cracking can initiate from stress concentrations at the surface. Bottom-up cracking develops faster because the lower layers carry greater tensile demand.

Three failure modes are associated with interface debonding. Adhesive failure occurs when the bond between the tack coat and the AC surface is broken. Cohesive failure occurs within the tack coat material itself. Mixed failure involves both surface and bulk material fracture.

The interface bond factor used in this analysis represents the mechanical continuity between adjacent asphalt layers. A factor of 1.0 means full composite action. The layers transfer strain completely. A factor below 1.0 means the interface allows some slip. The layers transfer only a fraction of the strain demand. As the factor decreases, the pavement responds progressively more like an unbound layered system than a composite structure.

4.2 Analysis Framework

The analysis was structured as a factorial comparison. Each binder grade was paired with each annual average daily truck traffic (AADTT) level. Each case was evaluated at three interface bond factors. The climate inputs were selected from nearby weather station data sources using latitude and longitude coordinates. Two climate data points were used in the analysis: 35.000, −106.875 and 35.000, −105.625. These coordinates represent the weather station locations used to define the local climatic conditions for the pavement performance simulations. This arrangement allows direct comparison of bonding effects across a consistent range of design variables.

The interface bond factor is the primary variable. It represents the mechanical continuity between asphalt layers at the interface. Reducing the factor limits the shear and tensile strain transfer across the interface. A weak interface changes the location and magnitude of critical pavement response. The analysis uses this variable to determine which distress types are most sensitive to the bonding condition.

The pavement structure modeled in this study consists of an AC surface course placed over a granular base and natural subgrade. The AC layer thickness and mixture properties are held constant across all cases. Changes in the interface bond factor, binder grade, traffic level, and weather input are the only sources of variation between runs. This design ensures that observed differences in predicted distress are attributable to those specific variables.

The Mechanistic Empirical Pavement Design Guide (MEPDG) software is used to generate distress predictions. The MEPDG is a comprehensive design and analysis tool based on mechanistic-empirical principles. It models the pavement as a multi-layer elastic structure subjected to realistic traffic loading and climate inputs. The software predicts pavement performance over a defined design life using transfer functions calibrated to field observations.

Level 3 inputs are used throughout this analysis. These inputs represent nationally calibrated default values and locally available material characterization data. They are appropriate for a comparative study where the objective is to assess relative differences in response rather than absolute performance predictions for a specific project.

TABLE 4.1. Analysis Matrix for Interface Bond Factor Study

Variable	Levels Used in This Chapter
Interface bond factor	0.5, 0.8, 1.0
PG binder grade	PG 58-22, PG 64-22, PG 76-22
Traffic level (AADTT)	5,000, 10,000, 12,000
Weather station	Station 1: Elv: 5613 ft, Temperature: 57 °F; Station 2: Elv: 6948 ft, Temperature: 52 °F
Distress outputs	AC rutting; IRI; top-down cracking; bottom-up cracking

4.3 Pavement Distress Measurement

Four distress measures are used to interpret pavement response. Each represents a different failure mechanism. Together, they provide a complete picture of how the interface condition influences structural and functional performance.

4.3.1 Asphalt Concrete Rutting

AC rutting is the predicted permanent deformation accumulated within the asphalt layer. It develops through repeated loading and shear flow of the asphalt material. Rutting is sensitive to binder stiffness, temperature, traffic volume, and the layer's ability to resist shear deformation under load.

The interface condition directly affects rutting. When layers are fully bonded, they share the shear demand imposed by traffic. When layers slip, the upper layer carries more of the shear stress alone. This concentrated loading accelerates permanent deformation. The result is higher rutting in partially or weakly bonded pavements.

A higher PG binder grade provides better resistance to rutting because it remains stiffer at high pavement temperatures. PG 76-22 is expected to outperform PG 58-22 in rutting resistance under otherwise identical conditions. This relationship holds for both bonded and partially bonded cases, but the benefit of a higher PG grade diminishes when the interface is weak.

4.3.2 International Roughness Index

IRI is a measure of pavement surface roughness. It reflects accumulated functional deterioration over time. A higher IRI indicates reduced ride quality. The index is sensitive to all sources of surface deformation, including rutting, cracking, and differential settlement.

IRI is an important service measure because it directly affects user perception and vehicle operating cost. A pavement that fails on IRI criteria may still appear structurally adequate by other measures. Including IRI as a separate output ensures that the serviceability impacts of the bonding condition are captured explicitly.

4.3.3 Top-Down Fatigue Cracking

Top-down fatigue cracking initiates near the pavement surface. It is associated with tensile and shear stresses generated by tire contact. These stresses are affected by tire pressure, tire contact geometry, AC stiffness, temperature, and surface aging. Near-surface tensile strains cause the asphalt to crack. The cracks then propagate downward under repeated loading.

Top-down cracking is primarily controlled by near-surface material properties. The binder grade and the traffic volume determine the magnitude of the tensile response at the surface. A softer binder grade or a higher traffic level produces greater tensile demand. The interface condition has limited influence on top-down cracking because this failure mode is governed by the behavior of the surface layer rather than the interaction between layers.

This behavior has a direct implication for design. The selection of a higher PG grade is the most effective tool for managing top-down cracking risk. Improving the interface bond alone is not expected to substantially reduce top-down fatigue cracking. The two interventions address different structural mechanisms.

4.3.4 Bottom-Up Fatigue Cracking

Bottom-up fatigue cracking initiates at the base of the asphalt structure. It is driven by tensile strain at the bottom of the AC layer under repeated traffic loading. The crack propagates upward through the layer. Eventually, it reaches the surface and becomes visible as alligator cracking.

This distress mode is the most sensitive to the interface bond factor. When the interface is weak, the asphalt layers no longer act as a composite beam. Each lift deflects independently under load. The tensile strain at the bottom of the structure increases dramatically. The predicted fatigue life shortens.

The relationship between interface bonding and bottom-up cracking has been documented in previous mechanistic studies. Willis and Timm (2006) provided strain gauge data from the

National Center of Asphalt Technology (NCAT) test track showing that measured strains in de-bonded sections exceeded strains in fully bonded sections. Those elevated strains directly shortened fatigue life. The current analysis confirms this relationship through predicted distress outputs.

Rich binder layers (RBL) are sometimes incorporated at the base of perpetual pavement designs. Their purpose is to absorb tensile strain and resist bottom-up fatigue cracking. However, when the interface above the RBL is debonded, the fatigue cracking initiates at the debonded interface rather than at the bottom of the structure. The RBL no longer provides its intended protective function.

AC Rutting Results

AC rutting decreased when the interface bond factor increased from 0.5 or 0.8 to 1.0. This trend held for all binder grades and all traffic levels tested. The reduction was large enough to shift several cases from failed or marginal performance to acceptable performance.

The 0.5 and 0.8 bond factor cases produced nearly the same rutting depth in most combinations. The pavement gained little rutting benefit from a modest improvement in bonding. The main performance gain occurred when the interface reached full bond. This suggests a threshold behavior. Below a critical level of bonding, improvements in interface quality do not translate into proportional improvements in performance.

Binder grade had a clear effect on rutting. PG 76-22 produced the lowest rutting values. PG 58-22 produced the highest values. This result is expected. A stiffer binder at high temperature provides better resistance to shear deformation within the asphalt layer. Traffic also increased rutting. The effect was most pronounced when AADTT increased from 5,000 to 10,000. A further increase to 12,000 AADTT produced additional rutting, though the rate of increase slowed.

Weather Station 2 generally produced lower rutting than Weather Station 1. The difference was consistent but smaller than the difference caused by shifting from partial bond to full bond. This indicates that interface condition and binder grade are more influential than climate input for rutting prediction in these cases.

The plots are organized by distress type. Each plot compares the two weather stations for one PG grade and one AADTT level. The horizontal axis shows the interface bond factor. The vertical axis shows the predicted distress. The same vertical scale is used within each distress category to allow direct visual comparison across plots.

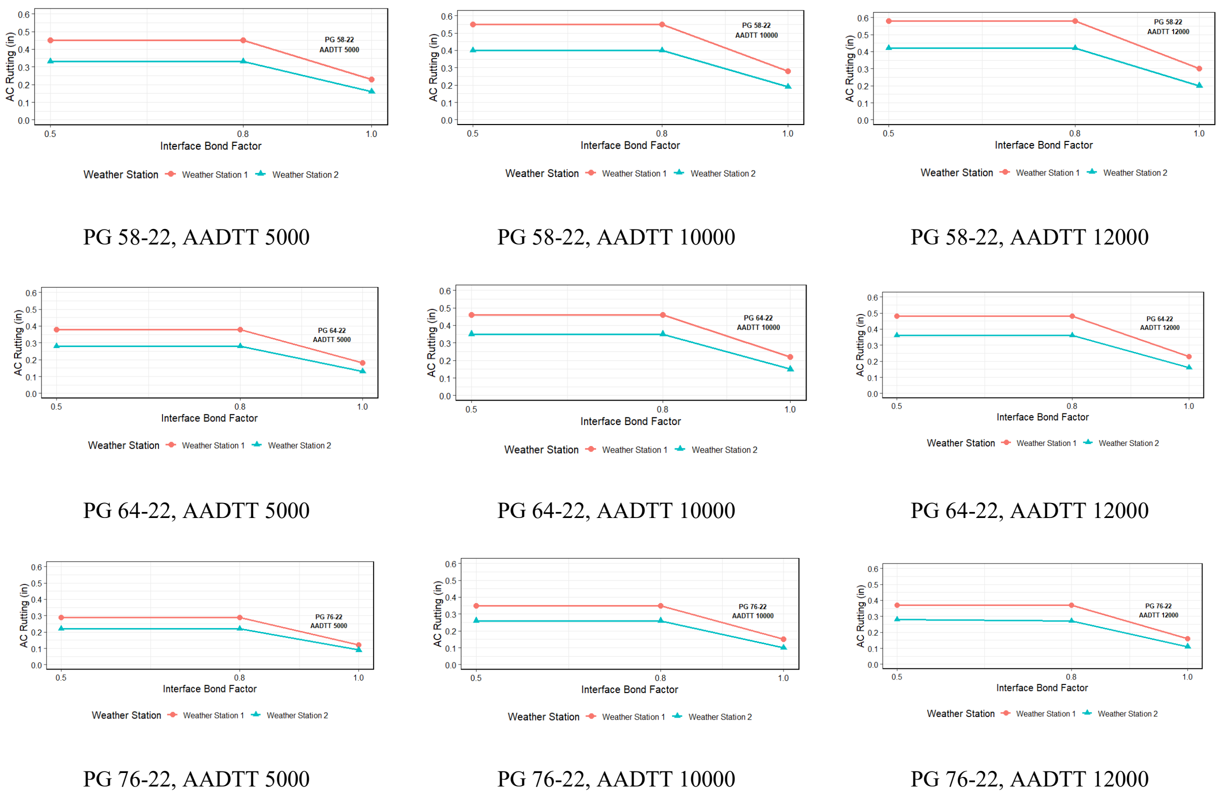

PG 58-22, AADTT 5000 | PG 58-22, AADTT 10000 | PG 58-22, AADTT 12000

PG 64-22, AADTT 5000 | PG 64-22, AADTT 10000 | PG 64-22, AADTT 12000

PG 76-22, AADTT 5000 | PG 76-22, AADTT 10000 | PG 76-22, AADTT 12000

FIGURE 4.1. Interface bond factor versus AC rutting for all PG grades and AADTT combinations

International Roughness Index Results

IRI followed the same direction as the AC rutting. Lower bond factors produced higher roughness. Full bonding reduced the predicted IRI for every PG group and both weather stations.

The IRI plots show a sharp improvement at the 1.0 bond factor. This supports the interpretation that serviceability improves substantially when asphalt layers achieve full composite action. The roughness values at 0.5 and 0.8 were close. Again, the most important change was not a small improvement in a weak interface, but a transition to a fully bonded condition.

PG 76-22 produced the lowest IRI values. PG 58-22 produced the highest values. IRI also increased with AADTT. The highest values occurred at higher traffic levels and softer binder grades. This confirms that a weak interface accelerates serviceability loss. The pavement loses its functional adequacy faster under combined conditions of weak bonding and high traffic demand.

The IRI results reinforce the rutting findings. Both measures respond to the same underlying mechanism: reduced composite action causes larger deformations, which accumulate into surface roughness over time. Managing interface bonding is therefore relevant not only to structural performance but also to functional pavement life.

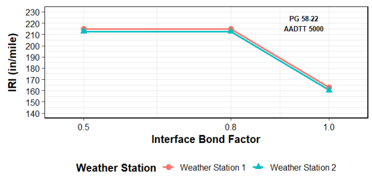

PG 58-22, AADTT 5000

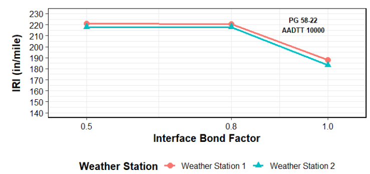

PG 58-22, AADTT 10000

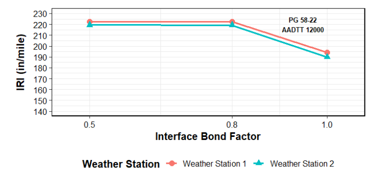

PG 58-22, AADTT 12000

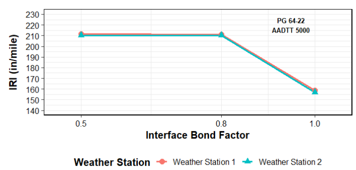

PG 64-22, AADTT 5000

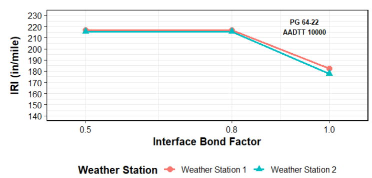

PG 64-22, AADTT 10000

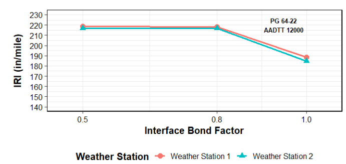

PG 64-22, AADTT 12000

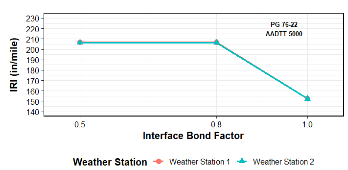

PG 76-22, AADTT 5000

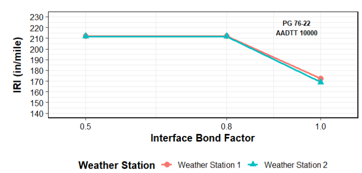

PG 76-22, AADTT 10000

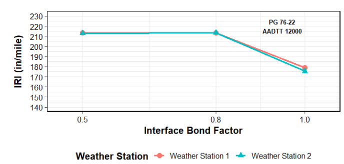

PG 76-22, AADTT 12000

FIGURE 4.2. Interface bond factor versus IRI for all PG grades and AADTT combinations

Top-Down Fatigue Cracking Results

Top-down fatigue cracking behaved differently from rutting and IRI. The three interface bond factors produced nearly identical cracking values for a given PG grade and AADTT level. This shows that top-down cracking was not controlled by the interface bond condition in this set of model outputs.

The primary driver for top-down cracking was the combination of PG grade and traffic. For PG 58-22, cracking increased sharply when AADTT rose from 5,000 to 10,000. It remained high at 12,000 AADTT. This pattern shows that a softer binder is more vulnerable at higher traffic levels. The near-surface tensile demand exceeds the material's resistance, and cracking accumulates rapidly.

PG 64-22 produced intermediate top-down cracking values. PG 76-22 produced the lowest values. These results confirm that high-temperature binder grade controls near-surface cracking response. The higher stiffness at service temperature limits the tensile strain that drives crack initiation at the surface.

The weather station effect was small for top-down fatigue cracking. Both stations produced similar cracking trends under the same PG and AADTT conditions. This suggests that the selected climate inputs did not produce sufficient difference in pavement temperature or thermal gradient to significantly alter the near-surface stress state.

The insensitivity of top-down cracking to the interface bond factor has a practical implication. Engineers addressing top-down cracking should focus on binder grade selection and traffic characterization rather than on interface bonding. In contrast, engineers addressing bottom-up cracking or rutting should consider interface bonding as a primary design variable.

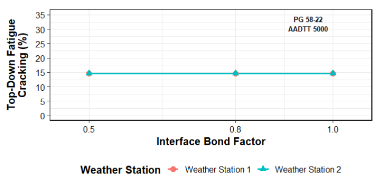

PG 58-22, AADTT 5000

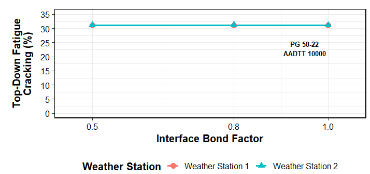

PG 58-22, AADTT 10000

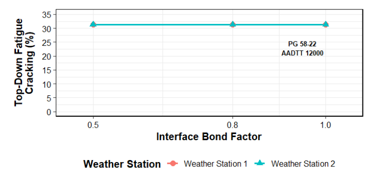

PG 58-22, AADTT 12000

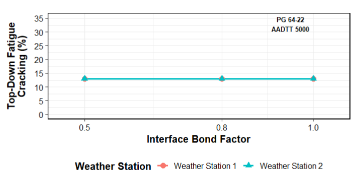

PG 64-22, AADTT 5000

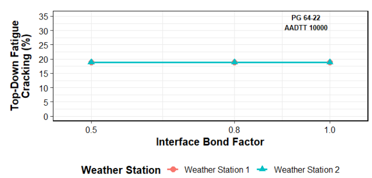

PG 64-22, AADTT 10000

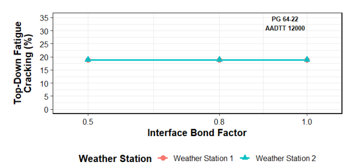

PG 64-22, AADTT 12000

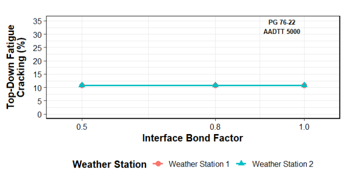

PG 76-22, AADTT 5000

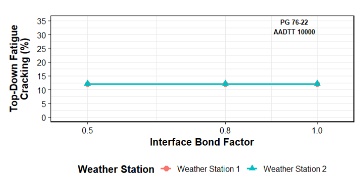

PG 76-22, AADTT 10000

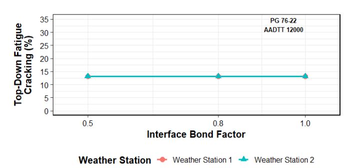

PG 76-22, AADTT 12000

FIGURE 4.3. Interface bond factor versus top-down fatigue cracking for all PG grades and AADTT combinations

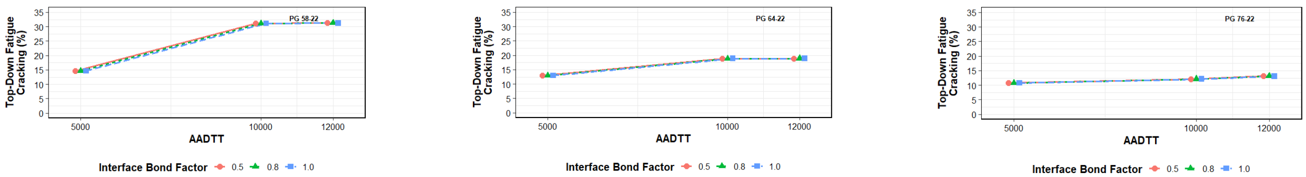

PG 58-22 **PG 64-22** **PG 76-22**

FIGURE 4.4. Top-down fatigue cracking versus AADTT using the average of both weather stations

Bottom-Up Fatigue Cracking Results

Bottom-up fatigue cracking was the most sensitive to the interface bond factor. At bond factors of 0.5 and 0.8, bottom-up cracking reached 100 percent in nearly every case. This indicates severe structural deterioration when the asphalt layers were not fully bonded.

The behavior at bond factors of 0.5 and 0.8 was similar in magnitude. Both conditions produced critical cracking. This pattern matches the rutting and IRI findings. A modest improvement in a weak interface does not substantially change predicted performance. The critical transition is from partial bond to full bond.

At the 1.0 bond factor, bottom-up cracking dropped sharply. The reduction was strong for all PG grades. However, several full-bond cases still exceeded a 25 percent cracking threshold. This finding is important. Full bonding improved structural performance, but it did not eliminate failure risk under high traffic or softer binder grades. Both conditions must be addressed together.

PG 76-22 showed the best bottom-up fatigue performance. The lowest cracking values occurred for PG 76-22 at 5,000 AADTT. PG 58-22 showed the most critical behavior at high traffic. These results confirm that bottom-up cracking is controlled by both interface condition and the structural response of the asphalt layer. Improving only one factor is not always sufficient to bring performance within acceptable limits.

This finding has direct implications for design. Bottom-up fatigue cracking is the distress mode most likely to be underestimated when a fully bonded assumption is used in design. If the constructed interface delivers partial bonding, the predicted fatigue life will be substantially shorter than the design target. The consequence is premature structural failure.

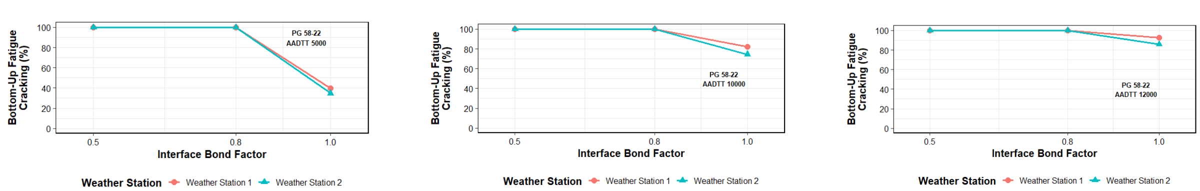

PG 58-22, AADTT 5000 PG 58-22, AADTT 10000 PG 58-22, AADTT 12000

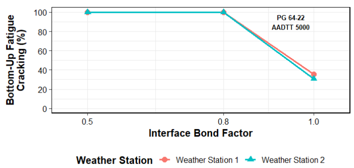

PG 64-22, AADTT 5000

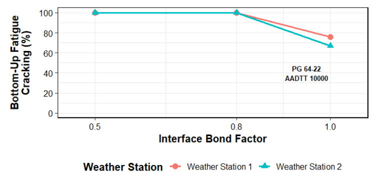

PG 64-22, AADTT 10000

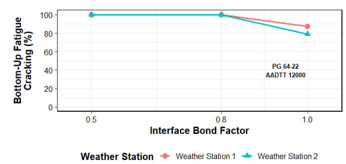

PG 64-22, AADTT 12000

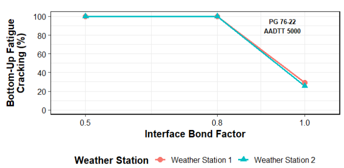

PG 76-22, AADTT 5000

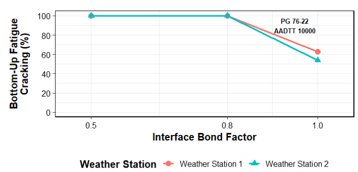

PG 76-22, AADTT 10000

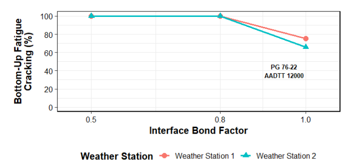

PG 76-22, AADTT 12000

FIGURE 4.5. Interface bond factor versus bottom-up fatigue cracking for all PG grades and AADTT combinations

4.4 Comparative Sensitivity of Distress Outputs

The four distress types did not respond equally to changes in the interface bond factor. Bottom-up fatigue cracking showed the strongest sensitivity. AC rutting and IRI showed moderate sensitivity. Top-down cracking showed very low sensitivity to bond factor across the cases studied.

This hierarchy of sensitivity has a practical interpretation. Engineers should prioritize interface condition as a design input for rutting and bottom-up fatigue prediction. For top-down cracking, binder grade selection and traffic characterization are more critical inputs. Each distress mode is governed by different structural mechanisms, and each responds to different design variables.

The following TABLE 4.2 summarizes the relative sensitivity of each distress output to the interface bond factor and identifies the controlling variables for each mode.

TABLE 4.2. Relative Sensitivity of Distress Outputs to Interface Bond Factor

Distress Type	Sensitivity to Bond Factor	Primary Controlling Variables
AC Rutting	Moderate to High	Interface bond, PG grade, AADTT
IRI	Moderate to High	Interface bond, PG grade, AADTT
Top-Down Fatigue Cracking	Low	PG grade, AADTT
Bottom-Up Fatigue Cracking	Very High	Interface bond, PG grade, AADTT

The strong response of bottom-up cracking to interface conditions reflects the structural role of composite action in pavement response. When the layers act as a unit, they distribute tensile strain efficiently across the full depth of the AC structure. When they slip, the base of the upper lift experiences concentrated tensile demand. The MEPDG transfer function for bottom-up cracking is highly sensitive to this concentration, which explains the sharp prediction difference between partial and full bond cases.

4.5 Effect of Weather Station

The analysis used two nearby New Mexico weather stations. Station 1 was Pajarito Mesa, NM, located at 35.0000° latitude and −106.8750° longitude, with an elevation of 5,613 ft. This station had a mean annual air temperature of 57.04°F, mean annual precipitation of 12.70 in, freezing index of 41.14°F-days, average annual freeze–thaw cycles of 105.27, and water table depth of 10 ft.

Station 2 was Clines Corners, NM, located at 35.0000° latitude and −105.6250° longitude, with an elevation of 6,948 ft. This station was cooler and wetter than Station 1. It had a mean annual air temperature of 52.39°F, mean annual precipitation of 16.70 in, freezing index of 146.29°F-days, average annual freeze–thaw cycles of 126.73, and water table depth of 10 ft.

The two weather stations produced consistent trends. Station 2 generally yielded slightly lower rutting and IRI than Station 1. This may be related to its lower mean annual air temperature and higher elevation. The difference was visible, but it was smaller than the difference caused by the transition from partial bond to full bond.

For fatigue cracking, the weather station effect was minor. Top-down cracking showed almost no difference between the two stations. Bottom-up cracking showed a modest station effect at the full bond level. Under partial bond conditions, both stations produced similarly critical results.

The consistent direction of results across both climate inputs provides confidence in the interpretation. The interface bond factor changed pavement response in the same way for both weather stations. This consistency supports treating the interface condition as a primary design variable rather than only a site-specific adjustment factor.

The limited influence of the weather station on the overall conclusions does not mean climate is unimportant. It means that, for the climate difference represented by Pajarito Mesa and Clines Corners, interface condition and binder grade were more influential. Larger climate contrasts may produce stronger effects, especially for top-down cracking, where temperature strongly affects near-surface binder behavior.

4.6 Interaction Between Bond Factor, Binder Grade, and Traffic

The three design variables — interface bond factor, PG binder grade, and AADTT — do not act independently. Their interaction determines the severity of pavement distress. Understanding these interactions is necessary for correct design decisions.

For rutting and IRI, the benefit of a higher PG grade was most visible at full bond. When the interface was weak, the rutting benefit of PG 76-22 over PG 58-22 was reduced. The interface condition limited the extent to which improved binder stiffness could improve performance. This is because a weak interface introduces shear deformation that binder stiffness alone cannot prevent.

For bottom-up cracking, the interaction was even more pronounced. PG 76-22 at full bond produced the lowest cracking values. PG 58-22 at partial bond produced the highest. However, even PG 76-22 at partial bond produced critical cracking in most cases. This indicates that achieving full bond is a prerequisite for binder grade improvements to deliver their full structural benefit.

Traffic level amplified the differences between bond conditions. At 5,000 AADTT, some partial bond cases produced acceptable performance. At 10,000 and 12,000 AADTT, partial bond cases consistently failed regardless of binder grade. Higher traffic removes the tolerance that might otherwise exist for a moderately weak interface. Under high-volume conditions, the demands placed on the interface exceed what partial bonding can sustain.

These interactions support a design principle: bond quality and binder selection are linked decisions. Selecting a higher PG grade without ensuring adequate bonding provides less benefit than expected. Ensuring adequate bonding while using a lower PG grade may also be insufficient under high traffic. Both conditions must meet their respective targets to achieve the intended design performance.

4.7 Interpretation for Design and Implementation

The results support a practical design conclusion. Interface bonding should not be treated as a construction detail alone. It has a direct effect on structural performance and functional service life. Weak bonding can increase distress even when a stronger binder grade is used. The two factors are not interchangeable.

The greatest performance benefit occurred when the bond factor reached 1.0. The difference between bond factors of 0.5 and 0.8 was small for rutting, IRI, and bottom-up cracking in most cases. This does not mean a bond factor of 0.8 is acceptable. It means the pavement response remained critical until full composite action was achieved. Any target that falls short of full bond should be considered a risk factor.

For design and construction practice, the interface must be controlled through deliberate attention to multiple factors. Tack coat type, application rate, and coverage uniformity all influence the achievable bond level. Surface cleanliness before paving is equally important. Dust, debris, or standing water at the interface reduces adhesion and lowers the effective bond factor.

Curing time also matters. The NMDOT research report documents that curing conditions affect shear strength across all tack coat types studied. Paving before adequate curing can trap moisture at the interface and reduce the bond developed between layers. Construction scheduling should account for curing requirements, particularly in humid conditions or when moisture-sensitive emulsions are used.

Surface texture affects the bond through mechanical interlocking. Milled surfaces consistently produce higher interface shear strength than non-milled surfaces. Where practical, milling the existing surface before overlay placement provides both improved texture and improved adhesion. This finding from the NMDOT laboratory program is consistent with the broader literature on interlayer bonding.

Only three interface bond factors were evaluated: 0.5, 0.8, and 1.0. The response between 0.8 and 1.0 may not be linear. A threshold likely exists somewhere in this range where pavement response begins to improve substantially. Additional bond factor levels would be needed to locate this threshold precisely. Future work should fill this gap.

The top-down fatigue cracking output showed little variation with the interface bond factor across all cases. This may reflect a genuine structural behavior or a model sensitivity limitation. The MEPDG top-down cracking model is primarily driven by the near-surface stress state, which is controlled by binder stiffness and tire contact. Different layer thicknesses, tire pressures, or interface locations might produce a different sensitivity pattern. This possibility should be examined in future analyses.

The analysis used two weather stations. These inputs were useful for comparison, but they do not represent all climate regions. The conclusions regarding climate effects are limited to the conditions represented by these stations. Regional recommendations should be supported by a wider range of climate inputs.

The interface bond factor as implemented in this analysis represents a global reduction in layer interaction. In practice, debonding occurs progressively and may be localized rather than uniform across the interface. The model does not capture spatial variability in bond condition. Future finite element modeling with cohesive zone elements could represent localized debonding more realistically.

4.8 Summary

The following conclusions follow from the distress plots and performance comparisons presented in this chapter.

The interface bond factor had a clear and consistent effect on AC rutting. Rutting was highest at bond factors of 0.5 and 0.8. It was lowest at full bond. The difference between 0.5 and 0.8 was small. The most significant reduction occurred at the transition to full bond.

IRI followed the same pattern as rutting. Full bonding improved ride-related performance in every PG grade and AADTT combination tested. Both measures confirm that interface quality is a functional serviceability factor as well as a structural one.

Top-down fatigue cracking was controlled mainly by PG grade and AADTT. It showed little sensitivity to the interface bond factor in the available results. Addressing top-down cracking requires appropriate binder grade selection. Interface bonding is not an effective lever for this distress mode.

Bottom-up fatigue cracking was the most critical distress in this study. Partial bond cases produced severe cracking across nearly all combinations. Full bonding reduced cracking substantially but did not eliminate failure risk under high traffic or softer binder grades. Both bond quality and binder selection must be addressed together.

PG 76-22 gave the best overall performance across all four distress measures. PG 58-22 gave the most critical response, particularly at higher traffic levels. The binder grade benefit was fully realized only when the interface bond was adequate.

Weather Station 2 generally produced slightly lower rutting and IRI than Station 1. Trends were consistent across both stations. Interface condition and binder grade were more influential than the weather station for all four distress outputs in these cases.

A recommended next step is to calibrate the interface bond factor using laboratory shear test data and field core measurements. This calibration would link the factor to measurable construction properties. It would allow the model to translate tack coat type, application rate, and surface texture into a predicted bond quality that can be used directly in mechanistic design.

CHAPTER 5
SELECTION OF DELAMINATION DESIGN PARAMETERS AND LIMITING VALUES

Previous chapters evaluated the effects of tack coat type, application rate, and curing condition on interface shear strength. These parameters play an important role in the development of interlayer bonding. However, the behavior of the asphalt interface during pavement service depends not only on construction practices but also on the mechanical and environmental conditions acting on the pavement structure.

Interfacial delamination occurs when the shear resistance of the interface is exceeded by stresses generated within the pavement system. Traffic loading produces shear stresses along the interface between asphalt layers. The magnitude of these stresses depends on the structural characteristics of the pavement, the loading conditions applied to the pavement surface, and the environmental state. If the interface cannot resist these stresses, relative movement may occur between asphalt layers. Continued loading may then lead to progressive separation of the layers and the development of interfacial delamination.

The resistance of an asphalt interface is controlled by several mechanisms. Adhesion provided by the tack coat residue contributes to bonding between the layers. Friction generated by normal stress acting across the interface also contributes to shear resistance. In addition, surface roughness can provide mechanical interlocking between the two asphalt layers. The combined contribution of these mechanisms determines the overall shear resistance of the pavement interface.

Normal stress plays an important role in the development of frictional resistance at the interface. When normal stress increases, the contact pressure between the two asphalt layers also increases. This increase in contact pressure improves frictional resistance and allows the interface to sustain greater shear stress before failure occurs. Shear loading rate can also influence interface behavior. Asphalt materials exhibit time-dependent mechanical properties, and the resistance of the interface changes depending on the rate at which shear is applied.

Environmental conditions further influence the behavior of asphalt interfaces. Temperature affects the stiffness and viscosity of asphalt binders. At higher temperatures, the binder becomes softer and more susceptible to deformation. This condition may reduce the resistance of the interface to shear loading. Moisture also weakens the bond between asphalt layers by reducing cohesion within the tack and adhesion between the coating and the aggregate surface. Exposure to moisture can therefore contribute to a reduction in interface shear strength.

A proper understanding of interfacial delamination requires evaluation of these mechanical and environmental factors. Measuring interface strength under a single test condition does not fully describe the behavior of the interface in service. The interface must be examined under different stress states and conditioning conditions in order to understand how shear resistance develops and how failure may occur.

The chapter first examines the influence of normal stress on interface shear strength. The effect of shear loading rate is then evaluated. The Mohr–Coulomb framework is used to determine cohesion and friction angle parameters that describe interface resistance. The influence of temperature and moisture conditioning on interface shear strength is also investigated. Surface condition of the interface also influences bonding behavior. Milled surfaces introduce higher macrotexture, which increases mechanical interlocking between layers. This additional roughness can improve shear resistance, especially under higher normal stress.

Controlled surface texturing was also considered in this study. Notched or grooved surfaces were prepared to isolate the effect of texture from other variables. These controlled patterns provide a consistent geometry for mechanical interlock. The results allow a clearer comparison with conventional milled surfaces, where texture is more variable. This approach helps to better understand the role of surface texture in interfacial delamination. In addition to surface condition, the effect of aging on interface behavior is examined in this study. Aged and unaged surfaces may respond differently due to changes in binder properties and bonding potential. The orientation of controlled surface texture relative to the direction of shear is also considered, as it can influence the degree of mechanical interlocking and resistance to shear. These factors are evaluated to better understand their role in interfacial shear performance.

The results provide a mechanistic understanding of how asphalt interfaces respond to loading and environmental conditions that may contribute to delamination during pavement service.

5.1 Design Parameters

The resistance of an asphalt interface to shear loading is governed by several mechanisms. These mechanisms include adhesive bonding, frictional resistance, and mechanical interlocking between AC layers. The relative contribution of each mechanism depends on the material properties of the tack coat, the surface condition of the asphalt layers, and the loading conditions applied to the interface.

Adhesion is provided by the residual asphalt binder present in the tack coat. After the emulsion breaks and cures, the asphalt residue forms a thin bonding layer between the two AC layers. This layer provides adhesive resistance that helps prevent relative movement between layers. The magnitude of this adhesive bond depends on the chemical and rheological properties of the binder and the condition of the surfaces in contact.

Friction also contributes to the resistance of the interface. Friction develops when normal stress acts across the interface between asphalt layers. Traffic loads applied to the pavement structure produce both vertical and horizontal stresses. The vertical component generates normal stress at the interface, while the horizontal component produces shear stress. The interaction of these stresses creates frictional resistance that helps prevent sliding between the layers.

Surface texture can also influence interface resistance. Rough surfaces increase mechanical interaction between asphalt layers. This mechanical interaction improves the resistance to relative movement and contributes to the overall shear strength of the interface. Smooth surfaces provide less mechanical interaction and therefore depend more strongly on adhesive bonding.

The combined effect of adhesion and friction is commonly represented using the Mohr–Coulomb failure criterion. In this approach, the shear strength of the interface is expressed as a function of normal stress. The relationship can be written as

$$\tau = c + \sigma \tan\varphi \qquad \text{Eq .1}$$

where,

τ = interface shear stress;

c = cohesion;

σ = normal stress;

φ = angle of internal friction.

The cohesion parameter is associated with the bonding provided by the asphalt material. The friction angle represents the frictional component of the interface resistance that develops under normal load.

The Mohr–Coulomb framework provides a convenient method for interpreting interface shear test results. By measuring shear strength at different levels of normal stress, the cohesion and friction angle of the interface can be determined. These parameters provide a mechanistic description of the interface behavior.

The experimental setup used in this chapter is the same direct shear testing system described in Chapter 3. The GCTS servo-controlled direct shear device was used to apply controlled shear and normal loads to the double-layer AC specimens. Details of the specimen preparation procedure, test configuration, and instrumentation are provided in the previous chapter and are not repeated here.

The objective of the present chapter is to evaluate the mechanical and environmental factors that influence interfacial delamination. For this purpose, the direct shear test was conducted under different levels of normal stress and shear loading rate. Additional tests were also performed under different environmental conditions. The specimens were tested at several temperature levels to evaluate the influence of temperature on interface shear strength. Moisture-conditioned specimens were also tested to examine the influence of moisture exposure on bonding performance.

The combination of these testing conditions allowed the interface behavior to be examined under a range of mechanical and environmental states. The resulting data were used to evaluate the shear strength characteristics of the asphalt interface and to determine the cohesion and friction angle using the Mohr–Coulomb failure relationship.

5.2 Effect of Normal Stress and Shear Rate

Normal stress plays an important role in the development of interfacial shear resistance between asphalt concrete layers. When normal stress increases, the contact pressure between the two asphalt layers increases, which enhances frictional resistance at the interface. As a result, the interface can sustain higher shear stresses before failure occurs. This behavior is commonly described using the Mohr–Coulomb failure framework, where shear strength increases linearly with normal stress due to the combined effects of cohesion and friction.

To evaluate the influence of normal stress on interface shear strength, direct shear tests were conducted on double-layer asphalt concrete specimens bonded with SS-1H tack coat. Tests were performed under three normal stress levels: 72.5 psi, 108.8 psi, and 145 psi (equivalent to 500 kPa, 750 kPa, and 1000 kPa, respectively). For each normal stress level, tests were conducted at several shear displacement rates, and three replicate specimens were used for each test condition.

FIGURE 5.1 shows the results found from the direct shear tests for shear rates of 1 mm/min, 2.54 mm/min, and 5 mm/min. To get a lower coefficient of variance, some sets (at specific shear rate and normal stress) were conducted more than three times to eliminate outliers. For all cases, there are two different phases in the load-displacement curves. In the first phase, the load initially increases as the displacement increases until it reaches a maximum value. This load increment is attributed to bonding between two layers due to adhesion from tack coating and interlocking from aggregate embedment. The maximum value of load is related to the bonding strength of the interface material. After reaching the peak point, the bonding between the interface materials starts to fail (second phase), when the load decreases as the displacement increases. Finally, the load decreases after the complete deterioration in interface bonding. Frictional resistance was present between the two surfaces. It should be mentioned that the load-displacement curves of three replicate specimens are close to each other, which confirms the repeatability of the direct shear test.

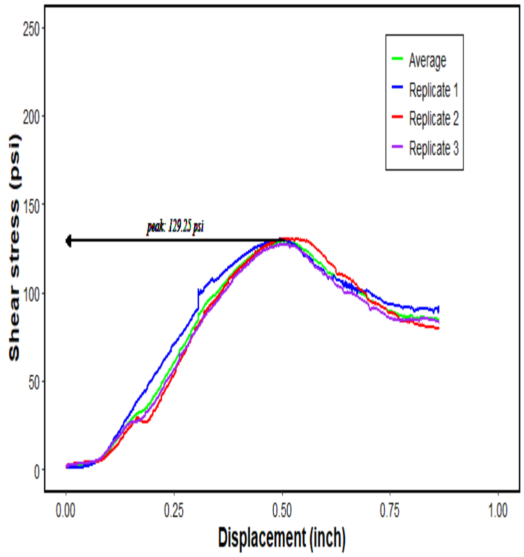

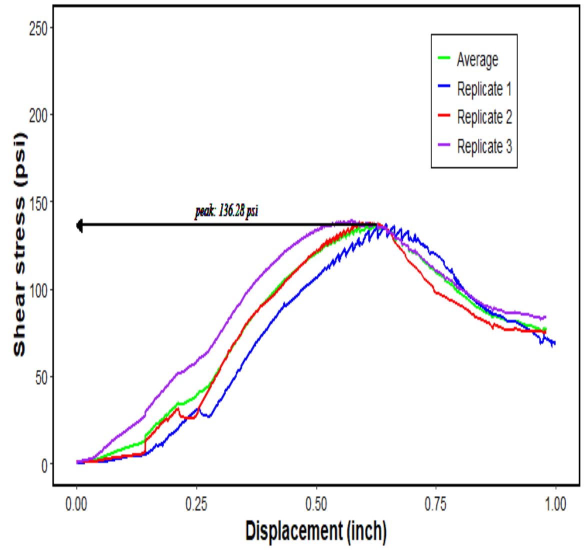

a. 1 mm/min b. 2.54 mm/min

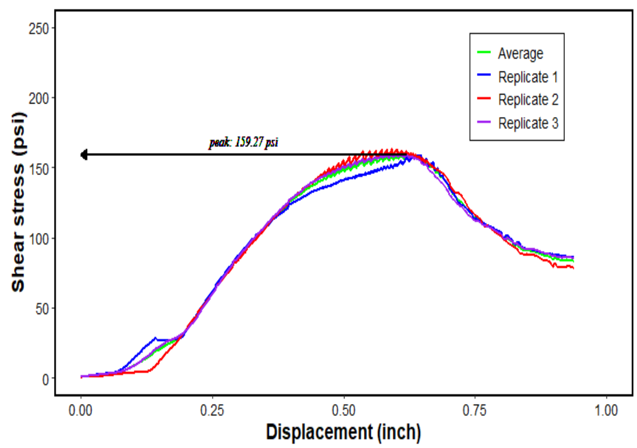

c. 5.0 mm/min

FIGURE 5.1: Direct shear test results for different displacement rates at 72 psi normal load

TABLE 5.1 summarizes the results as shown in FIGURE 5.1, where the tests were performed at a normal stress of 72 psi with displacement rates of 1 mm/min, 2.54 mm/min, and 5 mm/min.

TABLE 5.1: Conducted direct shear tests at 72 psi normal load on double-layered AC specimens

Normal stress (psi)	**72 psi**		
Loading rate (mm/min)	r_1=1	r_2=2.54	r_1=5
Shear strength (psi), Replicate 1	129.04	134.12	157.99
Shear strength (psi), Replicate 2	129.51	136.51	158.73
Shear strength (psi), Replicate 3	129.37	138.43	161.69
Coefficient of Variance (%)	0.209	1.95	1.12
Average shear strength (psi)	129.25	136.28	159.27

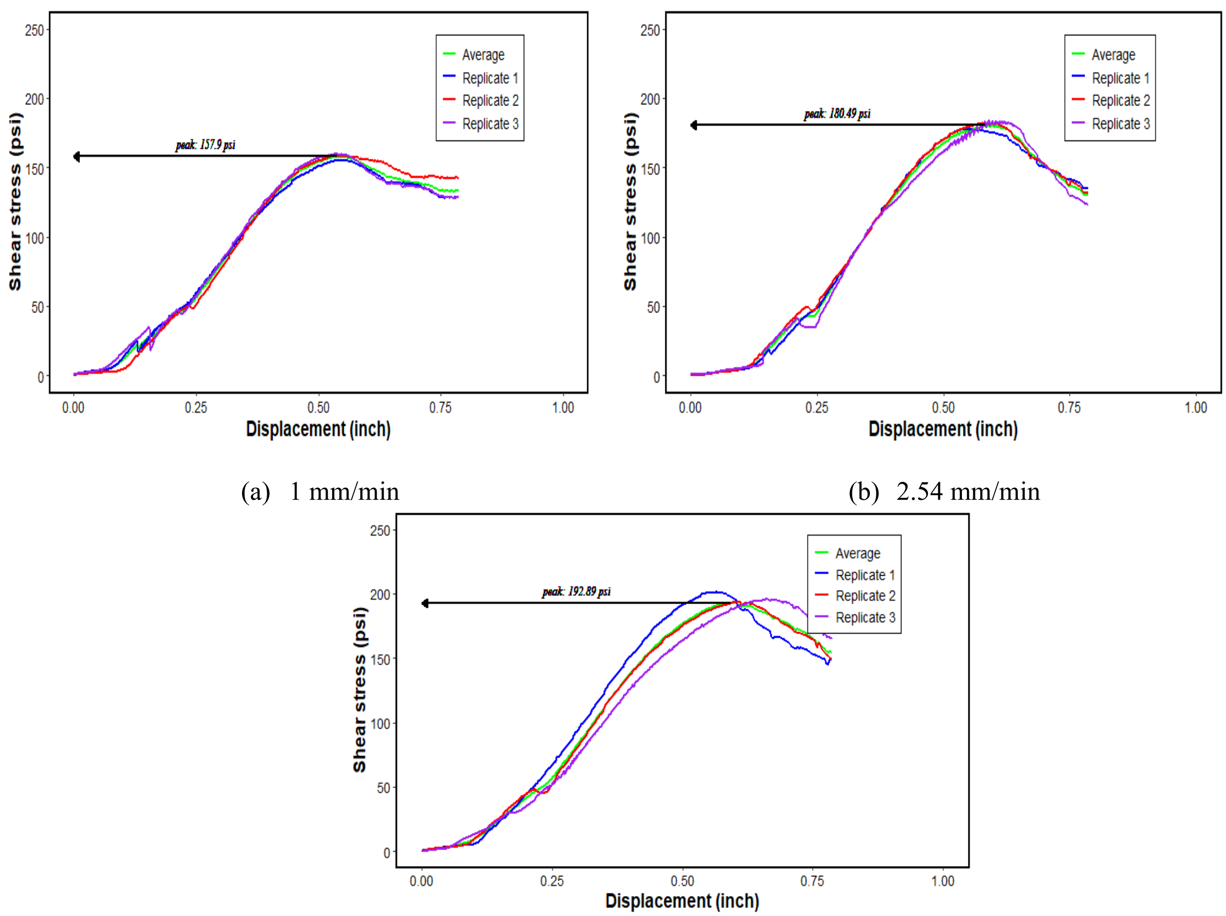

(a) 1 mm/min

(b) 2.54 mm/min

(c) 5.0 mm/min

FIGURE 5.2: Direct shear test results for different displacement rates at 108 psi normal load

TABLE 5.2 summarizes the results as shown in FIGURE 5.2, where the tests were performed at a normal stress of 108 psi with displacement rates of 1 mm/min, 2.54 mm/min, and 5 mm/min.

TABLE 5.2: Conducted direct shear tests at 108 psi Normal Load

Normal stress (psi)	**108 psi**		
Loading rate (mm/min)	$r_1=1$	$r_2=2.54$	$r_1=5$
Shear strength (psi) Replicate 1	155.45	177.50	201.32
Shear strength Rep 2 (psi) Replicate 2	158.84	182.04	193.87
Shear strength (psi) Replicate 3	159.84	183.98	195.78
Coefficient of Variance (%)	1.19	1.50	1.62
Average shear strength (psi)	157	180	192

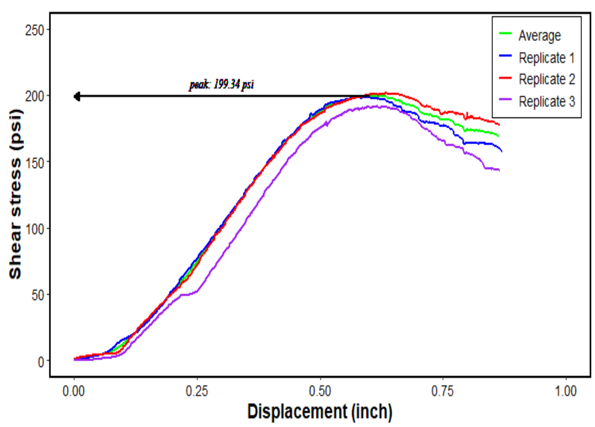

(a) 1 mm/min

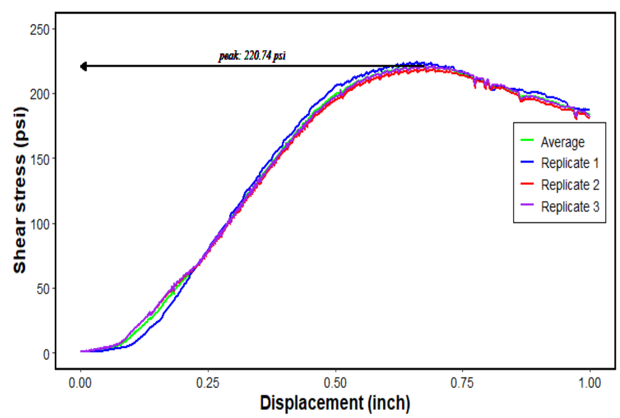

(b) 2.54 mm/min

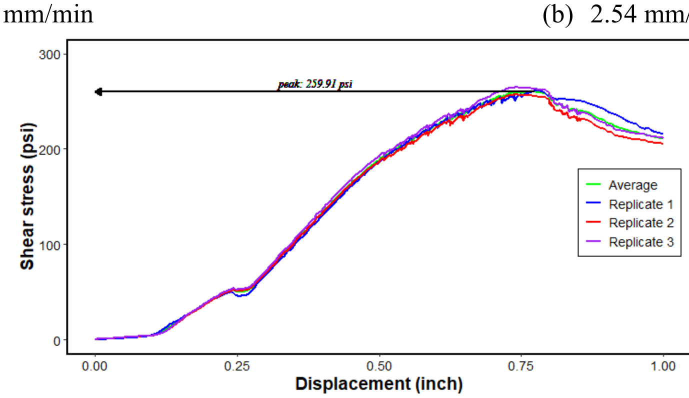

(c) 5.0 mm/min

FIGURE 5.3: Direct shear test results for different displacement rates at 145 psi normal load

TABLE 5.3 summarizes the results as shown in FIGURE 5.3, where the tests were performed at a normal stress of 145 psi with displacement rates of 1 mm/min, 2.54 mm/min, and 5 mm/min.

TABLE 5.3: Direct shear tests on double-layered AC specimens at 145 psi Normal Load

Normal stress (psi)	**145 psi**		
Loading rate (mm/min)	r_1=1	r_2=2.54	r_1=5
Shear strength (psi) Replicate 1	198.54	223.77	261.12
Shear strength Rep 2 (psi) Replicate 2	201.64	218.50	257.10
Shear strength (psi) Replicate 3	191.64	220.90	264.76
Coefficient of Variance (%)	2.12	0.97	1.2
Average shear strength (psi)	199	220	259

To analyze the Mohr-Coulomb principle, the average interface shear stress values obtained at 1 mm/min, 2.54 mm/min, and 5 mm/min displacement rates were plotted against the corresponding normal stress values. This resulted in a linear relationship, indicating that the interface shear strength increased with an increase in the normal stress.

TABLE 5.4 summarizes the mean interface shear stress values at a 1 mm/min displacement rate

TABLE 5.4: Summary of the mean interface shear stress at 1 mm/min displacement rate

Normal Stress σ (psi)	**Shear Stress τ (psi)**
72	129
108	136
145	199

FIGURE 5.4 illustrates the Mohr-Coulomb principle at a 1 mm/min displacement rate, based on the data presented in TABLE 5.4. The plot shows a linear relationship between shear stress and normal stress, with the corresponding angle of internal friction and cohesion values calculated from the linear equation.

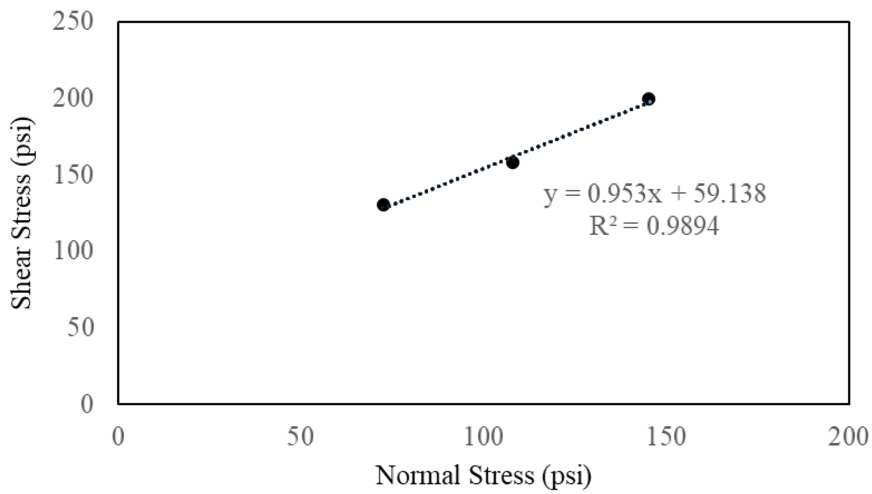

FIGURE 5.4: Mohr-Coulomb principle at 1 mm/min, based on the data in TABLE 5.4

TABLE 5.5 presents the interpreted shear strength parameters (angle of internal friction and cohesion) derived from FIGURE 5.4.

TABLE 5.5: The interpreted shear strength parameters

Friction Angle ϕ°	Cohesion C (psi)
43.62	59.138

TABLE 5.6 summarizes the mean interface shear stress values at a 2.54 mm/min displacement rate.

TABLE 5.6: Summary of the mean interface shear stress at 2.54 mm/min displacement rate

Normal Stress σ (psi)	Shear Stress τ (psi)
72	139
108	180
145	220

FIGURE 5.5 illustrates the Mohr-Coulomb principle at a 2.54 mm/min displacement rate, based on the data presented in TABLE 5.6. The plot also shows a linear relationship between shear stress

and normal stress, with the corresponding angle of internal friction and cohesion values calculated from the linear equation.

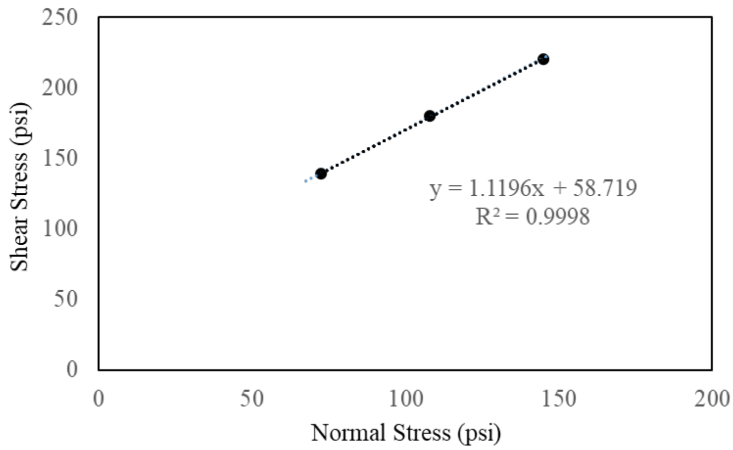

FIGURE 5.5: Mohr-Coulomb principle at 2.54 mm/min, based on the data in TABLE 5.6

TABLE 5.7 presents the interpreted shear strength parameters (angle of internal friction and cohesion) derived from FIGURE 5.5.

TABLE 5.7: The interpreted shear strength parameters

Friction Angle ϕ°	**Cohesion C (psi)**
48.21	58.719

TABLE 5.8 summarizes the mean interface shear stress values at a 5 mm/min displacement rate.

TABLE 5.8: Summary of the mean interface shear stress at 5 mm/min displacement rate

Normal Stress σ (psi)	**Shear Stress τ (psi)**
72	162
108	193
145	259

FIGURE 5.6 illustrates the Mohr-Coulomb principle at a 5 mm/min displacement rate, based on the data presented in TABLE 5.8.

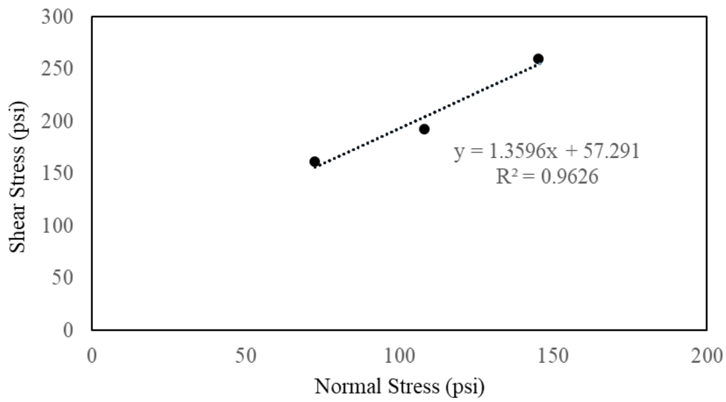

FIGURE 5.6: Mohr-Coulomb principle at 5 mm/min, based on the data in TABLE 5.8

TABLE 5.9 presents the interpreted shear strength parameters (angle of internal friction and cohesion) derived from FIGURE 5.6.

TABLE 5.9: The interpreted shear strength parameters

Friction Angle ϕ°	**Cohesion C (psi)**
53.65	57.291

At higher shear rates (1–5 mm/min), the friction angle increased with loading rate. The cohesion values did not change consistently. To examine this behavior further, additional tests were carried out at lower shear rates (0.1–0.5 mm/min). This was done to check whether the same trend holds for both friction and cohesion. The results from direct shear tests performed at shear rates of 0.1 mm/min, 0.25 mm/min, and 0.5 mm/min under normal stresses of 72 psi, 108 psi, and 145 psi, respectively, are shown in FIGURES 5.7 to 5.9.

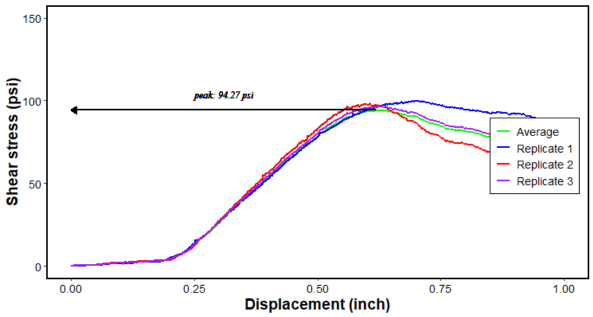

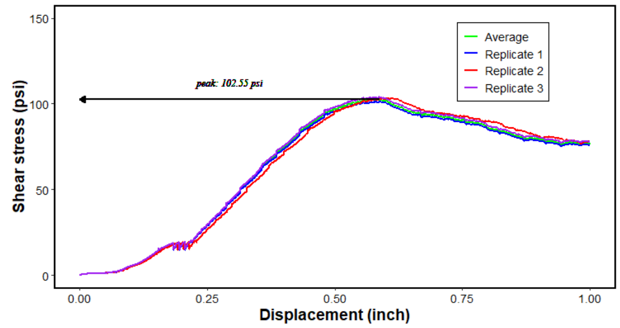

(a) 0.1 mm/min (b) 0.25 mm/min

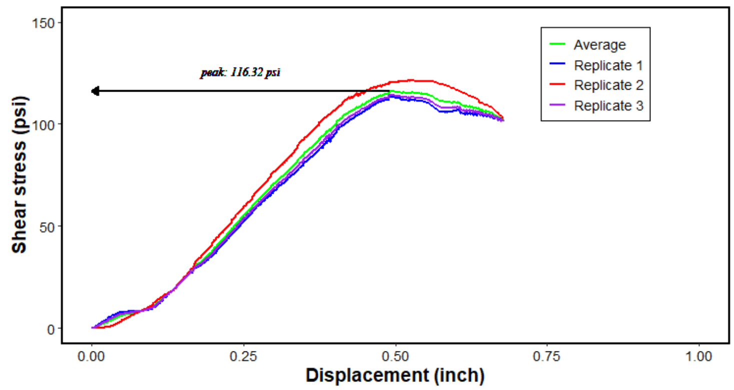

(c) 0.5 mm/min

FIGURE 5.7: Direct shear test results for different displacement rates at 72 psi normal load

TABLE 5.10 summarizes the results as shown in FIGURE 5.7, where the tests were performed at a normal stress of 72 psi with displacement rates of 1 mm/min, 2.54 mm/min, and 5 mm/min.

TABLE 5.10: Conducted direct shear tests at 72 psi normal load on double-layered AC specimens

Normal stress (psi)	**72 psi**		
Loading rate (mm/min)	r_1=0.1	r_2=0.25	r_3=0.5
Shear strength (psi) Replicate 1	92.84	101.33	113.80
Shear strength Rep 2 (psi) Replicate 2	98.53	103.36	121.40
Shear strength (psi) Replicate 3	91.44	102.93	114.62
Coefficient of Variance (%)	3.98	1.04	3.58
Average shear strength (psi)	94.27	102.94	116.61

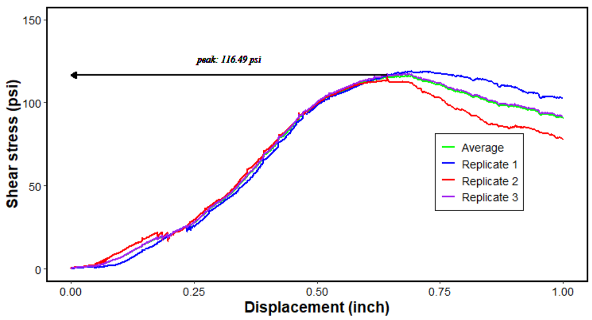

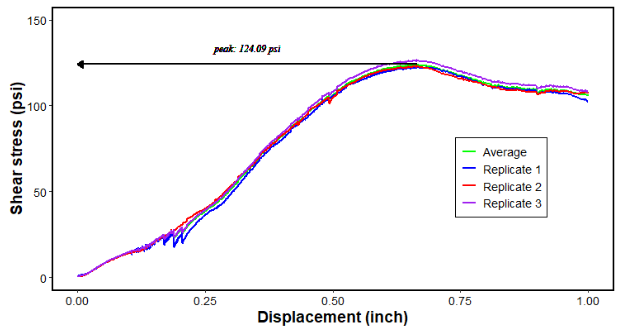

(a) 0.1 mm/min

(b) 0.25 mm/min

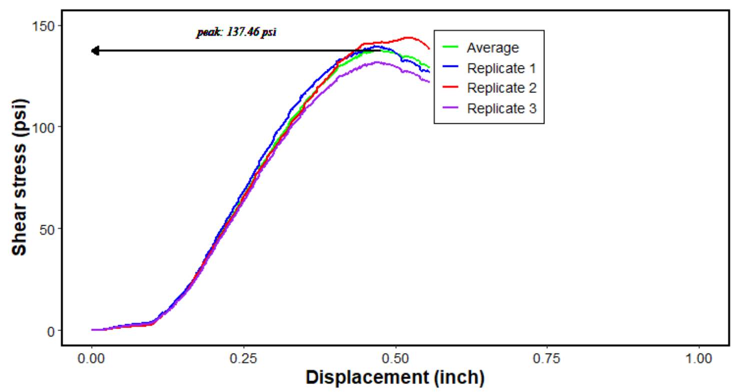

(c) 0.5 mm/min

FIGURE 5.8: Direct shear test results for different displacement rates at 108 psi normal load

TABLE 5.11 summarizes the results as shown in FIGURE 4.8a to 4.8c, where the tests were performed at a normal stress of 108 psi with displacement rates of 0.1 mm/min, 0.25 mm/min, and 0.5 mm/min.

TABLE 5.11: Conducted direct shear tests on double-layered AC specimens at 108 psi Normal Load

Normal stress (psi)	**108 psi**		
Loading rate (mm/min)	r_1=0.1	r_2=0.25	r_3=0.5
Shear strength (psi) Replicate 1	119.17	122.53	139.58
Shear strength Rep 2 (psi) Replicate 2	115.61	123.20	143.42
Shear strength (psi) Replicate 3	117.57	126.45	131.58
Coefficient of Variance (%)	1.52	1.69	4.37
Average shear strength (psi)	117	124	137

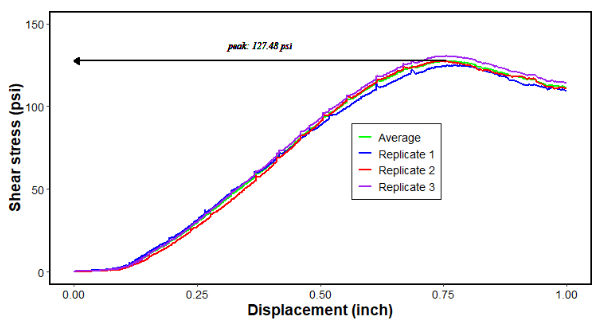

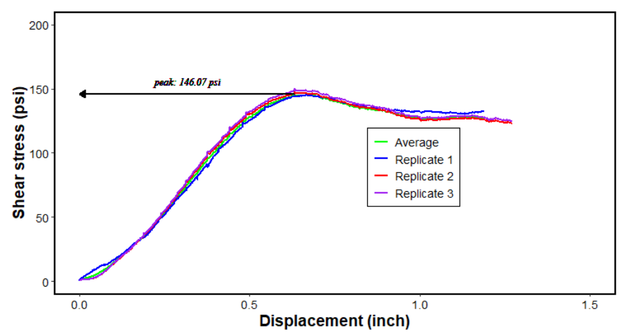

(a) 0.1 mm/min (b) 0.25 mm/min

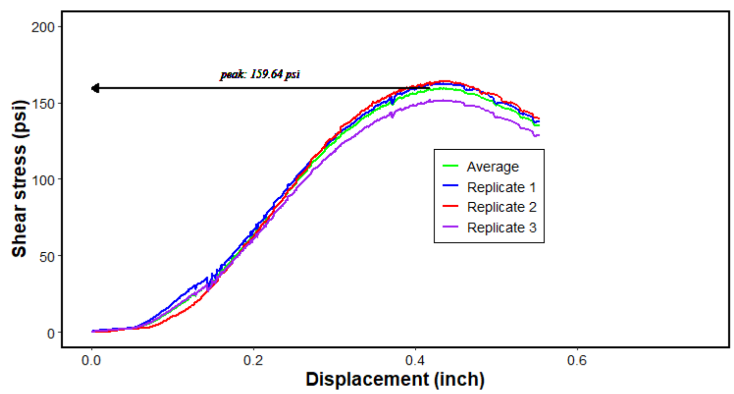

(c) 0.5 mm/min

FIGURE 5.9: Direct shear test results for different displacement rates at 145 psi normal load

TABLE 5.12 summarizes the results as shown in FIGURE 5.9a to 5.9c, where the tests were performed at a normal stress of 145 psi with displacement rates of 0.1 mm/min, 0.25 mm/min, and 0.5 mm/min.

TABLE 5.12: Direct shear tests on double-layered AC specimens at 145 psi Normal Load

Normal stress (psi)	**145 psi**		
Loading rate (mm/min)	r_1=0.1	r_2=0.25	r_3=0.5
Shear strength (psi) Replicate 1	124.83	139.18	163.57
Shear strength Rep 2 (psi) Replicate 2	127.42	142.46	164.06
Shear strength (psi) Replicate 3	130.50	144.45	152.05
Coefficient of Variance (%)	2.22	1.87	4.25
Average shear strength (psi)	127	142	159

To analyze by the Mohr-Coulomb principles, the average interface shear stress values obtained at 0.1 mm/min, 0.25 mm/min, and 0.5 mm/min displacement rates were plotted against the corresponding normal stress values. This resulted in a linear relationship, indicating that the interface shear strength increased with an increase in the normal stress.

TABLE 5.13 summarizes the mean interface shear stress values at a 0.1 mm/min displacement rate.

TABLE 5.13: Summary of the mean interface shear stress at 0.1 mm/min displacement rate

Normal Stress σ (psi)	**Shear Stress τ (psi)**
72	94.27
108	117.45
145	127.48

FIGURE 5.10 illustrates the Mohr-Coulomb principle at a 0.1 mm/min displacement rate, based on the data presented in TABLE 5.13. The plot shows a linear relationship between shear stress

and normal stress, with the corresponding angle of internal friction and cohesion values calculated from the linear equation.

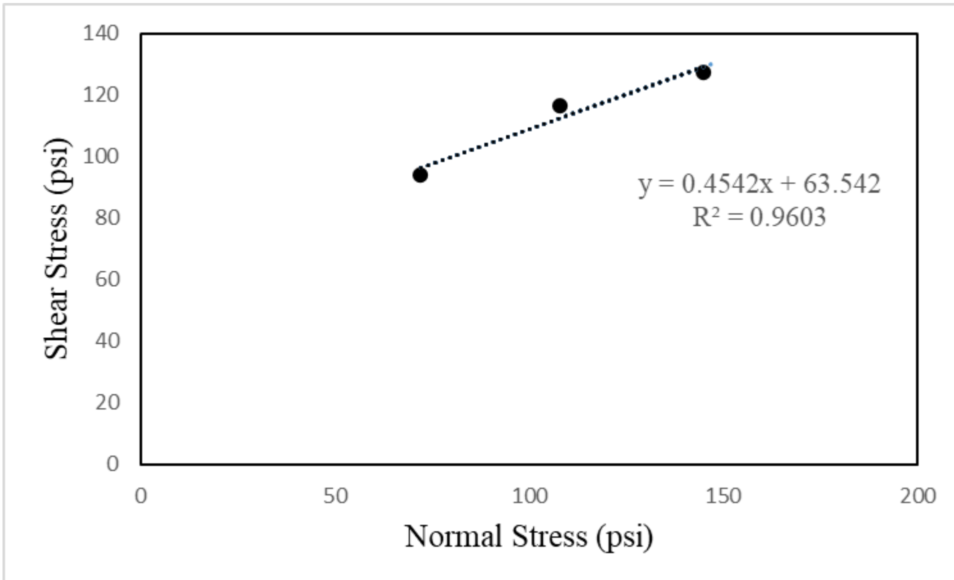

FIGURE 5.10: Mohr-Coulomb principle at 0.1 mm/min, based on the data in TABLE 5.13

TABLE 5.14 presents the interpreted shear strength parameters (angle of internal friction and cohesion) derived from FIGURE 5.10.

TABLE 5.14: The interpreted shear strength parameters

Friction Angle ϕ°	**Cohesion C (psi)**
24.42	63.52

TABLE 5.15 summarizes the mean interface shear stress values at a 0.25 mm/min displacement rate.

TABLE 5.15: Summary of the mean interface shear stress at 0.25 mm/min displacement rate

Normal Stress σ (kPa)	**Shear Stress τ (psi)**
72	102.94
108	124.08
145	142.03

FIGURE 5.11 illustrates the Mohr-Coulomb principle at a 0.25 mm/min displacement rate, based on the data presented in TABLE 5.15. The plot also shows a linear relationship between shear stress and normal stress, with the corresponding angle of internal friction and cohesion values calculated from the linear equation.

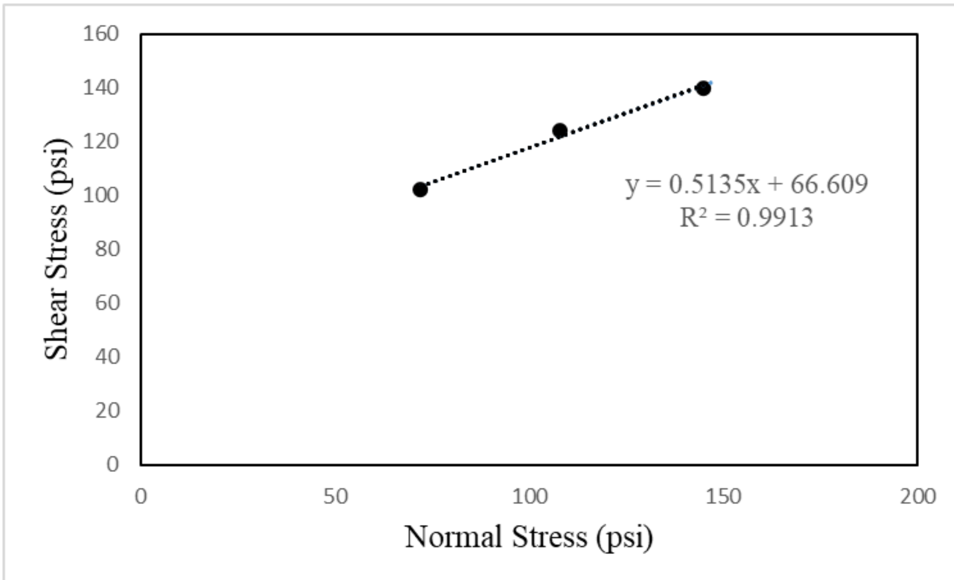

FIGURE 5.11: Mohr-Coulomb principle at 0.25 mm/min, based on the data in TABLE 5.15

TABLE 5.16 presents the interpreted shear strength parameters (angle of internal friction and cohesion) derived from FIGURE 4.11.

TABLE 5.16: The interpreted shear strength parameters

Friction Angle ϕ°	**Cohesion C (psi)**
27.15	66.61

TABLE 5.17 summarizes the mean interface shear stress values at a 0.5 mm/min displacement rate.

TABLE 5.17: Summary of the mean interface shear stress at 0.5 mm/min displacement rate

Normal Stress σ (kPa)	**Shear Stress τ (psi)**
72	116.61
108	137.45
145	159.64

FIGURE 5.12 illustrates the Mohr-Coulomb principle at a 0.5 mm/min displacement rate, based on the data presented in TABLE 5.17.

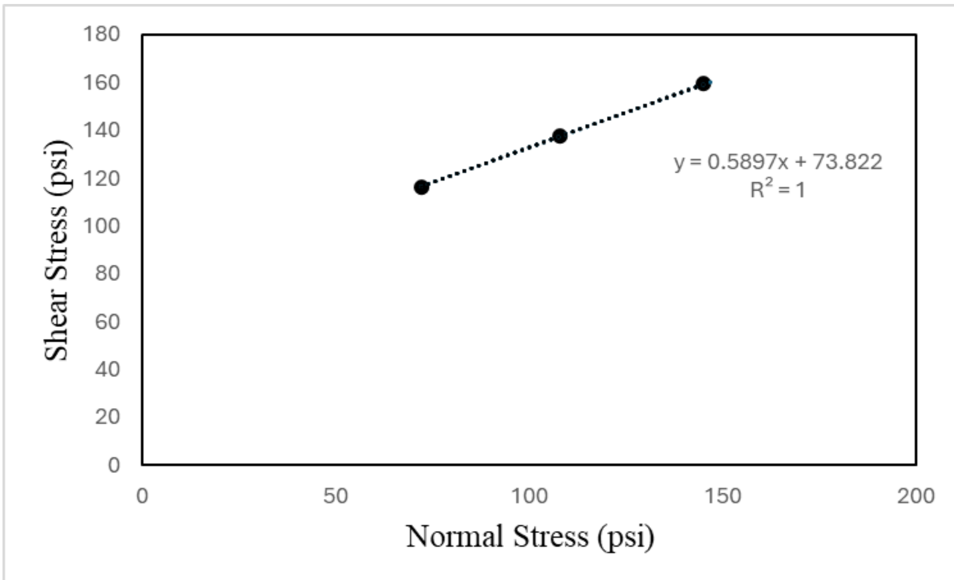

FIGURE 5.12: Mohr-Coulomb principle at 0.5 mm/min, based on the data in TABLE 5.17

TABLE 5.18 presents the interpreted shear strength parameters (angle of internal friction and cohesion) derived from FIGURE 5.12.

TABLE 5.18: The interpreted shear strength parameters

Friction Angle ϕ°	Cohesion C (psi)
30.52	73.82

5.2.1 Statistical Influence of Shear Rate on Shear Strength Parameters

The interpreted shear strength parameters obtained from the Mohr–Coulomb envelopes are summarized in TABLE 5.19.

TABLE 5.19: Summary of interpreted shear strength parameters at different shear rates

Shear Rate (mm/min)	Friction Angle (°)	Cohesion (psi)
0.1	24.42	63.52
0.25	27.15	66.61
0.5	30.52	73.82
1	43.58	406.95
2.54	48.23	402.71
5	53.59	395.07

The results show that the angle of internal friction increased as the shear rate increased. At lower displacement rates (0.1–0.5 mm/min), the friction angle ranged from 24.42° to 30.52°. At higher displacement rates (1–5 mm/min), the friction angle increased further, reaching 53.59° at 5 mm/min. This trend indicates that the frictional resistance at the asphalt interface becomes more dominant at higher shear rates.

In contrast, the cohesion parameter did not show a consistent increasing trend across the entire shear rate range. Cohesion values remained relatively stable within each testing group, although differences were observed between the lower and higher shear rate ranges.

To determine whether shear rate significantly influences the interpreted shear strength parameters, a one-way analysis of variance (ANOVA) was performed. The ANOVA results are summarized in TABLE 5.20.

TABLE 5.20: ANOVA results for the influence of shear rate on shear strength parameters

Parameter	*p*-value
Friction Angle	0.0527
Cohesion	0.0831

The ANOVA results indicate that the friction angle shows a near-significant dependence on shear rate**.** The *p*-value of 0.0527 is close to the commonly accepted significance level of 0.05. This suggests that shear rate may influence the frictional component of interface resistance.

In contrast, the cohesion parameter does not show a statistically significant dependence on shear rate. The p-value of 0.0831 indicates that variations in cohesion among the shear rate groups are not statistically significant.

These findings suggest that shear rate primarily affects the frictional component of interface shear resistance, while the adhesive bonding component, represented by cohesion, remains relatively stable.

5.3 Bending Stress of Beam-Shaped Samples

The bending test of an asphalt concrete beam was conducted to evaluate its mechanical properties when subjected to bending failure at loading rates of 1 mm/min. The beam used in this test had a length of 150 ± 2.0 mm and a cross-sectional area of 50 ± 2.0 mm in both width and height. During the test, the load was applied to the center of the beam until it fractured. The data collected from this test were used to determine the bending strength at the point of maximum load. FIGURE 5.13a-5.13d shows the test sample, sample schematic, test set-up, and some tested samples:

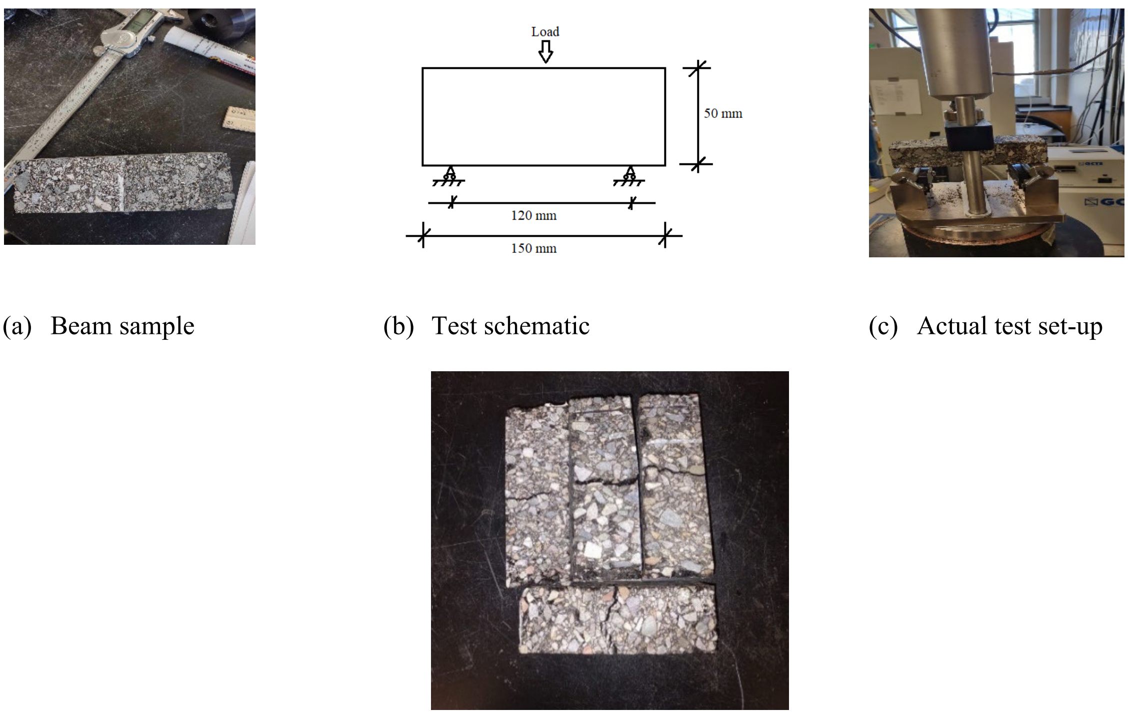

(a) Beam sample (b) Test schematic (c) Actual test set-up

(d) Tested samples

FIGURE 5.13: Beam bending test

FIGURES 5.14(a) – 5.14(d) show the average bending stress for the specimens with different tack coat application rates. The average bending stress for the specimens prepared with no tack coat is 8.25 psf. The bending stress is calculated from the formula:

$$\sigma = \frac{Mc}{I} \qquad \text{Eq. 2}$$

σ = bending stress (psf)

M = the internal bending moment about the section's neutral axis (kip-ft)
c = the perpendicular distance from the neutral axis to the farthest point of the section (ft)
I = the moment of inertia of the section area about the neutral axis (ft^4)

Similarly, test results for specimens prepared with 0.04, 0.06, and 0.08 gal/yd^2 tack coats are presented in FIGURES 4.14(b)-4.14(d). The average bending stress of specimens prepared with 0.04, 0.06, and 0.08 gal/yd^2 tack coats is 8.57, 8.42, and 8.31 psf, respectively. A one-way ANOVA analysis showed that the differences in bending stress with application rates are not significant.

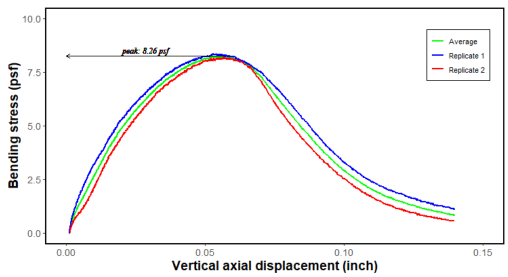

(e) No tack coat (0 gal/yd^2)

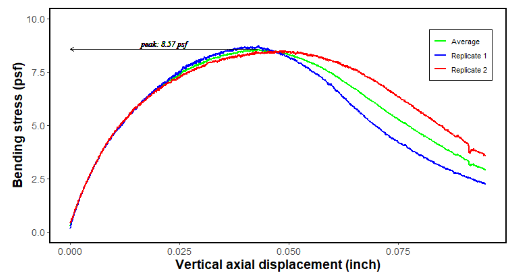

(f) 0.04 gal/yd^2

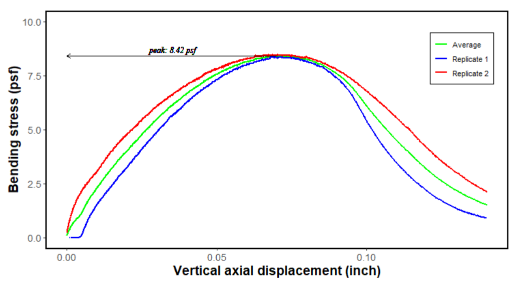

(g) 0.06 gal/yd^2

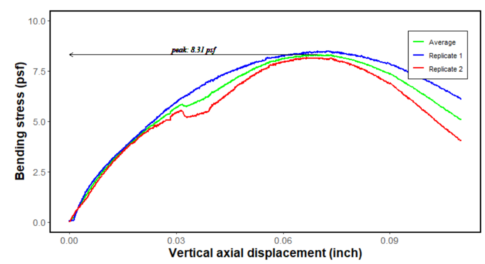

(h) 0.08 gal/yd^2

FIGURE 5.14: Beam Bending Test Results for Different Application Rates

5.4 Effect of Moisture Damage

To simulate the moisture damage, this study utilized the moisture-induced stress test (MIST) on the double-layered specimens. The MIST test (FIGURE 5.15) is used to simulate moisture damage by applying a cyclic hydrostatic pressure at an elevated temperature. The specimen was subjected to 3500 cycles of 39.9 psi pore pressure at 140°F to simulate moisture damage using a hydraulic pump and piston system.

(a)

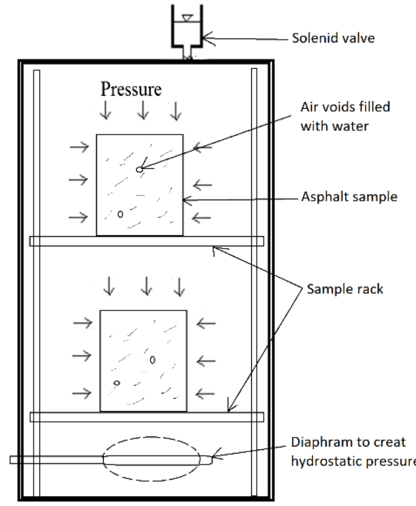

(b)

FIGURE 5.15: Moisture-induced stress test: (a) MIST chamber, and (b) test schematic

FIGURE 5.16 shows the results found from the direct shear test results for specimens prepared with different amounts of tack coat emulsion. The average shear strength for the unconditioned specimens prepared with SS-1H tack coat is 242.98 psi. Similarly, direct shear test results for specimens prepared with SS-1HP, CSS-1H, CSS-1HP, and trackless tack coats are presented in FIGURES 4.16(b)- 4.16(e). The average interface shear strengths of specimens prepared with SS-1HP, CSS-1H, CSS-1HP, and trackless tack coats are 264.22 psi, 228.75 psi, 253.97 psi, and 241.94 psi, respectively.

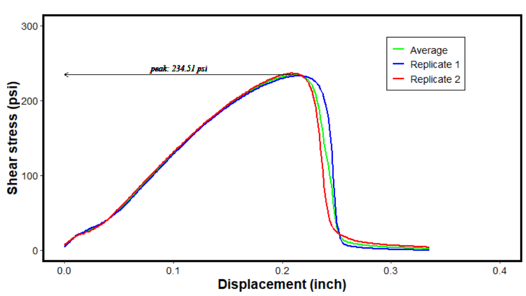

(a) SS-1H

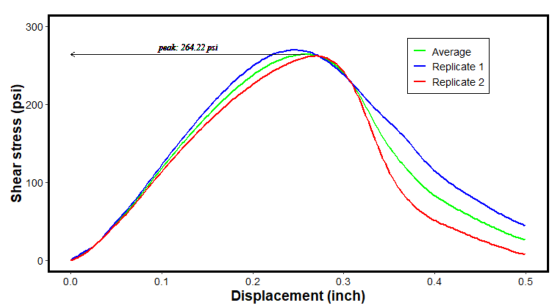

b) SS-1HP

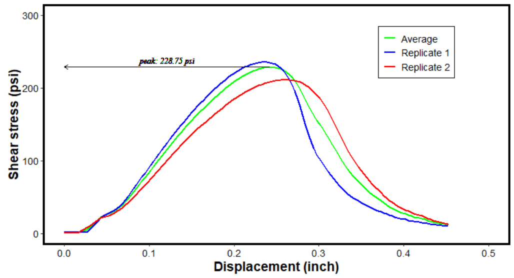

(b) CSS-1H

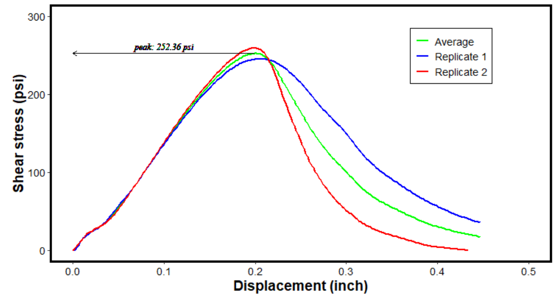

(c) CSS-1HP

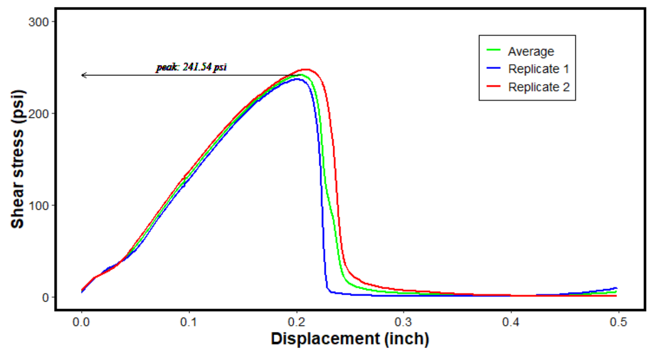

(d) **Trackless Tack**

FIGURE 5.16: Direct Shear Test Results for unconditioned Samples

The average shear strength for the MIST conditioned specimens prepared with SS-1H tack coat is 195.47psi (FIGURE 4.17a). Similarly, direct shear test results for specimens prepared with SS-1HP, CSS-1H, CSS-1HP, and trackless tack coats are presented in FIGURES 5.17(b)-5.17(e). The average interface shear strengths of specimens prepared with SS-1HP, CSS-1H, CSS-1HP, and trackless tack coats are 219.91psi, 172.09 psi, 214.21 psi, and 227.03 psi, respectively.

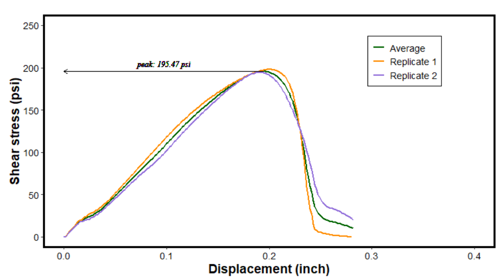

a) SS-1H

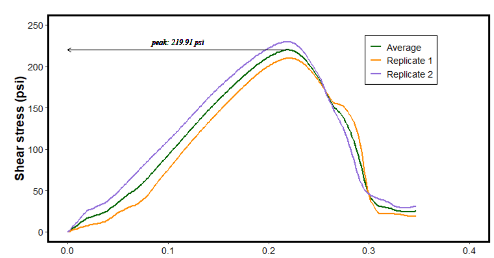

b) SS-1HP

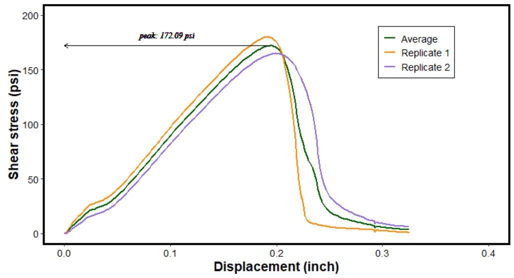

c) CSS-1H

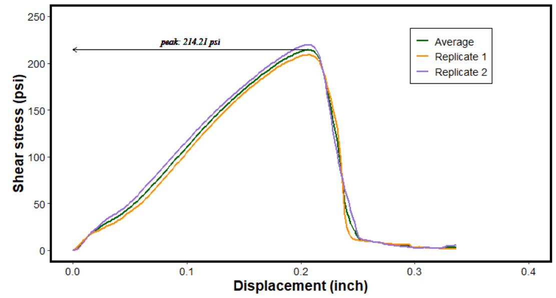

d) CSS-1HP

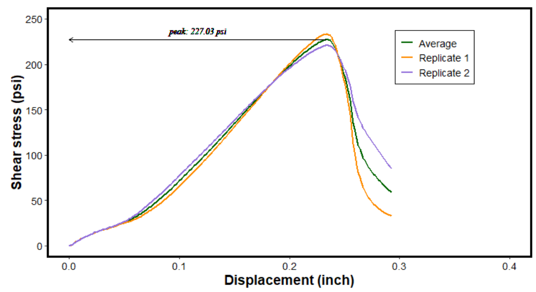

e) **Trackless Tack**

FIGURE 5.17: Direct Shear Test Results for MIST Conditioned Samples

TABLE 5.21 shows the interface shear strengths of the unconditioned specimens and MIST-conditioned specimens.

TABLE 5.21: Interface shear strength with different tacks for unconditioned and conditioned specimens

Conditioning states	ISS with SS-1H (psi)	ISS with SS-1HP (psi)	ISS with CSS-1H (psi)	ISS with CSS-1HP (psi)	ISS with Trackless Tack (psi)
Unconditioned	242.94	264.22	228.75	252.36	241.54
MIST conditioned	195.47	219.91	172.09	214.21	227.03
Difference	20%	16%	24%	15%	6%

FIGURE 5.18 shows the reduction in interface shear strength due to MIST conditioning. The largest reduction was observed for CSS-1H, and the smallest reduction was observed for trackless tack**.**

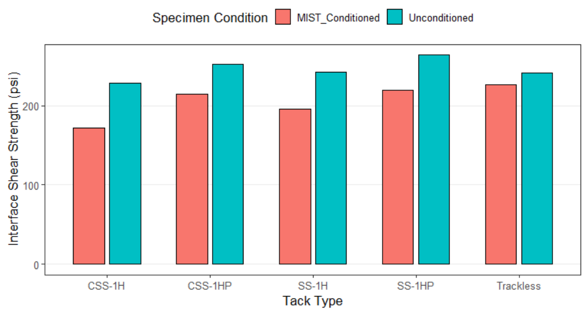

(a)

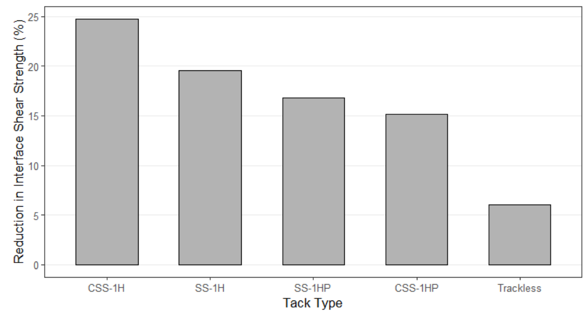

(b)

FIGURE 5.18: Comparison between unconditioned MIST conditioned states (a) Interface shear strength of different tack types at both states (b) Percentage reduction in interface shear strength due to MIST conditioning for the corresponding tack types

A paired t-test (TABLE 5.22) was conducted to determine whether there is a statistically significant difference between the paired measurements from the unconditioned and MIST-conditioned groups. The results indicate a significant difference ($p < 0.01$), with the MIST-conditioned group exhibiting a substantially lower mean value by approximately 40.22 psi. The 95% confidence interval shows that the true mean difference lies between 20.54 and 59.90 psi.

TABLE 5.22: Results of paired t-test comparing unconditioned and MIST-conditioned states

Parameter	Values
Test Statistic (*t*)	5.6742
Degrees of Freedom (*df*)	4
95% Confidence Interval (*CI*)	20.54 to 59.90
Significance (*p*)	0.004759

5.5 Temperature Effect

5.5.1 Temperature effect on CSS-1H

FIGURE 5.19 shows the results found from the direct shear test for specimens prepared with different amounts of tack coat emulsion. FIGURE 5.19(a) shows the direct shear test results of two specimens prepared with no tack coating. The average shear strength for the specimens prepared with no tack coat is 47.56 psi. Similarly, direct shear test results for specimens prepared with 0.04, 0.06, and 0.08 gal/yd^2 tack coats are presented in FIGURES 5.19(b)-5.19(d). The average shear strengths of specimens prepared with 0.04, 0.06, and 0.08 gal/yd^2 tack coats are 43.83, 40.76, and 33.49 psi, respectively.

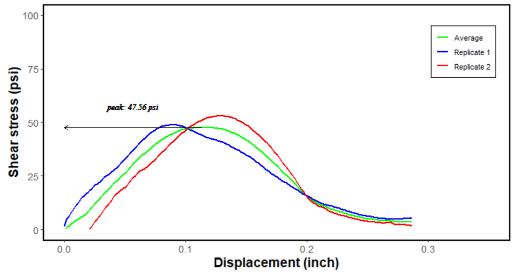

a. No tack coat (0 gal/yd²)

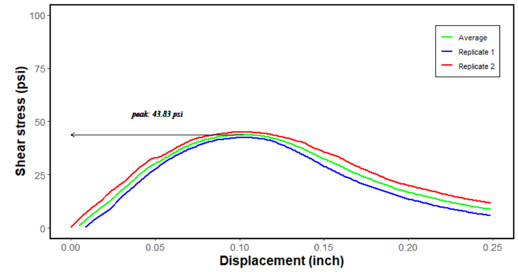

b. 0.04 gal/yd²

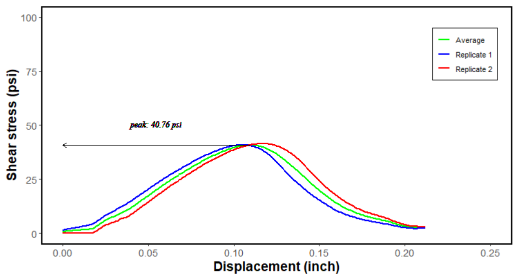

c. 0.06 gal/yd²

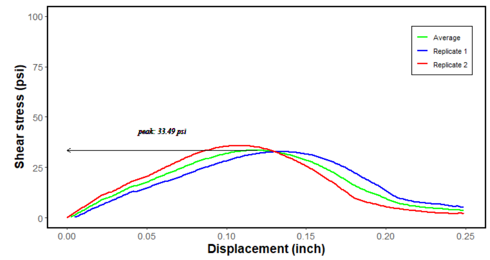

d. 0.08 gal/yd²

FIGURE 5.19: Direct Shear Test Results for Different Application Rates of CSS-1H at 131°F

FIGURE 5.20 shows an inverse relationship between the tack coat application rate and the shear strength of the interface. As the tack coat application rate increases, the shear strength decreases. The shear strength value decreases from 47.56 to 33.49 psi as the tack coat application rate increases from 0 to 0.08 gal/yd^2.

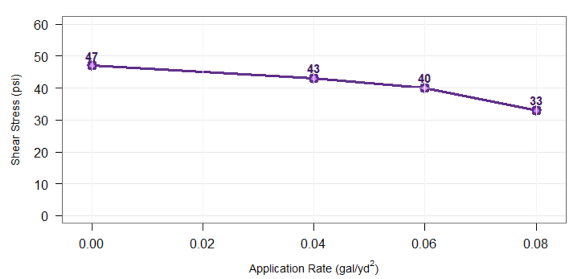

FIGURE 5.20: Shear strength at 131°F for different application rate of CSS-1H

FIGURE 5.21 shows the distribution of interfacial shear strength values obtained from direct shear tests conducted at two different temperatures.

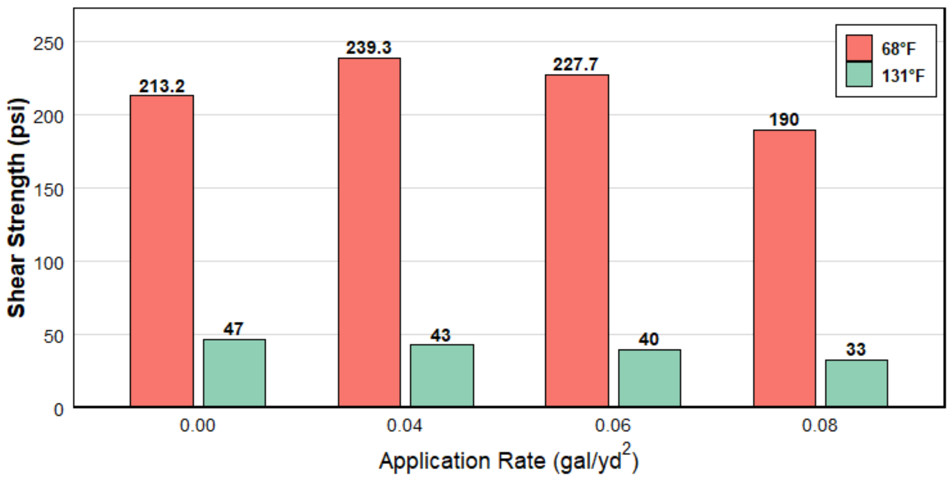

FIGURE 5.21: Shear strength at 68°F versus 131°F at different application rate

5.5.2 Temperature effect on SS-1H

FIGURE 5.22 shows the results found from the direct shear test results for tested specimens prepared with different amounts of tack coat emulsion. FIGURE 5.22 (a) shows the direct shear test results of two specimens prepared with no tack coating. The average shear strength for the specimens prepared with no tack coat is 47.56 psi. Similarly, direct shear test results for specimens prepared with 0.04, 0.06, and 0.08 gal/yd^2 tack coats are presented in FIGURES 5.22 (b)- 5.22 (d). The average shear strengths of specimens prepared with 0.04, 0.06, and 0.08 gal/yd^2 tack coats are 44.34, 42.59, and 34.57 psi, respectively.

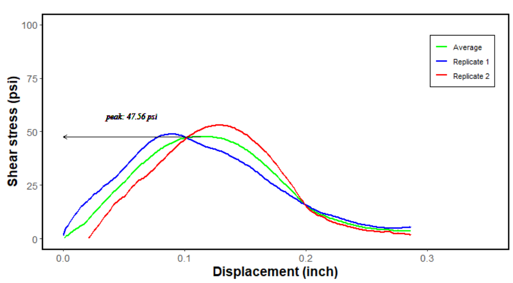

(a) No tack coat (0 gal/yd^2)

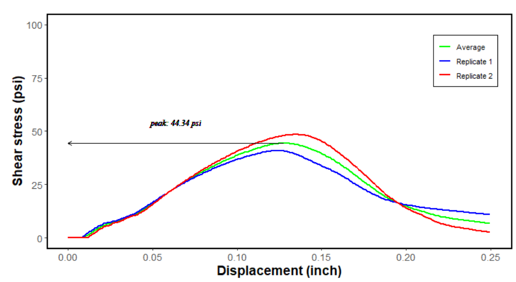

(b) 0.04 gal/yd^2

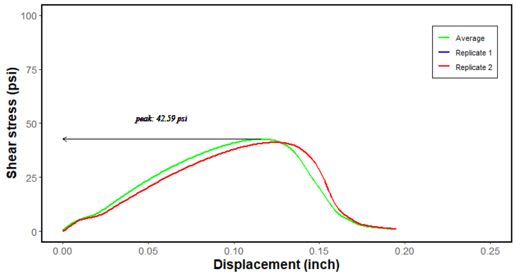

(c) 0.06 gal/yd^2

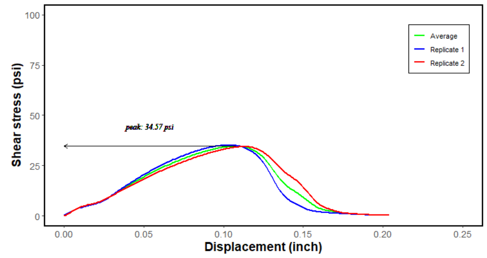

(d) 0.08 gal/yd^2

FIGURE 5.22: Direct Shear Test Results for Different Application Rates of SS-1H at 131°F

FIGURE 5.23 shows an inverse relationship between the tack coat application rate and the shear strength of the interface. As the tack coat application rate increases, the shear strength decreases. The shear strength value decreases from 48 psi to 35 psi as the tack coat application rate increases from 0 to 0.08 gal/yd^2.

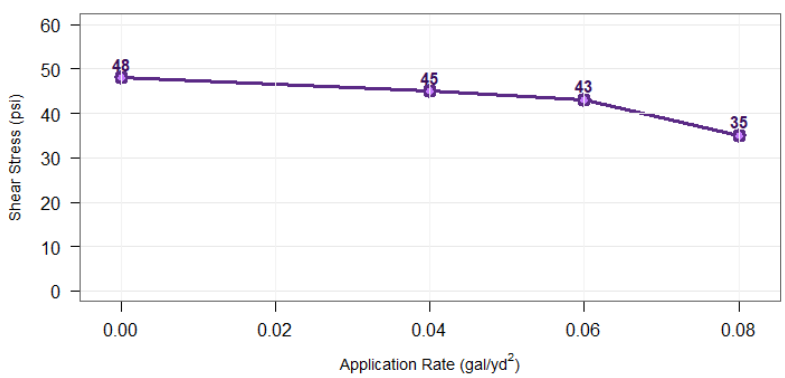

FIGURE 5.23: Shear strength of SS-1H samples at 131°F

FIGURE 5.24 shows the distribution of interfacial shear strength values obtained for SS-1H specimens from direct shear tests conducted at two different temperatures.

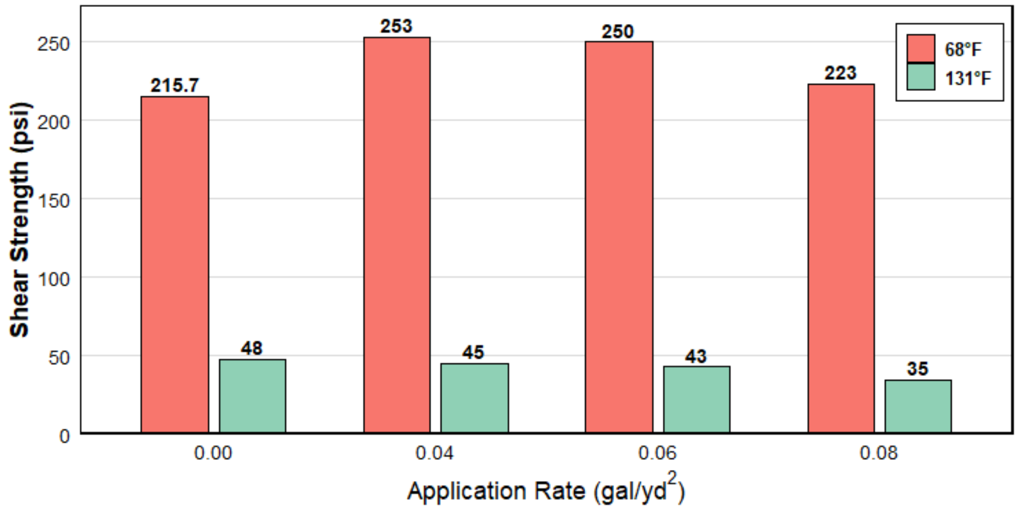

FIGURE 5.24: Shear strength at 68°F versus 131°F at different application rates for SS-1H

5.6 Effect of Surface Roughness

Surface texture plays an important role in interface behavior. Rougher surfaces promote mechanical interlocking between layers. This interaction increases resistance to shear loading along with friction and cohesion. As a result, higher interface shear strength is generally observed for rougher interfaces.

Field Core as Bottom Layer

Field cores were taken at various locations throughout the westbound lanes of I-40. The bottom end of the cored specimens was trimmed to 3" height (75 mm) with a saw machine, as shown in FIGURE 5.25.

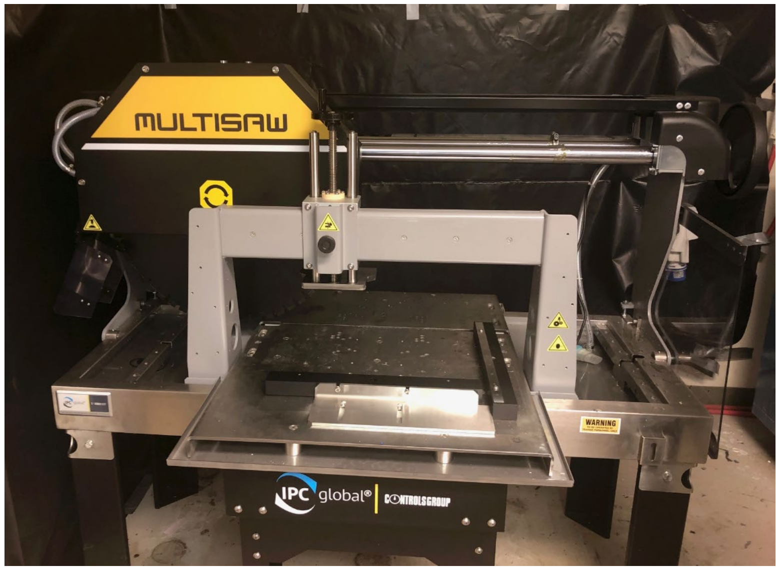

FIGURE 5.25: Saw Machine for Specimen Cutting

The diameter of the field cores was slightly larger than the inside diameter of the compaction mold. Therefore, the side of the specimen must be sanded so that it can be reinserted into the compaction mold. FIGURE 5.26 shows the belt sander used in this study.

(a) 6.11-Inch Dia Field Core

(b) Sand Grinding Field Core's Peripheral Side

FIGURE 5.26: Field Core’s Dia Measurement and Sand Grinding

Binder Content and Aggregate Gradation

The ignition method by the NCAT oven, standardized by AASHTO T 308, was used for determining the asphalt binder content in the field cores. In this process, an HMA sample is heated in a high-temperature oven to burn off the asphalt binder completely, leaving only the aggregate behind. The binder content is then calculated by comparing the sample's weight before and after ignition.

The formula used in this method:

$$Asphalt\ content\ = \frac{w_s - w_a}{w_s} \qquad \text{Eq. 3}$$

Where,

w_s = Initial weight of aggregates with binder

w_a = weights of the aggregate after the method.

The correction factor (*CF*) was calculated by averaging two known HMA specimens. The formula for calculating the correction factor:

$$CF\ =\ (known\ value\ of\ binder\ content\ -\ binder\ content\ from\ ignition\ oven) \qquad \text{Eqn. 4}$$

The binder content from the NCAT oven later matched with the binder content determined by the solvent extraction method as specified in AASHTO T 164. The calculated asphalt content was: (a) Ignition method's asphalt content = 4.8%, and (b) Solvent Extraction method's asphalt content = 4.3%.

FIGURE 5.27 shows the aggregates gradation found from these two methods:

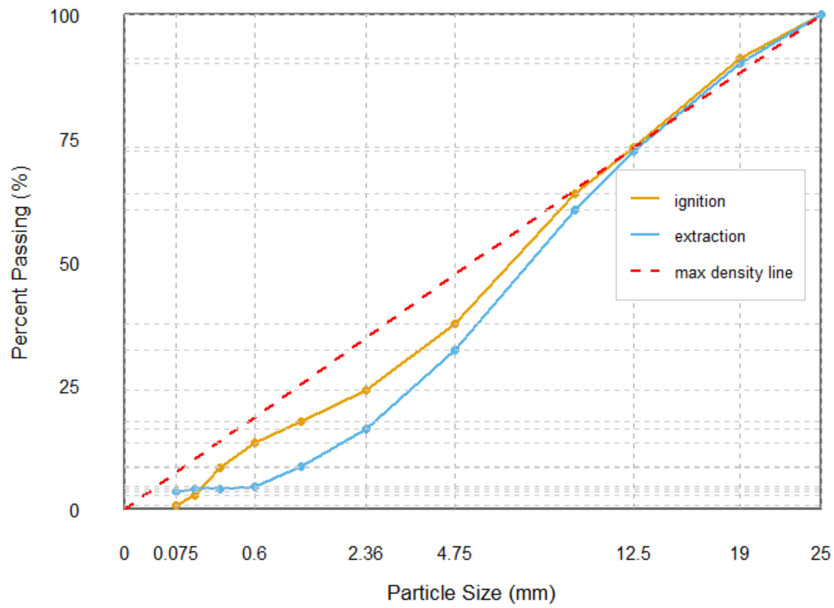

FIGURE 5.27: 0.45 Power Gradation Curve

Texture Roughness Determination

The sample roughness was measured with a sand-patch test with a modification of ASTM E965 for a lab experiment. The sand patch test involves filling the spaces between particles with sand, as shown in FIGURE 5.28.

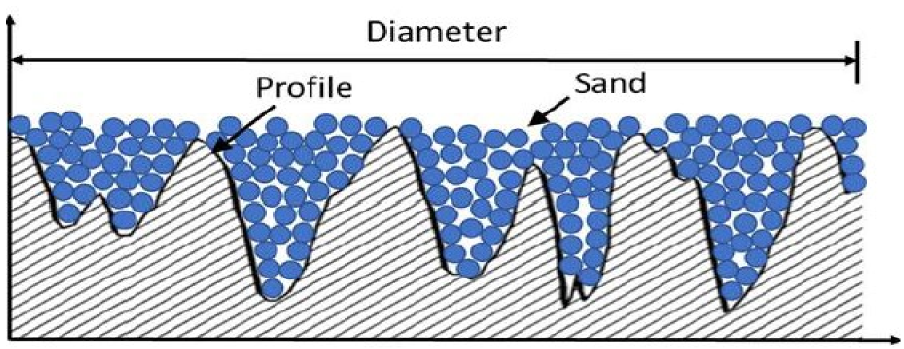

FIGURE 5.28: A Sand-Filled Milled Surface

The graduated cylinder and an ice hockey puck (according to ASTM E965), which is considered suitable for use as the hard rubber material in this test method to spread the sand, are shown in FIGURE 5.29.

FIGURE 5.29: Determination of Macrotexture Depth of Milled Surface Using the Sand Patch Test

Eq. 5 provides the formula for determining average texture depth. In millimeters cubed, *V* is the volume of sand utilized. *D* is the sand patch circle's average diameter, measured in millimeters (inches).

$$Texture\ depth\ = \frac{4V}{\pi D^2} \qquad \text{Eq. 5}$$

TABLE 5.23 shows the sand patch test results calculated by Equation 5.

TABLE 5.23**:** Milled Cores Macrotexture Depth

Sample #	**Diameter (mm)**	**Volume of sand (mm^3)**	**Texture depth (mm)**	**Texture Depth (inch)**
sample 1	150	17945.10	1.02	0.04
Sample 2	150	31403.93	1.78	0.07
Sample 3	150	44862.75	2.54	0.10
Sample 4	150	26917.65	1.52	0.06
Sample 5	150	62807.85	3.56	0.14
Sample 6	150	26917.65	1.52	0.06
Sample 7	150	40376.48	2.29	0.09
Sample 8	150	98698.05	5.59	0.22
Sample 9	150	49349.03	2.79	0.11
Sample 10	150	53835.30	3.05	0.12
Sample 11	150	31403.93	1.78	0.07
Sample 12	150	49349.03	2.79	0.11
Sample 13	150	53835.30	3.05	0.12
Sample 14	150	76266.68	4.32	0.17
Sample 15	150	62807.85	3.56	0.14
Sample 16	150	31403.93	1.78	0.07
Sample 17	150	80752.95	4.57	0.18
Sample 18	150	62807.85	3.56	0.14
Sample 19	150	26917.65	1.52	0.06
Sample 20	150	89725.50	5.08	0.20

The sand patch test results were subsequently validated using a digital caliper (see FIGURE 5.30) to measure 20 prominent data points across three sections of the top surface, from which the RMS roughness was calculated. This method is established for assessing the texture depth of geomaterials. The coefficient of variance was found to be between 8 to 12%.

(a) **(b)**

FIGURE 5.30: sand patch test results validation (a)Set Up a Reference Plane (b) Texture Depth

FIGURE 5.31 shows the results found from the direct shear tests. Mechanical interlocking was present between the two surfaces.

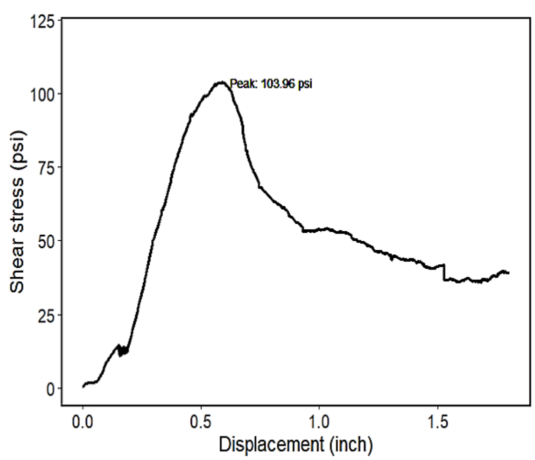

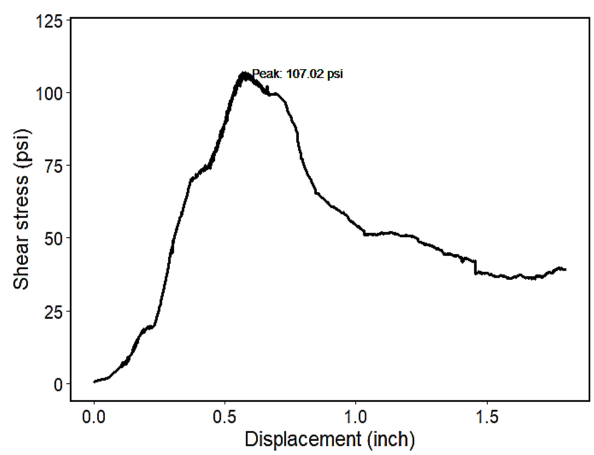

(e) 0.0712 inch

(f) 0.1124 inch

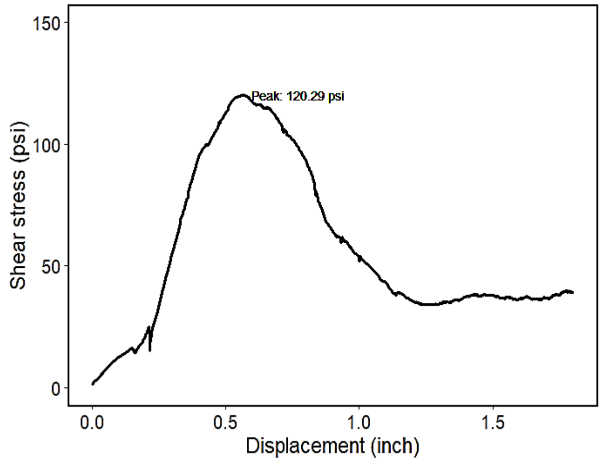

(g) 0.165 inch

FIGURE 5.31: Direct Shear Test Results for 0.08 gal/yd^2 Application Rate

TABLE 5.24 summarizes the results as shown in FIGURE 30a to 30c, where the tests were performed at a normal stress of 200 kPa with displacement rates of 2.54 mm/min. The tack coat application rate at the interface is 0.08 gal/yd^2.

TABLE 5.24: Conducted Direct Shear Tests at 0.08 gal/yd^2 Application Rate

Roughness (inch)	Shear Strength (psi)
0.0712	102.4431
0.1124	108.4790
0.1654	119.2537

FIGURE 5.32 shows the results found from the direct shear tests with a 0.06 gal/yd^2 application rate.

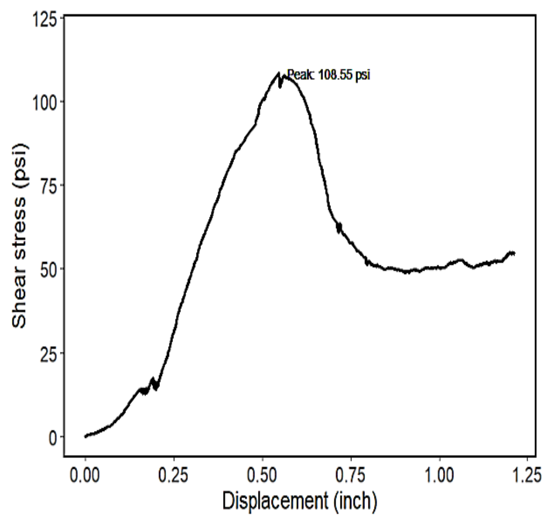

(a) 0.074 inch

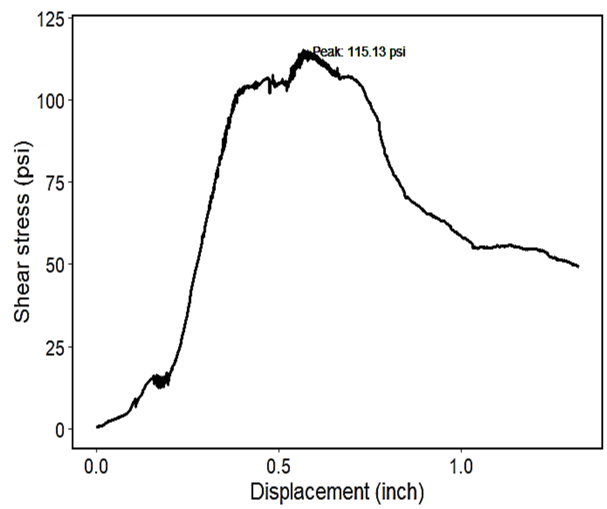

(b) 0.124 inch

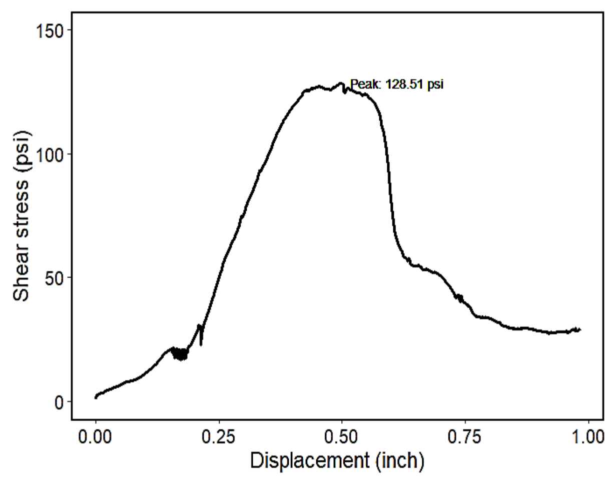

(c) 0.195 inch

FIGURE 5.32: Direct Shear Test Results For 0.06 gal/yd^2 Application Rate

TABLE 5.25 summarizes the results as shown in FIGURE 5.32, where the tests were performed at a normal stress of 29 psi with displacement rates of 2.54 mm/min. The tack coat application rate at the interface is 0.06 gal/yd^2.

TABLE 5.25: Conducted Direct Shear Tests at 0.06 gal/yd^2 Application Rate

Roughness (inch)	Shear Strength (psi)
0.074	107.6233
0.1235	115.6646
0.1952	127.3975

FIGURE 5.33 shows the results found from the direct shear tests with a 0.04 gal/yd^2 application rate.

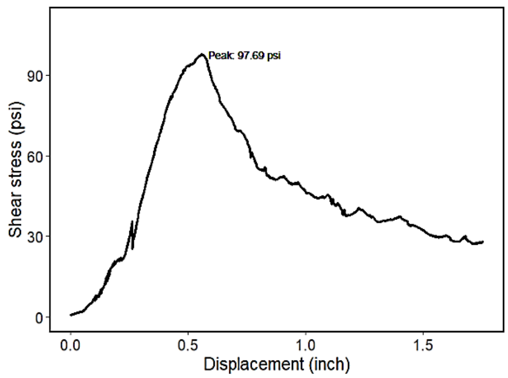

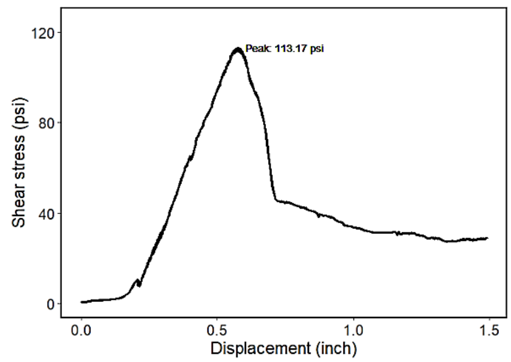

(a) 0.064 inch

(b) 0.0984 inch

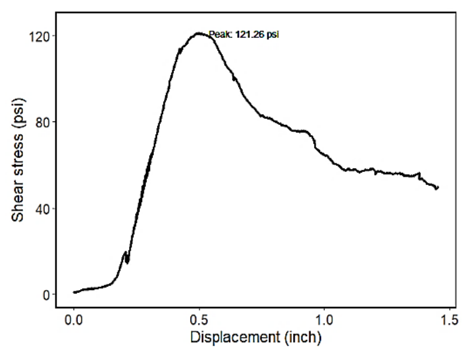

FIGURE 5.33: Direct Shear Test Results For 0.04 gal/yd^2 Application Rate

TABLE 5.26 summarizes the results as shown in FIGURE 4.33, where the tests were performed at a normal stress of 29 psi with displacement rates of 2.54 mm/min. The tack coat application rate at the interface is 0.04 gal/yd^2.

TABLE 5.26: Conducted Direct Shear Tests at 0.04 gal/yd^2 Application Rate

Roughness (Inch)	Shear Strength (Psi)
0.1823	121.2658
0.0984	113.2516
0.0635	98.2453

FIGURE 5.34 shows the results found from the direct shear tests with a 0 gal/yd^2 application rate.

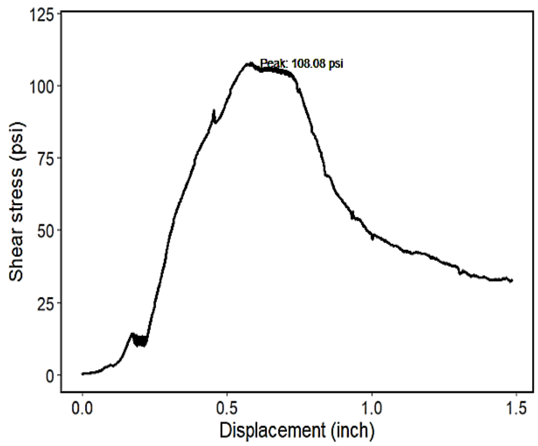

(a) 0.0446 inch

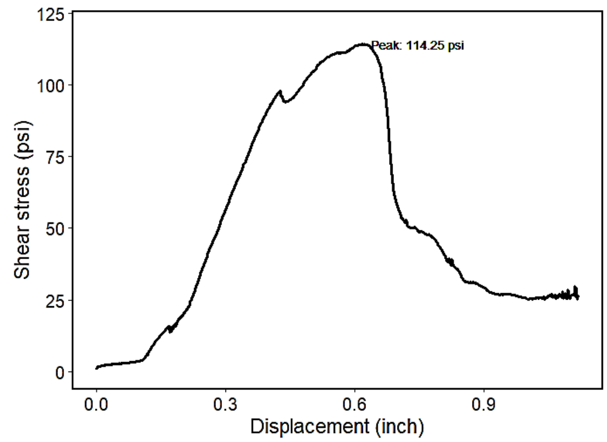

(b) 0.1097 inch

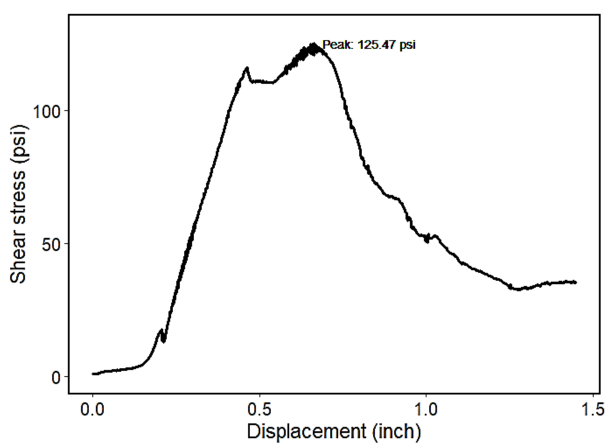

(c) 0.2157 inch

FIGURE 5.34: Direct Shear Test Results For 0 gal/yd^2 Application Rate

TABLE 5.27 summarizes the results as shown in FIGURE 4.34, where the tests were performed at a normal stress of 29 psi with displacement rates of 2.54 mm/min. The tack coat application rate at the interface is 0.04 gal/yd^2.

TABLE 5.27: Conducted Direct Shear Tests at 0 gal/yd^2 Application Rate

Roughness (Inch)	Shear Strength (Psi)
0.2157	125.4837
0.0446	108.0555
0.1097	114.2512

FIGURE 5.35 presents a detailed analysis of the relationship between tack coat application rate, surface roughness, and interface shear strength, derived from direct shear tests conducted under a normal stress of 29 psi and a shear rate of 2.54 mm/min. The data, from TABLES 5.24–5.27, are represented with surface roughness (measured in inches) plotted along the x-axis and interface shear strength (expressed in psi) along the y-axis. Four distinct trendlines were observed corresponding to tack coat application rates of 0.00 gal/yd^2 (untreated control), 0.04 gal/yd^2, 0.06 gal/yd^2, and 0.08 gal/yd^2. A consistent positive correlation between surface roughness and shear strength is observed across all tack coat application rates. For the untreated condition (0.00 gal/yd^2), shear strength increases from approximately 108 psi at a roughness of 0.0446 inch to 125 psi at 0.2157 inch. Similarly, at the highest application rate of 0.08 gal/yd^2, shear strength rises from 102 psi at 0.0712 inch to 119 psi at 0.1654 inches. This trend highlights the critical influence of surface texture in enhancing mechanical interlock between the AC layer and the milled surface.

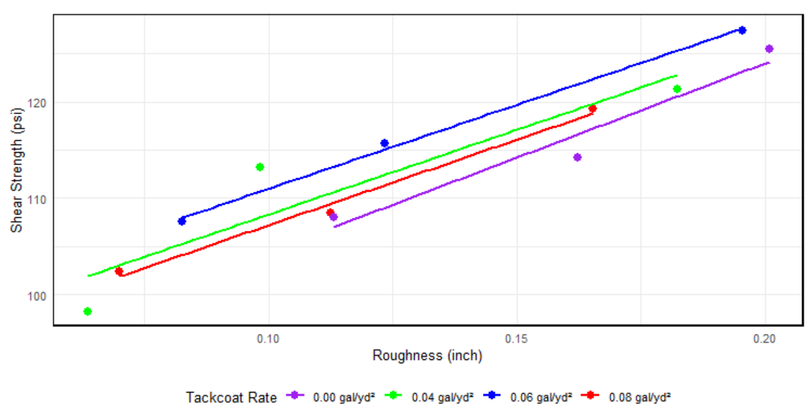

FIGURE 5.35: Effect of Tack Coat Rate and Surface Roughness on Interface Shear Strength

The shear stress vs. roughness slopes for 0.06 gal/yd^2 and 0.08 gal/yd^2 are specifically steeper than those for lower rates, suggesting a more evident increment of shear strength with increasing roughness at higher tack coat levels.

A linear regression equation (**Shear Strength = 145.365 × Roughness − 43.748 × Rate + 97.783**) was developed. It was used to normalize shear strength at a constant application rate of 0.08 gal/yd² to isolate the effect of surface roughness. FIGURE 4.36 shows the effect of roughness on interface shear strength.

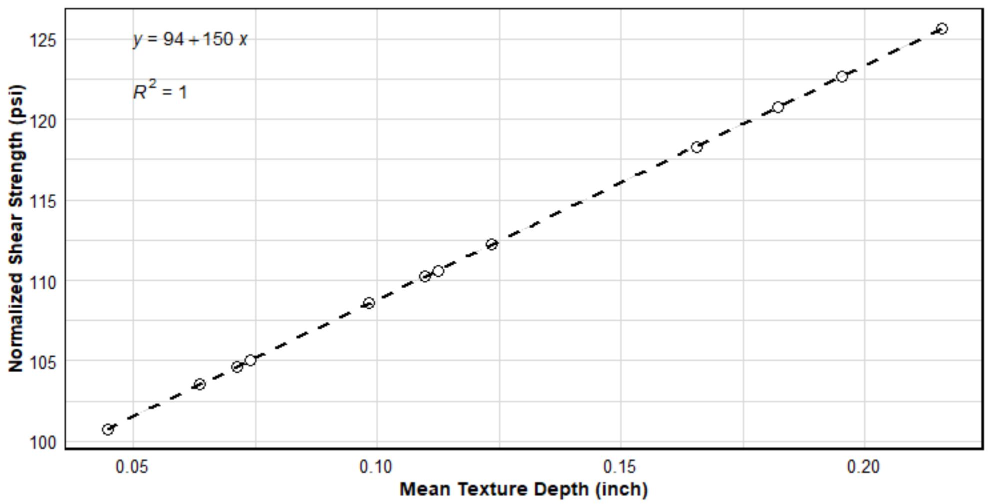

FIGURE 5.36: Surface roughness effect on interface shear strength

This observation points to a synergistic interaction between surface roughness and tack coat application on interface shear strength. To check the interaction significance, a two-way analysis of variance test (ANOVA) was conducted.

ANOVA Test

The two-way ANOVA results (TABLE 5.28) revealed a statistically significant effect of surface roughness on shear strength (*p*<0.05. In contrast, neither the main effect of tack coat rate (*p*=0.438) nor the synergistic effect of "roughness*tack coat rate" interaction (*p*=0.991) reached statistical significance. However, visual analysis from FIGURE 15 suggested a practical trend: higher tack coat rates (0.06 and 0.08 gal/yd²) exhibited steeper shear strength gains with increasing roughness, indicating a potential synergistic effect at elevated tack coat levels, which may not have been detected statistically due to limited sample size or residual variability.

TABLE 5.28**:** Two-Way ANOVA Results for The Effects of Surface Roughness and Tack Coat Rate on Shear Strength

Source	Df	Sum Sq	Mean Sq	F value	p-value
Roughness	1	779.39	779.39	58.38	<0.05
Tack coat Rate	3	45.07	15.02	1.13	0.438
Roughness × Tack coat Rate	3	1.29	0.43	0.03	0.991
Residuals	4	53.4	13.35		

Comparing Strength at 0.1 mm/min Shear Rate

Two types of specimens were tested to see how tack coat affects bond strength between asphalt layers: a new asphalt concrete (AC)-new AC double-layer specimen (tack coat application rate 0.04 gal/yd²) and a milled AC-new AC specimen (tack coat application rate 0.06 gal/yd²). The tests were conducted at a loading rate of 0.1 mm/min with a normal load of 78 psi. For a newly compacted AC double-layer specimen (roughness: 0.03 inch), the optimum application rate is 0.04 gal/yd². Compacted with a rougher (roughness: 0.12 inch) milled surface, 0.06 gal/yd² showed better performance in terms of interface shear strength (FIGURE 5.37).

Stronger bonding was shown by the milled specimen at 0.06 gal/yd² compared to the new AC-new AC specimen at the optimum application rate. At 0.06 gal/yd², a higher peak stress of 116 psi was achieved, which is a 26.09% increase compared to much less roughness (0.03 inch), and less tack coat applied (0.04 gal/yd²) newly compacted double-layer specimen. Some researchers, like Lee & Kim (2014), have claimed that tack coat doesn't greatly affect milled surfaces, but these results show otherwise—tack coat was found to improve bonding, especially with rougher surfaces like the milled AC (0.12-inch roughness).

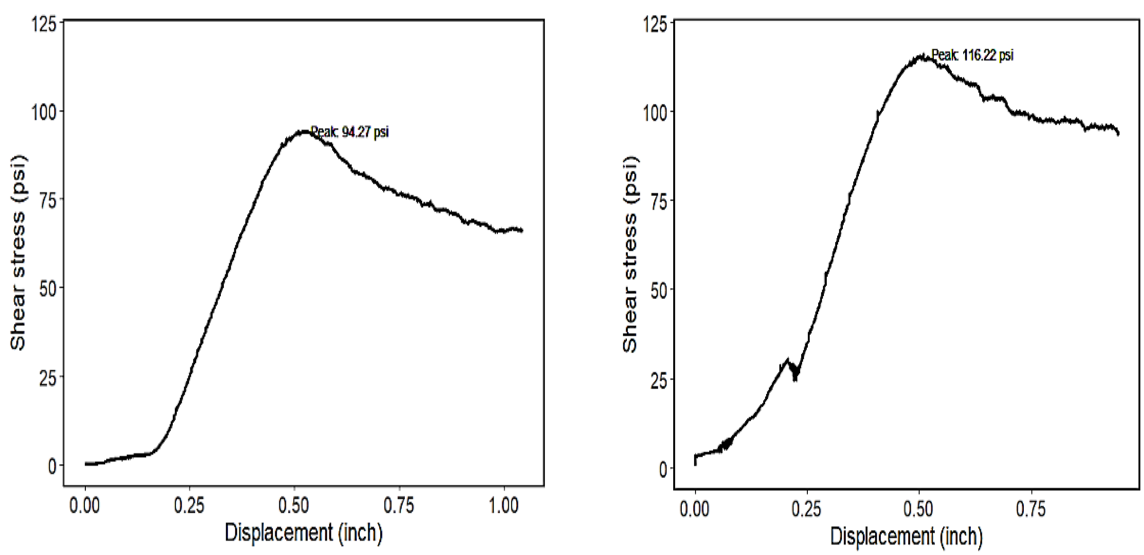

(a) New HMA-New HMA **(b)** Milled HMA-New HMA

FIGURE 5.37**:** Shear Strength Comparison Between compacted New AC- New AC vs. Milled AC-New AC Specimens

5.7 Controlled Surface Texture on Field Core

Controlled surface textures were introduced to better isolate the effect of mechanical interlocking. The regular notches provide a uniform and repeatable geometry for interaction between layers. This enhances mechanical interlocking and reduces variability compared to conventional milled surfaces. The applied tack coat helps to understand its interaction effect with the controlled rough texture by allowing evaluation of how adhesion and interlocking act together.

Controlled Surface Texture Preparation

Core samples with milled surfaces (see FIGURE 5.38c) were collected from the westbound shoulder of I-40. The controlled surface textures were prepared from these samples. For controlled texture, field cores were trimmed to a 3-inch height. A mold was created using "SolidWorks" as shown in FIGURE 5.38a. It was placed over the samples (see FIGURE 5.38b), and the spacings of notching were marked. Field cores were notched with a diamond saw (4 mm depth, 2 mm width, 12 mm spacing) to create controlled textures (FIGURE 5.38d). Finally, tack coat application and top layer sample compaction were done.

(e) Created a mold using SolidWorks

(f) Mold over the specimen

(g) Milled surface

(h) Notched surface of the field core

FIGURE 5.38: Controlled surface texture creation: (a) Created mold by SolidWorks, (b) Mold over the specimen, (c) Milled surface, (d) Notched surface of the field core

The mean texture depth (MTD) for the controlled texture and milled surfaces of field cores was determined using a modified sand patch method (ASTM E965-15). FIGURE 4.39 shows the distribution of measured mean texture depths (MTD) for typical milled and controlled textured specimens.

FIGURE 5.39 a to FIGURE 5.39 d show the results found from the direct shear tests. The average shear strength for the specimens prepared with no tack coat is 118 psi. Similarly, direct shear test results for specimens prepared with 0.04, 0.06, and 0.08 gal/yd^2 tack coat are presented in FIGURES 5.39 (b)- 5.39 (d). The average shear strengths of specimens prepared with 0.04, 0.06, and 0.08 gal/yd^2 tack coat are 125, 131, and 121 psi, respectively.

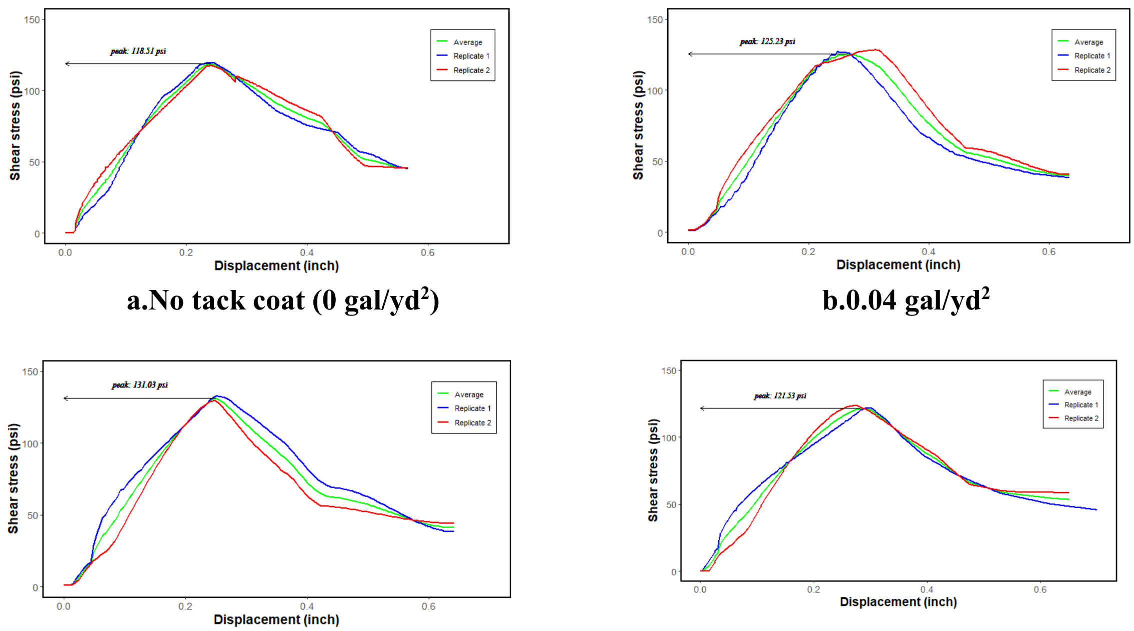

a.No tack coat (0 gal/yd^2)

b.0.04 gal/yd^2

c.0.06 gal/yd^2

d.0.08 gal/yd^2

FIGURE 5.39: Direct Shear Test Results for Different Application Rates

TABLE 5.29 shows the corresponding values for controlled-textured (notched) laboratory-compacted new hot-mix asphalt bottom layers. It was found that controlled grinding enhances interlayer bonding and reduces tack coat dependence.

TABLE 5.29: Interface Shear Strength of Controlled-Textured Specimens for Lab Notched Field Core

Bottom Layer Surface Type	Application Rate (gal/yd²)	Mean Texture Depth (inch)	Average ISS (psi)
Lab Grooved/Notched Field Core	0	0.092	118.24
Lab Grooved/Notched Field Core	0.04	0.0928	125.88
Lab Grooved/Notched Field Core	0.06	0.0958	131.05
Lab Grooved/Notched Field Core	0.08	0.0899	121.86

To evaluate the effect of application rate on interface shear strength (ISS), the controlled-textured specimens and conventional milled specimens cannot be compared directly using only the raw measured ISS values. The reason is that the two surface preparation methods did not have the same mean texture depth at each application rate. The controlled-textured specimens were intentionally prepared so that the mean texture depth remained nearly constant across all application rates, whereas the conventional milled specimens exhibited different texture depths at different application rates.

For the controlled-textured specimens, the measured mean texture depths were approximately 0.0920, 0.0928, 0.0958, and 0.0899 in for application rates of 0.00, 0.04, 0.06, and 0.08 gal/yd², respectively. These values are very close to one another, indicating that the surface texture was effectively controlled. In contrast, the conventional milled surfaces showed varying roughness values at each application rate. Therefore, a direct comparison of raw ISS between the two surface types would be influenced by both application rate and texture depth, making it difficult to isolate the true effect of application rate.

To make a fair comparison (shown in TABLE 5.30), the ISS of the conventional milled surface was estimated at the same texture depth as the corresponding controlled-textured specimen for each application rate. This was done using linear interpolation between the measured roughness-shear strength data points for the conventional milled specimens.

TABLE 5.30: Comparison of controlled-textured and conventional milled interface shear strength

Application rate (gal/yd²)	ISS for controlled texture	ISS for conventional milled (psi)	Difference (Controlled − Conventional) (psi)
0.00	118.24	112.57	5.67
0.04	125.88	110.84	15.04
0.06	131.05	111.16	19.89
0.08	121.86	105.18	16.68

ANOVA

A Type II analysis of variance (ANOVA) was performed to evaluate the effects of surface type (conventional milled vs. controlled texture) and residual tack coat rate (0, 0.04, 0.06, and 0.08 gal/yd²) on interface shear strength (ISS). The results are shown in TABLE 5.31. The mean texture depth (MTD) was treated as a continuous covariate in the Type II ANOVA model, resulting in 1 degree of freedom for its effect on interface shear strength.

TABLE 5.31: Type II ANOVA analysis with ISS Response

Term	*Sum Sq*	*Df*	*F* value	Pr(>*F*)	Significance Level ($p < 0.05$)
Surface type	3504	1	5.32	0.04136	Yes
Application Rate	22144.1	3	11.1996	0.003096	Yes
MTD	4615.9	1	7.0037	0.029418	Yes
Surface type: Application Rate	245.6	3	0.1242	0.943169	No
Surface type: MTD	215.8	1	0.3275	0.582881	No
Application Rate: MTD	398.4	3	0.2015	0.892481	No
Application Rate :MTD: Surface type	869.3	3	0.730917	0.93245	No
Residuals	5272.6	8			

5.8 Controlled Surface Texture on New HMA

All tests were performed at 29 psi normal stress and a shear rate of 2.54 mm/min. For the smooth specimens, the mean texture depth was approximately 0.0276 inches. For the controlled-textured specimens, the bottom surface was notched, and the mean texture depth was approximately 0.0935 inches (see FIGURE 5.40).

FIGURE 5.40: Prepared controlled notched/grooved specimens (used as bottom layer)

FIGURES 5.41a to 5.41d show the results found from the direct shear tests. The average shear strength for the specimens prepared with no tack coat is 125.8 psi. Similarly, direct shear test results for specimens prepared with 0.04, 0.06, and 0.08 gal/yd^2 tack coat are presented in FIGURES 5.41 (b)- 5.41 (d). The average shear strengths of specimens prepared with 0.04, 0.06, and 0.08 gal/yd^2 tack coat are 135.85, 138.65, and 123.93 psi, respectively.

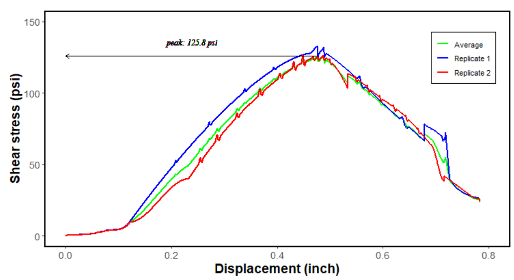

(a) No tack coat (0 gal/yd^2)

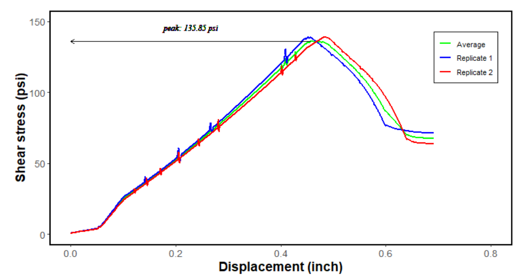

(b) 0.04 gal/yd^2

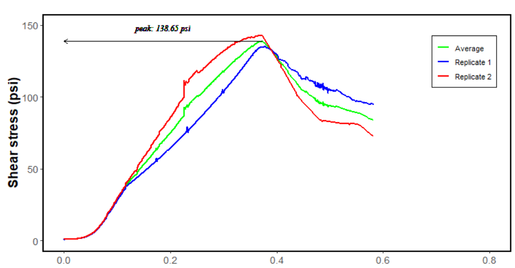

(c) 0.06 gal/yd^2

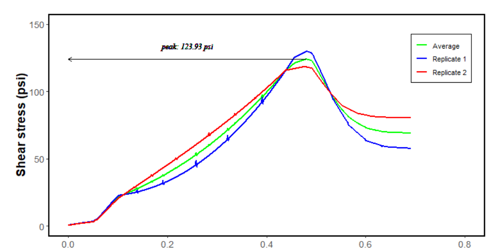

(d) 0.08 gal/yd^2

FIGURE 5.41: Direct Shear Test Results for Different Application Rates

TABLE 5.32 compares interface shear strength results from direct shear tests on smooth-surface and controlled-textured double-layer AC specimens.

TABLE 5.32: Comparison of ISS for smooth and notched double-layer AC specimens

Application Rate (gal/yd²)	Smooth Texture_Avg. ISS (psi)	Notched Texture_Avg. ISS (psi)	Notched Texture - Smooth Texture (psi)
0	83.01	125.8	42.79
0.04	99.10	135.85	36.75
0.06	107.68	138.65	30.97
0.08	83.79	123.93	40.14

ANOVA: Effects of Surface Type and Application Rate on ISS

A two-way ANOVA (see TABLE 5.33) was performed to evaluate the effects of surface type (smooth vs. textured) and tack coat application rate (0, 0.04, 0.06, and 0.08 gal/yd²) on interface shear strength (ISS), together with their interaction. The analysis shows that both main effects and their interaction are statistically highly significant.

TABLE 5.33**:** Two-Way ANOVA Results

Term	Sum Sq	Mean Sq	*F* value	*Pr*(>*F*)	Significance level
Surface Type	1	80504	80504	577.26	<0.05
Application Rate	3	79184	26395	189.27	<0.05
Surface Type: Application Rate	3	5386	1795	12.87	<0.05
Residuals	16	2231	139		

5.9 Effect of Aging on Interface Shear Strength

To evaluate the effect of aging on interface shear strength, controlled-textured specimens prepared with aged field-core bottom layers were compared with controlled-textured specimens prepared with unaged new HMA bottom layers. In both cases, the bottom layer surface was notched to provide a controlled texture and reduce variability in surface geometry. The comparison was made at four tack coat application rates: 0, 0.04, 0.06, and 0.08 gal/yd². The corresponding average interface shear strength values for aged specimens were 118.24, 125.88, 131.05, and 121.86 psi, respectively, while those for unaged specimens were 125.80, 135.85, 138.65, and 123.93 psi, respectively.

The results show that the unaged specimens consistently produced higher interface shear strength than the aged specimens at all tack coat application rates. For both surface conditions, the interface shear strength increased as the application rate increased from 0 to 0.06 gal/yd², and then decreased at 0.08 gal/yd². This indicates that 0.06 gal/yd² was the optimum application rate for both aged and unaged controlled-textured specimens.

The difference between unaged and aged specimens was 7.56 psi at 0 gal/yd², 9.97 psi at 0.04 gal/yd², 7.60 psi at 0.06 gal/yd², and 2.07 psi at 0.08 gal/yd². FIGURE 5.42 shows the comparison between the unaged and aged samples' interface shear strengths.

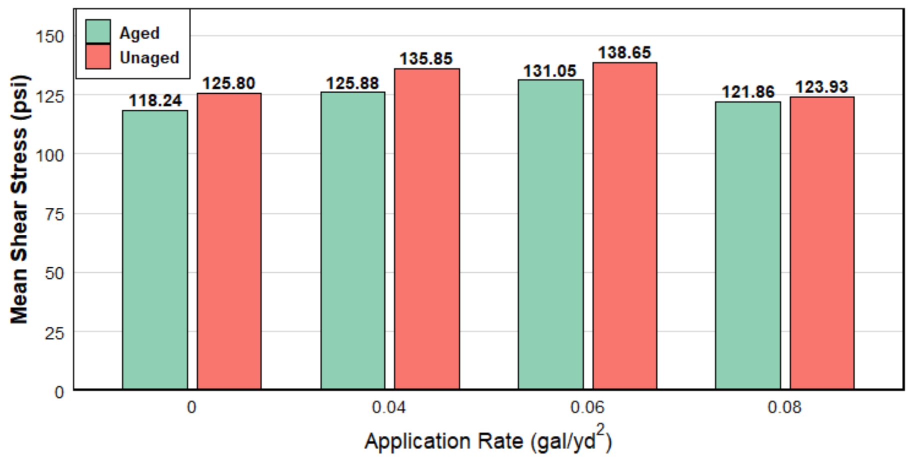

FIGURE 5.42: Comparison between unaged and aged samples' interface shear strengths

These results indicate that aging reduced the bonding capacity of the interface, even when a controlled texture was provided. A likely reason is that aging stiffens and oxidizes the asphalt surface, which reduces adhesive bonding with the tack coat. Although controlled texture improves mechanical interlocking, the aged surface still appears to provide a less favorable condition for interfacial bonding than the unaged surface. This suggests that both adhesion and mechanical interlocking contribute to interface resistance, and that the benefit of controlled texture cannot fully compensate for the effect of surface aging.

To statistically evaluate these observations, a two-way analysis of variance (TABLE 5.34) can be performed using surface condition and tack coat application rate as the main factors, with interface shear strength as the response variable. This analysis shows that aging has a significant effect on interface shear strength, and the interaction effect of tack coat application rate is also significant.

TABLE 5.34: Two-Way ANOVA Results for Aged vs Unaged Group

Source	*Df*	*Sum Sq*	*Mean Sq*	*F* value	Pr(>*F*)
Surface Condition	1	277.4	277.44	4.37e+31	<0.05
Application Rate	3	698.9	232.97	3.66e+31	<0.05
Surface Condition × Application Rate	3	50.5	16.82	2.65e+30	<0.05
Residuals	16	0.0	0.00	-	-

5.10 Effect of Surface Texture Orientation with Shear

During the direct shear test, these controlled textures are placed in three orientations: parallel, perpendicular, and 45° to the shear direction, to study the effect of texture orientations with shearing. In FIGURE 5.43a, the bottom controlled texture is parallel to the shear load. The bottom-controlled texture is perpendicular to the shear load in FIGURE 5.43b, and the controlled surface texture is 45° to the shear load in FIGURE 5.43c. It should be noted that the top layer is not shown in FIGURE 5.43 to make the shear and texture orientation clear. For better understanding, a blue line is created in FIGURE 5.43. This line indicates the texture direction, and the red mark indicates the shear load.

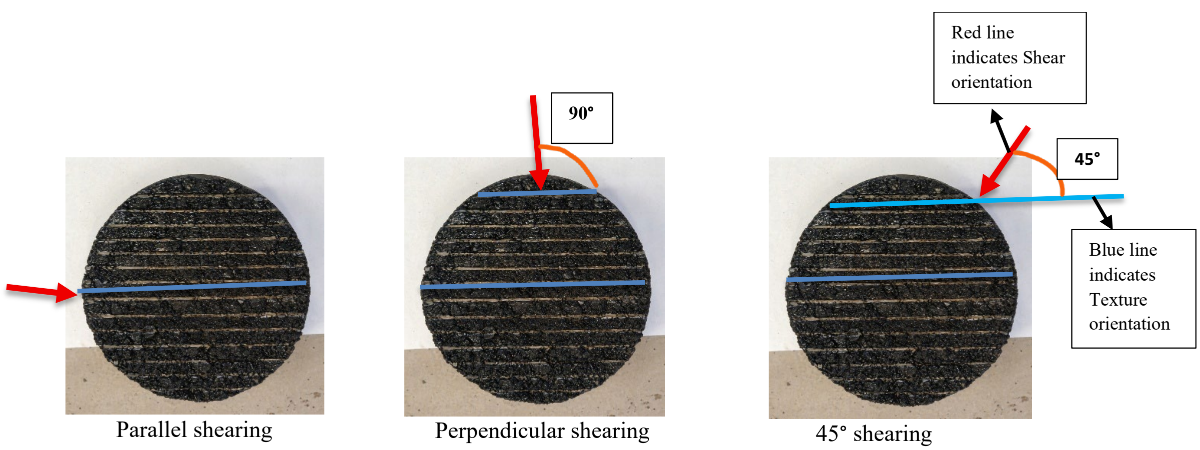

FIGURE 5.43: Shearing Direction During Direct Shear Test: **(a)** The Bottom Texture (blue color) is Parallel to the Shear Load (red color). **(b)** The Bottom Texture (blue color) is Perpendicular to the Shear Load (red color). **(c)** The Bottom Texture (blue color) is 45° to the Shear Load (red color).

FIGURE 5.44 shows the distribution of ISS across surface texture orientations for the new HMA group. The new HMA group uses a newly compacted bottom layer. Data vary by surface texture orientation relative to shear. Perpendicular orientation had the highest ISS (155.8 psi), whereas parallel orientation provided 135.9 psi, and 45° provided 143.2 psi. This indicates the best shear performance when the shear load is perpendicular to the texture of the bottom layer of new double-layer HMA specimens.

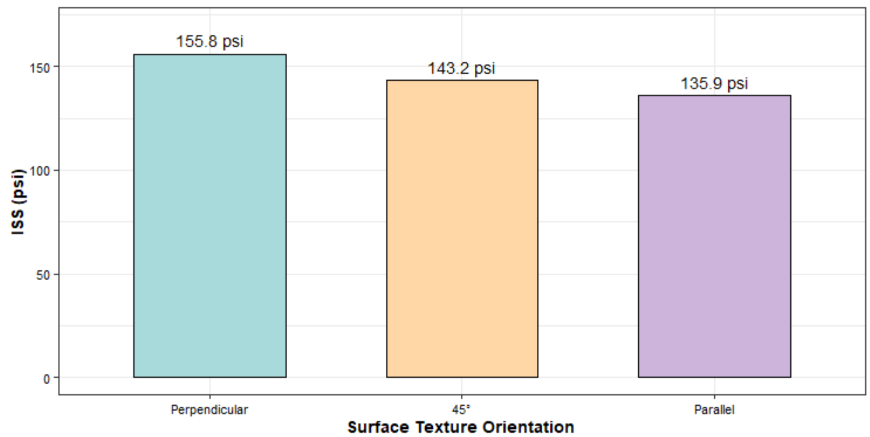

FIGURE 5.44: Interface shear strength for different surface texture orientations

One-way ANOVA compared ISS means across three orientations. Orientation served as the key factor. ISS was the dependent variable. Results showed a strong effect of orientation on ISS (F (2, 33) = 22.03, $p < 0.001$). Residuals were marginally normal (Shapiro-Wilk $W = 0.93638$, p = 0.03922). Variances were homogeneous (Levene's F (2, 33) = 0.5701, $p = 0.5709$). These checks support the ANOVA's validity.

5.11 **Evaluating Factors that Affect Interface Shear Strength**:

TABLE 5.35 presents ANOVA and Tukey HSD post-hoc results for factors affecting interface shear strength of AC. Tukey HSD shows mean differences in MPa and adjusted p-values (p adj). Partial eta-squared (η^2) represents the proportion of total variance in interface shear strength explained by each factor. In this highly controlled laboratory study, with low experimental variability (coefficients of variation <7% across replicates), most factors produced very large effect sizes ($\eta^2 > 0.9$), indicating that they account for the vast majority of the observed variation in ISS. Effect sizes between 0.8 and 0.9 were classified as large and very large, while the single factor with $\eta^2 = 0.628$ (curing time) was considered a medium effect. These descriptors are context-specific to the present experimental design and reflect the dominant influence of the tested variables under controlled conditions.

To address potential concerns about the large partial η^2 values in TABLE 5.35, comprehensive diagnostic checks were performed both on the full dataset and on the residuals of each of the individual one-way ANOVAs. The experimental design is fully balanced. Residuals from all models satisfied the ANOVA assumptions: normality (Shapiro–Wilk W ranged from 0.94 to 0.97, all $p \geq 0.08$), homogeneity of variance (Levene's test p ranged from 0.12 to 0.31). The coefficient of variation across the entire set of tests was low (overall $CV = 4.8$ %; range across factors 3.1–6.9 %). This experimental control produces large η^2 values that are statistically expected and desirable rather than things of imbalance or overfitting. Supporting evidence includes narrow 95 % confidence intervals for the largest effects (e.g., loading rate $\eta^2 = 0.999$, 95 % CI 0.997–1.000), 10-fold cross-validated $R^2 = 0.961$ (very close to adjusted $R^2 = 0.978$), and variance inflation factors < 2.1.

- Temperature has a strong effect on ISS. Its effect size is very large ($\eta^2 = 0.993$). Tukey HSD finds a large drop in ISS at 131°F compared to 20°C (p adj < 0.001). This shows that temperature reduces shear strength significantly.

- Mean texture depth (MTD) strongly correlates with ISS ($\eta^2 = 0.991$). Tukey HSD shows a gradual increase. High vs. low MTD gives p adj < 0.001.

- Moisture conditioning is significant ($\eta^2 = 0.984$). Tukey HSD measures ISS drops. MIST vs. unconditioned difference was found significant: p adj < 0.001. A significant difference was observed between MIST vs. AASHTO T283 (p adj = 0.004).

- Curing time is nearly significant ($\eta^2 = 0.628$). Tukey HSD picks one main comparison between 120 min vs. 0 min (p adj = 0.043).

- Surface texture orientation with relation to shear has a significant effect on ISS. Effect size is large ($\eta^2 = 0.894$). Tukey HSD shows that perpendicular orientation yields the highest shear strength. Key comparisons: Parallel vs. Perpendicular p adj < 0.003; 45° vs. Perpendicular p adj < 0.002; 45° vs. Parallel p adj < 0.002. This confirms that aligning surface texture perpendicular to the shear direction maximizes interface shear strength.

- Surface aging is highly significant (p = 7.84e-05, $\eta^2 = 0.983$). Tukey HSD shows aged surfaces have lower ISS (p adj < 0.001).

- Two-way ANOVA on tack coat type and rate shows strong main effects for application type and application rate (type: $p < 0.001$; rate: $p < 0.001$). Their interaction is also significant ($p < 0.001$). Effect sizes are large for both (type: 0.845; rate: 0.995). Tukey HSD shows differences between Trackless vs. SS-1h: p adj < 0.001. Higher rates reduce ISS (0.08 vs. 0.04 gal/yd²: p adj < 0.001).

TABLE 5.35: ANOVA test/ Tukey HSD pairwise test between various factors and shear strength

Factor	Significance Level from ANOVA $P < 0.05$	Effect Size (η^2)	Key Tukey HSD Comparisons (difference in psi, p adj)
Temperature	yes	0.993 (very large)	131°F-68°F: -153, <0.001
Mean Texture Depth	yes	0.991 (very large)	Mid-Low: 14.5, 0.002; High-Low: 29, <0.001; High-Mid: 14.5, 0.002
Texture Orientation	yes	0.894 (large)	Parallel-Perpendicular: 30.5, 0<.003; 45 degree-Perpendicular:: 18.9, <0.002; 45 degree- Parallel: 15.9, <0.002
Moisture	yes	0.984 (very large)	T283-Unconditioned: -34.1, <0.001; MIST-Unconditioned: -47, <0.001; MIST-AASHTO T283: -12.9, 0.004
Curing Time	yes	0.628 (medium)	120-0: 37.7, 0.043; 60-0: 18.9, 0.319; 120-60: 18.9, 0.319
Surface Aging	yes	0.983 (very large)	Unaged-Aged: 39.2, <0.001
Tack Coat Type and Rate	p (Type): yes p (Rate): yes p (Interaction): yes	Type: 0.845 (large) Rate: 0.995 (very large)	Type: Trackless-SS-1h: 28.6, <0.001 Rate: 0.08-0.04: -9.7, <0.001

The effect sizes (partial η^2) are summarized visually in FIGURE 4.45 as a ranked bar chart ordered from largest to smallest. Tack coat rate ($\eta^2 = 0.995$), temperature ($\eta^2 = 0.993$), mean texture depth ($\eta^2 = 0.991$), moisture ($\eta^2 = 0.984$), and surface aging ($\eta^2 = 0.983$) all exert very large effects ($\eta^2 > 0.9$) on interface shear strength.

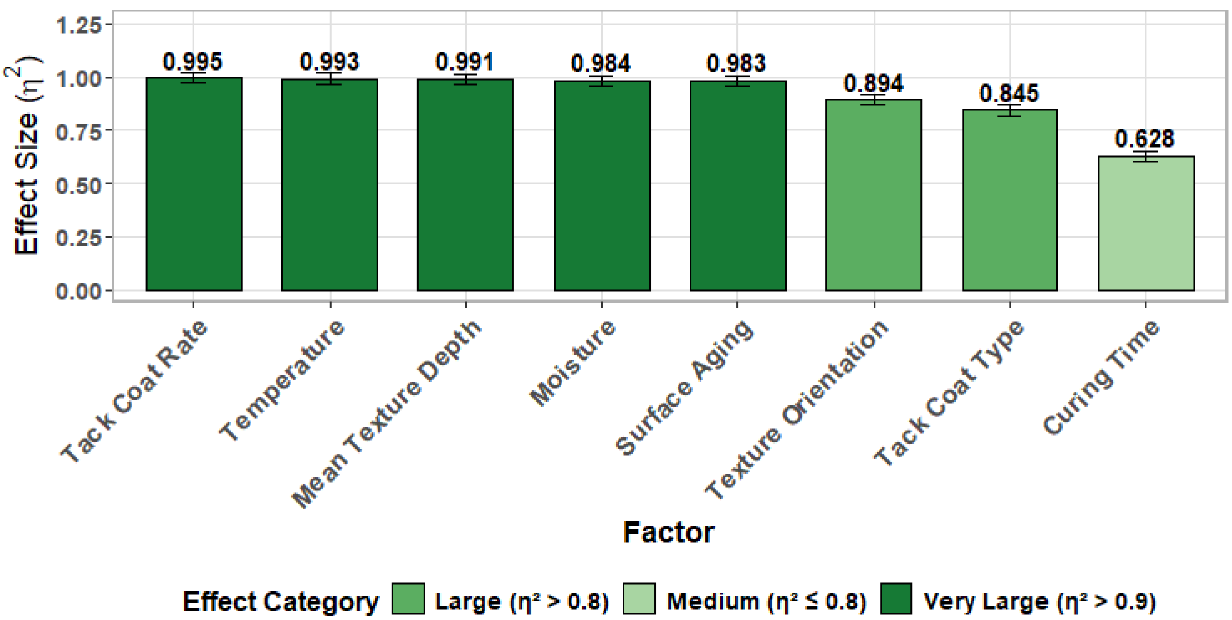

FIGURE 5.45: Ranked Effect Sizes (partial η^2) of Factors Influencing Interface Shear Strength

5.12 Finite Element Models and Limiting Values

Numerical modeling offers a useful approach for studying interfacial behavior in asphalt pavements. Finite element analysis can be used to evaluate stress and deformation within AC layers under controlled loading. It can also simulate the interaction between asphalt layers and represent the mechanical response of the interface under shear.

There are primarily three interfacial delamination failure modes: mode I or opening, mode II or sliding, and mode III or tearing. All three modes of failure are shown in FIGURE 5.1. The delamination failure can occur in the form of either of these modes, or it can be due to a mixed effect.

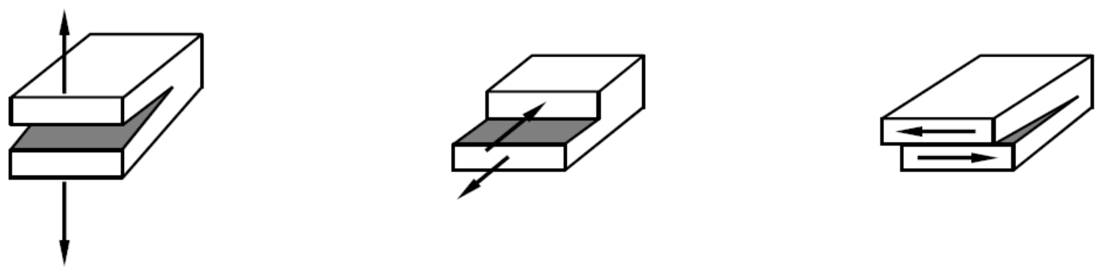

a) Mode I: opening **b)** Mode II: sliding **c)** Mode III: tearing

FIGURE 5.46: Modes of delamination failures

Crack surfaces can move relative to each other in three distinct ways. Mode I, the most common, involves the crack opening under tensile stresses, leading to its propagation. Mode II occurs when in-plane shear stresses cause sliding between the crack faces. Mode III refers to a tearing, similar to the action of pulling apart a piece of paper using both hands.

An interfacial crack grows only after a damage zone forms ahead of the crack tip. The size and shape of this damage zone can vary significantly, depending on the material's toughness and the applied stress state. For mode II and mode III loading, the damage zone is larger than that observed for mode I loading. This is due to the slower decay of the stress field in the shear modes. Additionally, the behavior differs between brittle and ductile materials. Brittle composites have a smaller damage zone compared to ductile ones. In practice, modes II and III are often connected, so computational analyses typically use the same interfacial strength and fracture energy for both.

Different models are available for numerical simulation of the delamination in a layered structure. Some of them are summarized below:

5.13 **Linear Elastic Fracture Mechanics**

Fracture mechanics is a key methodology for understanding interfacial delamination in materials over the years. When the influence of other material nonlinearities is negligible, LEFM becomes an effective approach to predict delamination growth. However, it is important to note that LEFM assumes the presence of an initial crack as a prerequisite for its application. Once delamination initiates, LEFM serves as a valuable tool for predicting its progression (Durix et al., 2012; Szeto et al., 2000).

LEFM relies on two primary parameters to evaluate failure near an existing crack or defect: the stress intensity factor (Irwin, 1948) and the strain energy release rate (Anderson, 2005). These parameters have been successfully employed in the study of cracking and delamination. Among these, recent studies mostly use the strain energy release rate approach due to its broader applicability. In all cases, fracture mechanics presumes the existence of a pre-existing crack or material defect.

Advanced techniques such as the Virtual Crack Closure Technique (VCCT) (Xie and Sitaraman, 2003), the J-integral method (Liu et al., 2013), the virtual crack extension method (Harries and Sitaraman, 2001), and the stiffness derivative approach (Sundararaman and Sitaraman, 2001) are widely applied to predict delamination growth. These methods are designed to compute the components of the energy release rate, which is critical for understanding crack propagation. Delamination occurs when the total energy release rate exceeds a critical value. However, implementing these methods in finite element analysis presents challenges. Calculating fracture parameters, such as stress intensity factors or energy release rates, requires detailed nodal and topological data from the region near the crack front. While such computations are manageable for stationary cracks, they become significantly more complex for cases involving progressive crack growth.

5.13.1 Stress Intensity Factor

In homogeneous materials, extensive research has focused on analyzing stress fields near crack tips. These studies have resulted in closed-form equations describing the stress distribution within the material (Irwin, 1948; Orowan, 1948). Using a polar coordinate system centered at the crack tip, subsequent research generalized these stress fields into a single parameter known as the stress intensity factor (SIF), denoted as *K*.

When both shear and normal stresses act near the crack tip, the loading condition is referred to as mixed-mode loading. For mode I loading, the stress field ahead of a crack tip can be expressed using the following equations:

$$\sigma_{xx} = \frac{K_I}{\sqrt{2\pi r}}\cos\left(\frac{\theta}{2}\right)\left[1-\sin\left(\frac{\theta}{2}\right)\sin\left(\frac{3\theta}{2}\right)\right] \quad \text{Eq. 1}$$

$$\sigma_{yy} = \frac{K_I}{\sqrt{2\pi r}}\cos\left(\frac{\theta}{2}\right)\left[1+\sin\left(\frac{\theta}{2}\right)\sin\left(\frac{3\theta}{2}\right)\right] \quad \text{Eq. 2}$$

$$\tau_{xy} = \frac{K_I}{\sqrt{2\pi r}} \cos\left(\frac{\theta}{2}\right) \sin\left(\frac{\theta}{2}\right) \sin\left(\frac{3\theta}{2}\right) \quad \text{Eq. 3}$$

In these equations, σ_{xx}, σ_{yy}, and τ_{xy} are the normal stresses in the x and y directions and the shear stress in the x-y plane, respectively. r and θ are polar coordinates, while K_I represents the mode I stress intensity factor.

For mode II loading, the stress field in front of the crack tip is described by the following equations:

$$\sigma_{xx} = -\frac{K_{II}}{\sqrt{2\pi r}} \sin\left(\frac{\theta}{2}\right) \left[2 + \cos\left(\frac{\theta}{2}\right) \cos\left(\frac{3\theta}{2}\right)\right] \quad \text{Eq. 4}$$

$$\sigma_{yy} = \frac{K_{II}}{\sqrt{2\pi r}} \sin\left(\frac{\theta}{2}\right) \cos\left(\frac{\theta}{2}\right) \cos\left(\frac{3\theta}{2}\right) \quad \text{Eq. 5}$$

$$\tau_{xx} = \frac{K_{II}}{\sqrt{2\pi r}} \cos\left(\frac{\theta}{2}\right) \left[1 - \sin\left(\frac{\theta}{2}\right) \sin\left(\frac{3\theta}{2}\right)\right] \quad \text{Eq. 6}$$

Here, K_{II} represents the mode II stress intensity factor. For two-dimensional problems, the stress field magnitudes are entirely determined by K_I and K_{II}. The critical stress intensity factor, K_{IC}, signifies the threshold value at which crack propagation begins. This value, a material property, is determined through fracture experiments. If the stress intensity factor K exceeds K_{IC}, a crack in the material will propagate.

5.13.2 Strain Energy Release Rate

In energy-based fracture mechanics, the strain energy release rate (SERR) is a critical parameter used to evaluate crack growth. When a crack propagates, it consumes energy to create two additional surfaces in the material. The rate at which this energy changes with respect to the crack area is denoted by G. Alternatively, G can be interpreted as the energy provided by applied loading that is available to propagate the crack. Irwin (1948) described the energy release rate as a modification of Griffith's energy balance, expressed as:

$$G = -\frac{d\Pi}{dA} \quad \text{Eq. 7}$$

Here, Π represents the potential energy stored in an elastic body, and A is the crack area.

In the framework of LEFM, G is directly proportional to the square of the stress intensity factor, K. The relationship is given by:

$$G = \begin{cases} \dfrac{K_I^2}{E} & \text{(plane stress)} \\ \dfrac{K_I^2(1-\nu^2)}{E} & \text{(plane strain)} \end{cases} \qquad \text{Eq. 8}$$

In these equations, E is the elastic modulus, ν is Poisson's ratio, and K_I is the mode I stress intensity factor.

Much like the stress intensity factor approach, crack propagation begins when G attains a critical value, referred to as the critical strain energy release rate (G_C). Like K_{IC}, G_C denotes a material-specific property determined experimentally. When G exceeds G_C, crack propagation occurs within the material.

5.13.3 Virtual Crack Closure Technique

Various computational methods are available in finite element modeling (FEM) software for calculating the strain energy release rate (SERR). These include the virtual crack extension method, the virtual crack closure technique (VCCT), and the J-integral method, each of which has been demonstrated to produce similar outcomes (Tran et al., 2013). In this study, the VCCT is applied to calculate SERR for interfacial fracture tests.

The VCCT, originally introduced by Rybicki and Kanninen (1977), incorporates the crack tip directly into the FEM model. Unlike other methods, the VCCT approach does not require singular elements at the crack tip. For two-dimensional analysis, crack tip nodes along the crack length a are modeled as uncoupled. This method typically uses eight-node quadratic elements. As the crack grows from $a + \Delta a$, where Δa indicates a small increment of a, the state of the crack tip is assumed to remain unchanged (Krueger, 2004; William, 1959).

In this context, crack tip opening displacements and forces are considered identical for small increments of Δa. Thus, the energy required to extend the crack by Δa is equivalent to the energy necessary to close the crack over the same length Δa. The total SERR for a two-dimensional case is given as $G = G_I + G_{II}$. The following equations describe G, calculated using eight-node elements:

$$G_I = -\frac{1}{2\Delta a}\left[Y_i(v_l - v_l^*) + Y_j(v_m - v_m^*)\right] \qquad \text{Eq. 9}$$

$$G_{II} = -\frac{1}{2\Delta a}\left[X_i(u_l - u_l^*) + X_j(u_m - u_m^*)\right] \qquad \text{Eq. 10}$$

In these equations, u and v are horizontal and vertical displacements, while X_i and Y_i denote the horizontal and vertical nodal forces at the crack tip. Only the forces from the upper surface are considered in the summation.

Crack propagation is predicted when the computed energy release rate (G_T) equals the material's fracture toughness, G_c:

$$G_T = G_C \qquad \text{Eq. 11}$$

An advantage of the VCCT is that it focuses on energy calculations rather than stress. However, its primary limitation is its reliance on the assumption of similar crack extension. Consequently, the method is best suited for short cracks, as it cannot accurately model long crack growth.

5.13.4 J-Integral Technique

The *J-Integral* is another method commonly used in FEM software to calculate the strain energy release rate (SERR) (Matos et al., 1989). Initially introduced by Rice (1968), the *J-Integral* provides a measure of the energy release rate for cracks in nonlinear elastic materials. For two-dimensional problems, the *J-Integral* can be simplified into a path-independent line integral taken around the crack tip, as expressed below:

$$J - \text{integral} = \int_{\Gamma} \left(w dy - T_i \frac{\partial u_i}{\partial x} dS \right) \qquad \text{Eq. 12}$$

In this equation, J denotes the nonlinear energy release rate that remains independent of the path and is evaluated along a contour Γ. The term w refers to the strain energy density, T_i denotes the components of the traction vector, and u_i represents the displacement vector components.

Since the *J*-Integral accounts for nonlinear effects, it is particularly useful for analyzing cracks in elastic-plastic materials. In cases where the material behavior is purely elastic, the *J*-Integral is equivalent to G.

5.14 Cohesive Zone Model

The Cohesive Zone (CZ) model originates from the works of Dugdale (1960), who introduced the concept of a plastic zone near the crack tip, and Barenblatt (1962), who focused on molecular-scale cohesive forces. This model was later extended by Hillerborg et al. (1976) to incorporate crack initiation and growth governed by tensile strength.

The CZ model describes interfacial separation as taking place within a designated cohesive damage zone once material damage exceeds a certain threshold. Traction stresses within this zone engage in interactions across the cohesive surfaces, and the behavior of these stresses is described by a traction-separation law.

5.14.1 Traction-Separation Damage Model

This model applies to cohesive elements and assumes a linear relationship between traction and separation until damage begins and evolves. The elastic behavior is defined by an elastic constitutive matrix that establishes a relationship between nominal stresses and nominal strains at the interface. Nominal stresses are evaluated as the ratio of force components to the initial area at integration points, whereas nominal strains are calculated as the separation distances normalized by the original element thickness at those points. The nominal traction stress vector, t, includes three components, t_n, t_s, and t_t, corresponding to separations δ_n, δ_s, and δ_t , respectively. The initial thickness of the cohesive element is represented by T_0. The nominal strain components are expressed as:

$$\varepsilon_n = \frac{\delta_n}{T_0};\ \varepsilon_s = \frac{\delta_s}{T_0};\ \varepsilon_t = \frac{\delta_t}{T_0} \qquad \text{Eq. 13}$$

The elastic behavior of the system is described using the following matrix relationship:

$$t = \begin{Bmatrix} t_n \\ t_s \\ t_t \end{Bmatrix} = \begin{bmatrix} K_{nn} & K_{ns} & K_{nt} \\ K_{ns} & K_{ss} & K_{st} \\ K_{nt} & K_{st} & K_{tt} \end{bmatrix} \begin{Bmatrix} \varepsilon_n \\ \varepsilon_s \\ \varepsilon_t \end{Bmatrix} = K\varepsilon \qquad \text{Eq.14}$$

Here, K is the elasticity matrix, which defines a fully coupled relationship between the components of traction and separation vectors. Uncoupled behavior is ensured by nullifying the off-diagonal components of the matrix.

5.14.2 Damage Initiation

Damage initiation marks the beginning of material degradation. This process starts when stresses or strains reach predefined criteria for damage initiation, as specified by the user. A variety of criteria can be utilized for this purpose. Each criterion is linked to an output variable, which indicates whether the specified condition has been met. An output value of 1 signifies that the initiation condition has been satisfied.

5.15 Finite Element Model and Limiting Values

The geometry of the CZM was constructed based on a two-layer HMA system for testing interface shear strength. The model consists of two rectangular HMA layers with an interface between them. The interface is a thin layer spanning 6 inches in length. Each HMA layer also has a length of 6 inches. A 2D plane stress condition was assumed, as shown in FIGURE 5.47 (a). A combination of 0.5 mm four-noded (CPS4R) and three-noded (CPS3) two-dimensional plane stress elements was used for mesh generation of the HMA layers.

For the interface, a four-noded two-dimensional cohesive element (COH2D4) was placed between the two HMA layers. A mesh size of 0.5 mm was selected for the interface. The interface contains a total of 300 cohesive elements. FIGURE 5.47 (b) shows the selected mesh used in the model.

The boundary conditions were set up to model a direct shear test for the two-layer asphalt concrete specimen, as shown in FIGURE 5.47 (a). The bottom edge of the bottom HMA layer was fixed in the vertical direction (Y-axis) to stop it from moving up or down. The right edge of the bottom layer was fixed in the horizontal direction (X-axis) to keep it from sliding side to side. A reference point (RP-1) was used to apply a shear load. This point was moved to the right at the shear rates of TABLE 5.37, creating shear between the layers, as indicated by the horizontal arrow at RP-1. The reference point was also fixed in the vertical direction and rotation to ensure it only moved sideways.

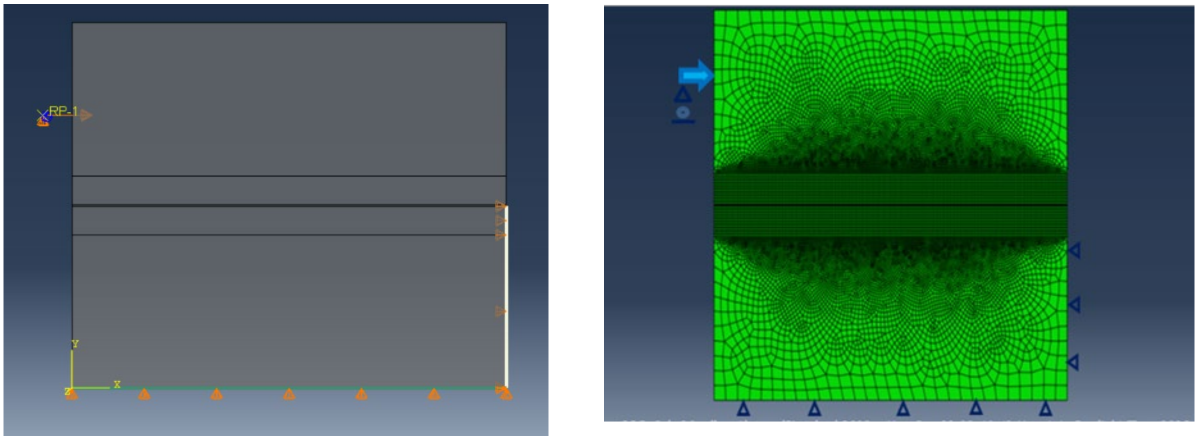

(a) Model Geometry **(b) Boundary Condition**

FIGURE 5.47: Model Geometry and FEM Model

5.15.1 Determination of Continuum Material Property

To simulate the deformation and fracture response of asphalt concrete in the finite element model, the undamaged continuum viscoelastic properties of the bulk material were determined. Because asphalt concrete is a viscoelastic material, its mechanical response depends strongly on temperature and loading rate. Therefore, characterization over a broad frequency range is required so that the finite element model can represent the rate-dependent response observed in laboratory testing.

In this study, the continuum material characterization was developed from binder rheological mastercurves. The binder complex shear modulus mastercurve and phase angle mastercurve were constructed at a reference temperature of 72°F using the time–temperature superposition principle and sigmoidal fitting. The Witczak–Bari model was used to predict the HMA dynamic modulus mastercurve, while the Hirsch model was used to estimate the HMA phase-angle mastercurve. The predicted modulus and phase-angle mastercurves were then used to develop the continuum viscoelastic representation for finite element analysis.

5.15.2 Binder Rheological Characterization

For the present study, the rheological behavior of the binder was characterized using a dynamic shear rheometer over a temperature range of 39°F to 158°F at 11°F increments. The applied frequency range was chosen from 1 to 100 rad/s with 6 record points per decade in log scale. The measured data were shifted to a common reference temperature of 72°F using the time–temperature superposition principle. A sigmoidal function was then used to fit the shifted complex shear modulus mastercurve.

The resulting mastercurve represents the undamaged binder response over a broad range of reduced frequencies. In addition, a phase-angle mastercurve was also developed at the same reference temperature. These binder mastercurves served as the rheological input for the predictive mixture models.

For the damage modeling, it is required to have the undamaged material responses at different loading rates (or frequencies). Mastercurve is a good way to express material responses for a wide range of frequencies at a given temperature. To construct a mastercurve, material responses at any temperature are transferred to a reference temperature by horizontally shifting the test data based on the time-temperature superposition principle. Though there are several mathematical models for the mastercurve, this study used the sigmoidal function, as shown in Eq. 15.

$$\log(G^*) = \delta + \frac{\alpha}{1+e^{\beta+\gamma\log(\omega_r)}} \qquad \text{Eq. 15}$$

where G^* is the complex modulus; α, β, δ, and γ are the fitting parameters; and ω_r is the reduced frequency, which can be calculated from the tested angular frequency, ω, and a shift factor, a_T, using Eq. 16.

$$\omega_r = \omega \cdot a_T \qquad \text{Eq. 16}$$

The purpose of a_T is to convert the ω of any temperature, T, to the reference temperature, T_r. There are many different shift factor functions found in the literature. One of the widely used shift factor functions is the Williams, Landel, and Ferry (WLF) equation, as shown in Eq. 17.

$$\log a_T = \frac{-C_1(T-T_{ref})}{C_2+(T-T_{ref})} \qquad \text{Eq. 17}$$

where C_1 and C_2 are the material fitting parameters that depend on T_r. Another popular shift faction equation is the Arrhenius equation, as shown in Eq. 18.

$$\log a_T = C\left(\frac{1}{T}-\frac{1}{T_r}\right) \qquad \text{Eq. 18}$$

where C is the material constant, and T and T_r are in the Kelvin scale. This study used the WLF equation to develop the relationship between the shift factor, a_T, and temperature, T. After constructing the complex modulus mastercurve, phase angle mastreccurve, δ_b can be predicted using the fitting parameters α, β, and γ, as shown in Eq. 19.

$$\delta_b = -90\alpha\gamma\frac{e^{\beta+\gamma\log(\omega_r)}}{\left(1+e^{\beta+\gamma\log(\omega_r)}\right)^2} \qquad \text{Eq. 19}$$

The time-temperature superposition was used to construct the mastercurves using the average test data of 4 replicate samples. The developed complex modulus mastercurve at 72°F is shown in FIGURE 5.48.

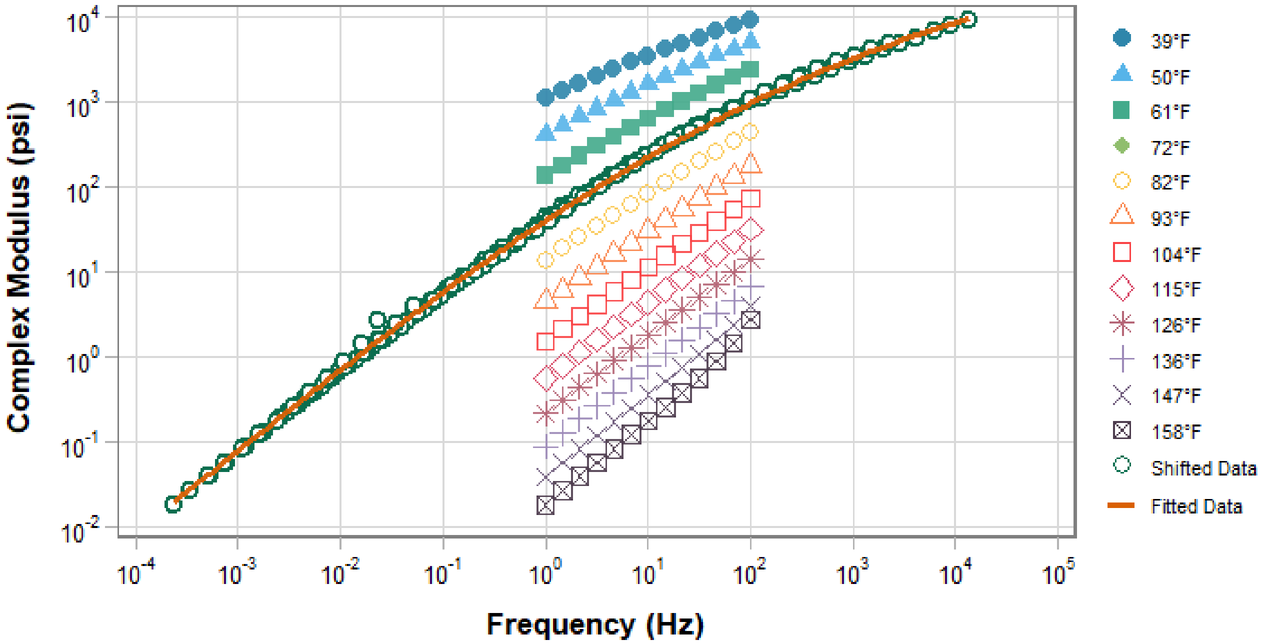

FIGURE 5.48: Complex modulus mastercurve at 72 °F

The markers (except green circles) represent the test data at different test temperatures. The complex shear modulus decreases as the temperature increases. Similarly, the complex shear modulus increases as the frequency increases. However, complex shear modulus increasing rates with frequency for all temperatures are not equal. The complex modulus increases with frequency as the temperature increases because at higher temperatures, the material becomes more fluid and loading rate sensitive. In this study, the time-temperature superposition principle was first used to construct mastercurve (represented using a green circle marker) by shifting the test data. It can be seen that the test data performed at lower temperatures than the reference temperature was moved rightward, and the test data performed at higher temperatures than the reference temperature was moved leftward. After constructing the mastercurve, it was fitted into the sigmoidal function represented using the red line. FIGURE 5.49 shows the shift factor master curve. It shows that the shift factor decreases as the temperature increases.

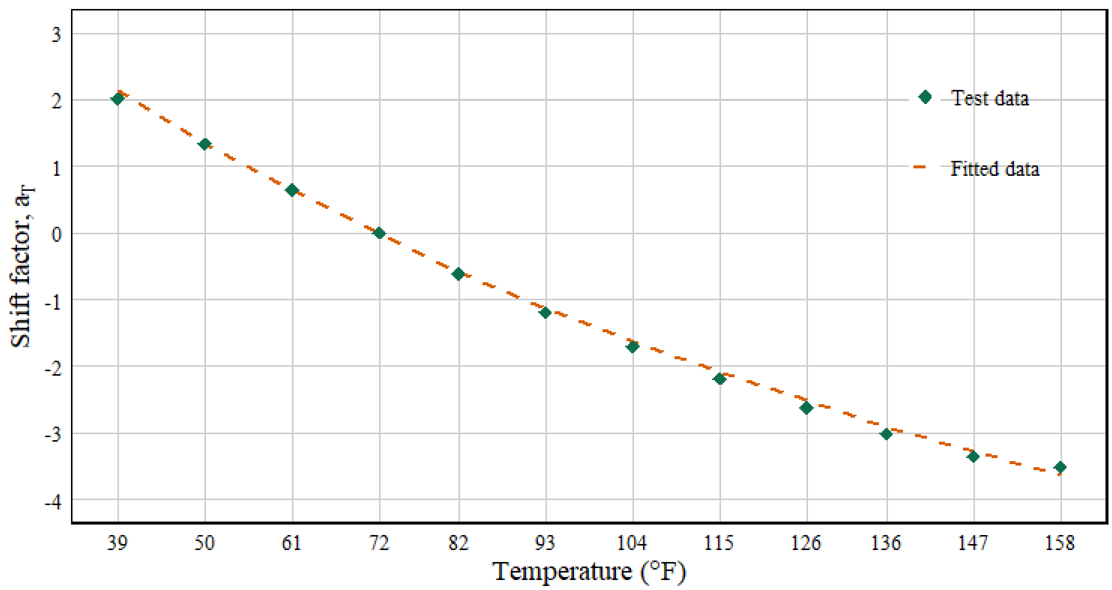

FIGURE 5.49: Shift factor mastercurve at 72 °F

The phase angle mastercurve is illustrated in FIGURE 5.50.

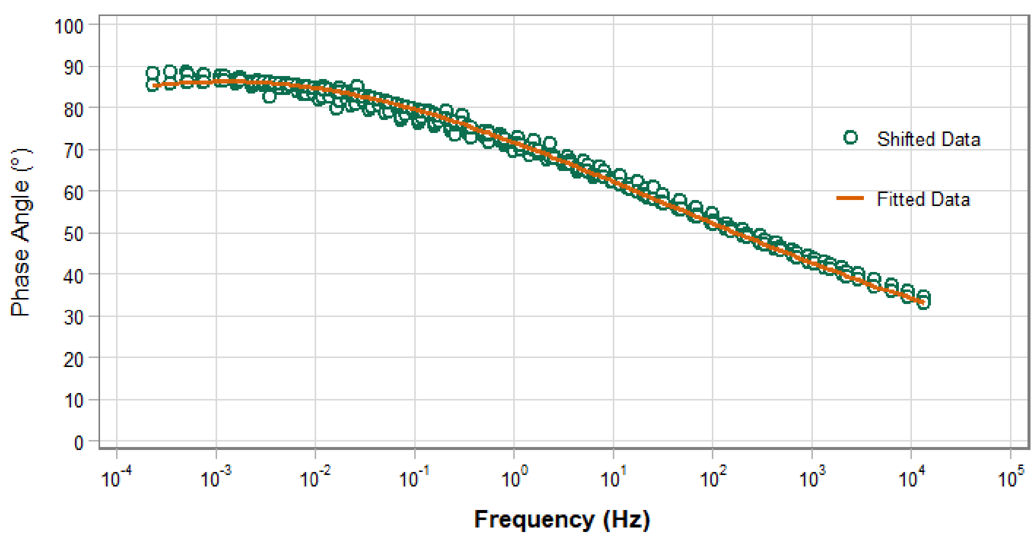

FIGURE 5.50**:** Phase angle mastercurve at 72 °F

5.15.3 HMA Dynamic Modulus Mastercurve

The dynamic modulus of the asphalt mixture was estimated using the Witczak–Bari predictive model. This model predicts the HMA dynamic modulus from binder rheological properties together with the mixture volumetric properties. The parameters adopted in this study are: $P_{200} = 8\%$, $P_4 = 60\%$, $P_{3/8} = 90\%$, $P_{3/4} = 100\%$, $V_a = 7.0\%$, $VMA = 14.2\%$. The model incorporates the binder complex shear modulus and binder phase angle over a wide range of loading frequencies. The Witczak-Bari model used in this study is expressed as:

$$\log(E^*) = -0.49 + 0.7544(G^*)^{-0.0052}\Big[6.65 - 0.032P_{200} + 0.0027P_{200}^2 + 0.011P_4 - 0.0001P_4^2 + 0.006P_{3/8} - 0.00014P_{3/8}^2 - 0.08V_a - 1.06\left(\frac{V_{be}}{V_{be}+V_a}\right)\Big] + \Big[\Big(2.56 + 0.03V_a + 0.71\left(\frac{V_{be}}{V_{be}+V_a}\right)\Big)/\big(1 + e^{--0.7814-0.5785\log(G^*)+0.8834\log(\delta_b)}\big)\Big]$$ Eq. 20

Where,

E^* = dynamic modulus of asphalt mixture

G^* = binder dynamic shear modulus

δ_b = binder phase angle

V_a = air void content

V_{be} = effective binder content

P_{200} = percent passing No. 200 sieve

P_4 = percent retained on No. 4 sieve

$P_{3/8}$ = percent retained on 3/8 in sieve

$P_{3/4}$ = percent retained on 3/4 in sieve

In the present study, the binder complex shear modulus mastercurve and phase angle mastercurve obtained at a reference temperature of 72°F were used as input rheological properties for the model. The predicted dynamic modulus values were then used to construct the HMA dynamic modulus mastercurve (FIGURE 5.51).

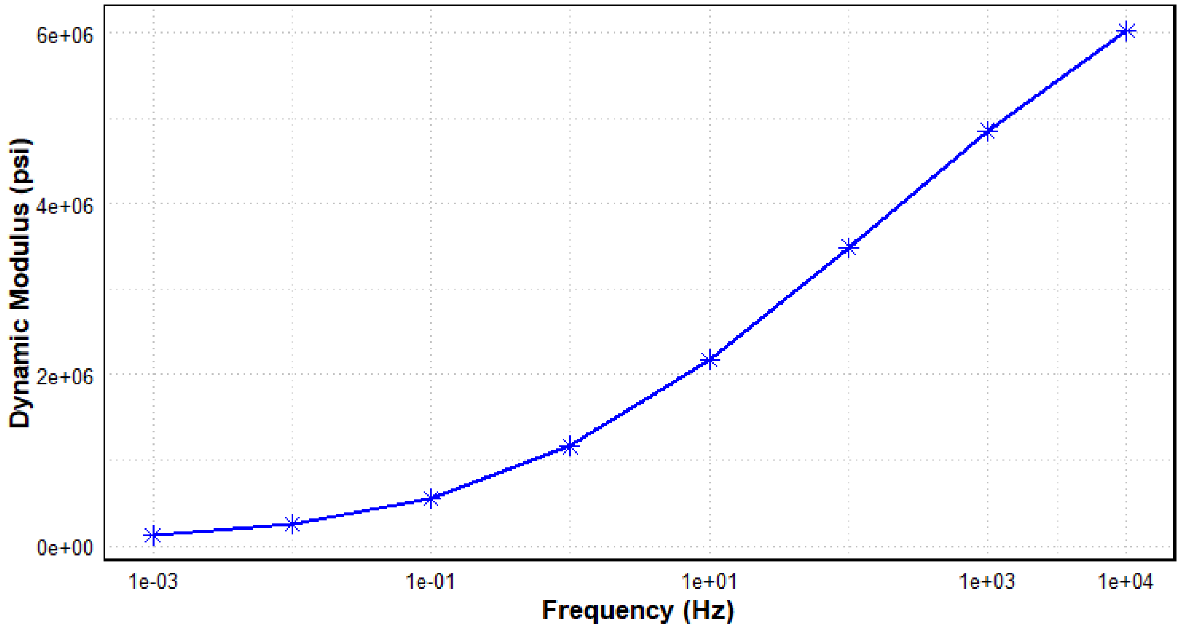

FIGURE 5.51: HMA Dynamic Modulus Mastercurve

5.15.4 HMA Phase Angle Mastercurve

The phase angle of the asphalt concrete was estimated using the Hirsch model. In this study, the Hirsch model was used to estimate the phase angle corresponding to each frequency obtained from the binder mastercurve. The phase angle of the HMA can be estimated as:

$$\phi = -21(\log P_c)^2 - 55\log P_c \qquad \text{Eq.21}$$

Where,

ϕ = Phase angle

P_c = model parameter

The model parameter P_c is calculated as

$$P_c = \frac{20+\left(\frac{3|G_b^*|(VFA)}{VMA}\right)^{0.58}}{650+\left(\frac{3|G_b^*|(VFA)}{VMA}\right)^{0.58}} \qquad \text{Eq.22}$$

For each frequency, the binder complex modulus obtained from the binder mastercurve was substituted into the Hirsch model to compute the parameter P_c. The corresponding phase angle was then determined using the above relationship. Repeating this procedure across the full frequency range produced the HMA phase-angle mastercurve (FIGURE 5.52).

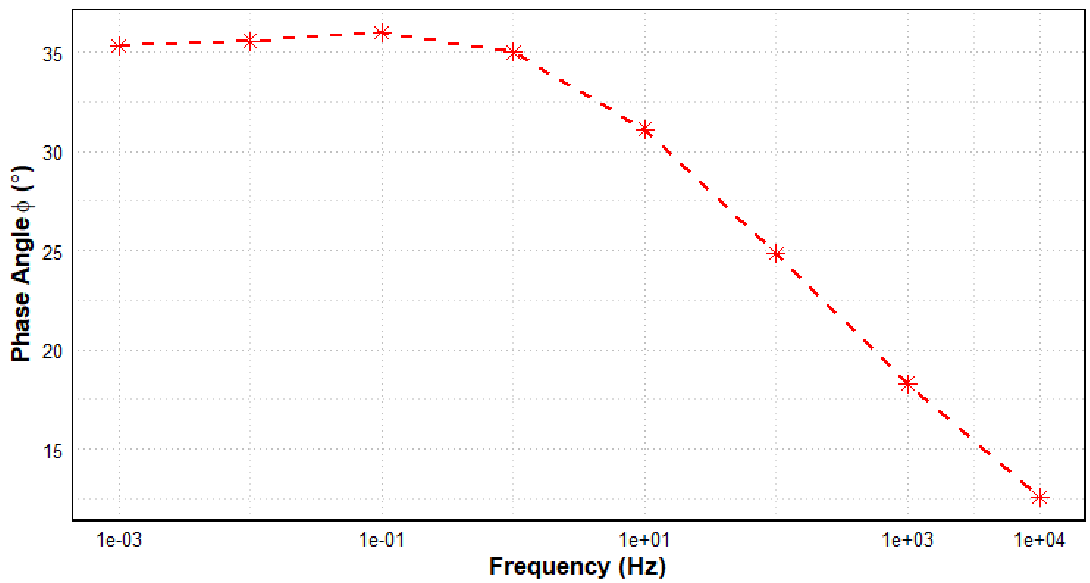

FIGURE 5.52 HMA Phase Angle Mastercurve

5.15.5 Development of Prony Series

After the HMA dynamic modulus and phase angle mastercurves were obtained, the viscoelastic response of the asphalt concrete was characterized in terms of storage modulus and loss modulus. These parameters describe the elastic and viscous components of the material response and are required for developing the time-domain viscoelastic representation used in finite element modeling.

The storage modulus E′ and loss modulus E″ were computed from the predicted dynamic modulus and phase angle using the following equations.

$$E' = |E^*|\cos\phi \qquad \text{Eq.23}$$

$$E'' = |E^*|\sin\phi \qquad \text{Eq.24}$$

The storage modulus represents the recoverable elastic portion of the material response, while the loss modulus represents the energy dissipated through viscous deformation. These parameters collectively describe the frequency-dependent viscoelastic behavior of the asphalt concrete.

Because finite element programs such as Abaqus require viscoelastic material properties in the time domain, the frequency-domain mastercurves were converted into a relaxation modulus representation. The relaxation modulus E(t) was expressed using a generalized Maxwell model (FIGURE 5.53) represented by a Prony series.

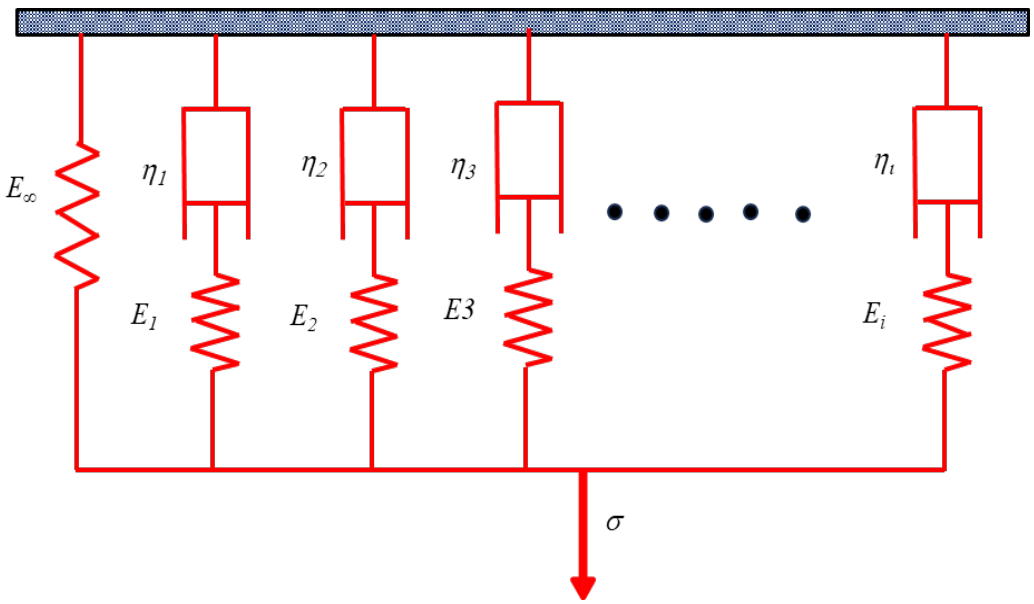

FIGURE 5.53: Generalized Maxwell Model

To determine the stress in the GMM model, the following steps are used:

$$\dot{\varepsilon} = \dot{\varepsilon}_s + \dot{\varepsilon}_d = \frac{\dot{\sigma}}{E} + \frac{\sigma}{\eta} \qquad \text{Eq.25}$$

It should be noted that the relaxation time is defined as the ratio of the viscosity and elasticity modulus of a single Maxwell element. Here, it is denoted by τ and $\tau = \eta/E$. Now, Eq.25 becomes:

$$\dot{\sigma} = E\dot{\varepsilon} - \frac{\sigma}{\tau} \qquad \text{Eq.26}$$

Laplace transformation of Eq.26 leads to:

$$s\sigma(s) = sE\varepsilon(s) - \frac{\sigma(s)}{\tau} \Rightarrow \sigma(s) = \frac{sE}{s + \frac{1}{\tau}}\varepsilon(s) \qquad \text{Eq.27}$$

Now, the inverse Laplace transform of Eq.27 back to the time domain yields the following form:

$$\sigma(t) = \int_{t'=0}^{t'=t} E e^{\left[-(t-t')/\tau\right]} \dot{\varepsilon} dt' \qquad \text{Eq.28}$$

It is the most basic integral form of the Maxwell model for stress-strain calculation. This equation is used later to derive a general integral form for the GMM.
Summing up the spring and the Maxwell elements using Eq.28, the generalized form is as follows:

$$\sigma(s) = \left(E_\infty + \sum_{i=1}^{n} \frac{sE_i}{s + 1/\tau_i} \right) \varepsilon(s) \qquad \text{Eq.29}$$

Inverse Laplace transformation of Eq.29 leads to:

$$\sigma(t) = \int_{t'=0}^{t'=t} \left\{ E_\infty + \sum_{i=1}^{n} E_i e^{\left[-(t-t')/\tau_i \right]} \right\} \dot{\varepsilon} dt' \qquad \text{Eq.30}$$

The simplest form of Eq.30 is as follows:

$$\sigma(t) = \int_{t'=0}^{t'=t} E(t-t') \dot{\varepsilon} dt' \qquad \text{Eq.31}$$

The Prony series representation of the relaxation modulus is given by,

$$E(t) = E_\infty + \sum_{i=1}^{n} E_i e^{\left(-t/\tau_i \right)} \qquad \text{Eq.32}$$

The storage modulus mastercurve can be obtained from the developed mastercurve for $|E^*|$ and the phase angle. The storage modulus as a function of angular frequency is fitted with the following Prony series expression:

$$E'(\omega) = E_\infty + \sum_{i=1}^{M} \frac{\omega^2 \tau_m^2 E_i}{1+\omega^2 \tau_i} \qquad \text{(Eq. 33)}$$

$$E''(\omega) = \sum_{i=1}^{M} \frac{\omega \tau_m E_i}{1+\omega^2 \tau_i} \qquad \text{(Eq. 34)}$$

Where $E'(\omega)$ and $E''(\omega)$ = storage modulus and loss modulus, that is, the real part and imaginary part of the complex modulus,

E_∞ = the longtime equilibrium modulus,

ω = the angular frequency,

τ_i is the relaxation time

E_i= spring constant in the generalized Maxwell model

For numerical implementation, the relaxation modulus is expressed in normalized form as:

$$\frac{E(t)}{E_0} = 1 - \sum_{i=1}^{N} g_i\left(1 - e^{-t/\tau_i}\right) \quad \text{Eq.35}$$

Where,

$$E_0 = \text{instantaneous modulus}$$

$$g_i = \text{dimensionless Pólya coefficients}$$

The Prony coefficients g_i and relaxation times τ_i were determined by fitting the predicted dynamic modulus mastercurve over the reduced-frequency range. This procedure ensures that the time-domain viscoelastic representation reproduces the frequency-dependent stiffness.

The storage and loss modulus equations were established over the selected frequency range. The Prony series parameters were obtained by solving the overdetermined system with nonnegative least squares. The fitted terms were then normalized to define the Abaqus Prony coefficients and relaxation times. The instantaneous and long-term moduli were calculated and verified before preparing the final Abaqus input TABLE. The Prony coefficients and relaxation times derived from the HMA mastercurves are summarized in TABLE 5.36. The long-term elastic modulus in the viscoelastic formulation was 33,935.82 psi with a Poisson's ratio of 0.30.

TABLE 5.36: Prony Series Parameters

Term (i)	Prony coefficient (g_i)	Relaxation time τ_i
1	0.264012	1.0E-04
2	0.189143	1.0E-03
3	0.220686	1.0E-02
4	0.160220	1.0E-01
5	0.090821	1.0E+00
6	0.041258	1.0E+01
7	0.016821	1.0E+02
8	0.012297	1.0E+03

5.15.6 Determination of Fracture Properties

Direct shear tests were conducted at loading rates of 0.197, 0.394, 1.181, 1.969, and 3.937 inch/min. The stress–displacement responses obtained from these tests were used to determine the peak stress and fracture energy. Representative stress–displacement curves are shown in FIGURE 5.54. The curves show an initial increase in stress with displacement, followed by a gradual reduction after the peak.

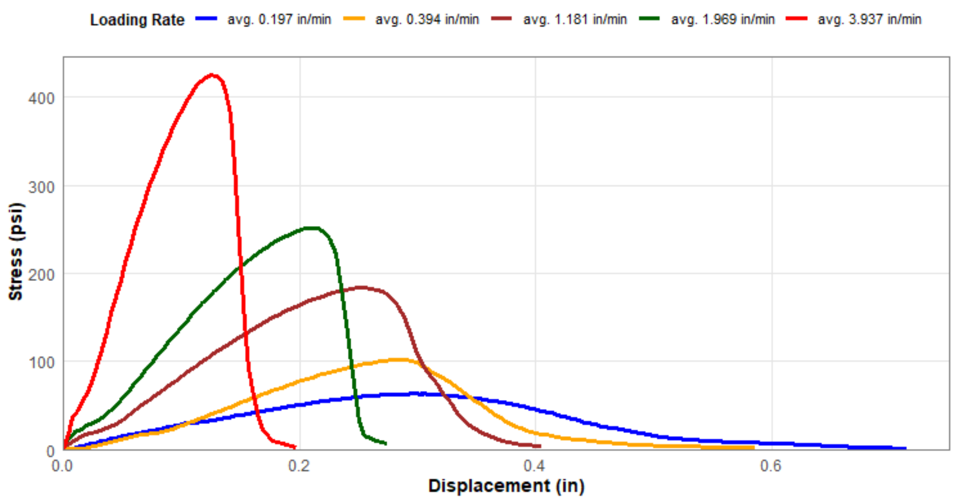

FIGURE 5.54 Shear stress–displacement curves obtained from direct shear tests at different loading rates.

Peak stress was defined as the maximum shear stress observed during each test. Fracture energy was calculated from the area under the load–displacement curve up to the point of failure. This approach is commonly used to quantify the energy required for interfacial fracture.

$$G_f = \frac{1}{A}\int_0^{\delta_f} P(\delta)\ d\delta \qquad \text{Eq.27}$$

where G_f is the fracture energy (kip.f-in/in^2), $P(\delta)$ is the applied load as a function of displacement, δ is the displacement, δ_f is the displacement at complete separation, and A is the bonded interface area.

The calculated peak stress and fracture energy values are summarized in TABLE 5.37.

TABLE 5.37: Lab-tested peak stress and fracture energy

Loading Rate (inch/min)	Peak Stress (psi)	Fracture Energy (kipf-in/in^2)
0.197	63.5	0.0214
0.394	102.3	0.0237
1.181	182.2	0.0324
1.969	252.5	0.0370
3.937	425.0	0.0419

TABLE 5.37 shows that both peak stress and fracture energy increase with loading rate. The peak stress increases from 63.5 psi at 0.197 inch/min to 425 psi at 3.94 inch/min. A similar increase is observed in fracture energy, indicating that greater energy is required to cause interfacial failure at higher loading rates.

The observed increase in peak stress with loading rate indicates a rate-dependent response of the asphalt interface. Similarly, the increase in fracture energy suggests that higher deformation rates require more energy for crack propagation. This behavior is consistent with the viscoelastic nature of asphalt materials, where stiffness and resistance to fracture increase as the loading rate increases.

5.15.7 Simulation Results

The developed finite element model was used to simulate the direct shear response of the asphalt concrete interface at different displacement rates. The numerical results were compared with the laboratory direct shear test results to evaluate the ability of the model to capture the interface bonding behavior. FIGURE 5.10 presents the comparison between the laboratory measurements and the ABAQUS simulation results for deformation rates of 0.197, 0.394, 1.181, 1.969, and 3.937 inch/min.

As shown in FIGURE 5.55, the load–displacement response obtained from both the laboratory tests and the numerical simulations follows a similar trend. In all cases, the shear stress initially increases with displacement until a peak value is reached. This stage represents the intact bonding condition between the two asphalt layers.

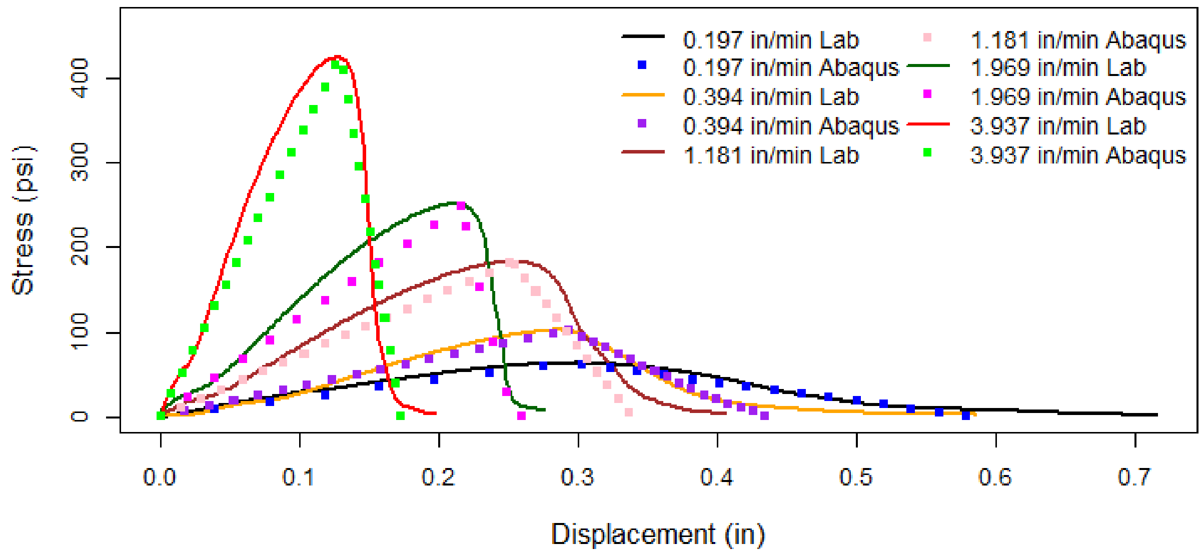

FIGURE 5.55: Model simulation and laboratory test results for different shear rates

After reaching the peak stress, the curves show a gradual decrease in shear stress with increasing displacement. This reduction indicates progressive damage and deterioration of the bonding at the interface. The softening region represents the failure of bonding between the two asphalt layers. Eventually, the stress approaches zero, indicating complete separation.

The ABAQUS simulation results capture both the peak stress and the softening behavior observed in the laboratory tests. For all deformation rates, the numerical curves closely follow the experimental trends in terms of stiffness, peak location, and post-peak response.

Overall, the comparison indicates that the developed cohesive zone model is capable of reproducing the shear failure mechanism at the asphalt interface. The good agreement between the experimental and simulation results confirms that the calibrated parameters used in the model reasonably represent the interfacial bonding characteristics of the tested specimens.

The model parameters obtained from the calibrated ABAQUS simulations were analyzed to develop deformation rate–dependent relationships for the asphalt concrete interface behavior. Two key parameters were considered in this analysis: the peak interfacial shear stress and the fracture energy. These parameters were extracted from the calibrated numerical simulations conducted at different deformation rates.

TABLE 5.38 presents the ABAQUS simulation results used for model development. The TABLE lists the deformation rate together with the corresponding peak shear stress and fracture energy values obtained from the calibrated cohesive zone simulations.

TABLE 5.38: ABAQUS Simulation Results

Loading Rate (inch/min)	**Peak Stress (psi)**	**Fracture Energy (kipf-in/in^2)**
0.197	63.53	0.0185
0.394	101.97	0.0218
1.181	182.75	0.0263
1.969	249.57	0.0311
3.937	435.23	0.0378

The results indicate that both peak stress and fracture energy increase with increasing deformation rate. This trend reflects the rate-dependent response of the asphalt interface. At higher loading rates, the interface becomes stiffer, resulting in higher peak stress values. Similarly, the fracture energy increases with loading rate, indicating that greater energy is required to propagate interface separation.

5.15.8 Peak Stress Model

The resulting peak stress power law is:

$$T = 167.9\,(\text{rate})^{0.6121} \quad \text{(psi)} \qquad \text{Eq.36}$$

where T represents the peak shear stress and rate represents the deformation rate in inches/min.

A regression analysis was performed to calibrate the power law relationship, and the predicted peak stress model is:

$$T = 181.7\,(\text{rate})^{0.6121} - 4.64 \quad \text{(psi)}, \quad R^2 = 0.98 \qquad \text{Eq.37}$$

FIGURE 5.56 shows the measured versus predicted peak shear stress with the calibrated model.

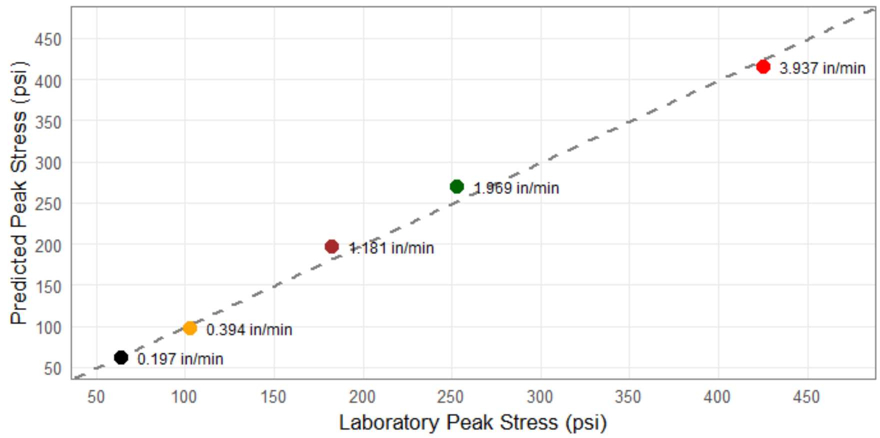

FIGURE 5.56**:** Measured Vs Predicted Peak Shear Stress

5.15.9 Fracture Energy Model

A similar regression procedure was used to develop the deformation rate–dependent model for fracture energy. The regression analysis yielded the following power-law relationship for fracture energy:

$$G_c = 0.0275\,(\text{rate})^{0.24} \quad (\text{kipf} \cdot \text{in/in}^2) \qquad \text{Eq.38}$$

where G_c represents the fracture energy and rate represents the deformation rate in inch/min.

A regression analysis was performed to calibrate the power law relationship, and the predicted fracture energy model is:

$$G_c = 0.0305\,(\text{rate})^{0.24} + 0.0018 \quad (\text{kipf} \cdot \text{in/in}^2), \quad R^2 = 0.97 \qquad \text{Eq.39}$$

FIGURE 5.57 shows the measured versus predicted fracture energy stress with the calibrated model.

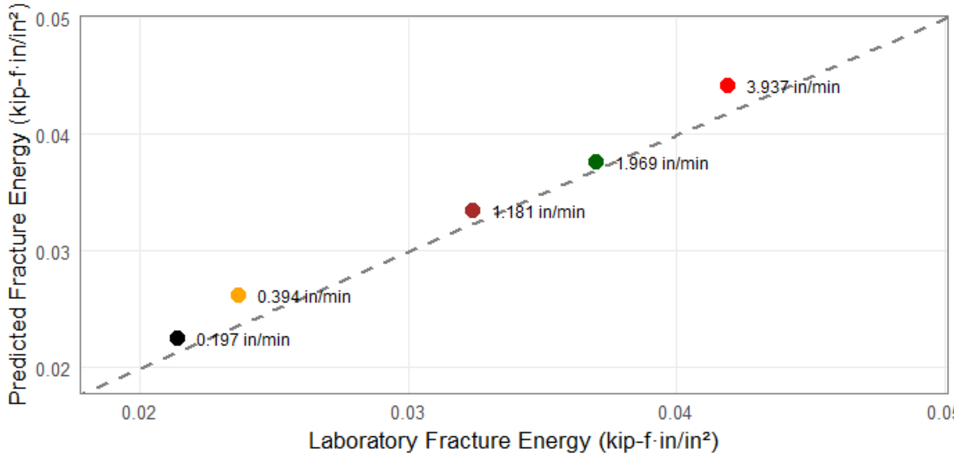

FIGURE 5.57**:** Measured Vs Predicted Fracture Energy

The rate-dependent models given by Equation 37 and Equation 39 were evaluated at two selected loading rates. The laboratory values were compared with the corresponding Abaqus simulated model predictions. The coefficient of variation was calculated for each laboratory-model pair. The results are summarized in TABLE 5.39.

TABLE 5.39: Validation of Abaqus simulated model results

Loading rate (inch/min)	Peak Shear Stress in psi (Lab)	Peak Shear Stress in psi (Model)	COV (%)	Fracture Energy in kipf-in/in^2 (Lab)	Fracture Energy in kipf-in/in^2 (Model)	COV (%)
0.0394	18.32	20.45	7.77	0.0149	0.0158	3.06
0.1000	42.87	39.75	5.34	0.0181	0.0194	4.58

The predicted peak shear stress was close to the laboratory result at both loading rates. The fracture energy values also showed good agreement. The largest variation was observed for peak shear stress at 0.0394 inch/min, with a coefficient of variation of 7.77%. For fracture energy, the coefficients of variation were 3.06% and 4.58%.

CHAPTER 6
CONCLUSIONS

This study evaluated the interfacial bonding performance between asphalt concrete layers by focusing on the effects of tack coat type, application rate, surface condition, curing, and environmental factors. Laboratory direct shear tests were conducted on specimens prepared to measure interface shear strength. Different tack coats and surface textures were considered to understand their influence on bonding behavior. Based on the results, the following conclusions can be drawn:

1. Tack Coat Type: Direct shear tests were conducted to evaluate the interface shear strength of double-layer AC specimens. The specimens used were trackless tack, CSS-1h, SS-1h, and SS-1hp. DSR tests were conducted to determine the high-temperature PG grade, percent of recovery, and non-recoverable creep compliance. The results show that trackless tack has the highest high-temperature PG grade of 82 °C, compared to 64 °C for SS-1h and CSS-1h, and 70 °C for SS-1hp. Trackless tack also shows higher elastic recovery, with values of 87% and 65% at 0.1 and 3.2 kPa, respectively, while CSS-1h shows the lowest recovery of 12% and 7%. In terms of non-recoverable creep compliance, trackless tack has the lowest values (0.13 and 0.27 kPa^{-1}), indicating better resistance to permanent deformation, whereas CSS-1h shows the highest values (0.56 and 0.62 kPa^{-1}). Overall, the higher PG grade, higher percent of recovery, and lower non-recoverable creep compliance of trackless tack make it superior compared to conventional and nanopolymer-modified tack coats.

2. Tack Coat Application Rate for Newly Compacted and Milled Surfaces: The study found the optimal tack coat application rates for both the new HMA layer and the milled surface. The optimal rates vary based on tack coat type and surface type. For example, the optimum application rates for SS-1h and CSS-1h were found to be nearly the same, approximately 0.04 gal/yd^2. The current NMDOT specification mentions applying up to 0.08 gal/yd^2 residual application rate. For conventional tack, they produce a slip plane at 0.08 gal/yd^2 residual application rate. For the nanopolymer modified SS-1hp tack, the optimum application rate was found to be 0.06 gal/yd^2. Using tack coat above the optimum rate not only increases cost but also negatively affects pavement performance.
For trackless tack, with the increment of application rate, the interface shear strength increases. The study went up to 0.10 gal/yd^2, which is 0.02 gal/yd^2 higher than the maximum residual application rate specified by NMDOT. The study found 0.06 to 0.08 gal/yd^2 application rate performs better for a typical milled surface.

3. Environmental Effect: This study evaluated the environmental effects on the interface by analyzing moisture damage and temperature.

3.1 ***Moisture Damage Analysis*****:** MIST conditioning reduced interface shear strength for all tack coats. For SS-1h, the strength decreased from 242.94 psi to 195.47 psi, showing a reduction of about 20%. Similarly, CSS-1h decreased from 228.75 psi to 172.09 psi, with a higher reduction of 24%. Polymer-modified tack coats showed better resistance to moisture damage. SS-1hp decreased from 264.22 psi to 219.91 psi (16%), and CSS-1hp decreased from 252.36 psi to 214.21 psi (15%). Trackless tack showed the least reduction, decreasing from 241.54 psi to 227.03 psi, which is only about 6%. Overall, conventional tack coats are more sensitive to moisture, while polymer-modified and trackless tacks provide better resistance and maintain higher interface shear strength.

3.2 *Temperature Effect Analysis*: This study analyzed the effect of temperature on the interface shear strength at different application rates. The results show that interface shear strength decreases significantly as temperature increases. At 68°F, the highest strength was observed at 0.04 gal/yd² with 253 psi, followed by 250 psi at 0.06 gal/yd², 223 psi at 0.08 gal/yd², and 215 psi at 0.0 gal/yd². At 131°F, the reduction was more significant, where the values dropped to 48 psi, 45 psi, 43 psi, and 34 psi for application rates of 0, 0.04, 0.06, and 0.08, respectively. Overall, increasing temperature leads to a sharp decrease in interface shear strength, and the effect becomes more severe at higher temperatures.

4. Evaluating Eight Factors: Eight factors were evaluated to understand their effect on interface shear strength, including tack coat type, application rate, mean texture depth, texture orientation, temperature, curing time, surface aging, and moisture damage. The ANOVA results show that all factors are statistically significant. Among them, application rate has the strongest influence, with very large effect sizes (η^2 = 0.995 for rate and 0.885 for type). Trackless tack provides higher strength compared to other tack coats with statistical significant difference. Mean texture depth also has a very large effect (η^2 = 0.992), where higher texture depths result in higher shear strength. Temperature shows a very strong effect (η^2 = 0.942), with shear strength decreasing significantly as temperature increases. Texture orientation has a large effect (η^2 = 0.894), where parallel orientation shows higher strength than perpendicular and 45-degree orientations. Moisture also has a large effect (η^2 = 0.885), and moisture reduces strength significantly. Curing time has a moderate effect (η^2 = 0.628), with strength increasing with complete curing. The interface shear strength increases by approximately 20–40% from no curing to full curing. Surface aging also has a strong effect (η^2 = 0.846), where unaged specimens show higher strength than aged ones.

5. Interface Shear Strength Variation with Tack Type and Application Rates: The results show that shear strength varies with both tack coat type and application rate. For SS-1h, the strength increased from 215 psi at 0.0 gal/yd² to a peak of 253 psi at 0.04 gal/yd², then decreased to 250 psi at 0.06 and 223 psi at 0.08 gal/yd². For SS-1hp, higher strengths were observed, reaching 264 psi at 0.04 and 275 psi at 0.06 gal/yd², before decreasing to 253 psi at 0.08 gal/yd². CSS-1h showed relatively lower values, with 234 psi at 0.04, 223 psi at 0.06, and a drop to 186 psi at 0.08 gal/yd². Trackless tack showed the best performance, increasing from 237 psi at 0.04, 274 psi at 0.06, and 282 psi at 0.08 gal/yd². The highest value of 298 psi was achieved at 0.10 gal/yd² for trackless tack. Overall, trackless tack provides the highest interface shear strength, followed by SS-1hp, SS-1h, and CSS-1h.

6. Interface Shear Strength of Typical Milled Surface: For a typical milled surface, rougher surfaces showed higher interface shear strength. At zero application rate, the shear strength increased from 108.06 psi to 125.48 psi as the mean texture depth increased from 0.0445 to 0.2157 inch. A similar trend was observed at other application rates. At 0.04 gal/yd², the strength increased from 98.25 psi to 121.27 psi with increasing texture depth. At 0.06 gal/yd², it increased from 107.62 psi to 127.4 psi. At 0.08 gal/yd², the strength also increased from 102.44 psi to 119.25 psi with higher texture depth. Overall, the results clearly show that increasing mean texture depth improves interface shear strength, and rougher milled surfaces provide better bonding performance.

7. Controlled Grinding: The results show that controlled-textured (lab grooved/notched) surfaces improve interface shear strength across different application rates for both field cores and new HMA. For lab-notched field cores, the strength increased from 118.24 psi at 0 gal/yd² to 125.88 psi at 0.04 gal/yd² and reached a peak of 131.05 psi at 0.06 gal/yd², then slightly decreased to 121.86 psi at 0.08 gal/yd². A similar trend was observed for new HMA. The strength increased from 125.11 psi at 0 gal/yd² to 132.59 psi at 0.04 gal/yd² and reached the highest value of 139.32 psi at 0.06 gal/yd², followed by a decrease to 123.75 psi at 0.08 gal/yd². Overall, controlled grinding increases interface bonding for both aged and new surfaces.

8. Curing Guidelines: Current NMDOT curing specification is unclear (e.g., 24 hours or until cured). This study identified the minimum curing time required for each tack to achieve the best performance. For SS-1h, the shear strength increased from 172 psi without curing to 210 psi at 120 minutes, showing gradual improvement with time. CSS-1h showed a similar trend, increasing from 149 psi to 191 psi at 120 minutes. For SS-1hp, the strength increased from 204 psi without curing to 231 psi at 10 minutes and reached a peak of 270 psi at 50 minutes, then remained almost constant at 60 minutes. Trackless tack showed the fastest curing behavior, increasing from 211 psi without curing to 289 psi at 15 minutes, 301 psi at 25 minutes, and reaching 303 psi at 30 minutes. Based on these results, the minimum curing times required are about 120 minutes for SS-1h, 100 minutes for CSS-1h, 50 minutes for SS-1hp, and only 25 minutes for trackless tack. Overall, curing time significantly affects interface shear strength, and trackless tack achieves high strength in a much shorter time compared to other tack coats.

9. Delamination Mechanism: The mechanics of delamination can be evaluated using PMED by comparing full and partial interface bonding conditions. Two New Mexico weather stations were selected to represent different climatic conditions. Under full bond conditions, the asphalt layers acted together as a composite structure and transferred traffic loads more efficiently. Under partial bond conditions, the layers did not act fully together, which increased predicted pavement distresses such as AC rutting, IRI, top-down cracking, and bottom-up cracking. Therefore, interface bond condition should be considered as an important parameter in pavement design and performance evaluation.

The results show that interface shear strength increases with both loading rate and normal stress. At a normal stress of 72 psi, the shear strength increased from 94 psi at a low loading rate of 0.1 mm/min to 162 psi at 5 mm/min. A similar trend was observed at higher normal stresses. At 108 psi, the strength increased from 113 psi to 192 psi, and at 145 psi, it increased from 128 psi to 260 psi as the loading rate increased. This indicates that higher loading rates and higher normal stresses improve interface resistance to shear.

The cohesion values remained relatively stable across loading rates, ranging from about 58 psi to 66 psi. In contrast, the angle of internal friction increased significantly with loading rate, from about 24° at 0.1 mm/min to about 54° at 5 mm/min. This shows that friction plays a more important role at higher loading rates, while cohesion remains relatively constant. Overall, the delamination mechanism is controlled by both cohesion and friction, but friction becomes dominant at higher loading conditions.

10. Finite Element Model: A finite element model is developed and validated by laboratory experiments. It can be used to simulate field pavement interface behavior under complex geometry and traffic loading, and materials.

REFERENCES

Al-Qadi, I. L., & Wang, H. (2011). Prediction of tire-pavement contact stress and analysis of asphalt pavement response: A decoupled approach. In *Proceedings of Asphalt Pavement Technology* (pp. 289-315). Association of Asphalt Paving Technologists.

Al-Qadi, I. L., Hasiba, K. I., Cortina, A. S., Ozer, H., Leng, Z., Parish, D. C., & Worsfold, S. J. (2012). *Best practices for implementation of tack coat: Part I-Laboratory study* (Research Report No. FHWA-ICT-12-004). Illinois Center for Transportation.

Ali Shafabakhsh, G., & Akbari, A. (2013). Numerical study of airplane wheel characteristics on the runway rigid pavement failure. *Journal of Scientific & Industrial Research, 72*, 348-357.

Anderson, T. L. (2005). *Fracture mechanics: Fundamentals and applications* (3rd ed.). Taylor & Francis.

Bae, A., Mohammad, L. N., Elseifi, M. A., Button, J., & Patel, N. (2010). Effects of temperature on interface shear strength of emulsified tack coat and its relationship to rheological properties. *Transportation Research Record: Journal of the Transportation Research Board, 2180*, 102-109.

Banerjee, A. (2012). *Breaking and curing rates in asphalt emulsions*.

Banerjee, A., Prozzi, J. A., Smit, A. d. F., Bhasin, A., & Aguiar-Moya, J. P. (2010). *Curing rates for asphalt emulsions*.

Barenblatt, G. I. (1962). The mathematical theory of equilibrium cracks in brittle fracture. *Advances in Applied Mechanics, 7*, 55-129.

Belytschko, T., Liu, W. K., & Moran, B. (2000). *Nonlinear finite elements for continua and structures*. John Wiley & Sons.

Brown, S. F., & Brunton, J. M. (1984). The influence of bonding between bituminous layers. *Highways and Transportation, 31*(5), 16-17.

Buchanan, M. S., & Woods, M. E. (2004). *Field tack coat evaluator (ATACKer)*. Mississippi State University.

Buonsanti, M., & Leonardi, G. (2012). A finite element model to evaluate airport flexible pavement response under impact. *Applied Mechanics and Materials, 138-139*, 257-262.

CalTrans. (2003). *CPB 03-1 paint binder (tack coat) guidelines*. California Department of Transportation.

Canestrari, F., & Santagata, E. (2005). Temperature effect on the shear behaviour of tack coat emulsions used in flexible pavements. *International Journal of Pavement Engineering, 6*(1), 39-46.

Canestrari, F., Ferrotti, G., Lu, X., Millien, A., Partl, M. N., Petit, C., Phelipot-Mardele, A., Piber, H., & Raab, C. (2013). Mechanical testing of interlayer bonding in asphalt pavements. In *Advances in interlaboratory testing and evaluation of bituminous materials* (pp. 303-360). Springer.

Chang, F., Yaacob, H., Hainin, M. R., & Rashid, A. S. A. (2014). Compilation of pavement interface bond strength devices for bond strength quantification. *Jurnal Teknologi, 71*(3), 15-22.

Charmot, S., Romero, P., & Dunning, M. (2005). Forensic analysis of slippage cracking. In *Proceedings of the 84th TRB Annual Meeting*. Transportation Research Board.

Chen, J.-S., & Huang, C.-C. (2010). Effect of surface characteristics on bonding properties of bituminous tack coats. *Transportation Research Record: Journal of the Transportation Research Board, 2180*, 142-149.

Chen, J.-S., Chang, M. K., & Lin, K. Y. (2005). Influence of coarse aggregate shape on the strength of asphalt concrete mixtures. *Journal of the Eastern Asia Society for Transportation Studies, 6*, 1062-1075.

Collop, A. C., Sutanto, M. H., Airey, G. D., & Elliott, R. C. (2009). Shear bond strength between asphalt layers for laboratory prepared samples and field cores. *Construction and Building Materials, 23*, 2251-2258.

Covey, D., Coleri, E., & Mahmoud, A. (2017). Tack coat rheological properties and the effects on interlayer shear strength. *Journal of Materials in Civil Engineering, 29*(11), 04017221.

D'Andrea, A., Russo, S., & Tozzo, C. (2013). Interlayer shear testing under combined stress conditions. *Advanced Materials Research, 723*, 381-388.

De Beer, M., Fisher, C., & Jooste, F. J. (2002). Evaluation of non-uniform tyre contact stresses on thin asphalt pavements. In *Proceedings of the 9th International Conference on Asphalt Pavements*. International Society of Asphalt Pavements.

Desai, C. S. (2001). *Mechanics of materials and interfaces: The disturbed state concept*. CRC Press.

Desai, C. S. (2007). Unified DSC constitutive model for pavement materials with numerical implementation. *International Journal of Geomechanics, 7*(2), 83-101.

Diakhate, M., et al. (2007). Comparison of direct shear and torque tests for determining viscoelastic shear behavior of tack coats. In *Proceedings of Advanced Characterisation of Pavement and Soil Engineering Materials* (pp. 281-290). Taylor & Francis.

Diakhate, M., Phelipot, A., Millien, A., & Petit, C. (2006). Shear fatigue behaviour of tack coats. *Road Materials and Pavement Design, 7*(2), 201-222.

Donovan, E., Al-Qadi, I., & Loulizi, A. (2000). Optimization of tack coat application rate for geocomposite membrane on bridge decks. *Transportation Research Record: Journal of the Transportation Research Board, 1740*, 143-150.

Dugdale, D. S. (1960). Yielding of steel sheets containing slits. *Journal of the Mechanics and Physics of Solids, 8*, 100-104.

Durix, L., Dressler, M., Coutellier, D., & Wunderle, B. (2012). On the development of a modified button shear specimen to characterize the mixed mode delamination toughness. *Engineering Fracture Mechanics, 84*, 25-40.

Estakhri, C., Saylak, D., Button, J., & Jenkins, P. (1991). *Investigation of laboratory test methods to determine curing rate of asphalt emulsion*.

Hachiya, Y., & Sato, K. (1997). Effect of tack coat in bonding characteristics at interface between asphalt concrete layers. In *Proceedings of the Eighth International Conference on Asphalt Pavements* (Vol. 1, pp. 349-362). International Society of Asphalt Pavements.

Hakimzadeh, S. (2015). *Evaluation of bond between pavement layers: Fracture mechanics approach* [Doctoral dissertation, University of Illinois].

Hakimzadeh, S., Kebede, N. A., Buttlar, W. G., Ahmed, S., & Exline, M. (2012). Development of fracture-energy based interface bond test for asphalt concrete. *Road Materials and Pavement Design, 13*(sup1), 76-87.

Harries, R. J., & Sitaraman, S. K. (2001). Numerical modeling of interfacial delamination propagation in a novel peripheral array package. *IEEE Transactions on Components and Packaging Technologies, 24*, 256-264.

Hillerborg, A., Modeer, M., & Petersson, P. E. (1976). Analysis of crack formation and crack growth in concrete by means of fracture mechanics and finite elements. *Cement and Concrete Research, 6*, 773-782.

Irwin, G. R. (1948). Fracture dynamics. *Fracturing of Metals, 147*, 166.

Isailovic, I., Falchetto, A. C., & Wistuba, M. (2017). Fatigue investigation on asphalt mixture layers' interface. *Road Materials and Pavement Design, 18*(sup4), 514-534.

Krueger, R. (2004). Virtual crack closure technique: History, approach, and applications. *Applied Mechanics Reviews, 57*, 109-143.

Kruntcheva, M. R., Collop, A. C., & Thom, N. H. (2005). Properties of asphalt concrete layer interfaces. *Journal of Transportation Engineering, 131*(11), 880-888.

Li, H. (2016). Evaporation rate and evaporative cooling effect of pavement materials. In *Pavement materials for heat island mitigation* (pp. 135-153).

Lysenko, J. E. (2006). Development of shear testing of a bond coat emulsion. In *Proceedings of the CME Congress*.

Maina, J. W., Dennerman, M., & De Beer, M. (2008). Introduction of new road pavement response modelling software by means of benchmarking. In *Proceedings of the 27th Annual South African Transportation Conference*.

Matos, P. P. L., McMeeking, R. M., Charalambides, P. G., & Drory, M. D. (1989). A method for calculating stress intensities in bimaterial fracture. *International Journal of Fracture, 40*, 235-254.

Mohammad, L. N. (2012). *Optimization of tack coat for HMA placement* (NCHRP Report No. 712). Transportation Research Board.

Mohammad, L. N., Bae, A., Elseifi, M., Button, J., & Scherocman, J. (2009). Interface shear strength characterisation of emulsified tack coats. In *Proceedings of Asphalt Pavement Technology* (Vol. 78, pp. 250-277). Association of Asphalt Paving Technologists.

Mohammad, L. N., Elseifi, M. A., Das, R., & Cao, W. (2018). *Validation of the Louisiana interlayer shear strength test for tack coat*.

Mohammad, L. N., et al. (2010). Effects of pavement surface type and sample preparation method on tack coat interface shear strength. *Transportation Research Record: Journal of the Transportation Research Board, 2180*, 93-101.

Mohammad, L. N., Hassan, M., & Patel, N. (2011). Effects of shear bond characteristics of tack coats on pavement performance at the interface. *Transportation Research Record: Journal of the Transportation Research Board, 2209*, 1-8.

Mrawira, D., & Damude, D. J. (1999). Revisiting the effectiveness of tack coats in HMA overlays: The shear strength of tack coats in young overlays. In *Proceedings of the 44th Annual Conference of the Canadian Technical Asphalt Association* (pp. 115-129). Polyscience.

Orowan, E. (1948). Fracture and strength of solids. *Reports on Progress in Physics, 12*, 185-232.

Ozer, H., Al-Qadi, I. L., & Leng, Z. (2008). Fracture-based friction model for pavement interface characterization. *Transportation Research Record: Journal of the Transportation Research Board, 2057*, 54-63.

Raab, C., Partl, M. N., & Abd El Halim, A. O. (2010). Effect of gap width on interlayer shear bond results. *International Journal of Pavement Research and Technology, 3*(2), 79-85.

Rice, J. R. (1968). A path independent integral and the approximate analysis of strain concentration by notches and cracks. *Journal of Applied Mechanics, 35*, 379-386.

Romanoschi, S. A., & Metcalf, J. B. (2002). The characterization of pavement layer interfaces. In *Proceedings of the 9th International Conference on Asphalt Pavements*. International Society for Asphalt Pavements.

Rybicki, E. F., & Kanninen, M. F. (1977). A finite element calculation of stress intensity factors by a modified crack closure integral. *Engineering Fracture Mechanics, 9*, 931-938.

Sangiorgi, C., Collop, A. C., & Thom, N. H. (2002). Laboratory assessment of bond condition using the Leutner shear test. In *Proceedings of the 3rd International Conference on Bituminous Mixtures and Pavements*.

Santagata, E., & Canestrari, F. (1994). Tensile and shear tests of interfaces in asphalt mixes: A new perspective on their failure criteria. In *Proceedings of the 2nd International Symposium on Highway Surfacing*.

Santagata, F. A., et al. (2008). Layer characteristics affecting interlayer shear resistance in flexible pavements. In *Proceedings of Asphalt Pavement Technology* (Vol. 77, pp. 221-256). Association of Asphalt Paving Technologists.

Shaat, A. A. (1992). *Investigation of slippage of bituminous layer in overlaid pavement in Northern Ireland* [Consultancy report]. Department of the Environment in Northern Ireland.

Sholar, G. A., Page, G. C., Musselman, J. A., et al. (2004). Preliminary investigation of a test method to evaluate bond strength of bituminous tack coats (with discussion). *Journal of the Association of Asphalt Paving Technologists, 73*, 771-806.

Sholar, G. A., Page, G. C., Musselman, J. A., Upshaw, P. B., & Moseley, H. L. (2002). *Preliminary investigation of a test method to evaluate bond strength of bituminous tack coats* (Research Report No. FL/DOT/SMO/02-459). Florida Department of Transportation.

Su, K., et al. (2008). Analysis of shear stresses in asphalt pavements under actual measured tire-pavement contact pressure. In *Proceedings of the 6th International Conference on Road and Airfield Pavement Technology* (pp. 11-18). Pavement Engineering Society.

Sundararaman, V., & Sitaraman, S. K. (2001). Interfacial fracture toughness for delamination growth prediction in a novel peripheral array package. *IEEE Transactions on Components and Packaging Technologies, 24*, 265-270.

Sutanto, M. H. (2011). Development of automatic torque bond test. *Jurnal Transportasi, 11*(3).

Szeto, W., Xie, M., Kim, J., Yuen, M., Tong, P., & Yi, S. (2000). Interface failure criterion of button shear test as a means of interface adhesion measurement in plastic packages. In *Electronic Materials and Packaging, 2000: International Symposium* (pp. 263-268).

Tashman, L., Nam, K., & Papagiannakis, T. (2006). *Evaluation of the influence of tack coat construction factors on the bond strength between pavement layers* (Report No. WCAT 06-002). Washington Center for Asphalt Technology, Washington State University.

Tashman, L., Nam, K., Papagiannakis, T., Willoughby, K., Pierce, L., & Baker, T. (2008). Evaluation of construction practices that influence the bond strength at the interface between pavement layers. *Journal of Performance of Constructed Facilities, 22*(3), 154-161.

Tayebali, A. A., et al. (2004). *A mechanistic approach to evaluate contribution of prime and tack coat in composite asphalt pavements* (Research Report 2001-2004). North Carolina State University.

Tozzo, C., D'Andrea, A., Cozzani, D., & Meo, A. (2014). Fatigue investigation of the interface shear performance in asphalt pavement. *Modern Applied Science, 8*(2), 1.

Tran, H. T., Shirangi, M. H., Pang, X., & Volinsky, A. A. (2014). Temperature, moisture and mode-mixity effects on copper leadframe/EMC interfacial fracture toughness. *International Journal of Fracture, 185*, 115-127.

Tran, N., Willis, R., & Julian, G. (2011). *Refinement of the bond strength procedure and investigation of a specification* (Report No. 12-04). National Center for Asphalt Technology.

Transportation Research Board. (2012). *Optimization of tack coat for HMA placement* (National Cooperative Highway Research Program Report 712).

Tschegg, E. K., Kroyer, G., Tan, D., Stanzl-Tschegg, S. E., & Litzka, J. (1995). Investigation of bonding between asphalt layers on road construction. *Journal of Transportation Engineering, 121*(4), 309-316.

Tsubokawa, Y., et al. (2007). Study on infrared thermographic inspection of de-bonded layer of asphalt flexible pavement. In *Proceedings of the FAA Worldwide Airport Technology Transfer Conference*. Federal Aviation Administration.

Uzan, J., Livneh, M., & Eshed, Y. (1978). Investigation of adhesion properties between asphaltic-concrete layers. *Journal of the Association of Asphalt Paving Technologists, 47*, 495-521.

Vallejo, M. (2012). *Predicting failure behavior of polymeric and asphalt composites using damage models* [Doctoral dissertation, University of New Mexico].

Wang, H., Al-Qadi, I. L., & Stanciulescu, I. (2012). Simulation of tyre-pavement interaction for predicting contact stress at static and various rolling conditions. *International Journal of Pavement Engineering, 13*(4), 310-321.

Wellner, F., & Hristov, B. (2015). Numerically supported experimental determination of the behavior of the interlayer bond in asphalt pavement. *Transportation Research Record: Journal of the Transportation Research Board, 2506*(1), 116-125.

West, R. C., Zhang, J., & Moore, J. (2005). *Evaluation of bond strength between pavement layers* (NCAT Report No. 05-08). National Center for Asphalt Technology.

Williams, M. L. (1959). The stresses around a fault or crack in dissimilar media. *Bulletin of the Seismological Society of America, 49*, 199-204.

Xie, W., & Sitaraman, S. K. (2003). Investigation of interfacial delamination of a copper-epoxy interface under monotonic and cyclic loading: Modeling and evaluation. *IEEE Transactions on Advanced Packaging, 26*, 441-446.

Xu, J., Li, N., & Xu, T. (2022). Temperature changes of interlaminar bonding layer in different seasons and effects on mechanical properties of asphalt pavement. *International Journal of Pavement Research and Technology, 15*(3), 589-605.

Yoo, P. J., et al. (2006). Flexible pavement responses to different loading amplitudes considering layer interface conditions and lateral shear forces. *International Journal of Pavement Engineering, 7*(1), 73-86.